The Pennsylvania State University

The Graduate School

Department of Aerospace Engineering

EXTENDING ACOUSTIC DATA MEASURED WITH SMALL-SCALE SUPERSONIC MODEL JETS TO PRACTICAL AIRCRAFT EXHAUST JETS

A Dissertation in

Aerospace Engineering

by

Ching-Wen Kuo

Submitted in Partial Fulfillment
of the Requirements
for the Degree of

Doctor of Philosophy

December 2010

The dissertation of Ching-Wen Kuo was reviewed and approved* by the following:

Dennis K. McLaughlin
Professor of Aerospace Engineering
Dissertation Advisor
Chair of Committee

Philip J. Morris
Boeing / A.D. Welliver Professor of Aerospace Engineering

Kenneth S. Brentner
Professor of Aerospace Engineering

Stephen C. Conlon
Assistant Professor of Aerospace Engineering

Tony Jun Huang
Associate Professor of Engineering Science and Mechanics

George A. Lesieutre
Professor of Aerospace Engineering
Head of the Department of Aerospace Engineering

*Signatures are on file in the Graduate School

ABSTRACT

Modern military aircraft jet engines are designed with variable geometry nozzles to provide optimum thrust in different operating conditions within the flight envelope. However, the acoustic measurements for such nozzles are scarce, due to the cost involved in making full-scale measurements and the lack of details about the exact geometry of these nozzles. Thus the present effort at The Pennsylvania State University and the NASA Glenn Research Center, in partnership with GE Aviation, is aiming to study and characterize the acoustic field produced by supersonic jets issuing from converging-diverging military style nozzles. An equally important objective is to develop a scaling methodology for using data obtained from small- and moderate-scale experiments which exhibits the independence of the jet sizes to the measured noise levels. The experimental results presented in this thesis have shown reasonable agreement between small-scale and moderate-scale jet acoustic data, as well as between heated jets and heat-simulated ones. As the scaling methodology is validated, it will be extended to using acoustic data measured with small-scale supersonic model jets to the prediction of the most important components of full-scale engine noise.

When comparing the measured acoustic spectra with a microphone array set at different radial locations, the characteristics of the jet noise source distribution may induce subtle inaccuracies, depending on the conditions of jet operation. A close look is taken at the details of the noise generation region in order to better understand the mismatch between spectra measured at various acoustic field radial locations. A processing methodology was developed to correct the effect of the noise source distribution and efficiently compare near-field and far-field spectra with unprecedented accuracy. This technique then demonstrates that the measured noise levels in the physically restricted space of an anechoic chamber can be appropriately extrapolated to represent the expected noise levels at different noise monitoring locations of practical interest.

With the emergence of more powerful fighter aircraft, supersonic jet noise reduction devices are being intensely researched. Small-scale measurements are a crucial step in evaluating the potential of noise reduction concepts at an early stage in the design process. With this in mind, the present thesis provides an acoustic assessment methodology for small-scale military-style nozzles with chevrons. Comparisons are made between the present measurements and those made by NASA at moderate-scale. The effect of chevrons on supersonic jets was investigated, highlighting the crucial role of the jet operating conditions on the effects of chevrons on the jet flow and the subsequent acoustic benefits. A small-scale heat simulated jet is investigated in the over-expanded condition and shows no substantial noise reduction from the chevrons. This is contrary to moderate-scale measurements. The discrepancy is attributed to a Reynolds number low enough to sustain an annular laminar boundary layer in the nozzle that separates in the over-expanded flow condition. These results are important in assessing the limitations of small-scale measurements in this particular jet noise reduction method.

Lastly, to successfully present the results from the acoustic measurements of small-scale jets with high quality, a newly developed PSU free-field response was empirically derived to match the specific orientation and grid cap geometry of the microphones. Application to measured data gives encouraging results validating the capability of the method to produce superior accuracy in measurements even at the highest response frequencies of the microphones.

TABLE OF CONTENTS

LIST OF FIGURES

LIST OF TABLES

NOMENCLATURE

a	ambient speed of sound
AR	exit-to-throat area ratio
C_{act}	actuator response coefficient (in dB)
C_{atm}	atmospheric attenuation coefficient (in dB)
C_{ff}	free-field response coefficient (in dB)
D	diameter of nozzle exit
D_e	equivalent diameter of nozzle exit
D_j	average diameter of the full-expanded jet plume
f	frequency (Hz)
f_c	characteristic frequency
I	noise intensity
k	wave number
L	shock cell length
M_a	acoustic Mach number
M_c	convective Mach number
M_d	design Mach number of nozzle
M_f	Mach number of co-flow for forward flight simulation
M_j	jet Mach number
NPR	nozzle pressure ratio
$OASPL$	overall sound pressure level
p, P	atmospheric pressure

PSD	power spectra density
r	radial coordinate
R	physical distance of the microphones from the jet exit
R_e	Reynolds number
R_{gas}	gas constant
St	Strouhal number
SPL	sound pressure level
T	atmospheric temperature
T_{ij}	Lighthill stress tensor
T_o	jet stagnation temperature
TTR	total temperature ratio
U_j	mean exhaust velocity
v	transverse velocity component
x	axial coordinate
x_c	length of the jet potential core
Δf	frequency resolution bandwidth

Greek:

α	atmospheric absorption coefficient
β	nozzle off-design parameter
γ	ratio of specific heats
δ	vorticity thickness
η	normalized radial distance
θ	polar angle, measured from the jet downstream direction

ρ	local density
τ	shear stress
ω	frequency (radian)

Subscripts:

∞	quantity relative to the ambient condition
core	quantity relative to the core of the jet
heated	quantity relative to the heated jet
j	quantity relative to the jet
mix	quantity relative to the mixed jet
max	quantity relative to the maximum value
prop	quantity relative to the propagation distance
raw	quantity relative to the raw signal data

ACKNOWLEDGEMENTS

I would like to express my sincere gratitude to my thesis advisor Prof. Dennis McLaughlin. I am very thankful for his academic advices and deliberate communication skills. I am always encouraged by his persistent working attitude, thorough thinking tactics, and methodical management.

I would also like to thank Prof. Philip Morris for his profound lectures and valuable comments on my research. I also appreciate my other committee members, Prof. Kenneth Brentner, Prof. Stephen Conlon, and Prof. Tony Huang for bringing up insightful aspects on my work.

I am grateful to Strategic Environmental Research and Development for sponsorship of this research. I would also like to thank Drs. James Bridges and Brenda Henderson of NASA for providing experimental data presented in this thesis, and Dr. Viswanathan of Boeing and Dr. Papamoschou of UCI for helpful discussions on some parts of this thesis.

Many thanks to the facility and technical help from Richard Auhl, Mark Catalano, and Kirk Heller. I am thankful to Drs. Jeremy Veltin and Steve Miller and fellow graduate students Benjamin Day, Brian Wallace, Brenton Forshey, Russell Powers, Ujas Patel, Yongle Du, Susan Ha, and Jeffrey Kauffman for their help and contribution.

Lastly I would like to thank the spiritual and financial support from my lovely family, the unforgettable company from Meng-Hsiu Lin, Po-Chun Chen, and Ting Liang with me at State College.

Chapter 1

Introduction

1.1 Motivation

The airplane industry has flourished since the Wright Brothers successfully flew the first airplane in 1903. During World War I and II, there were many rapid developments with military aircraft. The first military aircraft that operated with jet engines came out for service during the end of World War II. Ever since the debut of the jet engine, the aerospace industry has gradually unveiled the potential of modern aircraft to people around the globe. With the intense development of flights across the sky, lawmakers created regulations mainly concerning the aircraft noise generated by civil commercial airliners, whereas military-used aircrafts could be excempted by selecting remote locations for training bases. However, as the environmental laws become more stringent and draw people's attention to the noise levels of the airport communities, it is important to control the noise generated in take-off and landing as much as possible.

To assess the noise levels at the development stage of a novel engine, industry and aircraft manufacturers have acknowledged that the noise exhausting from scale model nozzles can represent the actual acoustics issuing from the full size engines for scale size ratios of approximately 1/7 scale. Even though the moderate-scale measurements are conducted as a primary data source for the evaluation of noise levels, these noise measurements still require more time and resources than small-scale model experiments typical of university laboratories. In such jet noise facilities, small-scale models can efficiently provide the newest and fastest experimental results and observations with various design configurations. As depicted in Figure **1-1**, besides commonly-used numerical prediction, researchers can conduct experiments assessing

the noise levels of jets issuing from various sizes of nozzles.. However, the consensus reached among governmental research institutes, industry, and aircraft manufacturers is that the noise measurements conducted with the moderate-scale nozzles simulate reasonably well the acoustics issuing from the actual size engine. The noise measurements conducted with small-scale nozzles still need further verification to evaluate the quality of experimental data. A scaling methodology for both small- and moderate-scale models can demonstrate that the measured noise levels are independent of the jet scales from the experiments. While the moderate-scale jet is frequently recognized as the adequate replicators of full size jets, the small-scale jets can also radiate the equivalent amount of noise of a full-scale aircraft engine. Under these considerations, the acoustic data acquired from the carefully conducted experiments in the low-cost small-scale jet facilities can be extended to the prediction of practical aircraft exhaust jet noise.

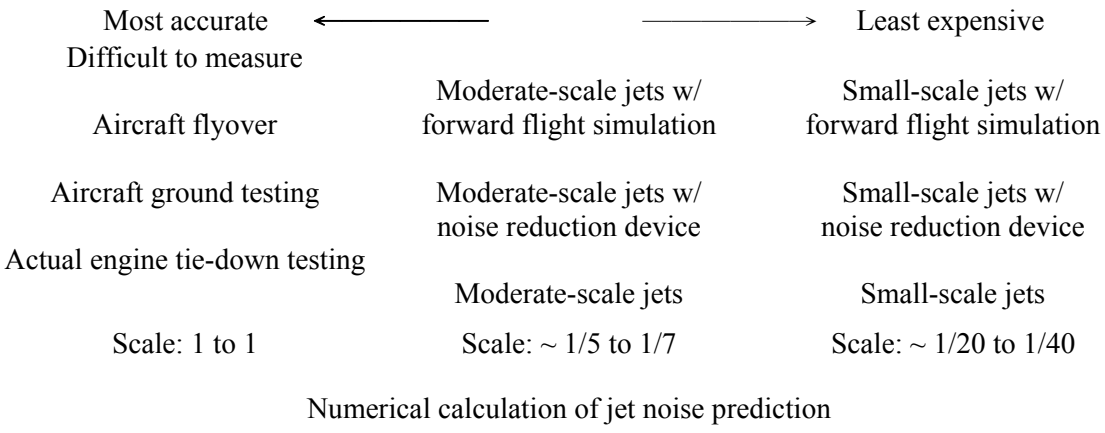

Figure **1-1**: Overview of the noise assessments from the experiments of various scale jets and numerical prediction.

1.2 Theory of aerodynamic noise

1.2.1 The acoustic analogy theory

Sir James Lighthill [1] published a paper in 1952 entitled 'On sound generated aerodynamically I. General theory', in which he used the term "sound generated aerodynamically" to describe the sound generated by aerodynamic forces and turbulence. Lighthill became the founder of this field: aeroacoustics. He began with the momentum equation and ended with a general theory which is called the acoustic analogy theory. Lighthill deliberately moved terms to the right side of the equation and obtained the inhomogeneous wave equation

$$\frac{\partial^2 \rho}{\partial t^2} - a_\infty^2 \nabla^2 \rho = \frac{\partial^2 T_{ij}}{\partial x_i \partial x_j}, \qquad \textbf{1.1}$$

where $T_{ij} = \rho v_i v_j + (p - \rho a_\infty^2)\delta_{ij} - \tau_{ij}$ is known as the Lighthill stress tensor. In his derivation, the left side of Equation **1.1** is the acoustic wave propagation and the right side of Equation **1.1** becomes the effective source of sound and describes the influences of the hydrodynamic field. In the absence of mass flow sources and internal surfaces (that generate forces) Lighthilll showed that these effective sources have a quadrupole nature. By applying dimensional analysis to the solution of Equation **1.1** he concluded that the radiated acoustic power of a jet increases in proportion to the eighth power of the jet velocity U_j in the flow; the so-called $U_j^{\,8}$ law.

As the noise sources move downstream with the mean flow, these moving sources radiate more noise in the direction of motion. This phenomenon was described as the convective amplification effect in the paper published by Lighthill [2] in 1954. He obtained a convection factor, $(1 - M_C \cos\theta)^{-6}$, which can be used to multiply the sound intensity field, where θ is the angle between the direction of convection and the direction of emission. The experimental data confirmed his theory that this factor signifies an increase in the sound intensity field while the

angle is small. He further argued that the flow convection is able to interpret the directional distribution of sound intensity. This convection effect on the directivity of jet noise was thoroughly investigated by Ffowcs Williams [3]. Ffowcs Williams concluded that for very high speed jets the value of power of U^8 law needs to be altered to U^3.

The refraction effect mentioned by Lighthill is caused by the different velocities of the wave front. While the sound radiates through the jet, its path will bend away from the jet centerline. This will create a relatively quiet region near the jet centerline known as the cone of silence where the noise intensity drops by more than 20 dB, which was experimentally demonstrated by Atvars *et al* [4]. Lilley [5] modified Lighthill's equation to include the effect of mean-flow refraction.

Ribner [6] started from Lighthill's analysis and derived the sound power per unit length downstream of a jet categorized in three regions as shown in Figure **1-2**. Ribner hypothesized that the sound power per unit length is approximately constant within the initial mixing region and starts to decrease in the subsequent transition region. While entering the fully developed jet region, the sound power per unit length reduces rapidly and is inversely proportional to the seventh power of axial distance. Ribner hypothesized that most sound noises are radiated in the first 10 diameters downstream of the nozzle exit plane. Powell [7] presented a similar analysis to Ribner but further proposed a similar pattern of spectra measured from turbulent jets. The spectrum of high frequency content is radiated from the annular mixing region while the spectrum of low frequency content is emitted farther behind the end of the jet potential core. It was also suggested that the peak noise may be located slightly downstream of the end of the jet potential core. Nagamatsu *et al.* [8] proposed an analytical calculation of the sound power per unit length issued from the supersonic jet and a reasonable matching with the experimental results. A similar conclusion showed that the peak noise is generated upstream of the axial location of the sonic point (the end of the supersonic core) along the jet downstream.

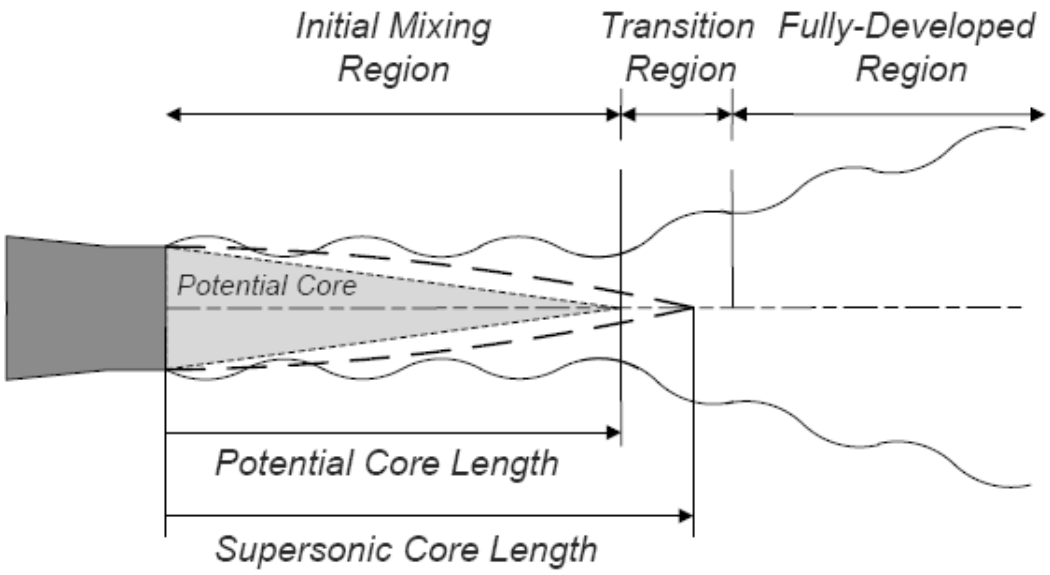

Figure **1-2**: Schematic of a supersonic jet.

1.2.2 Noise source mechanisms

The noise source mechanisms of a supersonic jet comprise two components, turbulent mixing noise, and shock associated noise. The shock associated noise appears only when the shock cells occur in the jet flow. Each of these noise sources radiates from specific flow regions and contributes to dominant noise at far-field observation positions. The description of these noise source mechanisms is as follows.

1.2.2.1 Turbulent mixing noise

One school of thought on the noise generation mechanisms stems from the acoustic analogy theory; the noise prediction in the peak noise emission angle from this approach is not as accurate as the calculation at the sideline direction. When Phillips [9] first described the noise

emission mechanism of the Mach wave radiation through the development of the convective wave equation Ffowcs Williams [3] then emphasized the importance of the convection effect. Ffowcs Williams demonstrated that as the turbulence convection velocity is higher than the ambient acoustic velocity, there is the presence of noise generation in the form of the Mach wave radiation. He also provided a theoretical prediction of the magnitude and directional characteristics of the noise mechanisms for the Mach wave radiation, and correlated the radiated acoustic power to the cubic power of the jet velocity. Another school of thought, however, argues the appropriateness of the instability wave model that confirms the peak noise emission radiating from the noise source mechanism. Turbulent mixing noise is described as being composed of large turbulent structure noise and fine scale turbulence noise. Both are dependent on the observation angle measured from the jet direction.

The large turbulent structure noise dominates the jet downstream region and contributes to the most dominant noise in the spectra. Components of the large turbulent structures that travel downstream supersonically will generate Mach wave radiation. This Mach wave radiation propagates at specific angles depending on the turbulence convection Mach number. Typically the large turbulent structures dominate the jet downstream region, especially at the peak noise emission angle.

The instability wave model can be used to describe the motion of the large turbulent structures in the jet flow. The theoretical work developed by Tam and Morris [10] and successive studies [11-13] have demonstrated that the noise radiation is associated with the large turbulent structures. These structures are treated as a linear superposition of instability waves and the process of the Mach wave radiation is somewhat similar to the one described in the wavy wall analogy. This model is more straightforward to implement than the acoustic analogy theory. Experimental confirmation of the instability wave model in the past resulted from the measurements of McLaughlin *et al.* [14], Morrison and McLaughlin [15], and Troutt and

McLaughlin [16]. These measurements provided substantial evidence that the dominant noise generation mechanism can be described by the instability wave model.

As the instability waves start at small amplitude near the nozzle exit, and grow rapidly and reach the maximum amplitude at some point downstream. After reaching the maximum amplitude, the amplitude of the instability waves starts to decrease as they propagate further downstream. This physical phenomenon can be described as the growing, emerging, and breaking down of the large turbulent structures convecting downstream in the jet shear layer. The growth and decay of the amplitude of the instability waves broadens the wave number (k) spectrum. The phase velocity depends on ω / k , where ω is frequency. When the phase velocity is higher than the ambient acoustic velocity, Mach wave radiation is generated. The strength of the Mach wave radiation increases as the jet convection velocity rises. Tam *et al.* [17] and Seiner *et al.* [18] demonstrated that for a series of jet Mach numbers and temperature ratios the experimental data compare well to the predicted peak noise emission angle and peak frequency contributed by the most amplified instability wave.

The common literature appears to draw a sharp distinction between jets with predominantly subsonic turbulence convection velocities (relative to the ambient air) and those with supersonic values of M_c. For fully supersonically convecting turbulence, ample evidence of Mach wave radiation exists. However, as clarified most recently by Veltin, Day, and McLaughlin [19-21], measurements and theoretical predictions from a number of sources show that often the convection velocity spectra contain subsonically travelling waves at low frequencies and supersonic traveling turbulence at high frequencies. Thus the process of noise generation of moderately heated, supersonic jets can include quite complicated processes.

The empirical similarity spectra proposed by Tam *et al.* [22] further emphasizes the noise generation mechanisms of the large turbulent structure noise as it is distinguished from the fine scale turbulence noise. This study of the similarity spectra was empirically concluded from the

experimental data of Seiner at the NASA Langley Research Center. As shown in Figure **1-3**, two spectra are individually responsible for the noise generation of the large turbulent structure and fine scale turbulence. The proposed spectrum dominated by the large turbulent structure noise at jet downstream axis has a sharp peak and drops off linearly at high and low frequencies. The spectrum dominated by the fine scale turbulence at jet sideline direction has a broad peak and gradually rolls off in both end of spectrum. These empirical similarity spectra can be fitted with reasonable accuracy to any measured spectrum in the jet downstream observation angle particularly in the absence of the broadband shock-associated noise.

As the fine scale turbulence is approximately isotropic in the flow field, the fine scale turbulence noise should be present in all observation angles. However, based on the characteristics of noise radiation simultaneously generated by the large turbulent structure and the fine scale turbulence, it is summarized that the fine scale turbulence noise dominates the jet upstream and sideline direction and the large turbulence structure noise dominates the jet downstream direction. While the measured spectrum at a given observation angle is not mainly dominated by either the large turbulent structure noise or the fine scale turbulence noise, there is a weighting factor for each of the similarity spectra. The combination of two similarity spectra then represents the spectrum at that observation angle. Tam and Zaman [23] follow up to present that the similarity spectra can also match well the spectra from measurements conducted with the non-axisymmetric and tabbed nozzles. It is noted that the model of noise from large scale and fine scale turbulent structures is strictly only applicable to supersonic jets operating at perfectly balanced (shock free) conditions.

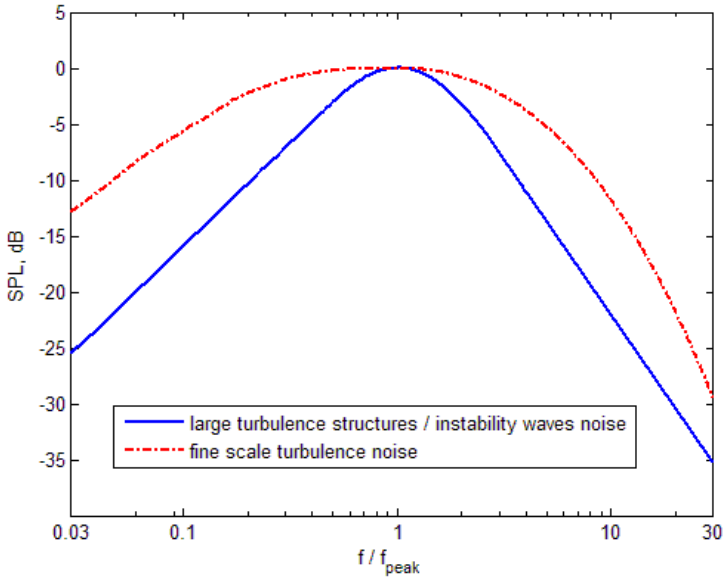

Figure **1-3**: Similarity spectra for the two components of turbulent mixing noise.

1.2.2.2 Shock associated noise

Supersonic jets operating at an off-design pressure ratio contain a standing shock wave pattern. Shock-associated noise is composed of discrete tones (screech) and broadband shock-associated noise (BBSAN). The two different shock-associated noise components possess very distinct characteristics. These two shock-associated noise components can easily be identified in the acoustic spectra when the shock cell structure appears in the jet flow at supercritical pressure ratio conditions.

The broadband shock associated noise has a broadband frequency range with a well-defined peak frequency in the measured spectra. In the 1970s Harper-Bourne and Fisher [24] demonstrated a relationship between the sound intensity and the jet Mach number, $I \propto \beta^4$, where $\beta^2 = \left(M_j^2 - 1\right)$. They showed that the intensity of broadband shock-associated noise is

only a function of the operating pressure ratio and showed that the peak frequency can be estimated by

$$f_p = \frac{U_C}{L\left(1 - M_C \cos\theta\right)}, \qquad \textbf{1.2}$$

where U_c and M_c are the average values of the convective velocity and Mach number of the turbulence, L is the shock spacing proportional to β and the jet diameter D, and can be written as

$$L = K\beta D, \qquad \textbf{1.3}$$

where K is a constant. The peak frequency of broadband shock-associated noise decreases as the observation angle, θ, increases from the jet direction as shown in Figure **1-4** and Figure **1-5** with the jets operated at various conditions. This shows the broadband shock-associated noise has strong directional dependence. Figure **1-6** shows the measurements conducted with the nozzle operating at fully-expanded jet condition as a comparison to Figure **1-4** and Figure **1-5**. The broadband shock-associated noise emerges and becomes comparative to the turbulent mixing noise when the measurements performed with the nozzle operating at off-design jet Mach numbers. The noise source mechanism of broadband shock-associated noise is the interaction between the shock cell structures and the large turbulent structure convecting downstream in the jet mixing layer. In a larger observation angle, the broadband shock-associated noise dominates the noise radiation. This, therefore, leads to higher noise contributions in the jet upstream and sideline directions than in the jet downstream directions.

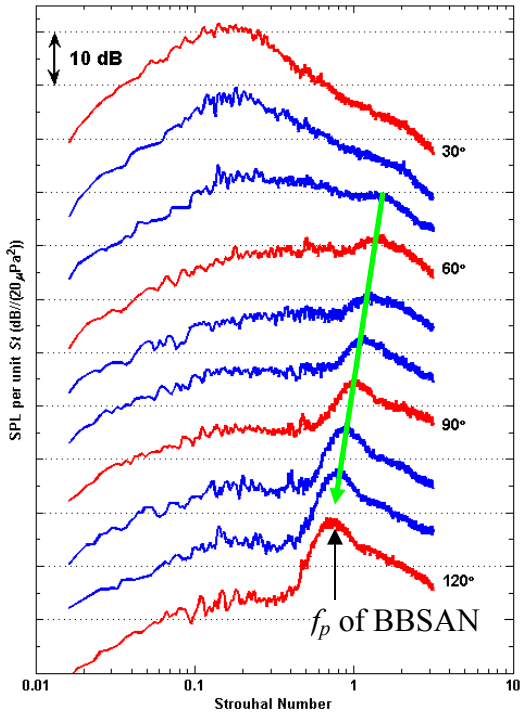

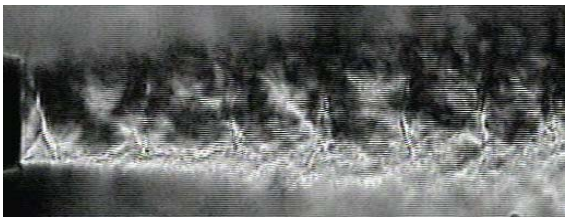

M_j = 1.3

Figure **1-4**: Spectra measured with the converging-diverging nozzle of M_d = 1.5 operated at M_j = 1.3, cold, accompanied with a schlieren image.

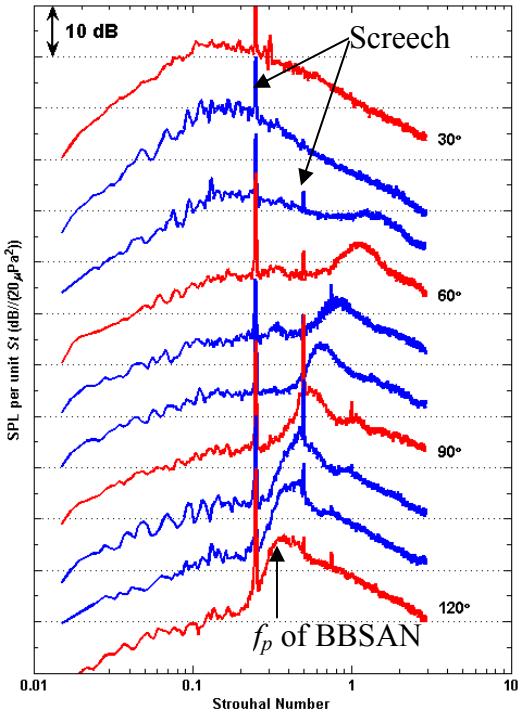

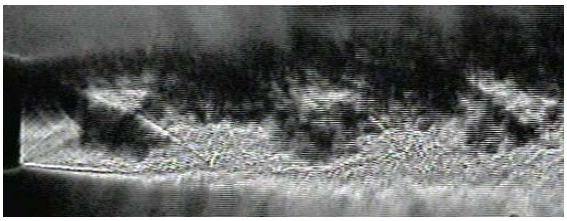

M_j = 1.7

Figure **1-5**: Spectra measured with the converging-diverging nozzle of M_d = 1.5 operated at M_j = 1.7 cold, accompanied with a schlieren image.

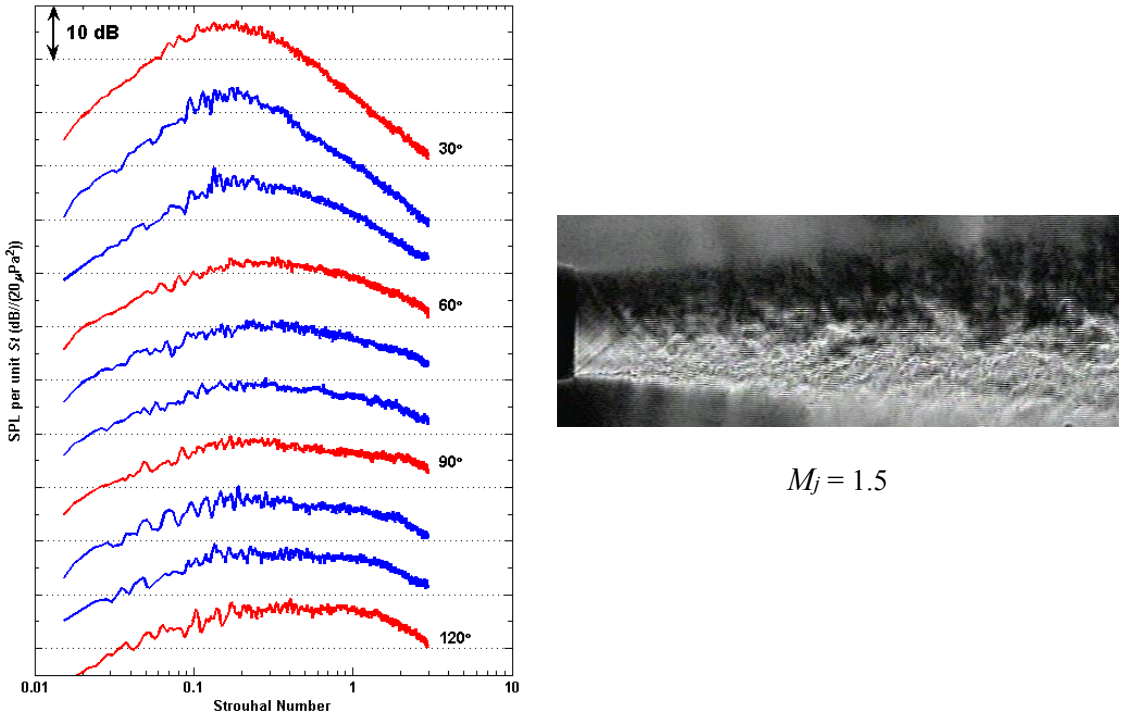

M_j = 1.5

Figure **1-6**: Spectra measured with the converging-diverging nozzle of M_d = 1.5 operated at M_j = 1.5, cold, accompanied with a schlieren image.

Readily apparent in the data of Figure **1-5** are screech tones that are discrete in the spectra with several harmonics. Powell [25] was first to observe this phenomenon and gave a solid explanation as follows. The acoustic waves radiated by the large scale instability waves downstream of jet flows can propagate back to the vicinity of nozzle lip and excite the jet mixing layer. As the excited jet flow grows in scale and convects downstream, again the acoustic waves are radiated upstream creating a feedback loop as shown in Figure **1-7**. Poldervaart *et al.* [26] presented a way to calculate the peak frequency of the screech tone with the photographic evidence of the feedback loop. Some studies [27] demonstrated a method of eliminating the screech tones by wrapping the nozzle exit surfaces with sound absorbing material or sticking a small projection in the nozzle lip. Although the peak frequency of broadband shock-associated noise has a dependence on observation angle, the peak frequency of screech tones is constant regardless of the observation angles. The fundamental screech tone is always lower than the peak

frequency of broadband shock-associated noise whose peak frequency will approach the fundamental screech tone as the observation angle increases, but won't be lower than the fundamental screech tone frequency. Due to this observation, Tam [28] proposed the relationship between the broadband shock-associated noise and the screech tones. From the experimental observation and numerical simulation comparison, he concluded that the screech tone is a special case of broadband shock-associated noise and the screech tone frequency can be determined by

$$\frac{fD_j}{U_j} \cong 0.67\left(M_j^2-1\right)^{-1/2}\left[1+0.7M_j\left(1+\frac{\gamma-1}{2}M_j^2\right)^{-1/2}\left[\frac{T_a}{T_j}\right]^{-1/2}\right]^{-1}, \qquad \textbf{1.4}$$

where T_a/T_j is the ratio of the ambient to the jet temperature. This semi-empirical equation agrees with experimental measurements.

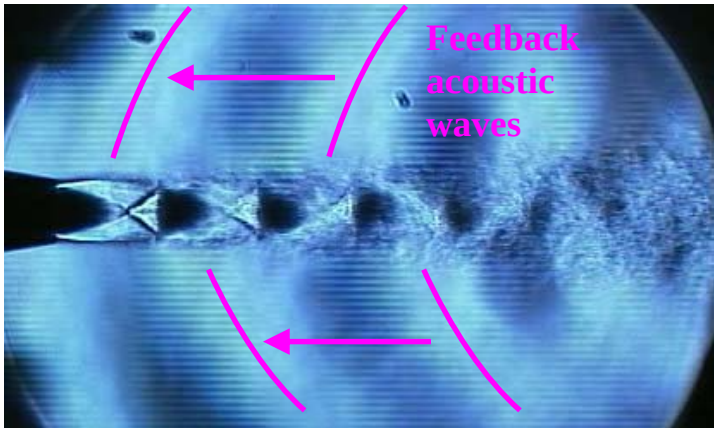

Figure **1-7**: Schlieren image conducted with a converging nozzle of $M_d = 1.0$ operated at $M_j = 1.5$ cold for the interpretation of the feedback loop of screech tones (taken at Penn State).

1.3 Full-scale experiments

Few public jet noise experimental tests have been conducted with the engine on a test stand or on a tied-down aircraft or with aircraft fly-over measurements. It requires huge amounts of resources and coordination to conduct full-scale experimental measurements. The experimental

data need careful treatment to provide reasonable results. Two main effects are involved in the fly-over measurements and ground testing: the effect of forward flight, and ground reflection effects.

1.3.1 Forward flight effect

From experimental observations, forward flight decreases the turbulent mixing noise within the frequency range at all observation angles and shifts the peak of shock associated noise to a lower frequency with a narrower broadband peak. An outer shear layer that originates from the vehicle boundary layer surrounds the jet exhaust plume causing the convection effect and noise source modification. The outer shear layer decreases the shear gradient and the spreading rate across the jet mixing layer such that the refraction angle is different from the static environment. The radiated sound waves are forced to propagate through a moving medium to the observation location. Due to the isotropy of fine scale turbulence, the spectra at the same observation angle only differ in the sound intensity level. However, the directional shock-associated noise lowers the peak frequency as the forward flight velocity increases. This external flow surrounding the jet exhaust plume also alters the shock cell spacing and the potential core length. These changes affect the noise source emission of shock-associated noise and the overall noise emission directivity.

1.3.2 Ground reflection effect

Tie-down jet engine tests always suffer from ground reflection. The intensity of reflected sound waves is related to the ground impedance and the reflection path. This ground reflection effect is simplified by using the concept of local reaction in the reflection location. A single

reflection path is approximated in a model of the effect of ground reflection. When the length difference between the wave propagation path and reflection path is the half wavelength of the propagation wave, cancellation of acoustic waves at the observation point occurs. The first cancellation frequency induced by ground reflection is known [29] by

$$f = \frac{r * a}{4 * h * z}, \qquad \textbf{1.5}$$

where r is the distance between measured microphone and noise source, and h and z is the height of noise source and microphone accordingly. This can be referred to as the frequency of negative reinforcement (FNR). The simplest assumption for the ground is rigid with direct reflection. Albeit numerical calculation methods have been developed to cancel out the ground reflection, it is not possible to eliminate the ground reflections that also vary with different operating conditions and different observation positions.

1.4 Model scale experiments

To avoid contamination and complication, model scale experiments are usually conducted in an anechoic chamber. An anechoic chamber is a room covered with sound absorbing material to simulate the free-field condition in sound propagation. The nozzle scale is usually built with a factor of 1/5 to 1/40 of the actual engine size depending on the capability of jet facility. The accuracy and discrepancy of experimental results conducted at various model-scale jets has been investigated [30], [31]. Several critical issues are raised and discussed below.

1.4.1 Nozzle scaling effect

The nozzle contour is the first issue for model scale experiments. In order to present similar experimental results across various model-scale jets, the test nozzles need to share a common physical geometry. It is critical to fabricate the identical nozzle inner geometry to generate similar flow conditions. Some studies [32-34] investigated the acoustic spectra from measurements conducted with various nozzle inner geometries, using conical, cubic, and contoured surfaces. It was found that the sound intensity levels are reasonably close, but not exactly identical when the nozzle contour is the only variable in the measurements.

The nozzle outer geometry was also studied by some researchers [35], [36]. The entrained flow around the nozzle body at the nozzle exit plane was affected slightly on the streamline plot and the relatively higher pressure variation was measured. However, the measured spectra presented negligible difference for the supersonic jets, except for the screech tone. Ponton and Seiner [37] conducted a series of measurements with nozzles possessing various lip thickness. The screech tone was found to be very sensitive to the nozzle lip thickness since this relates to the formation of the acoustic feedback loop.

For extending the measured data from model-scale jets to the prediction of full-scale exhaust jets, the similar nozzle geometry is the first requirement. Behind the similar nozzle geometry and operating condition, Reynolds number is another physical parameter in evaluating the flow condition under various sizes of jets. Several studies [38-40] showed that the measurements conducted with the low Reynolds number subsonic or supersonic jets (less than 100,000) still exhibit the comparative sound intensity level to the high Reynolds number jets to a reasonable level of accuracy. Moreover, Viswanathan [41] showed that there is an extra hump of noise contamination in the low frequency regime of spectra from the measurements that are conducted with the nozzle operating at subsonic hot jets possessing low Reynolds number. He,

therefore, concluded and suggested that the minimum Reynolds number of the jets is around 400,000 for obtaining accurate experimental results of the acoustic measurements.

1.4.2 Noise source distribution effect

As mentioned earlier in Figure **1-2**, the noise source of jets widely distributed along the jets downstream and the dominant noise source is located around the end of the potential core. For subsonic jets, the length of the potential core is roughly four times the nozzle diameter. For supersonic jets, the length of the potential core can extend to eight diameters or more [8]. Moreover, the distribution range of the noise source of supersonic jets is wider than the subsonic jets. It is clear that the jet noise source should not be treated as a compact noise source radiated from the representative location. However, Zaman [42] suggested that the reasonable results of the subsonic jet measurements still can be reached without the noise source locations correction. This statement is not quite true for supersonic hot jet measurements.

To avoid the noise source distribution effect, the measuring microphones should be placed at the far-field. The term of far-field is used to describe the noise source radiating spherically from its origin. Due to the broadband characteristics of jet noise, the noise emission locations are widely distributed along the jet downstream axis according to the noise frequency. While the noise directivity is related to the dominant noise source, there is no absolute threshold value of the far-field. Papamoschou and Debiasi [43] presented experimental results as a function of radial distances and observed polar angles for the threshold of the acoustic far-field. Koch *et al.* [44] showed similar observations for the noise source issued from the jets to be efficiently far-field for the acoustic measurements. Viswanathan [45] suggested the value of 35 to 50 nozzle diameters to be the sufficient radial distance for the noise of unheated subsonic jet radiating

spherically to sideline direction. The current study will contribute to a re-evaluation of these previous criteria.

1.5 Noise reduction mechanisms

From early efforts with one tab (a delta tab) attached in the nozzle exit, these experiments reported the noise level is reduced due to the additional vortex generated by the tabs. Nowadays the most promising noise reduction mechanism is the chevron nozzle. It is easily installed without significant weight or drag penalties.

When the jet plumes exhaust from the nozzle exit and flow through the array of chevrons, there are streamwise vortices generated on the upper surface of the chevrons. The pressure imbalance in the different sides of the chevrons affects the near-field flow generation and the far-field noise. From the experimental observations, two streamwise vortices are generated in the trough of the notch as shown in Figure **1-8**. This is the physical phenomena of the induced flow field due to chevrons attached in the nozzle exit plane. As the number of chevrons increase, the flow field has more alterations. An example is shown in Figure **1-9** with different numbers of chevrons. This streamwise vortex increases the jet mixing in the initial jet shear layer and improves the jet entrainments. As the jet mixing increases, the improved jet mixing rapidly transports flow momentum from the core high speed jet to the entrained ambient low speed flow. The improved jet mixing causes several effects. First, the convective velocity of the downstream large turbulent structures decreases and these contribute to the noise reduction in the low frequency regime. Secondly, the improved jet mixing in the jet shear layer generates more fine scale turbulence, and these cause excess high frequency noise. Third, the modification of the length of the jet potential core and the shock cell structures alters the interactions between the large turbulent structures and the shock cells causing the magnitude changes and the shift of the

peak frequency of the broadband shock-associated noise. These effects modify the spectra observed in the far-field. However, while the sound waves propagate to the far-field, the atmospheric attenuation absorbs some parts of high frequency noise and some reports suggest that by adequately selecting the number of chevrons the acoustic penalty from the high frequency noise can be practically reduced. Since the turbulent mixing noise can be substantially reduced due to chevrons, some commercial aircraft are already flying with them. For the shock-associated noise, the nozzle with chevrons can cause a change in the peak frequency of the broadband shock-associated noise.

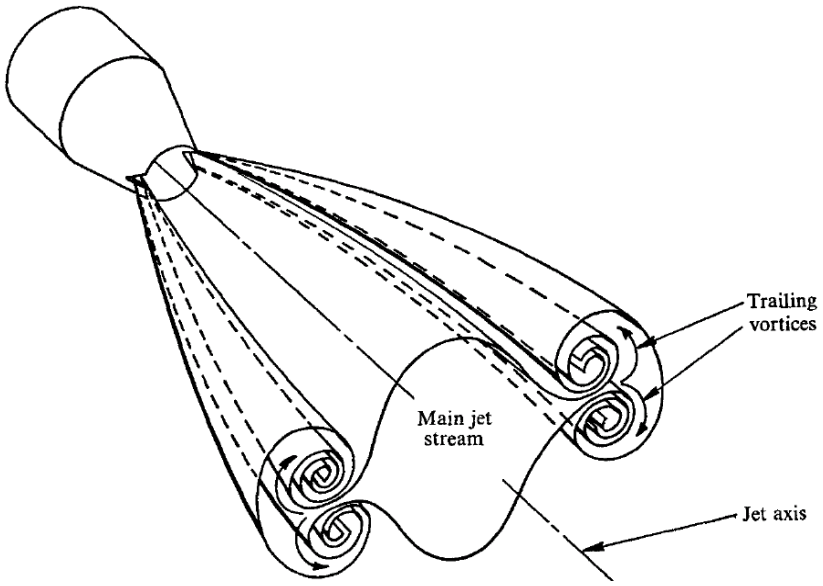

Figure **1-8**: Streamwise vortices generated in the trough of the notch. From Pannu and Johannesen [46].

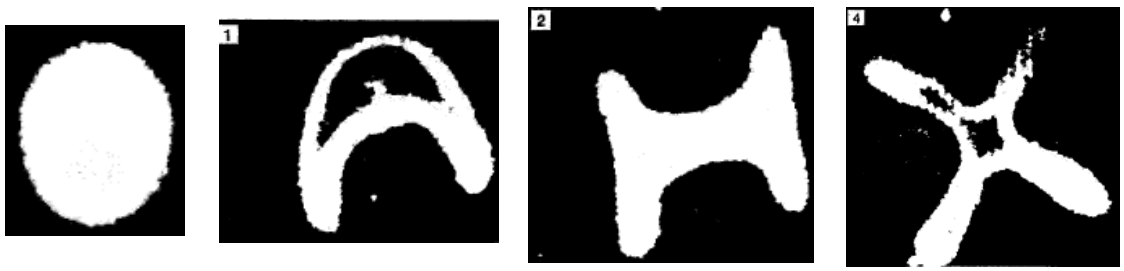

No chevron One chevron Two chevrons Four chevrons

Figure **1-9**: Photograph of the jet cross section at $x/D = 2$ conducted with nozzle possessing various counts of chevrons, operated at $M_j = 1.63$. From Zaman *et al.* [47].

The penetration angle of chevrons relates to the strength of the induced streamwise vortices. However these induced streamwise vortices not only cause the low frequency noise reduction but also amplify excess high frequency noise. The tradeoff between low and high frequency noise depends on the degree of the penetration angle of chevrons. To optimize the noise reduction, proper matching of the chevron geometry is needed for specific nozzle operating conditions. Bridges and Brown [48] have conducted a series of acoustic measurements with the parametric study of the length, width, penetration, and number of chevrons applied with a purely converging nozzle.

1.6 Scope of thesis

1.6.1 Research objectives

The goals of this thesis are to:

- Perform extensive acoustic measurements with several supersonic nozzles operating at various pressure and simulated temperature ratios to create a data base with which to develop improved understanding of supersonic jet noise relevant to military (fighter) aircraft.
- Through extensive comparison with moderate-scale (NASA) supersonic jet acoustic measurements, develop a methodology for using small-scale data, supported by computations, to reliably predict the noise at moderate-scale. (Ultimately this will be used to carry the predictions to full-scale engine noise.)

- Investigate the ability of newly developed scaling methodology to accurately predict the ability of chevron nozzles to accomplish noise reduction in a series of representative chevron designs and jet operating conditions.

The accuracy and capability of the high speed jet facility at Penn State was validated first. The NASA Glenn Research Center provided the related experimental results for these validations and supported the following experiments with comparative moderate-scale jets. An extensive database of small-scale models of acoustic far-field measurements with various baseline nozzles was collected at Penn State. All these experimental data contributed to the equivalent noise emission assessment on the scaling of the small-scale heat-simulated jets to the moderate-scale heated jets. A study of the characteristics of the jet noise source distribution strengthens the experimental accuracy on the scaling of the noise measurements acquired at disparate facilities. It also provides a fundamental understanding of military engine noise source mechanisms. The noise reduction concept was then assessed with chevrons attaching in the nozzle exit plane. The chevron configurations are provided by GE Aviation and NASA Glenn Research Center. The efficiency of the noise reduction devices installed in the small-scale model jets was examined. The noise reduction mechanisms were investigated as well. The capability of forward flight simulation was developed at Penn State providing a database of the above experiments in simulating the forward flight condition of airplane take-off and landing.

To develop the scaling methodology, a series of experiments were simultaneously conducted at NASA with moderate-scale models and PSU with small-scale models. The experimental program conducted at PSU is summarized below.

A. Baseline round nozzle experiments

A baseline round nozzle with three area ratios and internal contours conforming to the GE F414 family of military aircraft engines was supplied by GE Aviation. The experiments replicate the

same operating conditions of the moderate-scale measurements conducted at NASA. The scaling methodology compares the experimental results from the measurements individually conducted at small and moderate-scale jet facilities and assesses the noise intensity level to be independent of the jet plume sizes. In order to accomplish this goal, two major objectives were undertaken to obtain the appropriate accuracy of data.

- Measurements on accuracy improvement of 1/8 in. microphone

The accuracy on the high frequency response of 1/8 in. microphone was examined from the measurements with the microphone capped with the protective grid and oriented at grazing incidence. The data processing methodology was then examined in detail. This activity developed new microphone free-field response corrections for use in data processing.

- Near-field / Far-field acoustic measurements

A series of acoustic measurements were conducted to first evaluate the impact of the measured microphone locations at the same polar angle originating from the nozzle exit plane. An empirical approximation of the noise source distribution concluded from the phased array microphone measurements (performed by previous researchers) was used. A methodology was developed to interpret the discrepancy observed on the near-field / far-field acoustic measurements in terms of the true geometric far-field.

B. Baseline round nozzle with chevrons experiments

These experiments were undertaken with several various chevron designs supplied by GE Aviation and NASA Glenn Research Center. These experiments performed an assessment of the noise reduction devices with small-scale superonic jets. The efficiency of the noise reduction levels of chevrons was evaluated under various operating jet conditions. Direct comparisons were

made with data from experiments at NASA GRC using similar geometries and operating conditions.

C. Accompanying experiments

- Schlieren visualization experiments

The schlieren flow visualizations were undertaken with various chevron configurations and flow conditions to provide an extensive database of schlieren flow visualization and enable the validation of the location of the shock cells. The schlieren photographs reveal the flow-field modifications with the changes of the jet operating conditions.

- Pitot probe experiments

Pitot probe measurements were conducted to assist in the noise reduction assessment of chevrons in supersonic jets. The flow-field modifications, physically caused by chevrons, were documented with radial and axial distributions. The statistics of these flow-field modifications were examined and correlated with the chevron configurations and jet operation conditions. These sets of measurements accompanying the schlieren visualization are used to interpret the effect of chevrons on the noise reduction mechanisms.

- Combined forward flight experiments

The simulated forward flight condition was included in the above experiments to provide an extensive database of various nozzle configurations, jet flow conditions, and forward flight conditions. The experimental data of small-scale jets in forward flight further advance the experimental feasilibity of small-scale model jets.

1.6.2 Thesis synopsis

This thesis is to validate the data obtained from small-scale experiments which exhibits the independence of the jet sizes to the measured noise levels.

The remainder of this thesis consecutively presents related experiments, results, and discussions conducted in the high speed jet facility at Penn State. Chapter 2 provides the necessary descriptions of the high speed jet facility at Penn State. Chapter 3 provides the data processing steps and description of each experiment setup. The procedure of the acoustic near/far-field measurements conducted with both cold and heat simulated jets are introduced. The technique of schlieren visualizations is presented.

Chapter 4 presents the acoustic measurements of the small and moderate-scale jets in validating the scaling methodology. The related issues in successfully performing this scaling methodology are discussed. Chapter 5 shows the preliminary investigations on the effect of jet noise source distribution critical to the highly heated supersonic jets. Chapter 6 discusses the capability of model scale measurements involving advanced acoustic assessment on small-scale nozzle with chevrons. The effect of the empennage on sound scattering for model-scale measurements is demonstrated. The effect of forward flight is also examined. These extensive measurements substantially exhibit the capability and evaluate the contribution of small-scale supersonic jets. Finally Chapter 7 provides the conclusions drawn from these experimental results and gives recommendations for future work. In the end Appendix A presents the facility validation of the acoustic measurements with the small-scale supersonic jets. The capability and accuracy of the 1/8 in. microphone used in the small-scale jets are substantially improved by the current proposed method.

Chapter 2

Experimental Facilities

2.1 Facility overview

The experiments presented in this thesis were conducted in The Pennsylvania State University high-speed small-scale jet noise facility as shown in Figure **2-1**. This facility is located in Room 30 and Room 26 in the basement of the Hammond Building. Entrance to the main working area of this facility is in Room 30. Major experiments are conducted in an anechoic chamber manufactured by Eckel Industries Inc. in 1968. It was renovated into the current jet noise facility during 1999. The anechoic chamber is a 16.47 X 19.82 X 9.15 ft (5.02 X 6.04 X 2.79 m) room covered with fiberglass wedges and with an approximate cut-off frequency of 250 Hz. A thermometer, barometer, and hygrometer are screwed on a wooden board set next to the forward flight duct facing the entrance of the anechoic chamber to monitor the temperature,

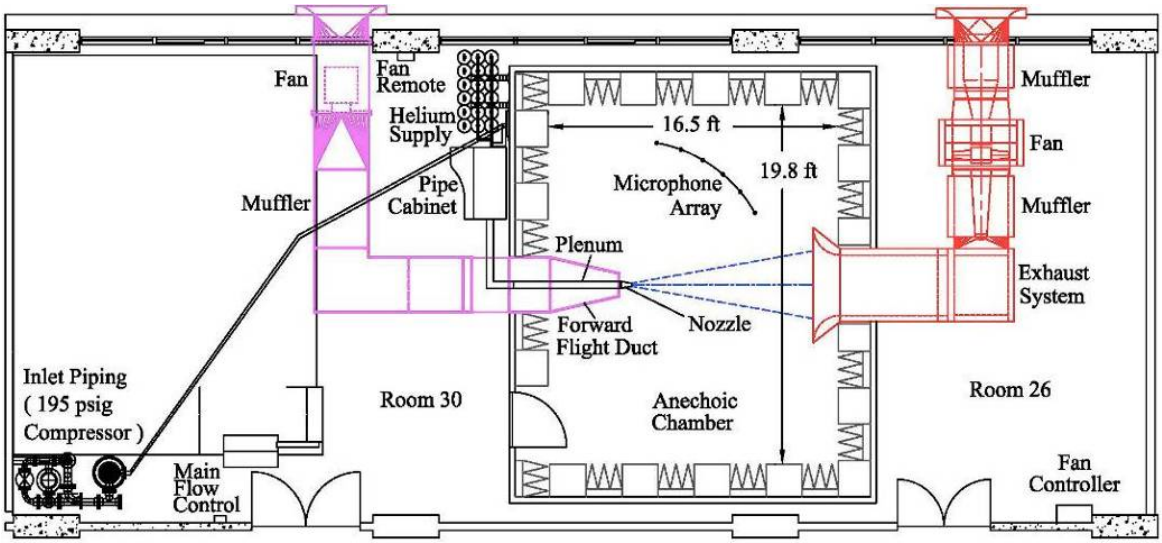

Figure **2-1**: The Pennsylvania State University high speed jet noise facility.

pressure, and relative humidity as the ambient reference condition inside the chamber for each experiment. An exhaust fan, installed in the downstream direction of the plenum, collects the jet exhaust and minimizes air circulation and possible local helium accumulation in the anechoic chamber. An inlet fan installed with a square duct surrounding the plenum draws air into the chamber to simulate the forward flight condition for testing the nozzle.

2.2 Microphone array

There is a microphone array hanging from a boom that extends from the plenum stand located in the chamber, as can be seen in Figure **2-2**. The microphone array can only rotate physically between the jet centerline to the corner away from the door of the chamber around a point located at the center of the nozzle exit plane. Six 1/8 in. microphones are usually positioned at a grazing incidence horizontal to the jet centerline plane and equally spaced by 10 degrees on the microphone array. The physical distance from each microphone to the nozzle exit is around 70 in. (180 cm). This distance is sufficient to ensure the microphones are in the far-field when testing nozzles up to 0.7 in. (1.8 cm) in diameter. Microphones also can be set on any ground spot inside the chamber by floor stand to support specific experimental needs as shown in Figure **2-2**.

Figure **2-2**: Microphone array in The Pennsylvania State University high speed jet noise facility.

2.3 High-pressure air supply system

High-pressure air is drawn from a tank with a capacity of 2000 ft^3 (56.6 m^3), pressurized by a *CS-121* compressor located in the subbasement of the Hammond Building. The air supply is first filtered by a *KAD-370* air dryer coming out of the compressor. Both the compressor and air dryer were manufactured by *Kaeser Compressors*. The air supply pipe comes into the door side corner of Room 30 and the main flow control of it is a pneumatic valve located next to the entrance of Room 30 as shown in Figure **2-1**. This pneumatic valve mainly controls the flow into the pipe across the ceiling of Room 30 to the air inlet of the pipe cabinet. The pipe cabinet is composed of two inlet pipes transmitting different air supplies (one for pure air and one for helium) and one outlet pipe with the capability of He-air mixture jets. Figure **2-3** shows the schematic of these piping systems (flow direction is from left to right) where top blue arrow represents air supply and bottom red arrow represents helium supply. The pipe cabinet with this control panel shown in Figure **2-3** is designed for easy control of the flow incorporating a series of solenoid valves, pressure regulators, gate valves, and ball valves.

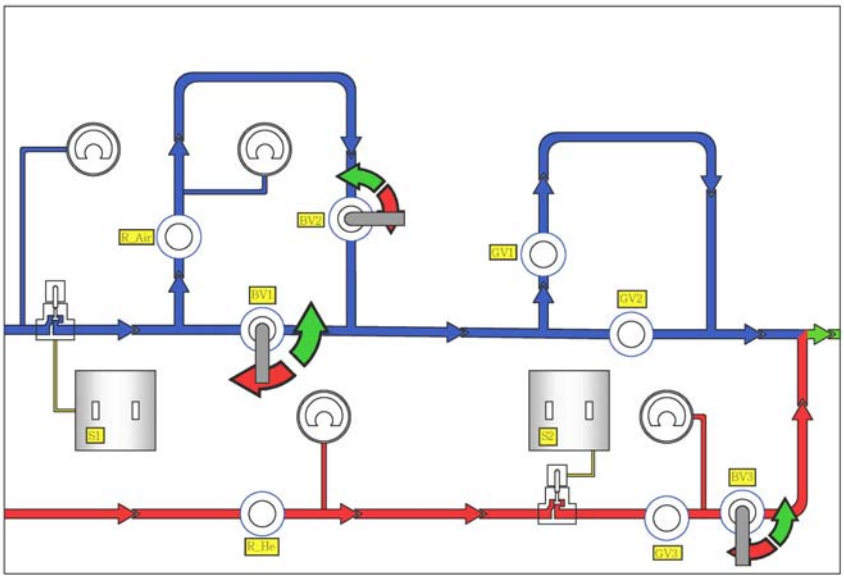

Figure **2-3**: Schematic of the control panel of pipe cabinet with helium-air mixture capability.

The helium supply is provided directly by helium bottles supplied by the general stores at Penn State. These helium bottles can provide high-pressure helium initially at 2000 psig (13.8 MPa). Up to six bottles can simultaneously provide helium into the helium inlet of the pipe cabinet. This helium-air mixture capability provides the heat simulated jets to simulate the aeroacoustics issuing from the actual heated jets. This system was developed by Doty and McLaughlin [49] over 10 years ago and has been refined since that time. A Fortran code *Helium.f90* developed by Doty [50] calculates each partial flow pressure of air and helium for specific operating condition. A detailed description of the helium-air mixture calculation is discussed in section **3.1.2**.

The pure air flow or helium-air mixture flow comes out of the pipe cabinet, and the outlet pipe is connected to the plenum made of aluminum pipe with a 4.5 in. (11.4 cm) inner diameter and 6 foot (1.83 m) length. The turbulence treatment inside this 6 foot long pipe includes a conical perforated plate of 5 in. in length facing upstream and a honeycomb plate of 3 in. in length. These turbulence treatment devices are located in a 19 in. long section at the inlet of the plenum. It was installed to reduce the turbulence intensity level and enhance the helium-air mixing before flow delivering to downstream nozzle.

Inside the plenum, there is a temperature probe and pitot probe accordingly installed on the bottom half 3 in. and 2 in. respectively upstream of the end of the plenum. This pitot probe is fed into a pressure transducer located next to the instruments monitoring ambient conditions inside chamber. The pressure transducer is regularly calibrated and documented. The output of the pressure transducer is connected to a voltmeter standing on the desk next to the pipe cabinet. The reading of voltmeter represents the nozzle pressure ratio or jet Mach number for specific nozzles mounted on the plenum end operating at specific jet conditions. Experiments proceed by controlling each valve in the control panel of the pipe cabinet to a specific partial pressure

established in advance of the experiment. The detailed operational procedure to set these pressure values to reach the specific jet conditions is discussed in section **3.1.3**.

The current capability of the air compressor can blow pure air through a 0.7 in. or 1 in. nozzle operating at M_j = 1.5 for continuous 50 and 7 minutes respectively under stable flow conditions. The maximum jet Mach number of the current facility is M_{jmax} = 2.3 and 1.7 conducted with the 0.5 in. or 1 in. exit diameter nozzles respectively for completing one time acquisition of acoustic measurements.

2.4 Nozzle description

A series of nozzles are involved in the measurements presented in this thesis. They are presented accordingly in the following figures with corresponding dimensions.

Two steel nozzles with 0.5 in. in nozzle exit diameter possessing physically identical outer geometries were designed with contoured inner nozzle surfaces: one is a purely converging nozzle; the other is a converging-diverging (CD) nozzle with an area ratio AR = 1.18 producing a nominal Mach number of 1.5 as shown in Figure **2-4**.

Two conical converging nozzles with 1 in. nozzle exit diameter were designed with chevrons as shown in Figure **2-5**. This series of convergent nozzles were used for preliminary study on noise reduction mechanism generated from chevron nozzles.

Three ‘baseline’ CD nozzles fabricated by the rapid prototyping technique with the original designs provided by General Electric are shown in Figure **2-6**. They share identical outer nozzle geometry and only differ in the area ratio of the nozzle divergent section. A three-dimensional schematic is shown accompanying a photograph viewing the nozzle upstream. These GE baseline nozzles replicate military style nozzles representative of the exhaust of aircraft engines from the GE F414 family. The exact inner contours are the property of General Electric

and were provided under a contract for the Strategic Environmental Research and Development Program (SERDP). While such military engines possess nozzles with variable geometry, adapting to different flight regimes, for this specific research, three nozzles with different exit-to-throat

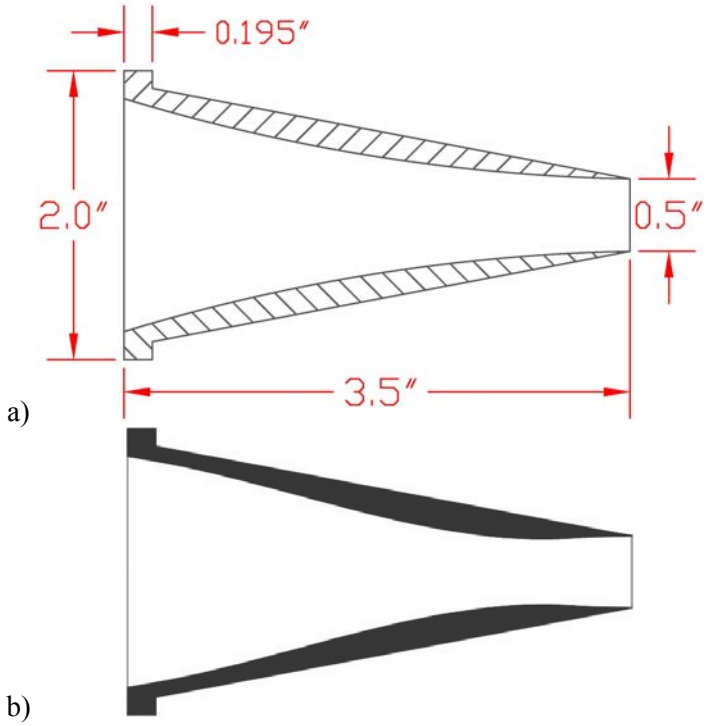

Figure **2-4**: Steel nozzles with 0.5 inch in nozzle exit diameter possessing physically identical outer geometries. a) Converging nozzle. b) Converging-diverging nozzle with nominal Mach number of 1.5 (AR = 1.18).

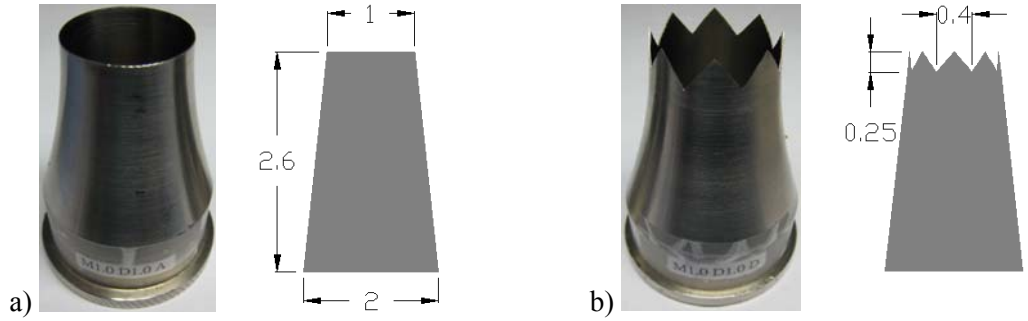

Figure **2-5**: Conical converging nozzles with 1 inch in nozzle exit diameter. a) Baseline nozzle. b) Chevron nozzle (8 chevrons).

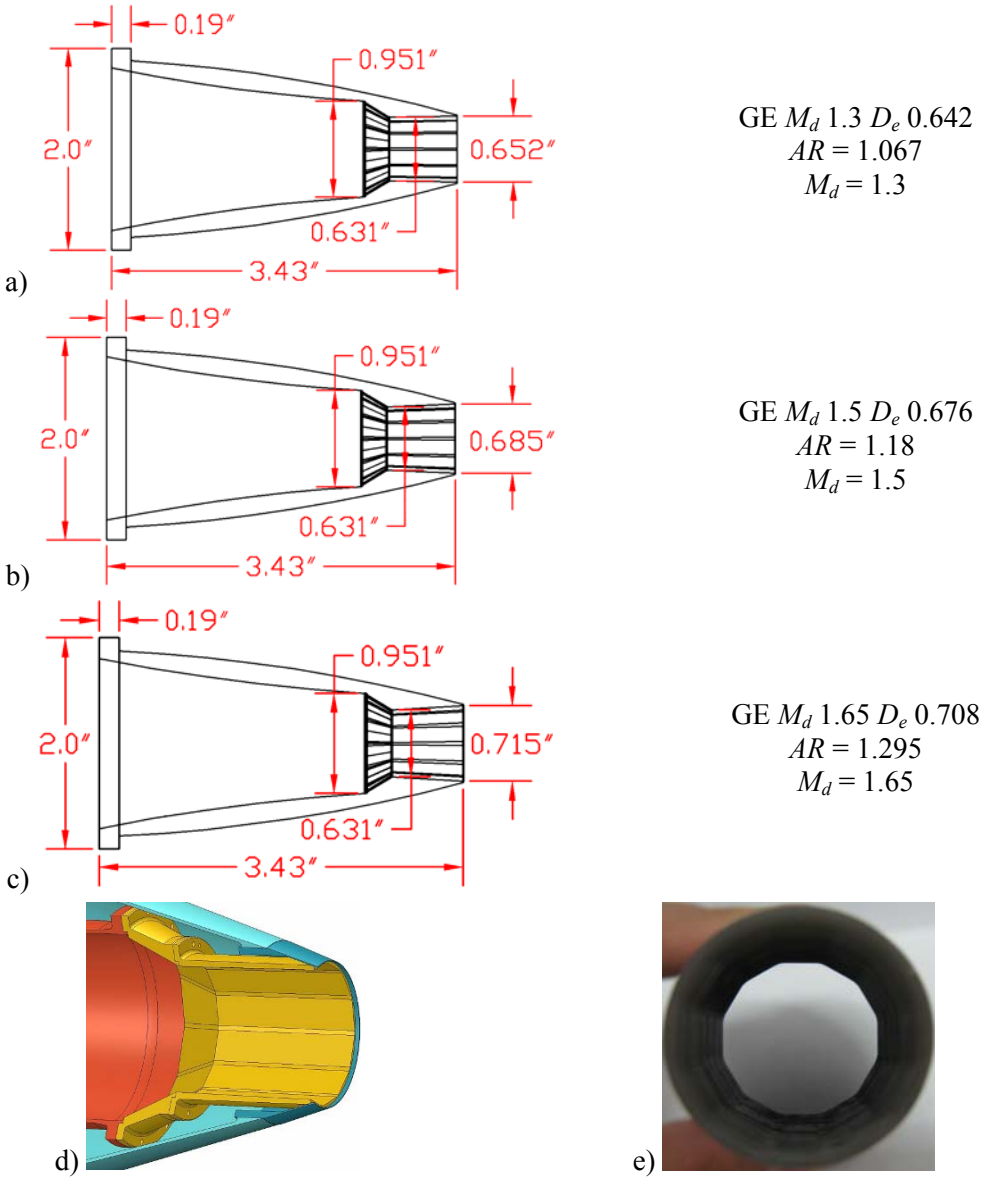

Figure **2-6**: GE baseline CD nozzles. a) M_d 1.3 nozzle. b) M_d 1.5 nozzle. c) M_d 1.65 nozzle. d) Three-dimensional schematic of nozzle. e) Nozzle upstream view.

area ratios were used, as specified by GE Aviation. These nozzles are designed with a multi-faceted inside conical contour. The design Mach number (M_d) is a convenient identifier used to show the Mach number that would result for perfectly expanded jet flow expanding through the design area ratio. At Penn State, the nozzles were fabricated using a rapid prototyping technique (stereolithography) and nozzles of similar inner geometry and larger scale nozzles (scaling factor 7.16) built by GE Aviation, were delivered to NASA for the medium scale experiments

conducted at the NASA Glenn Research Center [51]. In the current study, one of the goals is to examine the scaling methodology in extending the acoustic data measured with small scale supersonic model jets to practical aircraft exhaust jets. Therefore, a series of acoustic measurements were conducted with these GE baseline nozzles in performing the cross-scale comparison.

To further examine the noise reduction mechanism on military style supersonic nozzle, three chevron nozzles were fabricated respectively based on the designs from either GE Aviation or NASA Glenn Research Center. Following the parametric study of chevrons investigated by Henderson and Bridges [51], the chevron configuration is defined as shown in Figure **2-7**. The corresponding dimensions of the chevrons under study are listed in Table **2-1**. The width of the chevrons is as same as the width of each facet at the nozzle exit plane.

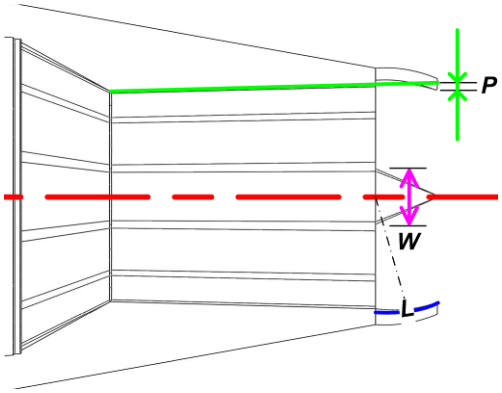

Figure **2-7**: Schematic of parameter definition on chevron configuration.

Table **2-1**: Defined parameters of chevrons on military-style chevron nozzles.

M_d	D (inch)	Chevron Counts	Penetration	Length	Width
1.5	0.676	12	0.04 D	0.16 D	0.2 D
			0.05 D	0.23 D	0.2 D
1.65	0.708		0.12 D	0.35 D	0.2 D

Figure **2-8** shows the plane view at the nozzle exit of GE baseline and chevron nozzles. These military-style nozzles contain nozzle geometry different from conventional axis-symmetric nozzles. A detailed examination of the acoustic measurements shows that there is no azimuthal sensitivity in the nozzle exit plane from both GE baseline and chevron nozzles. Figure **2-9** shows the result of comparing the measurements of the same chevron nozzle from two different tips and notch planes. (The tip and notch plane are defined in red and blue line in Figure **2-8**.) A good agreement is reached within 1 dB deviation. This demonstrates that there is no azimuthal sensitivity in the measurements conducted with the military-style nozzles.

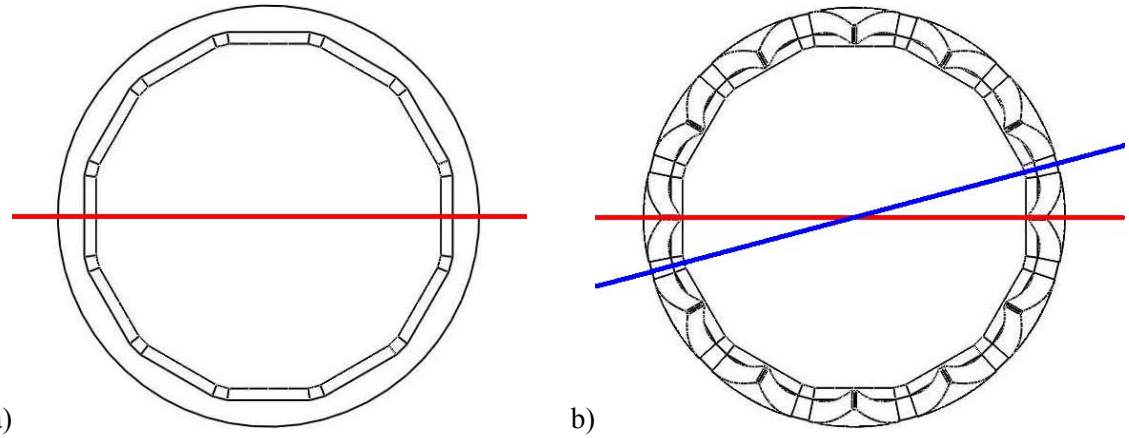

Figure **2-8**: Plane view at the nozzle exit. a) GE baseline nozzle. b) GE chevron nozzle where red line represents tip plane and blue line represents notch plane.

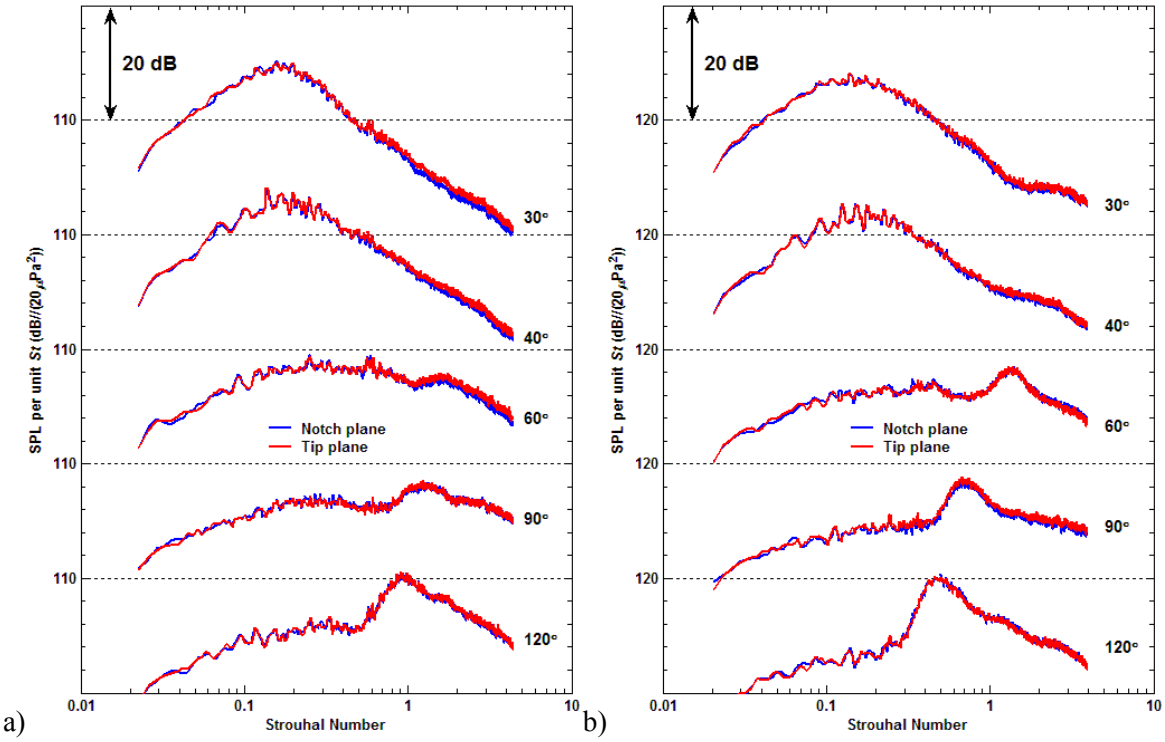

Figure **2-9**: Acoustic measurements conducted with GE chevron nozzle (M_d = 1.5, D = 0.676 in.) measuring accordingly at tip and notch plane. a) M_j = 1.22, TTR = 1. b) M_j = 1.64, TTR = 1.

2.5 Empennage model description

In order to make the small scale experiments conducted in the anechoic chamber more practical, a plastic aircraft model was built and used in the acoustic measurements to observe the impact due to the empennage model presence. The 1/48 scale F-35 JSF model was selected to generate reasonable physical geometric similarity between the aircraft model and nozzle exit diameter of the small scale GE nozzle. This single engine aircraft model was trimmed to fit the GE nozzles and upstream plenum adapter, and also meet the aerodynamic needs for the forward flight simulation. Figure **2-10** shows the empennage model where the aircraft tailplane extends around 2 times of GE nozzle diameter downstream from the nozzle exit plane and the distance between GE nozzle lip to the tail plane is around half nozzle exit diameter. The horizontal

projected blockage area percentage between the extended tail plane from nozzle exit plane and downstream jet plume column is about 35%.

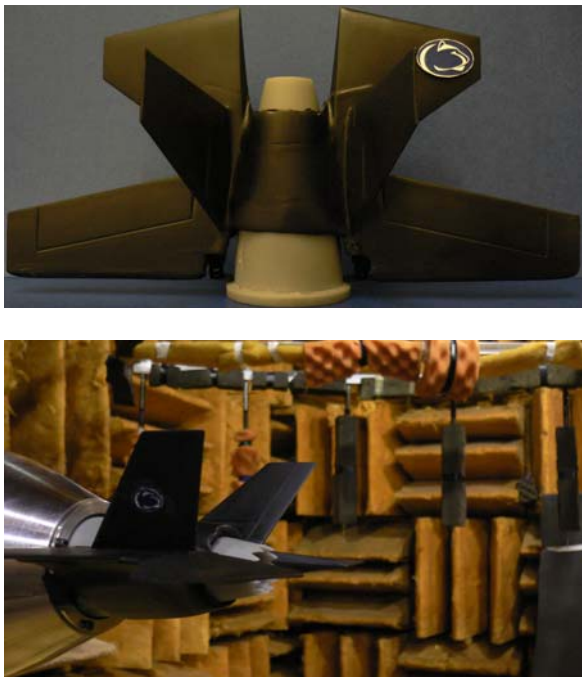

Figure **2-10**: 1/48 scale single engine aircraft model with GE military style CD nozzle.

2.6 Forward flight simulation

The forward flight simulation uses the inlet fan and exhaust fan as shown in Figure **2-1** to generate a co-flow surrounding the nozzle in order to simulate the ambient flow field conditions during aircraft flight (particularly take-off and landing). The inlet fan draws air from outside of the building passing through a muffler and an acoustically treated 36 inches square duct into the anechoic chamber. This fan is a *Twin City* Mixed Flow fan, model QSL 270. Inside the anechoic chamber the square duct then contracts to a 15 inches square duct, located around 12 inches from the exit plane of the testing nozzle (shown in Figure **2-11)**. The contracted square duct section has corner fillets in order to eliminate the generation of strong vortices from the upstream square

corner that could possibly contaminate the acoustic measurements and distort the mixing layer of the forward flight co-flow. The jet exhaust area ratio between the forward flight duct and the maximum nozzle diameter of 1 inch is around 250. In the jet direction, a large exhaust collector is connected to a *Buffalo* vane-axial exhaust fan, model 38A9, that draws the jet plume outside of the building. By simultaneously raising the fan speed to maximum on both fans the co-flow reaches a flow speed of 190 ft/s for forward flight simulation inside the anechoic chamber.

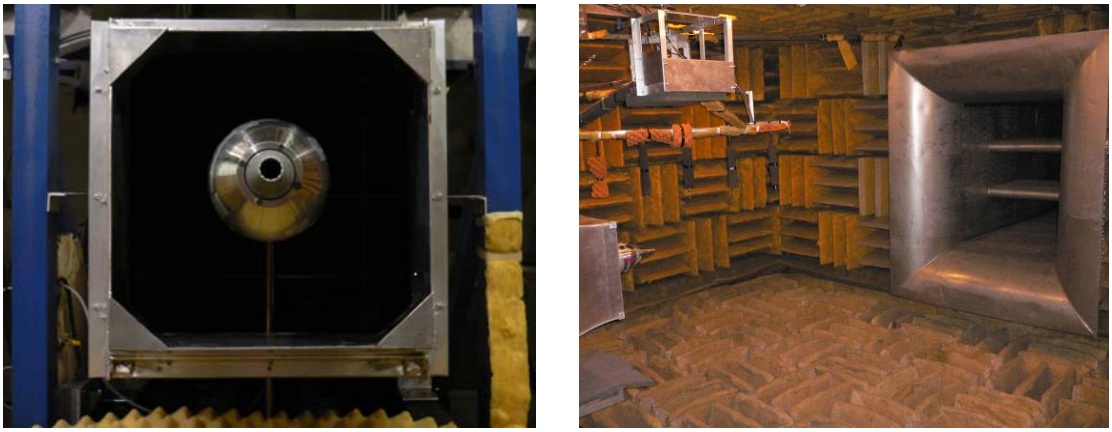

Figure **2-11**: Pictures of upstream 15 inches square duct and downstream exhaust collector for forward flight simulation of acoustic measurements inside the anechoic chamber at Penn State.

After reviewing the jet noise facilities, the Penn state has equipped sufficient capability to conduct high-quality jet noise measures. In the next chapter, a thorough description of the experimental setups and data processing procedures for acoustic measurement, Schlieren visualization, and pitot measurement will be introduced.

Chapter 3

Experimental Procedures

3.1 Acoustic measurements

3.1.1 Acoustic acquisition system setup for 1/8 in. microphone

A standard microphone boom (extending from a steel stand used to support the plenum) has the capability of supporting 6 microphones. The microphones used are 1/8 in. pressure-field microphones, type 4138 from *Brüel and Kjaer* (*B&K*), and type 40DP from *GRAS* with frequency response up to 140 kHz and an upper intensity level limit of 168 dB. Microphones are connected to the preamplifiers connected to the power supplies, a *Nexus*, *B&K* signal conditioner or a *GRAS* model 12AN power module where the output signals are amplified and filtered for anti-aliasing, thus enabling their accurate digital conversion in the following acquisition. The signals are then routed to a high-pass filter set to 500 Hz, removing any undesirable low frequency noise that could contaminate the data. Finally, cables carrying these signal all connect to a PCI-6123 *National Instruments* DAQ board. This DAQ board is capable of simultaneously acquiring 8 channels of time domain data that are then stored in binary files that are passed to the next stage for data processing and analysis. The microphone calibration constants are needed for conversion from recorded voltages to equivalent acoustic pressures. The microphone calibration is performed with a *B&K* acoustic calibrator, model 4231, possessing a sound pressure level of 94 dB at frequency of 1000 Hz. The values of microphone calibration constant are recorded for each microphone at each time of measurements and the uncertainties of the microphone calibration constant are within half decibel.

3.1.2 Heated jets simulation by Helium/Air mixture

In order to produce acoustic measurements that can be compared directly to aircraft engine exhaust measurements, the temperature of the jet is an important parameter that needs to be replicated. A heated jet results in different acoustical characteristics, due to the increase in jet exit velocity and decrease in jet density. Actually heating the air that exhausts through the nozzles is performed in facilities such as the one used at the NASA Glenn Research Center [52], [53] and the Boeing Low Speed Aeroacoustic Facility [45], [54]. However, it requires an extensive amount of power and infrastructure, raising the overall operating costs of the facility. In order to simulate the flow and acoustic properties of a hot jet, Kinize and McLaughlin [55] have demonstrated that the mixture of helium and air is able to capture the dominant noise characteristics of actual heated jets. Doty and McLaughlin [49] and Papamoschou [56] have shown that mixtures of helium and air can appropriately simulate the noise of heated jets to a reasonable accuracy. Recently, Miller and Veltin [57] showed a good agreement of the flow properties between the experimental data from helium-air mixture jets and numerical calculation of heated air jets. The features of heated jets are lowered density and increased acoustic velocity (for a given nozzle pressure ratio), and both of these features are achieved by helium-air mixture jets.

Hot air jets possess lower density and increased velocity compared to cold air jets. Both of these can be achieved by the addition of helium since it has a significantly lower density than air resulting in greater gas constant. This, for a given temperature and Mach number, results in a greater acoustic velocity. However, both parameters, the acoustic velocity a and the density ρ_j, can not be precisely matched simultaneously. Two different matching methods were introduced by Doty and McLaughlin [49] and only briefly described here.

The first methodology consists in matching the acoustic velocity between a helium-air mixture and a corresponding hot air jet.

$$a_{heated} = \sqrt{\gamma R_{gas} T_j} \quad \leftrightarrow \quad a_{mix} = \sqrt{\gamma_{mix} R_{gas\,mix} T_{j\,mix}} \tag{3.1}$$

γ_{mix} and R_{mix} are dependent on the helium concentration. The proper molar mass of helium can easily be calculated in order to equate a_{heated} and a_{mix}. From there, the partial pressure of helium and air can be computed and the pressure regulators can be adjusted based on these values in the experiment.

The second method consists of matching the density between a heated jet and a helium-air mixture jet, as shown below.

$$\left(\frac{\rho_j}{\rho_\infty}\right)_{heated} = \left(\frac{T_\infty}{T_j}\right)_{heated} \leftrightarrow \quad \frac{\rho_{j\,mix}}{\rho_\infty} = \frac{T_\infty R_{gas\,\infty}}{T_{j\,mix} R_{gas\,mix}} = \frac{R_{gas\,\infty}}{R_{gas\,mix}}\left[1 + \frac{\gamma_{mix} - 1}{2} M^2\right] \tag{3.2}$$

The molar mass of helium required to equate $\rho_{j\,mix}$ with ρ_j can be calculated, and from it the partial pressure of helium is once again derived. The two matching methods typically lead to slightly different values for the partial pressures of the mixture. However, previous experimental results [49], [56] have demonstrated that the two methods result in acoustic spectra in agreement within 1 dB. Figure **3-1** presents a comparison of spectra and *OASPL* polar plot from the helium-air mixture jets measurements respectively conducted with the method of density matching and acoustic velocity matching. It is shown that the discrepancy is within 1 dB across the frequency range in spectra and polar angle in the *OASPL* plot between the two matching methods. The acoustic velocity matching method is therefore selected as an operating standard for a consistent experimental methodology.

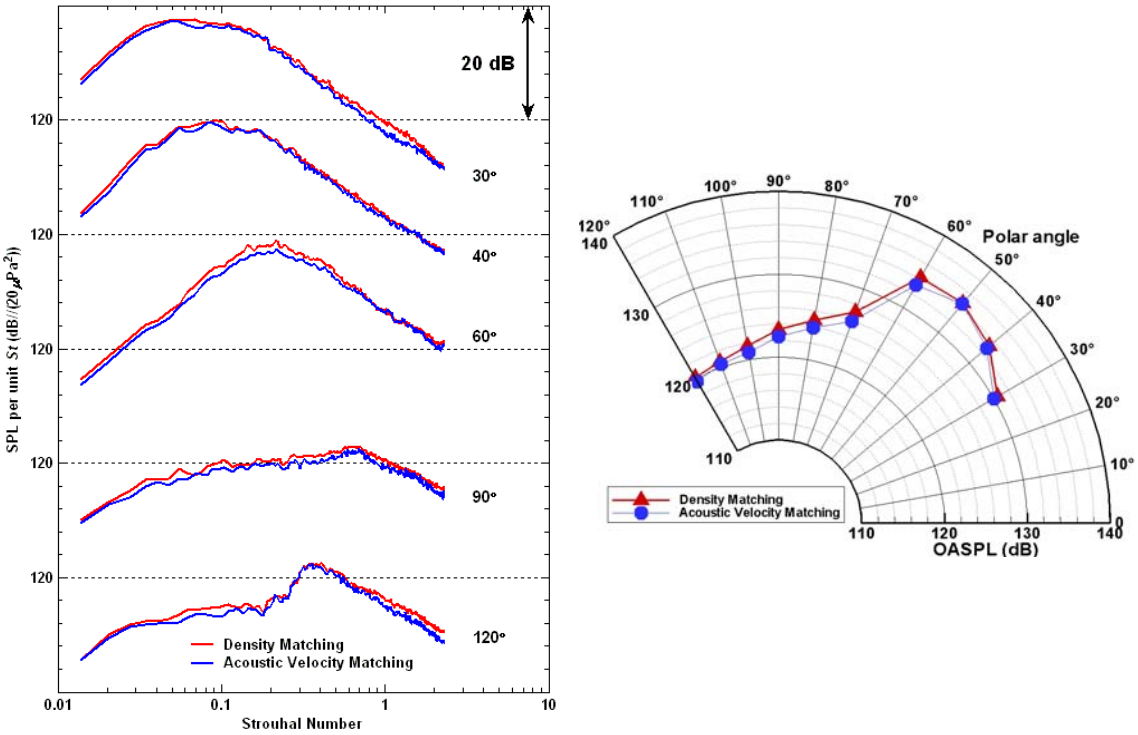

Figure **3-1**: Spectra and *OASPL* comparison from the helium-air mixture jets measurements respectively conducted by the method of density matching and acoustic velocity matching.

3.1.3 Description on pipe cabinet operation for specific jet condition

As mentioned in section **2.3**, there is a pipe cabinet between the compressor and plenum as the pressure regulator for specific jet condition exhausting from nozzle exit into the chamber. Figure **3-2** shows the front panel of this pipe cabinet. There are two main pipes inside this pipe cabinet: one is referred to as the blue line for air supply and the other is referred to as the red line for helium supply. These two pipes merge as one leaving the pipe cabinet into the downstream plenum. When there is no need for helium, the red line is totally shut off with the Ball Valve Control 3 fully closed. All control valves and regulators are fully closed at the beginning of the standard operational procedures. The reading on the Air Pressure Reading 1 represents the air pressure of the inlet pipe into the pipe cabinet. When the measurements are conducted with the 1

in. exit diameter nozzle, the flows go through the pipe with Ball Valve Control 1 fully open. Otherwise the flows pass through downstream with Ball Valve Control 2 fully open with finer flow control via the Air Pressure Regulator. The knobs of Gate Valve Control 1 and 2 downstream are used for flow volume control. After regulating these two valves to reach a stable state of a desired jet condition, one can trigger the code to complete the data acquisition for the cold jet acoustic measurements.

For the simulation of heated jets, helium is first fed into the pipe and the corresponding pressure reading is shown in Helium Pressure Reading with control by the He Pressure Regulator. Based on the calculation from section **3.1.2**, the pressure inside the plenum is first set to meet the desired partial value of pure air with the Ball Valve Control 2 fully open. The pressure reading in Air Pressure Reading 2 must be higher than the choking pressure at this specific operating condition to prevent Helium/Air mixture overflowing upstream. The desired partial value of helium is regulated by the He Pressure Regulator. Gate Valve Control 3 is then always maintained at fully open status while the Ball Valve Control 3 is fully open to release the helium. A LabView acquisition code in the meantime is set to automatically acquire the data with the targeted pressure range. After the data are automatically collected, Ball Valve Control 3 is quickly shut off. Then one time acquisition of heat simulated jets is completed. The acquisition of the results times from 0.7 second to 1.3 second varied by the amount of data points acquired.

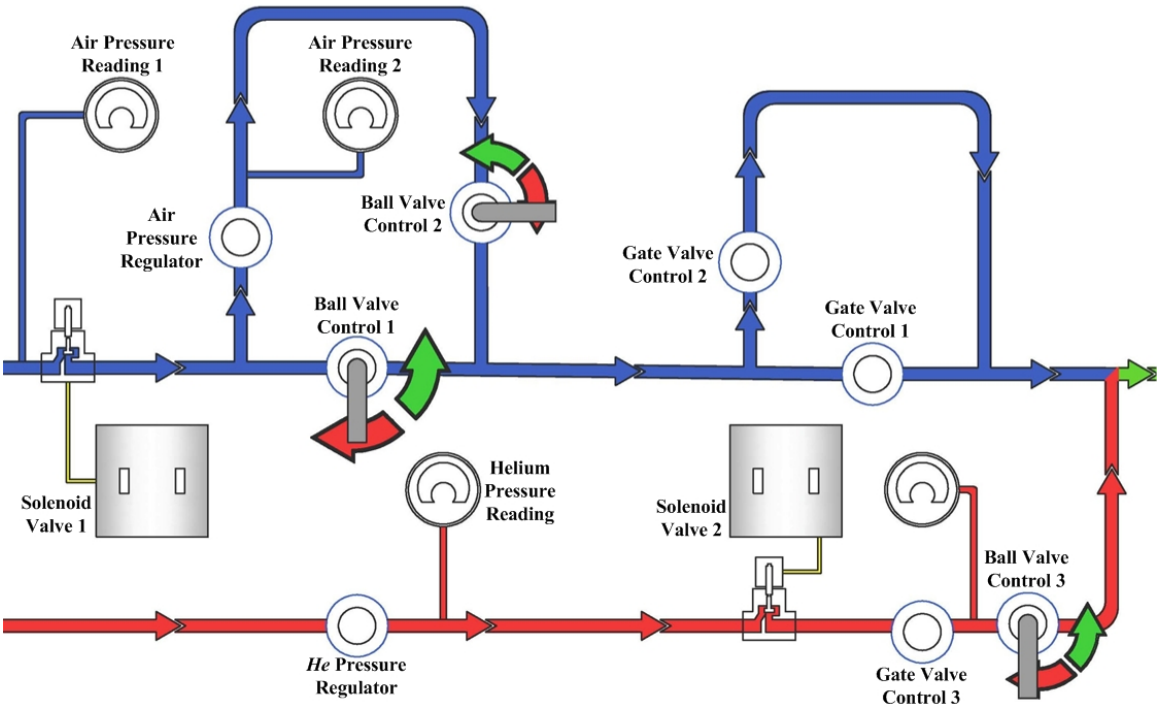

Figure **3-2**: Schematic of the control panel of pipe cabinet with the helium-air mixture capability.

3.1.4 Description of forward flight simulation

Inside the anechoic chamber there is a 15 inches square duct located around 12 inches upstream from the exit plane of testing nozzle as previously shown in Figure **2-9**. This square duct is used to provide a co-flow surrounding the jet exhaust plume to simulate the external flow at aircraft take-off and landing. A series of hot-wire and pitot probe measurements were conducted at various locations downstream from this square duct exit plane to investigate the co-flow condition. Figure **3-3** presents the experimental results individually with a pitot and hot-wire probes. The flow exits the duct with an average jet speed of around 190 ft/s. Figure **3-3** presents a velocity profile of the mixing layer around duct edge location in downstream measurement planes. Both measurements show consistent results of velocity profiles in cross-stream direction at each downstream measurement plane. The speed at the duct exit is therefore recorded as the reference

velocity for forward flight simulation and is also referred to as the simulated forward flight Mach number of 0.17.

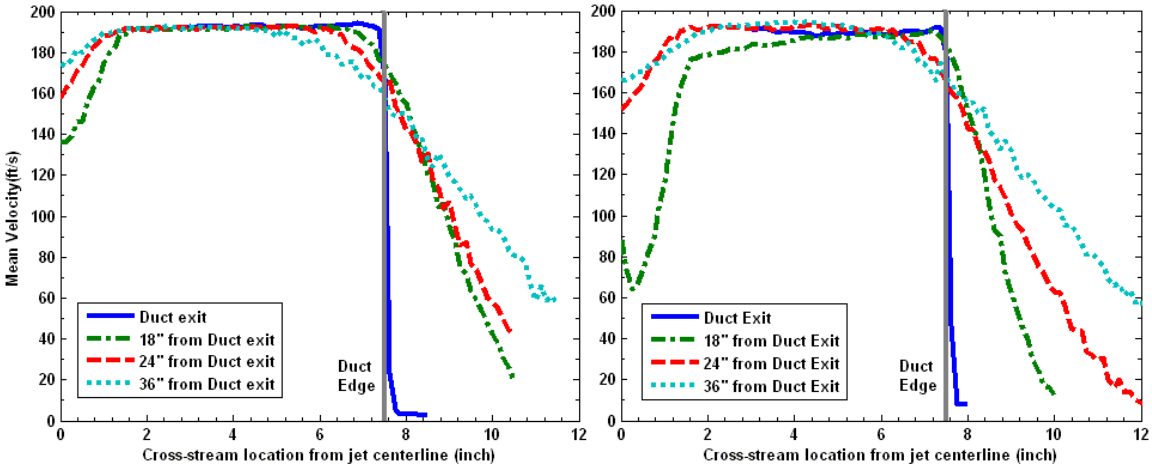

Figure **3-3**: Examination on flow condition exhausting from forward flight duct measured at various downstream locations via the pitot probe measurements (left figure), and the hot-wire measurements (right figure). The averaged Mach number across the duct exit is 0.17.

While there is a need to conduct the forward flight simulation, the inlet fan and exhaust fan both operate at full speed to reach desired flow velocity. When the duct flow becomes stable, one can start the operating procedure for acoustic measurements or other experiments. The duct flow is maintained until any kinds of measurements are finished. The capability of forward flight simulation expands the Penn State experimental capability substantially.

3.1.5 Acoustic data acquisition and processing methodology

A flow chart of the data acquisition process is shown in Figure **3-4**. A Pentium II computer was operated with *LabView* installed for data acquisition. A screen shot of the acquisition code for acoustic measurements is shown in Figure **3-5**. This acquisition code was originally developed by Doty [50] and subsequently revised. The data sampling rate is usually set

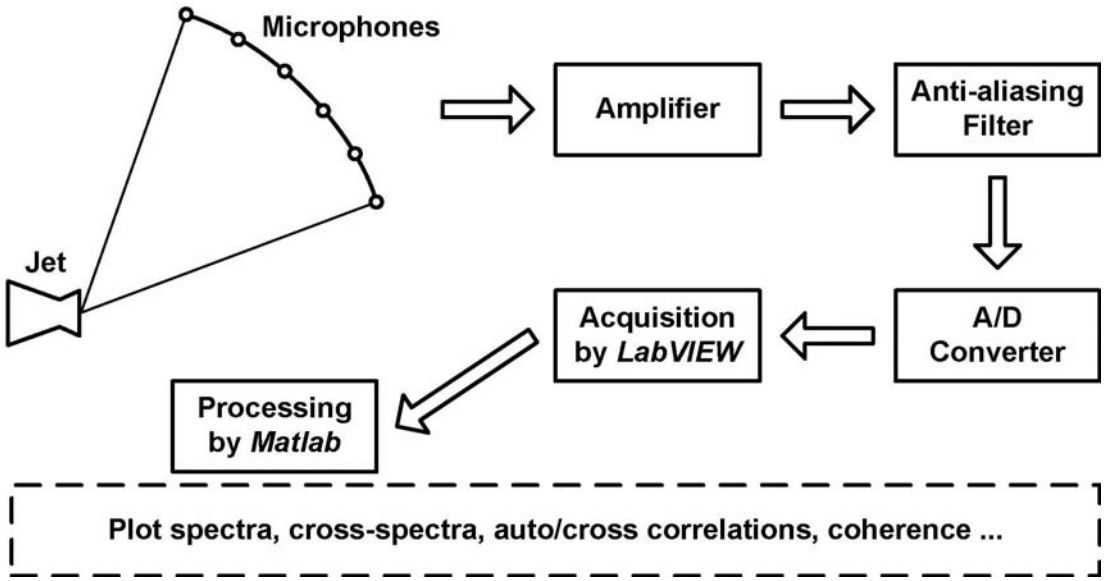

Figure **3-4**: Flow chart of the data acquisition process in acoustic measurements.

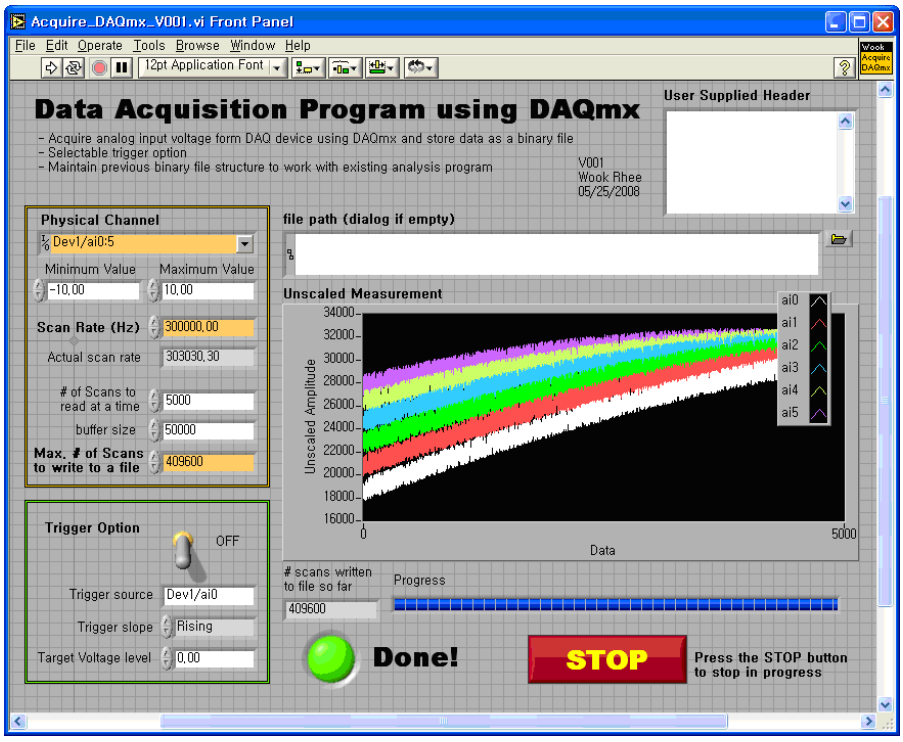

Figure **3-5**: Screen shot of the acquisition code for acoustic measurements (LabView application).

at 300 kHz and 102,400 to 409,600 data points are collected, the reduced dataset being used for helium-air mixture jets in order to reduce the amount of helium used during an experiment. In a measurement of a cold jet condition, personnel will operate the pipe cabinet to reach the desired jet condition and acquire data by *LabView*. For a measurement of heat simulated jet condition, personnel will setup the acquisition code first with the trigger switched on for a target voltage level corresponding to the desired pressure value. The operator then moves to manipulate the flow controls to reach the desired jet condition. Once the jet condition is reached, the acquisition code will be automatically triggered to complete the acquisition. In doing so, the consumption of helium can be reduced to minimum.

After finishing data acquisition, personnel can move experimental data to a folder for data processing. Raw data are fed into *Matlab* for data processing. In the beginning of the processing code, raw data are split into 1024 or 4096 points segments and a Hanning window function is applied with 50 percent overlap between each window. The Fast Fourier Transform (FFT) is calculated in each window and an averaged value is calculated from the 199 segments. This yields the power spectral density (PSD) which is then converted to decibels (dB) using a reference pressure of 20 μPa. Three corrections are then applied to the raw sound pressure level (SPL) to compute the lossless SPL. Finally, the spectra are non-dimensionalized to SPL per Strouhal number. Equation **3.3** summarizes the different steps that lead to the SPL per unit Strouhal number.

$$\underbrace{SPL(St)}_{\text{Lossless Spectrum}} = \underbrace{SPL_{raw}(f)}_{\text{Raw Spectrum}} - \underbrace{\Delta C_{act}(f) - \Delta C_{ff}(f)}_{\text{Microphone Responses}} + \underbrace{\Delta C_{atm}(f)}_{\text{Atmospheric Correction}} - \underbrace{10\times\log_{10}\Delta f}_{\text{Scaling to 1 Hz Bandwidth}} + \underbrace{10\times\log_{10} f_C}_{\text{Strouhal Number Scaling}} \qquad \textbf{3.3}$$

The Strouhal number is defined as $St = f / f_c$, with f_c the characteristic frequency of the jet defined by $f_c = U_j / D_j$, where $\boldsymbol{U_j}$ is the fully expanded jet velocity, and D_j is the fully expanded

diameter of the jet. Besides evaluating jet noise spectra measured at various polar angles, one can also present an *OASPL* contour plot by integrating the spectrum. From the SPL per resolution bandwidth, the *OASPL* is calculated from the following formula:

$$OASPL = 10\log_{10}\left[\sum\left(10^{\frac{\mathrm{SPL(f)}/\mathrm{resolution\ bandwidth}}{10}}\right)\right] \qquad \textbf{3.4}$$

When making cross-scale comparisons, the *OASPL* is calculated for all sets of data using the same non-dimensionalized frequency range in order to obtain an unbiased comparison.

The experimental data acquired at Penn State are typically processed into lossless spectra per unit Strouhal number to make comparison easier across scales. This correction is included in Equation **3.3**. The measurements were made predominantly at distances R = 100 D or 144 D, depending on the nozzle diameter. The spectra were (back) propagated to R_{prop} = 100 D, assuming spherical spreading of the acoustic field. This "back" propagated SPL can be determined from the following equation:

$$SPL(St)_{R_{prop}} = SPL(St)_R + 20\times\log_{10}(R/R_{prop}) \qquad \textbf{3.5}$$

While there is a need to propagate the spectra to a specific non-dimensional distance, Equation **3.5** is applied into the processing. When making cross-scale comparisons, all spectra normally propagate to identical non-dimensional distance.

The experimental repeatability is demonstrated in Figure **3-6**. The experimental results agree well within 1 dB when testing on the same nozzle in different time periods, thus ensures the reliability of the experiments.

These acoustic data acquisition and processing methodology used to examine the jet noise have been refined at the Penn State. The uncertainties of each correction in data processing are examined and shown in Appendix **A**. To advance the accuracy of the high freqeuency resolution of the 1/8 in. microphone, a method is proposed to replace the published free-field

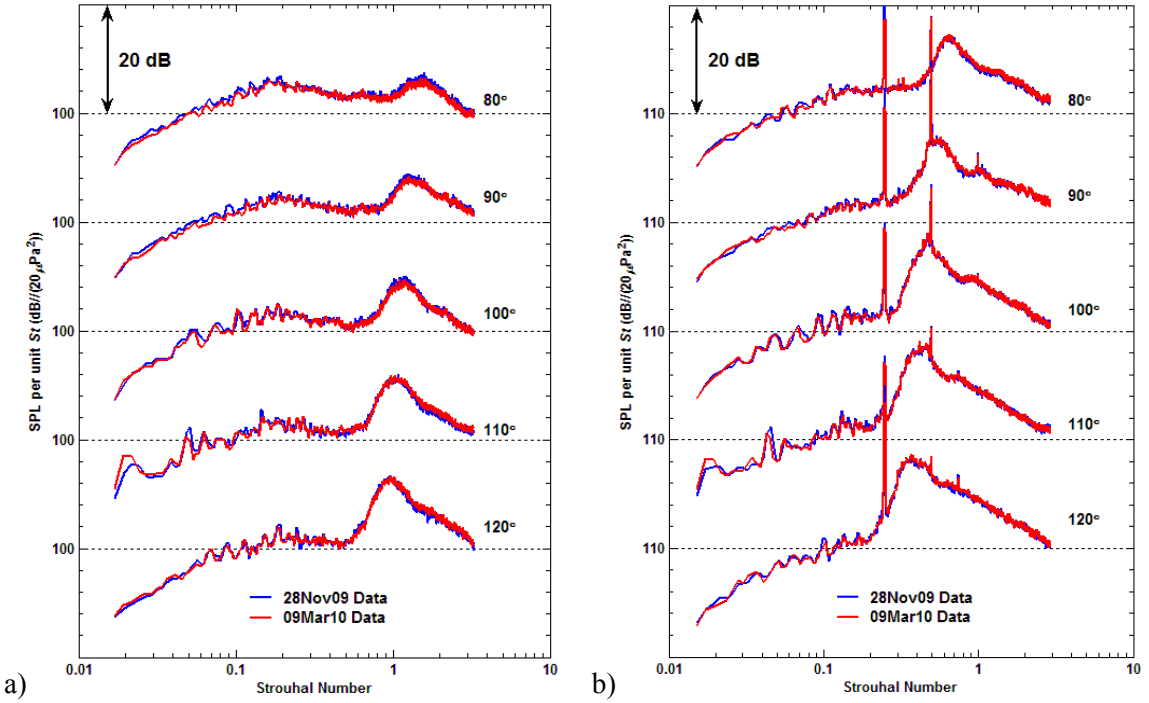

Figure **3-6**: Demonstration of the experimental repeatability. Spectral comparison of unheated jets issued from CD nozzle (M_d = 1.5, AR = 1.18) measured in different days. a) M_j = 1.2. b) M_j = 1.7.

response during data processing ($\Delta C_{ff}(f)$ as shown in Equation **3.3**) by an experimentally determined free-field response specifically for the 1/8 in. microphones operated at grazing incidence with the grid cap on. Several comparisons using this new response demonstrated the significantly improved accuracy of high frequency components of the acoustic spectra, as high as 100 kHz. Thus the usable range of acoustic measurements of the spectra of the Penn State high speed small scale jets has been effectively extended. The detailed explanation and derivation of the empirical free-field response are documented in Appendix **A**. All acoustic measurements conducted at Penn State in the current dissertation were processed with this empirical free-field response.

3.2 Schlieren visualization

Schlieren visualization is a non-intrusive technique used to observe the flow-field development. The setup at Penn State follows the conventional Z-type Schlieren system as shown in Figure **3-7**. The light source comes from a short duration spark light of xenon lamp (Spectrum Dynamics Spectralite Model 900). The stroboscopic rate of the lamp is driven at 60 Hz using a signal generator (Agilent model 33220A). The light source then passes through a focusing lens and focuses to a point at the slit location. The slit is set at the focal distance (4 ft) of the sending side mirror. Two parabolic mirrors of 6 in. (15.2 cm) in diameter are individually located at both sides of the jet exhausting direction as the mirror of sending light and the mirror of receiving light. In doing so, a parallel beam of light is normal to the jets and illuminates the jets. The mirror at the receiving side re-focuses the light to a point at the location of the knife edge. The knife edge is usually set at horizontal to the jet direction axis. As the parallel beam of light penetrates the testing jets section, some amounts of light are deflected due to the fluctuation of the jet density gradients. Any deflection of the parallel beam of light leads to more or less light blockage by the

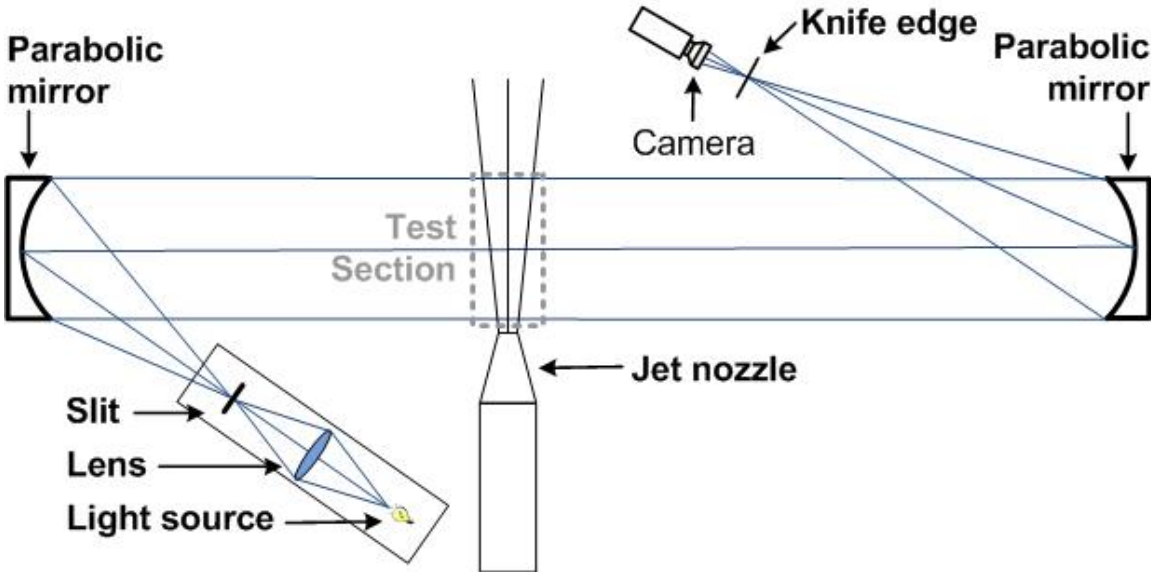

Figure **3-7**: Schlieren setup used in the Jet Noise Facility at The Pennsylvania State University.

knife edge. This causes some darker or brighter areas of the testing jets section on the visualized images recorded by the camera. A black and white CCD camera made by *Minolta*, MD 50/17, is used for the image acquisition.

3.3 Pitot probe measurements

Pitot probe measurements are mainly conducted to demonstrate the effect on the amplified jet spreading of the nozzle with chevrons. In order to provide the flow-field contour plot with good resolution, a five pitot rake was set up and used for the measurements. Each probe has an outer diameter of 0.025 in. and the center-to-center probe separation is 0.065 inch. Each probe records the total pressure at defined locations simultaneously. Figure **3-8** shows the whole setup of the pitot rake and the zoom-in photograph with the pitot rake located just downstream of

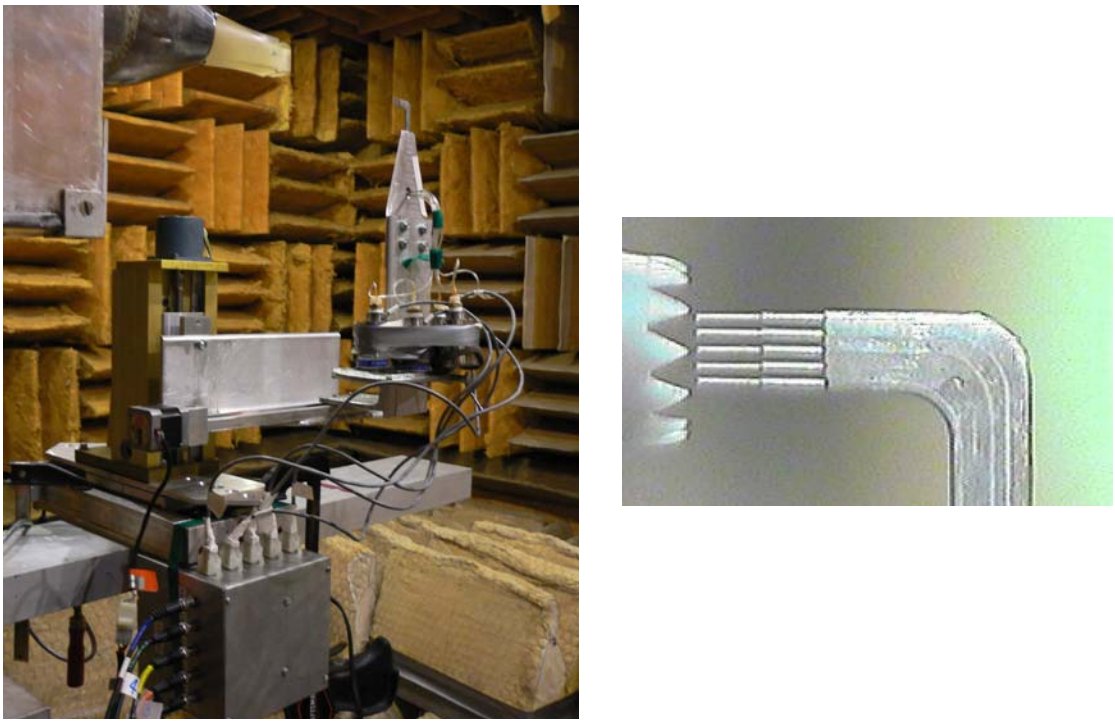

Figure **3-8**: The pitot rake setup and the zoom-in photograph with the pitot rake located just downstream of the chevron nozzle.

the chevron nozzle with nozzle exit diameter of 0.676 inch. This pitot rake setup has the capability of three-dimensional movement provided by three independent traverses. During the data acquisition, only two traverses are motorized and controlled by the acquisition code. The step increment of the pitot rake is usually set at the same amount of the probe separation distance (0.065 in.) in order to provide the measurements with fine grid. The data processing follows the methodology developed by Veltin [20] and subsequently revised.

Figure **3-9** shows the schematic of the pitot probe immersed in the supersonic flow. For the supersonic flow measurements, the measured pitot pressure (P_p) is the total pressure (P_{t2}) after the bow shock in the front of the probe in the supersonic flow region. The ratio of the measured pitot pressure (P_p) and the upstream static pressure (P_1) is then given by the Rayleigh-Pitot tube formula as follows.

$$\frac{P_p}{P_1} = \left(\frac{(\gamma+1)\ M_1^{\,2}}{2} \right)^{\gamma/(\gamma-1)} \left(\frac{\gamma+1}{2\gamma\ M_1^{\,2} - (\gamma-1)} \right)^{1/(\gamma-1)} \qquad \textbf{3.6}$$

When the value of P_p is measureable and the value of P_1 is assumed to be the ambient pressure, the corresponding local jet Mach number and local jet velocity in the measured locations of the pitot probe are derived.

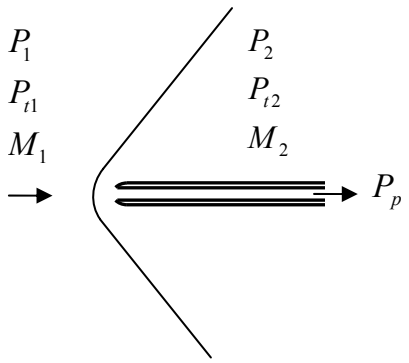

Figure **3-9**: Schematic of pitot probe immersed in the supersonic flow.

As for the probe in the subsonic flow region, the ratio of the measured pitot pressure (P_p) and the upstream static pressure (P_1) is then given by the isentropic flow formula as follows.

$$\frac{P_p}{P_1} = \left(1 + \frac{(\gamma + 1)\ M_1^{\,2}}{2} \right)^{\gamma/\gamma - 1} \qquad \textbf{3.7}$$

The corresponding local jet Mach number and local jet velocity in the measured locations of the pitot probe are then derived.

After introducing each experimental setup and data processing procedure, next chapter presents the spectral comparisons from the measurements acquired with small- and moderate-scale supersonic jets.

Chapter 4

Cross-scale Comparisons from Acoustic Data Measured with Small- and Moderate-Scale Supersonic Jets

4.1 Motivation

The high speed jet noise research team at The Pennsylvania State University has been conducting a project with partners at GE Aviation and the NASA Glenn Research Center. The aim of the overall project was to study and characterize the acoustic field produced by supersonic jets issuing from converging-diverging military style engine exhaust nozzles, and to identify and test promising noise reduction techniques. An equally important objective was to develop a methodology for using data obtained from testing at small and moderate scale, supported by computations, to reliably predict full scale engine noise. Therefore, an important step of this project was to conduct and compare small-scale and medium-scale experimental results with nozzles representative of military jet engine exhaust nozzles. Comparisons across scales with data obtained in different facilities will provide an additional measure of the quality of the measurements performed, and the ability of the methodology to extrapolate the subscale data to the full size aircraft. After forming a quality scaling methodology, the second stage is to conduct similar experiments on noise reduction devices by examining with chevrons of different designs. Eventually, comparison with flight data obtained with aircraft such as an F-16XL or an F-18 will be performed. This chapter focuses solely on the first step of the study: making extensive comparisons between small-scale measurements performed at Penn State and medium-scale measurements gathered at the NASA Glenn Research Center, in order to determine whether the

small-scale, heat simulated, jets can accurately simulate the acoustics issuing from moderate-scale jets.

4.2 NASA Glenn facility and measurements overview

Comparisons are shown in this chapter with acoustic measurements from similar nozzles at a larger scale acquired at the AeroAcoustic Propulsion Laboratory (AAPL) of the NASA Glenn Research Center. This facility is a high speed flow jet exit rig (HFJER) located in a 65 feet radius anechoic geodesic hemispherical dome with the capability of operating hot jets as shown in Figure **4-1**. A microphone arc is mounted at the top of the dome with 24 microphones separated by 5 degree increments, and the height of the microphone is 60 feet measured from the floor. Jet diameters up to 5 inches (12.7 cm) are typically used in this facility, with the capability to use a co-flow to simulate jets with a small bypass ratio of around 0.3. Extensive description and qualification measurements of this facility can be found in Bridges and Brown [53].

As noted above, the NASA HFJER has the capability to operate as a dual flow facility, shown schematically in Figure **4-2** a), and in the upper half of Figure **4-2** b). Additionally the annular flow passage can be closed to provide single stream jets. In all cases presented in this thesis, the upstream (staganation) pressures of the inner and outer flows are maintained at the same value (within experimental uncertainty). The annular flow was kept unheated when performing hot jet measurements in the dual flow mode, in an arrangement that more closely replicates actual engine operations. The testing of moderate-scale nozzles mentioned earlier in section **2.4** was performed in this facility operated in both the single and the dual-flow mode. The experimental data from the NASA Glenn Research Center, provided by Dr. J. E. Bridges [58], are used to generate the cross-scale acoustic spectra comparisons following the data processing methodology mentioned earlier in section **3.1.5**.

Figure **4-1**: The AeroAcoustic Propulsion Laboratory with high flow jet exit rig in the NASA Glenn Research Center.

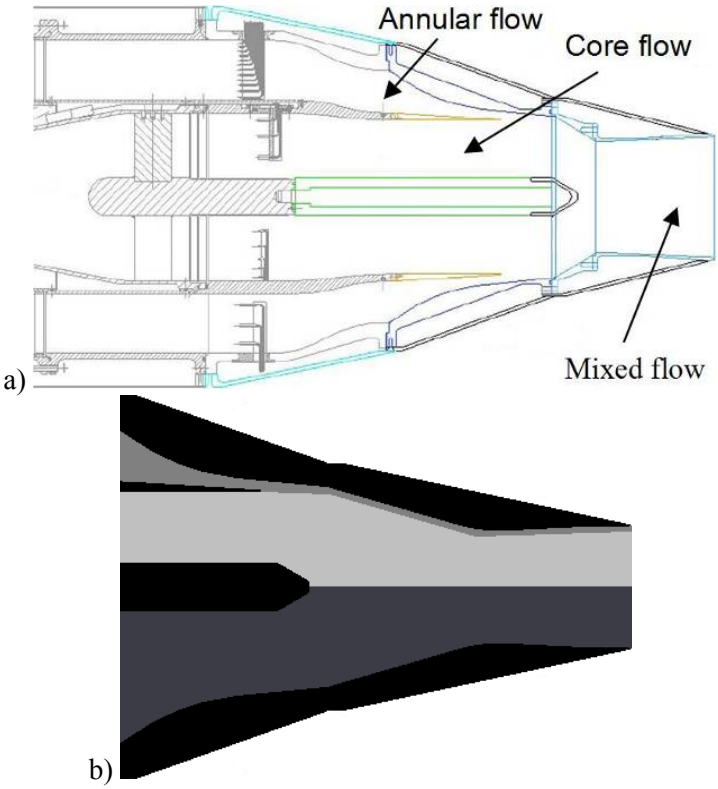

Figure **4-2**: a) Schematic of high flow jet exit rig (HFJER) in the NASA Glenn Research Center with the bypass air for low bypass nozzle systems. b) Schematic of the rig in dual-stream mode via splitter (top) with heated core jets and cold annual jets operated at the same nozzle pressure ratio, and in single-stream mode (bottom) premixed with heated core jets and cold annual jets operated at the same nozzle pressure ratio.

4.3 Acoustic spectra and details of flow fields in jets issuing from the military style supersonic nozzles and CD nozzle

In order to characterize the acoustic field produced by supersonic jets issuing from converging-diverging (CD) military style nozzles, comparison to contoured CD nozzle experiments were conducted. Recall that the GE design has 12 facets around the perimeter and is designed with straight walls in the flow direction in both the converging and diverging sections. Flaps and seals in variable area ratio nozzles create faceted conic nozzle for military aircraft engine operating in different flight envelopes. Measured spectral comparisons are shown in Figure **4-3** through Figure **4-5** between the contoured M_d 1.5 CD nozzle and the GE nozzle with a design Mach number M_d 1.5 (AR = 1.18) operated with cold jets. While acoustic measurements were gathered from $\theta = 30°$ to $\theta = 120°$, the main differences between the noise generated by the two nozzles appear in the broadband shock associated noise. This noise component is only (strongly) apparent at angles sideline to the jet and in the forward quadrant (i.e. $\theta > 90°$). Therefore, only spectra at $\theta = 90°$ and $\theta = 120°$ are shown here.

All jet flows shown in Figure **4-3** to Figure **4-5** are issuing from area ratio AR = 1.18 nozzles that produces approximately M_d 1.5 exit Mach numbers. The figures have three different pressure ratio conditions, however, yielding spatially averaged jet Mach numbers of 1.3 (overexpanded), 1.5 (perfectly expanded), and 1.7 (underexpanded) respectively. Schlieren images of the jets are presented next to the spectra in order to obtain some qualitative information of the flows. Comparisons are first shown for an over-expanded jet in Figure **4-3**. The Schlieren images show a maximum of 10 % discrepancy between the shock cell lengths within the first and second shock cells, and the spectra from the two jets compare fairly well within a 2 dB deviation across the whole frequency range. In the over-expanded jet condition, the jet exhausting from both nozzles needs to go through an oblique shock (possibly a strong normal shock) in order to balance the exit

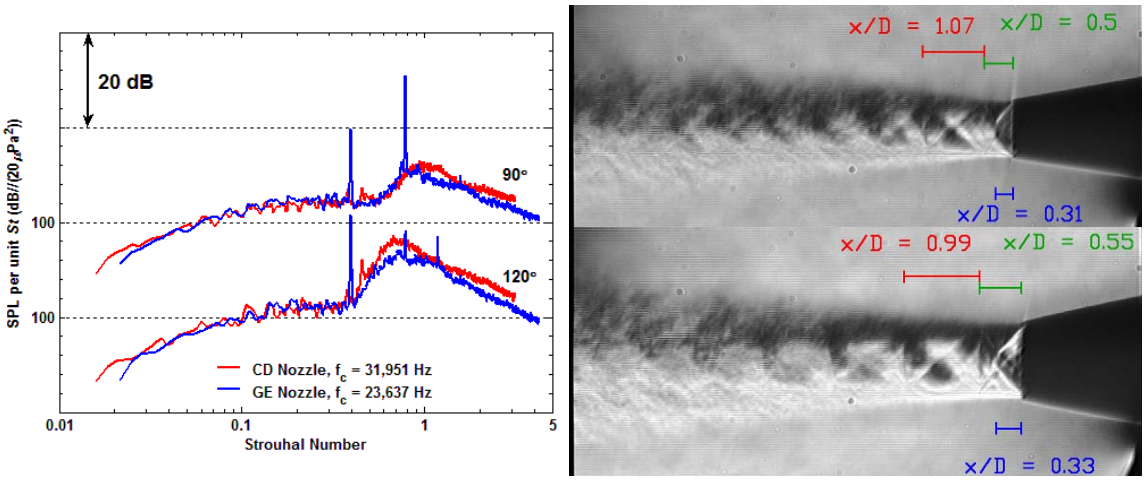

Figure **4-3**: Spectra of unheated jets from CD and GE nozzle (both with $M_d = 1.5$, $AR = 1.18$) operated at $M_j = 1.3$, schlieren images of CD nozzle (top) and GE nozzle (bottom).

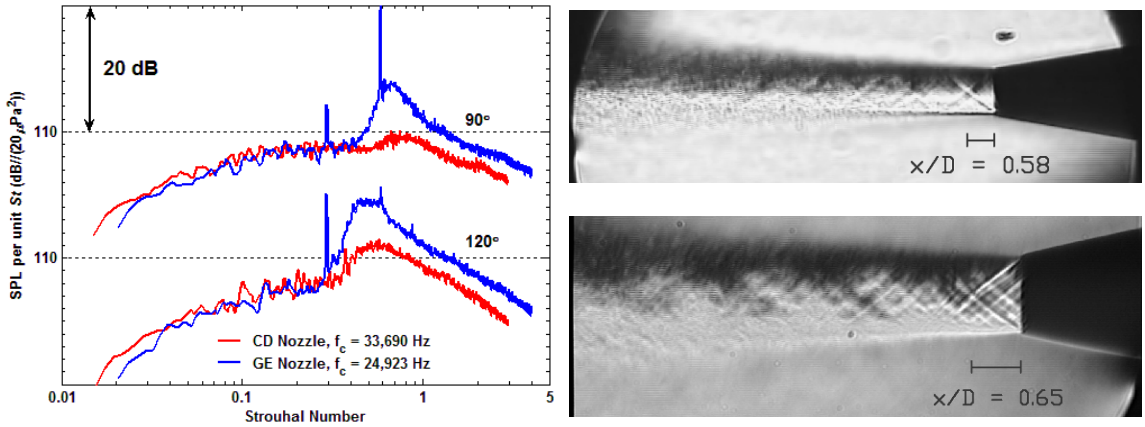

Figure **4-4**: Spectra of unheated jets from CD and GE nozzle (both with $M_d = 1.5$, $AR = 1.18$) operated at $M_j = 1.5$, schlieren images of CD nozzle (top) and GE nozzle (bottom).

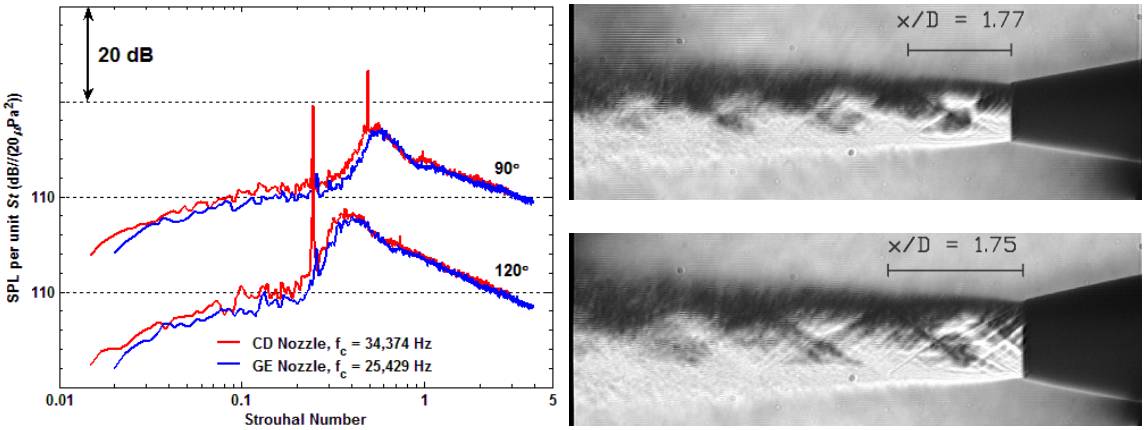

Figure **4-5**: Spectra of unheated jets from CD and GE nozzle (both with $M_d = 1.5$, $AR = 1.18$) operated at $M_j = 1.7$, schlieren images of CD nozzle (top) and GE nozzle (bottom).

pressure to the ambient pressure. Thus, it is reasonable that the spectra are close to each other at the polar angle of 90 and 120 degree since the jet exhausts consist of similar flow fields.

Figure **4-4** shows the comparison obtained from both nozzles operating a fully expanded M_j = 1.5 jet. The Schlieren visualizations reveal the presence of weak shock and expansion waves in both nozzles, but they are not as strong in the case of the CD nozzle jet (designed to operate shock free at this specific pressure ratio). A large number of weak shock waves can be seen in the jet issuing from the GE nozzle, due to the presence of facets and the straight wall conical design of the diverging section. Since there are more shock waves in this flow, it is not surprising to observe that the broadband shock associated noise (BBSAN) part of the spectra is louder by about 8 dB. Figure **4-5** shows both nozzles operating at an under-expanded condition. In this comparison, the shock cell length is very similar between the two flows. As a result, the spectra from both jets closely overlap for the BBSAN regime and compare well within a 2 dB deviation. Furthermore, the screech tone present in the CD nozzle is mostly eliminated with the GE design. In typical aircraft operating conditions, the variable geometry nozzles are mostly operating at off-design condition based on the needs of engine thrust output. Since the difference in the noise spectra is less than 2 dB under such conditions when compared to a CD nozzle, the facetted conical design appears to be a reasonable nozzle candidate for military aircraft and meets the mechanical criterion of engine operations.

For a detailed examination, examples are presented in Figure **4-6** and Figure **4-7**. Figure **4-6** shows spectra from both nozzles operated with cold M_j 1.7 jets. As mentioned earlier, the difference is less than 2 dB across the frequency range and the difference in the magnitude of screech is due to the various nozzle exit plane geometries. These screech frequencies are consistent with analytical predictions, as described by Tam *et al.* [28]. Figure **4-7** presents spectra from both nozzles operated at M_j 1.64, *TTR* 3.6 and shows trends consistent with those observed

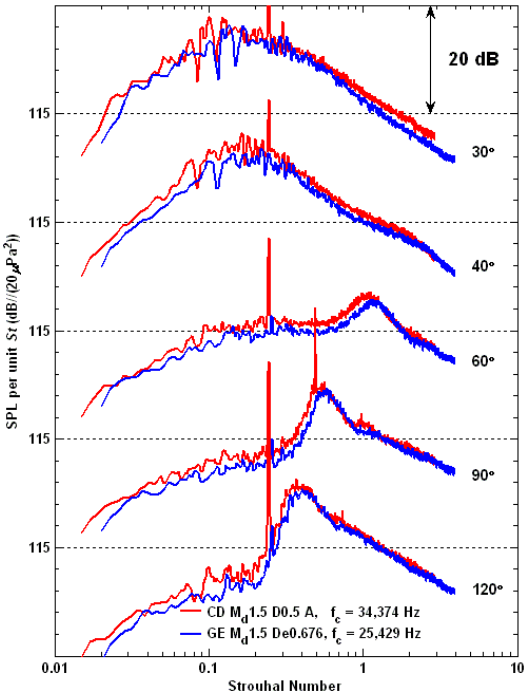

Figure **4-6**: Spectra of unheated jets from CD and GE nozzle (both with M_d = 1.5, AR = 1.18) operated at M_j = 1.7.

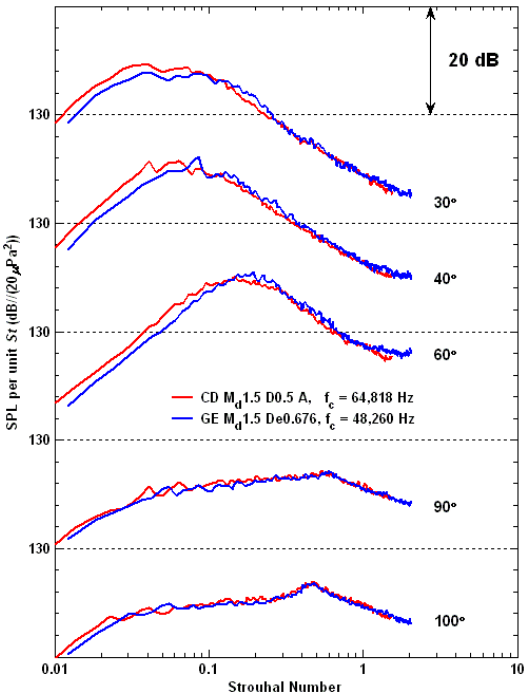

Figure **4-7**: Spectra of heat simulated jets from CD and GE nozzle (both with M_d = 1.5, AR = 1.18) operated at M_j = 1.64, TTR = 3.6.

earlier. This conclusion is identical to the experimental results observed in the moderate-scale CD and GE nozzle jets conducted at NASA Glenn Research Center as shown in Figure **4-8** and Figure **4-9**. It is encouraging to reach very similar conclusions as obtained with the PSU experiments. The significant difference in the spectral levels at the highest frequencies in Figure **4-9** will be discussed later.

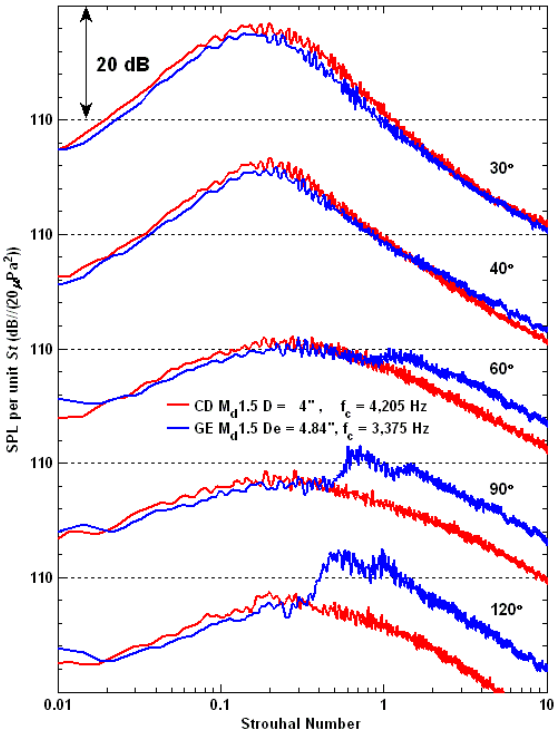

Figure **4-8**: Spectra of unheated jets from CD and GE nozzle (both with M_d = 1.5, AR = 1.18) operated at M_j = 1.5, conducted at NASA Glenn Research Center.

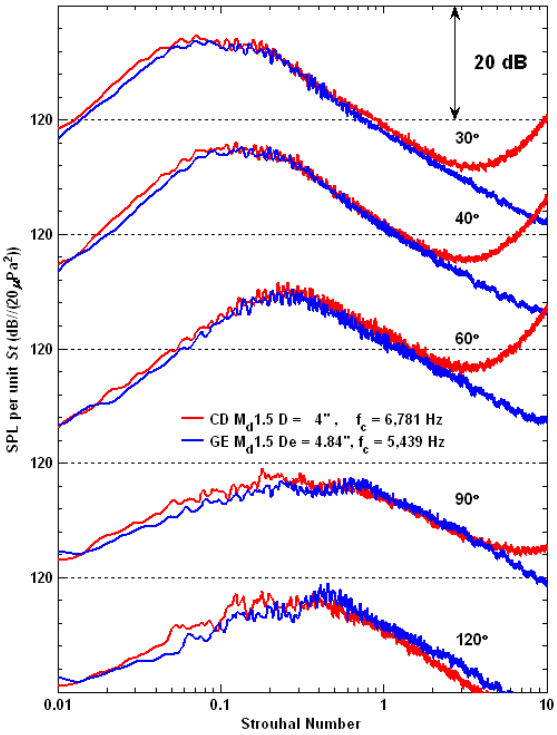

Figure **4-9**: Spectra of heated jets from CD and GE nozzle (both with M_d = 1.5, AR = 1.18) operated at M_j = 1.5, TTR_{core} = 3.1, TTR_{mix} = 2.6, conducted at NASA Glenn Research Center.

4.4 Cross-scale comparisons on acoustic measurements

In order to substantiate the scaling methodology on acoustic measurements, the following demonstrates the spectral comparisons from the measurements conducted at various facilities with different size supersonic jets. The matrix of operating conditions of the data acquired both at Penn State and at NASA is shown in Figure **4-10** and is summarized in Table **4-1** and Table **4-2**. In these tables, the jet Mach number M_j relates to the average Mach number of the fully expanded jet and is uniquely defined by the nozzle pressure ratio (NPR) and the nozzle total temperature ratio (TTR) defined from the jet stagnation temperature T_o and the ambient temperature T_∞ by $TTR = T_o / T_\infty$. For the data from NASA when operating in the dual flow mode, the subscript *core* is used to refer to quantities relative to the core of the jet, while the subscript *mix* relates to the

quantities relative to the mixture of the annular and core flow. The values of Reynolds number in this table were computed based on the M_d = 1.3 (AR = 1.067) GE nozzle and follow the calculation methodology described by Doty and McLaughlin [49]. In addition to the three GE nozzles, a contoured CD nozzle designed to operate fully expanded at a Mach number M_d = 1.5 was used for qualification of the spectral results. A series of unheated and simulated heated jet experiments was conducted at Penn State. As a first step, comparisons were made between cold measurements obtained at Penn State with similar measurements from NASA. These are presented in the first part of the results. Then, the heat simulated small-scale results are compared to the medium-scale hot jet measurements provided by NASA, with discussions of the results included.

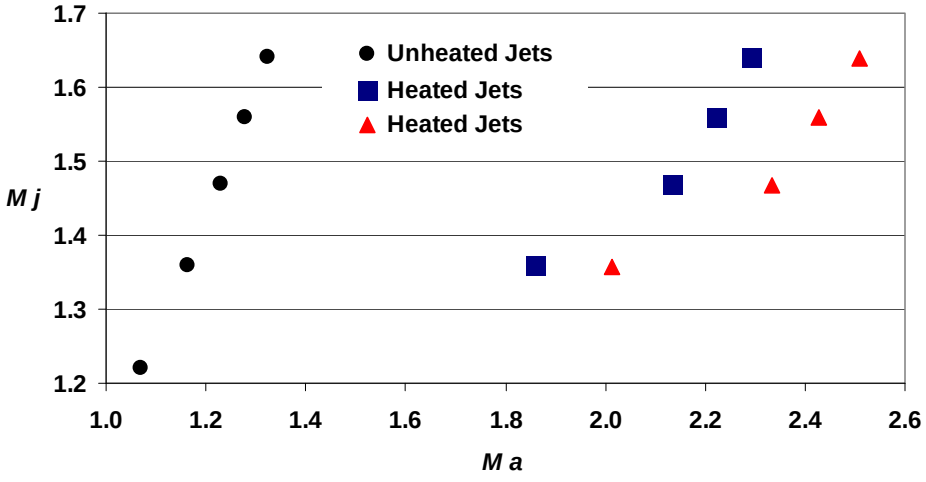

Figure **4-10**: Condition matrix of unheated and heated jets in acoustic Mach number (M_a) versus jet Mach number (M_j).

Table **4-1**: Operating conditions of unheated jets.

PSU Unheated Jets						NASA Unheated Jets				
NPR	M_j	T_j / T_∞	TTR	M_a	R_e	NPR	M_j	$T_{j\,mix} / T_\infty$	TTR_{mix} / TTR_{core}	$M_{a\,mix}$
2.5	1.22	0.77	1	1.07	595,400	2.5	1.22	0.77	1	1.07
3	1.36	0.73	1	1.16	727,800	3	1.36	0.73	1	1.16
3.5	1.47	0.7	1	1.23	857,200	3.5	1.47	0.7	1	1.23
4	1.56	0.67	1	1.28	989,000	4	1.56	0.67	1	1.28
4.5	1.64	0.65	1	1.32	1,119,700	4.5	1.64	0.65	1	1.32

Table **4-2**: Operating conditions of PSU heat simulated jets and NASA heated jets.

PSU Heat Simulated Jets						NASA Heated Jets				
NPR	M_j	T_j / T_∞	TTR	M_a	R_e	NPR	M_j	$T_{j\,mix} / T_\infty$	TTR_{mix} / TTR_{core}	$M_{a\,mix}$
3	1.36	1.87	2.56	1.86	499,500	3	1.36	1.87	2.56 / 3	1.86
		2.19	3	2.01	432,300					
3.5	1.47	2.11	3	2.14	553,400	3.5	1.47	2.11	3 / 3.6	2.13
		2.52	3.6	2.33	470,800					
4	1.56	2.03	3	2.22	636,600	4	1.56	2.03	3 / 3.6	2.22
		2.42	3.6	2.43	544,500					
4.5	1.64	1.95	3	2.29	723,300	4.5	1.64	1.95	3 / 3.6	2.29
		2.34	3.6	2.51	617,000					

4.4.1 Unheated jet measurements

First, comparisons are made between acoustic spectra from cold jets, between small-scale measurements acquired at Penn State and medium-scale measurements from NASA Glenn Research Center. This allows for a direct cross-scale comparison from jets issuing from nozzles of different sizes but the exact same geometry, without adding the complication of the heat simulation. Sample spectra are shown in Figures **4-11**, **4-12**, and **4-13** for three operating conditions: all jets are operated with a pressure ratio $NPR = 4$ ($M_j = 1.56$), they are issuing from the $M_d = 1.3$ ($AR = 1.067$), $M_d = 1.5$ ($AR = 1.18$), and $M_d = 1.65$ ($AR = 1.295$) GE nozzles respectively. Experiments were conducted with five cold jet conditions for each nozzle The data shown in Figures **4-11**, **4-12**, and **4-13** are representative of the consistent agreement obtained with all the other conditions. Meanwhile, the representative jet conditions describe the scenario of military style nozzles operating at over-expanded and under-expanded conditions well. In the figure, the blue curves represent data acquired at Penn State, with nozzles about 0.7 inch in diameter, and the red curves are spectra acquired at NASA with nozzles 7 times larger. One can conclude that there is a very good agreement - within a 2 dB deviation from the spectral comparison and *OASPL* polar plot between the data acquired from the two facilities - providing a check on the scaling methodology, and validating the quality of cold jet measurements acquired from both facilities. This is an encouraging comparison which validates the potential to develop noise reduction concepts in small-scale jets that accurately simulate the acoustics issuing from the actual engine exhausts.

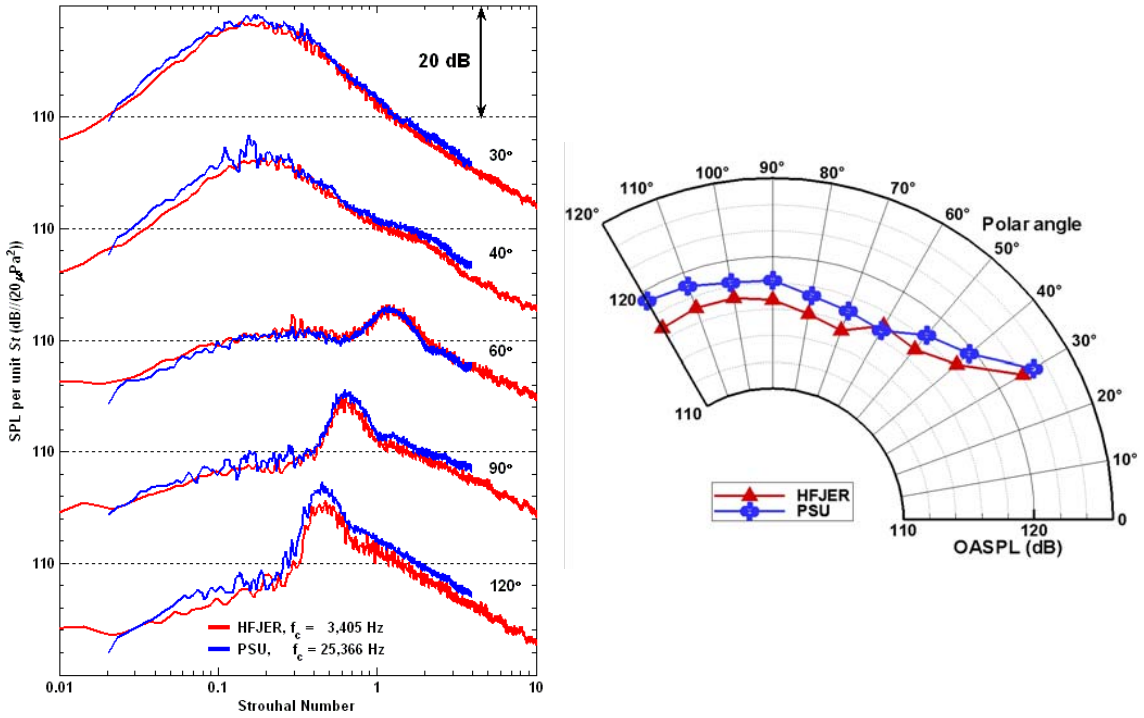

Figure **4-11**: Spectra and *OASPL* comparison of unheated jets from PSU and HFJER both issuing from GE nozzle with M_d = 1.3, M_j = 1.56 and scaled to R/D = 100.

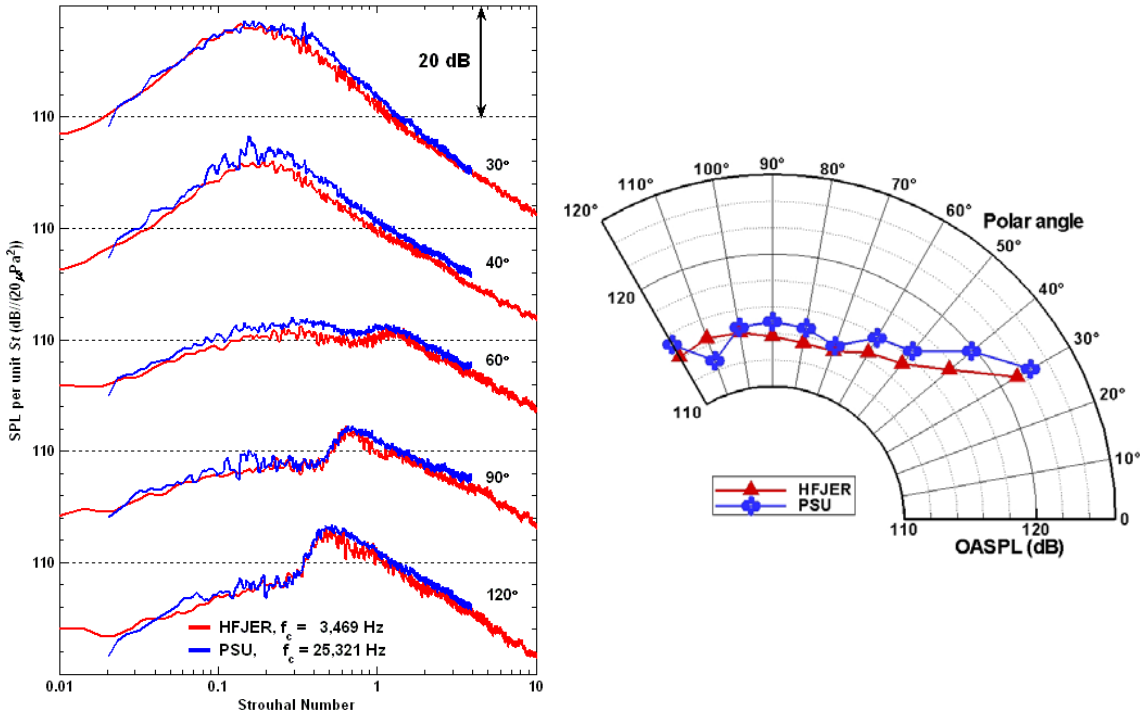

Figure **4-12**: Spectra and *OASPL* comparison of unheated jets from PSU and HFJER both issuing from GE nozzle with M_d = 1.5, M_j = 1.56 and scaled to R/D = 100.

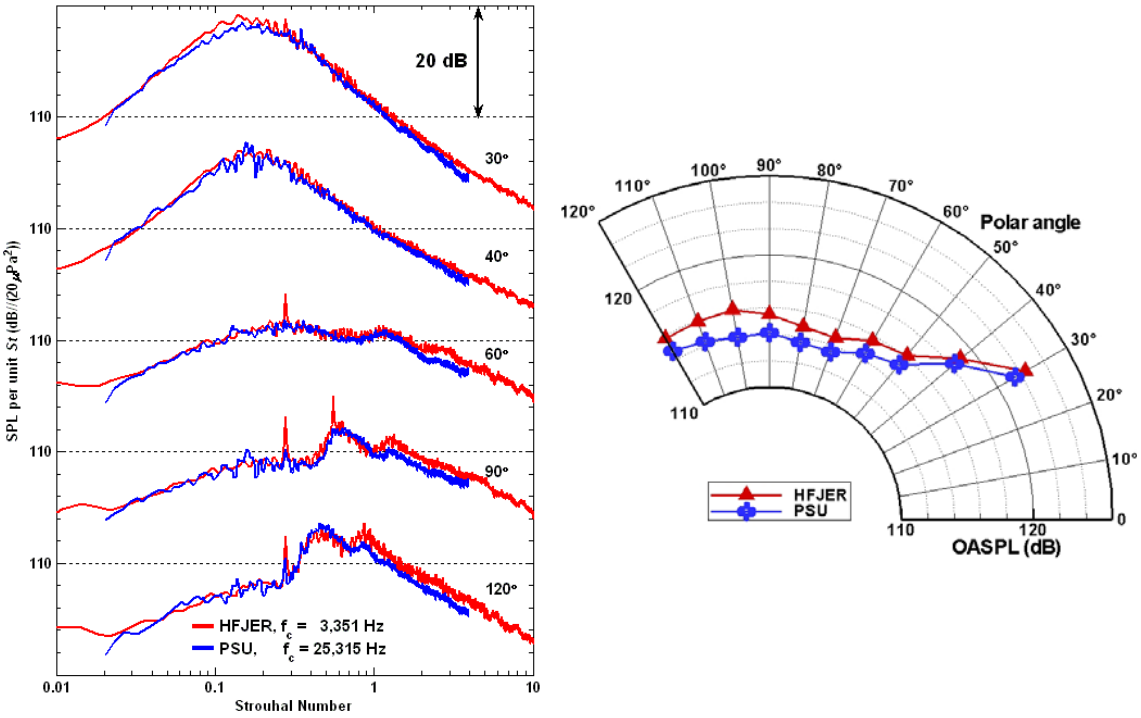

Figure **4-13**: Spectra and *OASPL* comparison of unheated jets from PSU and HFJER both issuing from GE nozzle with M_d = 1.65, M_j = 1.56 and scaled to R/D = 100.

Closer inspection of the details of the small scale nozzles used in conducting the experiments at Penn State shows that the internal nozzle surface is slightly rougher at this scale level in comparison with the moderate scale nozzle. The lip thickness is also not exactly reproduced, due to the limitations of the rapid prototyping technique and the brittleness of the material used. Therefore, the thickness of the boundary layer at the exit plane of the nozzle may not scale perfectly with the moderate scale measurements. In spite of these differences, the comparisons are very good.

4.4.2 Heat simulated jets and heated jets measurements

After the encouraging matching of spectra comparisons from cold jets measurements, Figure **4-14** shows acoustic spectra measured with the GE nozzles with AR = 1.295 conducted with single-stream jets at both Penn State and NASA GRC. The data recorded using the M_d = 1.65 (AR = 1.295) GE nozzle operating at a pressure ratio of NPR = 3.0 produce an average exit Mach number M_j = 1.36, and the simulated temperature ratio TTR = 2.6 for Penn State and TTR = 2.5 for NASA.

As in the case of the cold jets, the acoustic data for the small-scale experiments compare favorably with the NASA moderate-scale data across the frequency range. The individual spectral components are always within 3 dB for both sets of data and most spectral components agree within 2 dB.

The above demonstrations distinctly show that the small heat-simulated jet is capable of reproducing the acoustics issuing from a moderate-size heated jet when the precise simulated properties (*NPR, TTR)* are matched for the over-expanded CD nozzles, which are prevalent in practical supersonic aircraft. These data show that the scaling of small heat simulated jets measurements are in reasonable agreement provided that comparisons are made in the far-field past R/D = 100, with identical nozzles, and with matching Mach number and total temperature ratio. In this context “reasonable agreement” can be quantified to state that agreement of individual portions of the spectra agrees within 2 to 3 dB and the overall sound pressure levels agree within 2 dB.

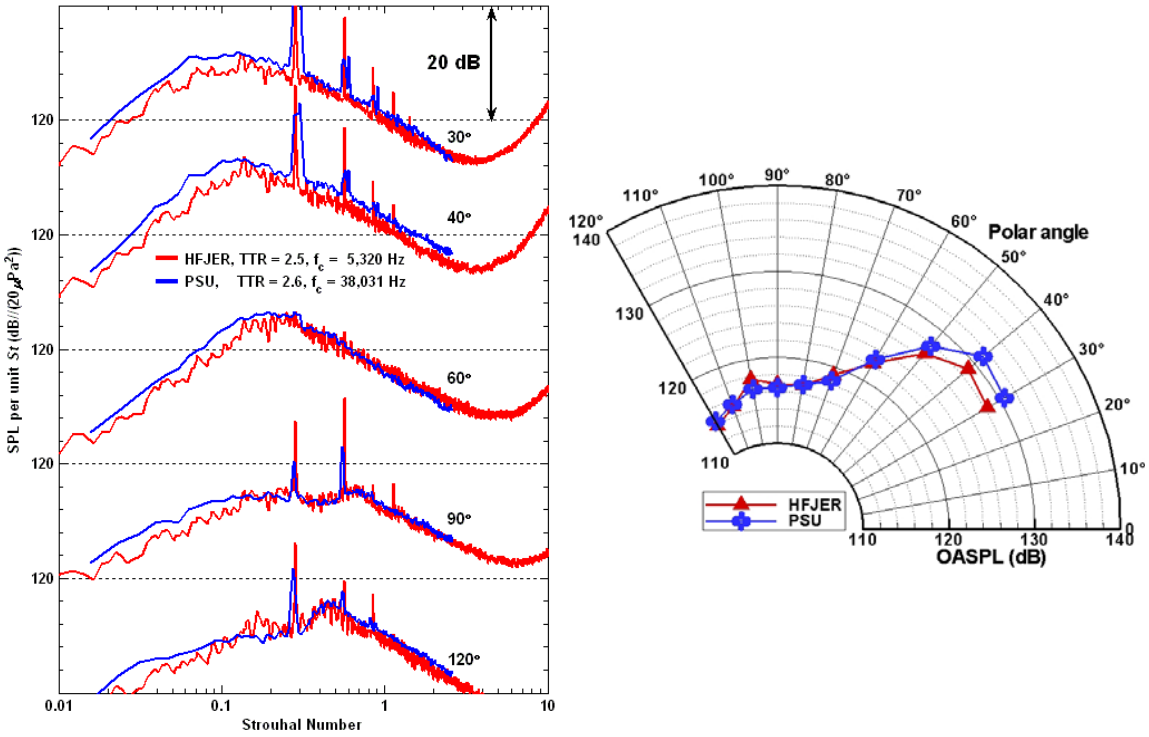

Figure **4-14**: Spectra and *OASPL* comparison of single-stream jet with heat simulation (*TTR* = 2.6) from PSU and heated jet (*TTR* = 2.5) from HFJER both issuing from GE nozzle with M_d = 1.65, M_j = 1.36, and scaled to *R/D* = 100.

4.4.3 Nonlinear propagation effect from the measurements conducted with various jet sizes

In the aircraft flyover measurements, it was found that spectra show less than expected atmospheric attenuation on the high frequency components of the spectra. This modification on spectrum presents that the noise attenuation between 5 to 10 kHz at 500 to 1000 m away from noise source is considerably less than the linear propagation prediction. The experimental results show that there is a strong nonlinear propagation effect involved in the aircraft flyover measurements [59], [60]. It is also concluded that when high-intensity, low-frequency noise appears in the acoustic field, the atmospheric attenuation is obviously less effective. In a demonstration of shadowgraph visualization [61] from supersonic cold jets, there are at least three kinds of sound waves forming and radiating into the acoustic field: a strong directional spherical

radiation wave emitted from nozzle exit, a spherically radiating sound wave generated from the interaction between the jet mixing layer and shock cells, and sound waves radiating from a further downstream location after the previous two waves. During the wave propagation, these three kinds of acoustic waves coalesce and involve complex wave interactions which may be responsible for the physical mechanisms of the nonlinear acoustic propagation. While there is a dominant high-intensity, low-frequency noise emerging in a highly heated supersonic jet, it is easy to spot the nonlinear propagation effect on spectra. Some researchers have attempted to demonstrate the onset of nonlinear propagation by convective Mach number, overall sound pressure level, and skewness [62-64]. In a more practical way, others provided numerical schemes on the nonlinear propagation prediction [65-70]. Currently there is no robust way to accurately evaluate the onset and effect of the nonlinear propagation.

While conducting the acoustic measurements to observe the nonlinear propagation effect, it is crucial to look at the background noise contamination. Figure **4-15** demonstrates the comparisons between the acoustic spectra and background electronic noise spectra from two jet operating conditions. Due to the lift up in the high frequency end of background noise spectrum, it is necessary to carefully avoid these contaminations.

One major feature has been present in Figure **4-14** that merits attention: the higher frequencies at which the HFJER data show a very strong rise (an upward “hook”). This sharp rise is not visible in raw data, but results from performing the atmospheric attenuation correction to obtain “lossless” data. Such a rise is not apparent in the Penn State data, which are not resolved to the same high non-dimensional frequency as is the HFJER data. This feature is most significant at the angles of strongest noise emission, e.g., aft angles, and typically appears at supersonic, hot jet conditions, as discussed in reference [71]. The physical explanation seems to be the presence of strong nonlinear distortion that is present in very high amplitude noise that is undergoing wave steepening (as discussed in several references, for example in reference [71]). It appears from the

data presented here, and much more which was not presented, that the increase in sound amplitude in absolute terms going from the 0.7 in. nozzle to 5 in. nozzle is sufficient to cause the onset of nonlinear propagation within the same relative measurement distance.

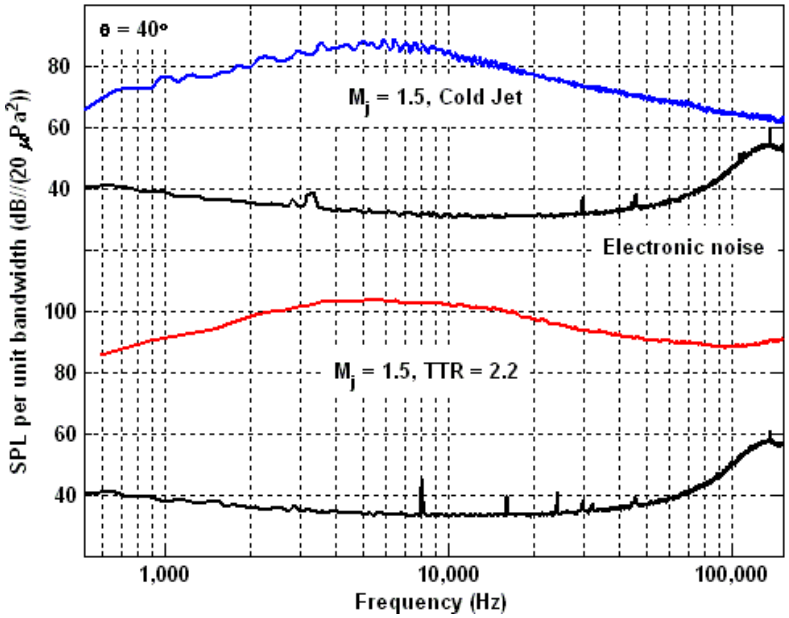

Figure **4-15**: Acoustic measurements conducted with CD nozzle (M_d = 1.5, D = 0.5 in.) operated at M_j = 1.5 for TTR = 1 and 2.2 measured at 40 degree with R/D = 280 in demonstrating the difference between measured signal and background noise.

It is noted that the rising spectral "hook" mentioned in the preceding paragraph is not seen in the Penn State data of Figure **4-14**. In both those data sets the small scale data agree with the moderate scale NASA data quite well but do not extend in frequency resolution to the point where the lossless spectral content begins to rise. The microphone's response limited the resolution. An experiment was conducted however, in which the microphones were placed 280 jet diameters from the nozzle exit over a range of polar angles at Penn State. Figure **4-16** presents the spectral comparisons from the measurements conducted at PSU and NASA HFJER with measured nondimensional distances of 280 and 140 respectively. These measurements were conducted with the contoured CD (M_d = 1.5, AR = 1.18) nozzle. The nozzle exit diameter is 0.5 in. for the Penn State data and 4 in. for the NASA data. For the jets operated at M_j = 1.5 with TTR =

1, there is a good agreement within a 2 dB deviation in the spectra of two measurements. For the jets operated at M_j = 1.5 with *TTR* = 2.2, reasonably good agreement is obtained within a 2 dB deviation in the spectra of two measurements except in the high frequency end of spectra where the nonlinear propagation effect dominates. The small scale data, presented in Figure **4-16**, show an almost identical shape as the moderate scale data, just shifted to a lower frequency. Such a shift in the location to the onset of the nonlinear distortion is consistent with the discussion presented by Petitjean *et al.* [71] on the onset of such effects. In summary, nonlinear propagation effects require the initially very high sound pressure levels, long propagation ranges within the facility, resolution of the frequency spectra to high frequencies and finally, properly applied correction of the spectra to remove the effect of atmospheric attenuation (to produce lossless data).

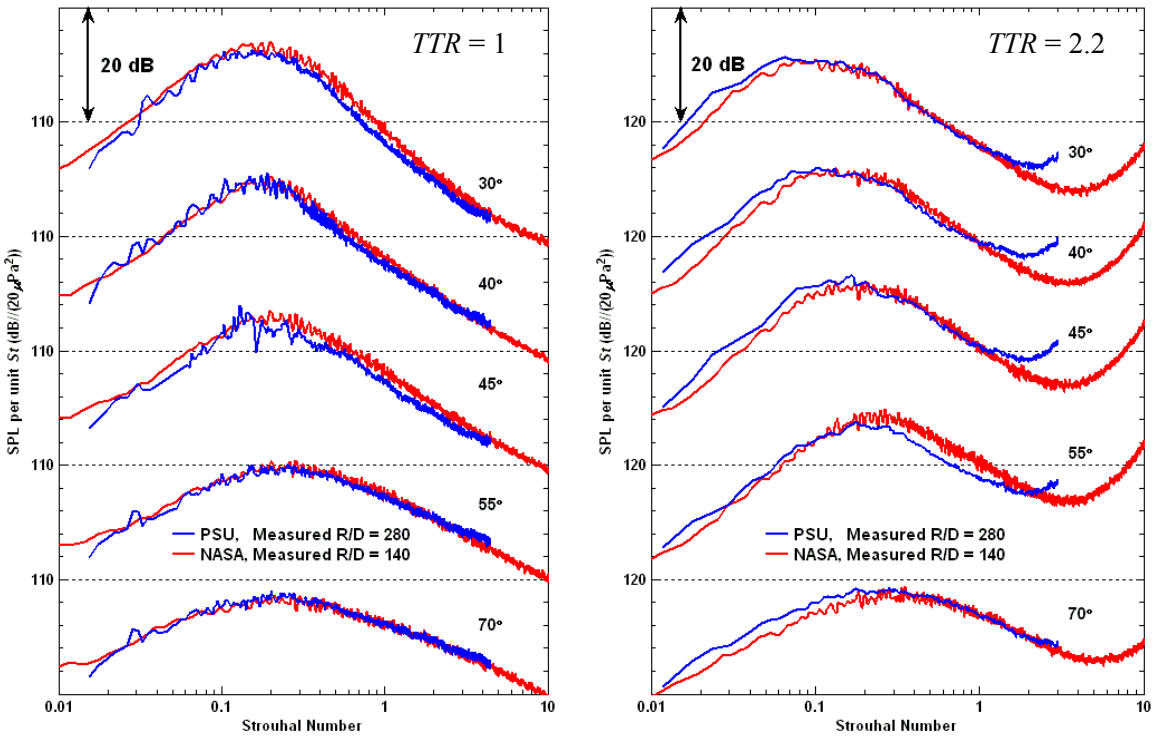

Figure **4-16**: Spectral comparison from the measurements of single-stream jet between PSU (D = 0.5 in.) and NASA HFJER (D = 4 in.) both conducted with CD M_d 1.5 nozzle operated at M_j = 1.5 for *TTR* = 1 and 2.2 with measured *R/D* = 280 and 140 respectively.

4.4.4 Small unheated bleed flow effect on the noise emission

The most common configuration for the NASA HFJER is with co-annular dual flow with a very low bypass ratio (*BPR* = 0.3) of unheated air. Such a configuration consists of a core flow surrounded by a thin annulus of cold air, whose initial thickness is less than 10% of the core radius. This configuration of nozzle is reasonably close to actual supersonic aircraft engines in which the annular fan flow plays a major role in cooling the nozzle walls. It does however introduce some uncertainty in how best to match these low *BPR* exhaust jet acoustic experiments to single-stream model jets for which a considerable amount of acoustic data are available. The experiments producing acoustic spectra are plotted in Figure **4-17** as a head-to-head single flow versus dual flow acoustic data comparison.

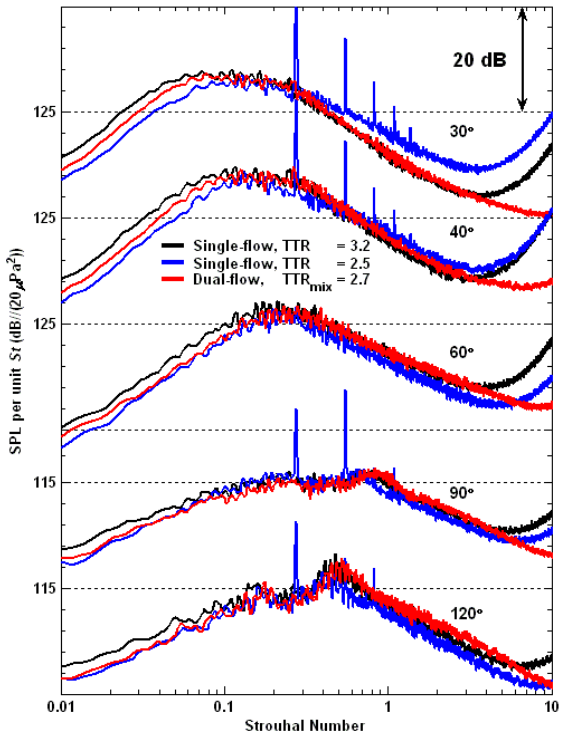

Figure **4-17**: Spectra comparison among single-flow heated jets (*TTR* = 3.2 and 2.5) and dual-flow heated jet (TTR_{core} = 3.2, TTR_{mix} = 2.7 with $St_{dual} = f D_j / U_{j\,mix}$) with *BPR* = 0.3 all from HFJER issuing from GE nozzle with M_d = 1.5, M_j = 1.36 and scaled to *R/D* = 100.

First, the HFJER was operated both as single-stream jet and in its standard configuration as a dual flow rig with a GE design nozzle with M_d = 1.5. Figure **4-17** compares data from the same facility when the single-stream *TTR* matched the core flow total temperature TTR_{core} (= 3.2) and also when it matched a hypothetical mixed flow temperature ratio TTR_{mix} (= 2.7) that assumes the core and cold annular flow to be fully mixed. As noted earlier, the bypass ratio was 0.3 in the dual flow experiment. In Figure **4-17** the difference between the two single-stream jet noise curves is roughly 3 dB for frequencies below the peak, in line with expectations from increasing jet velocity with increased temperature. The temperature change also affects the shift in peak frequency in the data in the aft quadrant (θ < 90°) and there are some differences in the high frequency roll off such that the colder jet produces more high frequency noise at shallow aft angles, but less high frequency noise on the sideline. It is believed that the explanation for this is the rotation of the peak noise emission direction toward steeper angles from the jet (and further from the jet axis) for the hotter single-stream jet. The dual-stream noise spectra generally lies between the two single-jet curves at low frequencies and follows the higher temperature (core conditions) single jet at high frequencies.

Having quantified the differences in simulating a low-bypass ratio practical CD nozzle with a single-stream jet, the next step is to add the effect of scale. The small-scale rig at Penn State was run in a similar fashion, with two total temperature values that match first the corresponding HFJER TTR_{core} and second, the TTR_{mix} value. The results are plotted in Figure **4-18**. Note that this case uses a slightly different nozzle than Figure **4-17**, with a M_d = 1.65; however, both cases are the faceted CD nozzles operating at the over-expanded condition. Here, the jet noise from the two single-stream jets at small scale differ by as much as 5 dB at low frequencies, more than did the same cases in the larger rig. Here the single-stream (PSU jet), run at simulated temperatures matching the dual flow fully mixed temperature condition, produced better agreement with the dual-stream data at low frequencies. At higher frequencies and aft

angles (θ < 90°), the single-stream jet matching the core conditions of the dual-stream jet best agreed with the dual-stream jet, in the same way as the medium-scale experiment did. It is noted that both the Penn State and the NASA data have shock screech components at virtually identical frequencies that are quite close in spectral level, assuring that the shock structure and details of the shock noise are well represented across the model scales (and with different methods of obtaining a "heated jet"). However, it can be concluded that there are imperfections in the matching of acoustic data between single-stream and dual-stream (BPR = 0.3) jets at frequencies below the peak frequency no matter what matching condition is used.

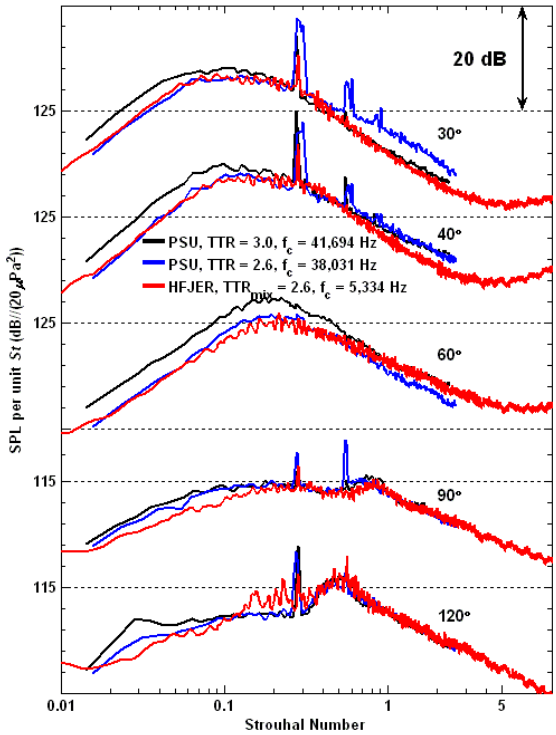

Figure **4-18**: Spectra comparison among heat simulated jets (TTR = 3.0 and 2.6) from PSU and heated jet (TTR_{core} = 3.0, TTR_{mix} = 2.6) from HFJER all issuing from GE nozzle with M_d = 1.65, M_j = 1.36 and scaled to R/D = 100.

4.4.5 Single-stream heat simulated jets and dual-flow heated jets measurements

Figure **4-19** and Figure **4-20** show acoustic spectra measured with the GE design nozzles conducted at both Penn State and NASA as the representative spectra for all heated jets measurements listed in Table **4-2**. As mentioned for the NASA experiments, a small amount of cold bleed flow surrounds the core flow (of temperature ratio TTR_{core}) and after some mixing yields a mixed flow temperature ratio TTR_{mix}. The mixed flow temperature ratio TTR_{mix} is selected as the simulated temperature ratio for the Penn State helium-air mixture jets. For the data shown in Figure **4-19**, the data recorded using the M_d = 1.3 (AR = 1.067) GE nozzle operating at a pressure ratio of NPR = 3.5 produces an average exit Mach number M_j = 1.47, and the simulated temperature ratio TTR = 3.0 for Penn State and TTR_{mix} = 3.0 (TTR_{core} = 3.6) for NASA. For the data shown in Figure **4-20**, the M_d = 1.5 (AR = 1.18) GE nozzle was used at both Penn State and NASA with a pressure ratio of NPR = 4.5. This yields a jet Mach number of 1.64 issuing from a nozzle whose AR corresponds to an M = 1.5 jet. In this case the Penn State jet was operated at a total temperature ratio of TTR = 3.0 corresponding to the NASA mixed flow temperature of the same value. The NASA core temperature ratio was 3.6 for this condition.

The data for the small scale experiments compare very favorably within a 2 dB deviation with the NASA moderate scale data, across the polar angle range (in the case of the $OASPL$ plot) and across the frequency range at the specific polar angles shown. To reiterate the experiments have been conducted with a non-dimensionally identical nozzle contour and with identical pressure ratios (both to engineering accuracy). The mixture simulated total temperature ratio of the Penn State small scale measurements match the mixture total temperature ratio of the NASA hot jet. Some questions may be raised due to using this mixed flow total temperature ratio in favor of the core total temperature ratio as the control parameter.

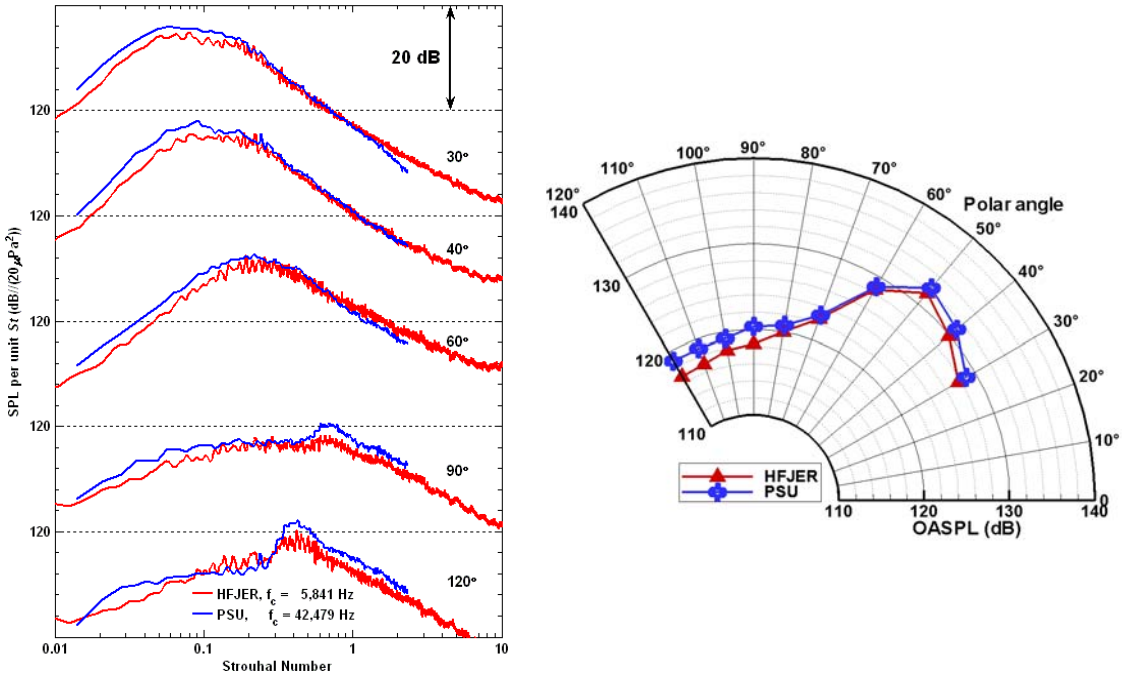

Figure **4-19**: Spectra and *OASPL* comparison of simulated heated jets (*TTR* = 3.0) from PSU and heated jets (TTR_{mix} = 3.0) from HFJER both issuing from M_d = 1.3 (*AR* = 1.067) GE Nozzle operated at *NPR* = 3.5, M_j = 1.47.

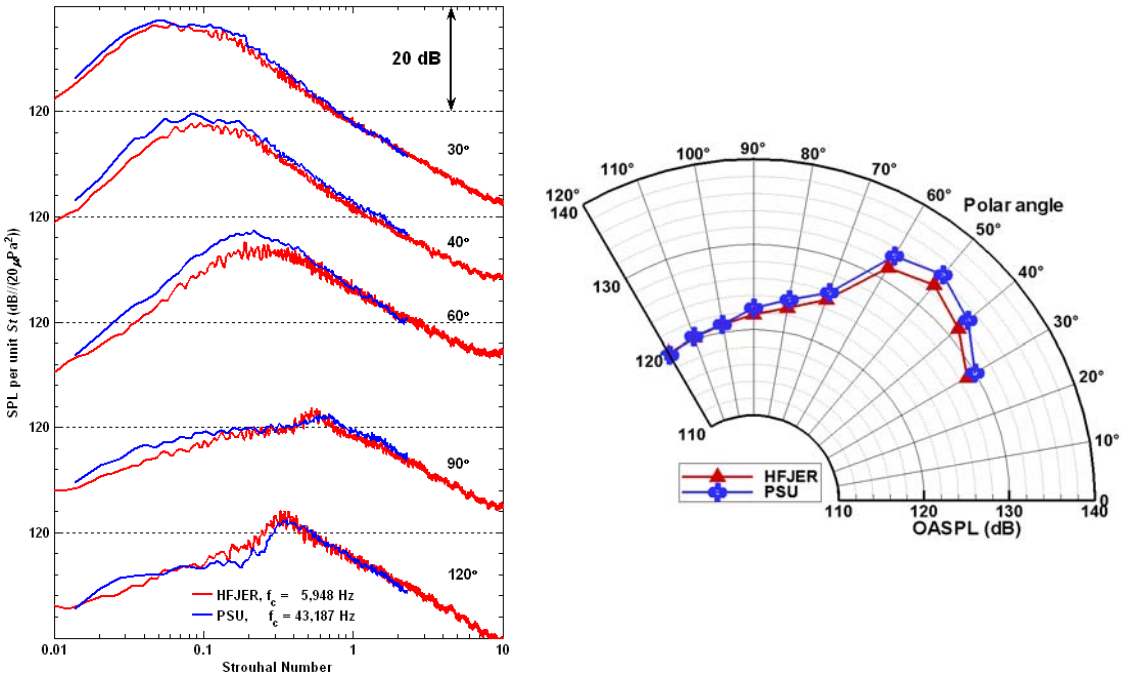

Figure **4-20**: Spectra and *OASPL* comparison of simulated heated jets (*TTR* = 3.0) from PSU and heated jets (TTR_{mix} = 3.0) from HFJER both issuing from M_d = 1.5 (*AR* = 1.18) GE Nozzle operated at *NPR* = 4.5, M_j = 1.64.

If this core temperature ratio is used as the basis of comparison for setting the Penn State simulated temperature ratio, the small scale acoustic data are higher than the NASA data by as much as 5 dB in the lower portion of the spectrum as shown in Figure **4-17** and Figure **4-18**.

In Figure **4-19** and Figure **4-20**, one can see that the overall sound intensity level is generally raised across radiated angles with jets maintaining at the same jets temperature and increasing the jet Mach number. There is also a slight lobe broadening of the overall sound intensity level in dominant noise emission direction accompanying the jet Mach number raises.

Overall, an agreement was reached from the heated jet measurements conducted independently with small- and moderate-scale nozzles. The consistency of results shows that the measured noise levels in small-scale supersonic jets can be applied to predict the noise issuing from a different size of jets.

4.5 Summary

Careful measurements and normalization were employed to produce direct comparisons between small-scale jet acoustic measurements made at Penn State and moderate-scale measurements from NASA GRC. In most cases the supersonic nozzles were of identical geometries (to engineering accuracy) and closely replicated the exhaust nozzles of GE 414 class turbojet engines. Initial experiments were performed with unheated, pure air jet flows. For these cold jets, non-dimensional acoustic data measured at identical scaled radial distances were shown to agree within +/- 1.5 dB across the spectra at numerous polar angles. The Reynolds numbers for all cold jet data presented exceeded 900,000 and imperfections in nozzle surface roughness and lip thickness did not appear to have any significant effect.

For hot jet comparisons of the single-stream measurements, the small-scale (Penn State) experiments simulated the hot-jet velocity conditions of experiments conducted at NASA GRC by using helium-air gas mixtures. Comparisons of the acoustic fields (measured in small and moderate sized facilities) of hot jets from practical CD nozzles in typical over-expanded conditions produced very good agreement on *OASPL* and spectra, typically within +/- 1.5 dB.

Realistic exhaust systems often have unmixed bypass flows exiting the nozzle, a feature incorporated into the medium-scale rig. For over-expanded jet conditions in realistic CD nozzles, there was an impact of the bypass flow on the noise. Comparisons of the small Penn State rig data with hot jet supersonic jet data from the NASA HFJER operating with low bypass ratio (*BPR* = 0.3) showed reasonable agreement (+/- 1.5 dB) provided the single-stream total temperature ratio *TTR* was matched to the theoretical mixed flow TTR_{mix} of the HFJER jet.

Chapter 5

Preliminary Investigations of the Effect of Jet Noise Source Distribution

5.1 Motivation

Supersonic jet noise has proven to be an extremely difficult phenomenon to control, or even to reduce in any measurable way. Because of this difficulty it is important to make all measurements as carefully and as accurately as possible. A part of the process of making and reporting accurate measurements is to make a number of comparisons with data from similar experiments conducted by other researchers at other institutions using similar but not precisely identical measurement and processing methodologies.

An example of such a comparison is shown in Figure **5-1** (data similar to data shown in Figure **4-13**) in which acoustic data obtained with a jet issuing from a 0.708 in. exit diameter nozzle at Penn State are compared with data obtained at the NASA Glenn Research Center (GRC) with a 5.068 in. exit diameter nozzle jet. In this case the nozzles replicated the inside contour of a GE F414 series engine exhaust nozzle to the accuracy of the machining and rapid prototyping process. Acoustic measurements were conducted with the circular microphone arrays set at non-dimensional radial distances that equaled or exceeded 100 D (and were centered at the nozzle exit plane). Care was taken to operate the nozzles at the same pressure ratio and at the same unheated temperature (ratio). Additionally, a consistent methodology was followed for the data processing, including the microphone and atmospheric attenuation corrections. This specific nozzle has an area ratio that produces an $M_d = 1.65$ exit flow using the isentropic flow approximation. Both jets were operated at pressure ratio of 4.0 which produces a spatially averaged exit Mach number M_j of 1.56. In such imperfectly balanced flow, a standard shock cell pattern is present and produces

broadband shock associated noise (BBSAN) that is easily identified in the spectra recorded at the polar angles of 60°, 90° and 120° from jet axis. The small shock screech components are replicated in frequency but not in amplitude. In the case of these data, the NASA Glenn data were "back propagated" from the measurement location of R/D = 120 to the location of R/D = 100 of the Penn State measurements (using spherical spreading, $p' \sim 1/R$). These data are part of a cooperative Penn State/NASA project in which numerous measurement comparisons with cold jets were performed. The supersonic jets were operated at various overexpanded and underexpanded conditions, and with three different jet area ratios. With cold jets, the two sets of data are typically in agreement within +/- 1.5 dB across the spectra.

Turning now to heated jets, those of primary interest to the aircraft and engine manufacturers and users, the agreement in the data is typically not as close (as mentioned in the chapter **4**). Figure **5-2** presents data recorded in three facilities: Penn State, NASA GRC and NASA Langley Research Center (LaRC) [72]. In this case the nozzles were contoured CD M_d = 1.5 and the jets were operated in the perfectly expanded M_j = 1.5 condition. All spectra were reported to have been measured in the far-field, with the closest microphones located at R/D = 85. In general the agreement between spectra acquired in different laboratories is not as good as was found from the cold jet data. The Penn State data, acquired with helium-air mixture jets to simulate the heated condition, fall for the most part in between the two NASA data sets. In fact, the discrepancy between the low frequency end of the two NASA spectra is approximately 5 dB for θ = 40° to 60°.

The imperfections in the data match led to the examination of the data in more detail from the GRC and the LaRC laboratories. These data comparisons led to the conclusions that when data are compared with measurements made at common radial distances from the nozzle, sufficiently in the far-field, the smaller heated jets at LaRC and Penn State agree across the spectra within about 1.5 dB over the range of polar angles typical of Figure **5-1** and Figure **5-2**.

When comparisons are made, *in the true geometric far-field* between any of these smaller jets and the GRC HFJER, the agreement at the peak amplitude and in the high frequency range is also within +/- 1.5 dB. However, at frequencies below the peak, the discrepancies between spectral levels grow to values as high as 5 dB.

The differences between the measurements at dissimilar *R/D* locations led to this part of the research. In gathering data with which to make comparisons, the usual assumption is that at ranges of $R/D > 50$ extrapolation of data to greater ranges can be quite accurate when using spherical spreading ($p' \sim 1/R$; or 6 dB per doubling of distance). While such scaling is straightforward, it relies on the underlying assumption that the noise radiates spherically, inversely proportional to distance between the source and the microphones, and the lateral extent of the noise generation region is assumed to be negligible.

The question of the minimum distance to the true geometric far-field was investigated more carefully by examining data recorded from the same jet (in the same laboratory) measured at different ranges. First are the comparative data of Figure **5-3** which show spectra of acoustic measurements performed (at Penn State) in the acoustic field of two supersonic jets exiting from CD nozzles operating fully expanded at $M_j = 1.5$ and simulated total temperature ratio of $TTR = 3.2$. The microphones for both jets were positioned at a radius of 70 in. on a polar arc centered on the nozzle exit. Since the two nozzles used in these measurements were 0.5 in. and 1 in. in diameter, the *R/D* value for the experiments were $R/D = 140$ and 70 respectively. In the data of Figure **5-3**, both sets of data were then scaled (by spherical spreading) to $R/D = 100$. Note that the spectral data are in reasonable agreement but differences of about 3 dB in magnitude are apparent between data of two size nozzles (and *R/D* positions). The discrepancies are most apparent at frequencies below the peak amplitude level and in the polar angle range from 40° to 60° from the jet axis corresponding to the region of largest gradient in the *OASPL* with polar angle.

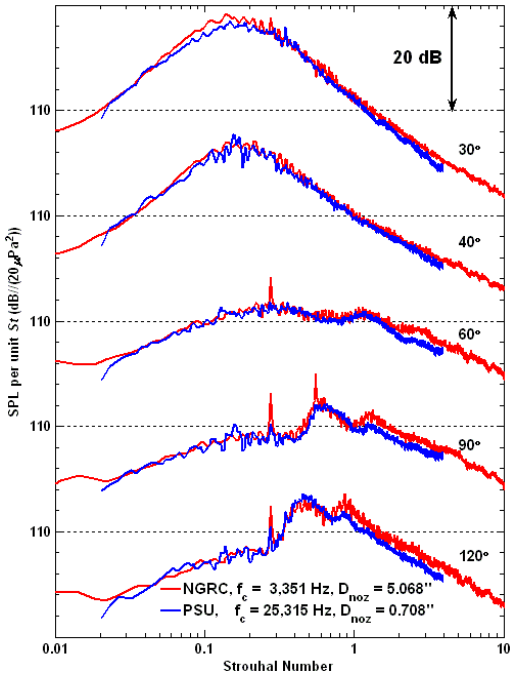

Figure **5-1**: Lossless spectra comparison of unheated jets from PSU and NASA Glenn Research Center (GRC) both issuing from M_d = 1.65 GE nozzle operated at M_j = 1.56, and scaled to R/D = 100.

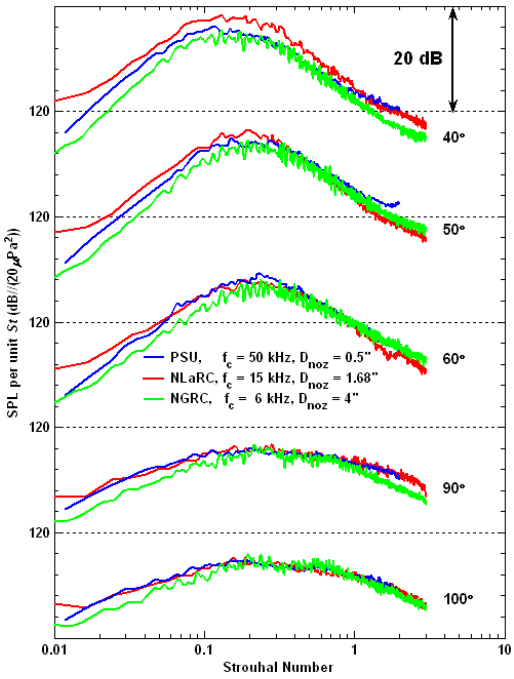

Figure **5-2**: Acoustic measurements from Penn State, NASA Langley Research Center (LaRC), and NASA Glenn Research Center (GRC) all conducted with CD nozzle (M_d = 1.5) operated at M_j = 1.5, TTR = 2.2, and scaled to R/D = 100.

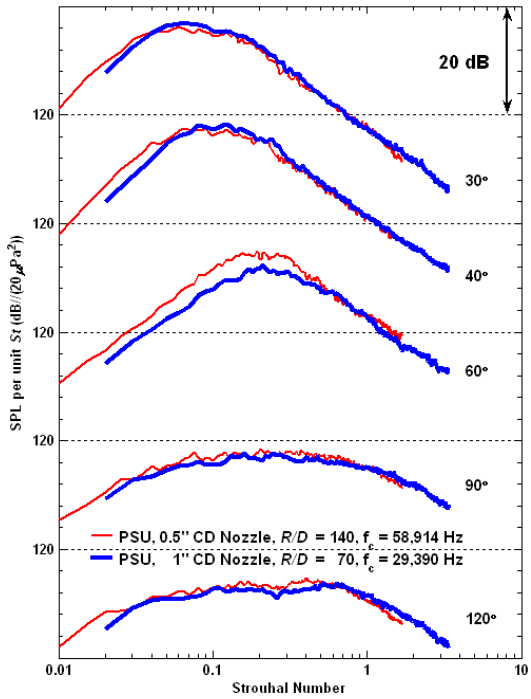

Figure **5-3**: Spectra comparison of heat simulated jets issuing from M_d = 1.5 (AR = 1.18) CD nozzle with 0.5 in. and 1 in. in diameter operated at M_j = 1.5, TTR = 3.2, and scaled to R/D = 100.

Figure **5-4** shows very similar data to Figure **5-3** this time recorded with a heated jet exhausting from the NASA GRC HFJER facility fitted with a CD nozzle (and a thin annulus of unheated bypass air). In this case the acoustic data were recorded simultaneously with microphones positioned on an arc at R/D = 147 and on a linear array displaced parallel from the jet axis by 33 D. The latter data, which are recorded at an average radius of R/D ~ 50, are clearly not in the geometric far-field. The plotted data are scaled to a non-dimensional radial position of R/D = 100 and discrepancies in the spectral level are observed as with the Penn State small-scale jet measurements of the previous figure.

Such discrepancies between the measurements made at the threshold of the near to far-field and those that are clearly in the geometric far-field are significant and render the comparisons of the effect of other parameters, in some cases, less effective. In essence the problem is much more acute with hot and heat-simulated jets, than it is with cold supersonic jets.

As demonstrated by Lee and Bridges [73] and McLaughlin *et al.* [74], the dominant region of noise sources in hot supersonic jets center around a non-dimensional axial distance x/D = 13, whereas the comparable location for cold jets is around x/D = 8. This shift of the dominant region of noise sources, as well as the extended length of the source region, is enough to distort the scaling of acoustic data to different radial positions using spherical spreading (when the measuring microphones are on a polar arc originating at the nozzle exit). This reason makes it more important to perform comparison measurements at the same non-dimensional radial positions. Due to physical restrictions and the different requirements of each experiment, such is not always possible practically when making comparisons to data recorded in experiments performed in past years.

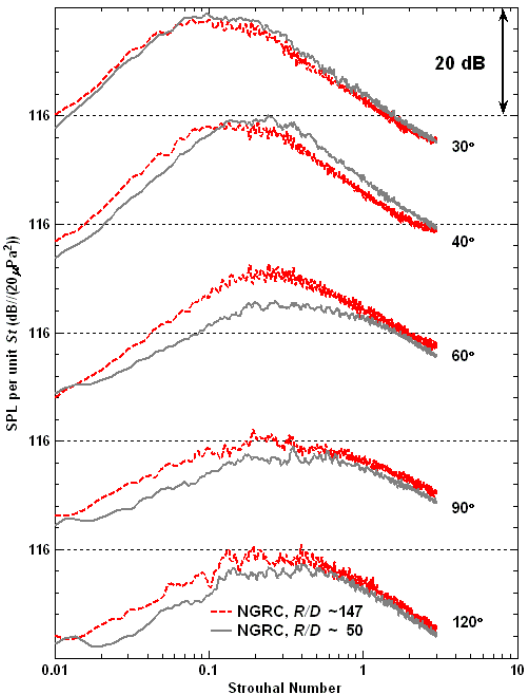

Figure **5-4**: Spectral comparison of experiments measured at various locations from NASA Glenn Research Center (GRC) issuing from M_d = 1.5 (AR = 1.18) CD nozzle operated at M_j = 1.5, TTR_{core} = 2.6, TTR_{mix} = 2.2, scaled to R/D = 100.

Until recently, the distance of 50 diameters has been widely accepted [43-45] as being the outer edge of the near field of high speed jets, and an appropriate distance to make measurements that can then be scaled to farther distances. However, when comparing the data obtained from different non-dimensional distances conducted in the same facility, as shown in Figure **5-3** for data acquired at Penn State and in Figure **5-4** for spectra measured at NASA, the agreement is not as precise as the comparisons in Figure **5-1** and Figure **5-2**. All these measurements were previously thought to meet the criterion of noise spherically radiating to the far-field. Albeit, one can easily observe that there is obvious discrepancy in the sound pressure level at low frequencies and an apparent shift of the peak frequency of the spectrum at some polar angles. These comparisons suggest that data previously measured and existing in the literature for some time might not have been made in the true geometric far-field. Table **5-1** summarizes some experiments for which comparisons have been made between data and the location of their microphones. Many of the data sets that have been widely referenced have been acquired at polar distances less than 100 jet diameters.

Table **5-1**: Testing nozzles and measured distances of acoustic measurements from each facility.

Author	Facility	Nozzle Diameter (D)	Measured Radius (R)	R/D	Reference Source
Tanna, H. K.	Lockheed-Georgia	2"	144"	72	*J. Sound Vib.*, 1977
Seiner, J. M. *et al.*	NASA Langley	1.68"	144"	85	NASA TM 86296, 1985
Viswanathan, K.	Boeing LSAF	1.5" up to 4.9"	Sideline array 180"	120 to 37	*AIAA J.*, 2006
Bridges, J. *et al.*	NASA Glenn, HFJER	4" up to 5"	588"	147 to 117	NASA TM-2002-211366, 2002
	NASA Glenn, SHJAR	2"	100"	50	AIAA Paper No. 2005-2846

It is also noteworthy at this time to mention that the extended range to the true geometric far-field is a direct result of the extended noise source region in supersonic jets, particularly those that have been heated. Beginning with Nagamatsu *et al.* [8], it has been established that the noise sources in supersonic hot jets extend much further downstream than do those in cold subsonic jets. The results of several noise source distribution measurements have been assembled and plotted collectively. Figure **5-5** and Figure **5-6** present the estimated downstream location of the peak noise source in low and high speed jets respectively as a function of non-dimensional frequency (Strouhal number). These data were collected from the literature where measurements were made with improved directional reflecting microphone systems [75-77] and with phased array microphone measurements [73], [78-79]. Even data from some early sound shadow measurements are included. These were conducted by systematically blocking noise generation regions from the acoustic far-field [80-82]. With these given peak noise emission locations, one can examine the relationship between the acoustic measurements conducted at pre-selected locations and the noise radiating from these peak noise emission locations. More experimental results [83]-[91] confirmed the nature of the noise source distributions.

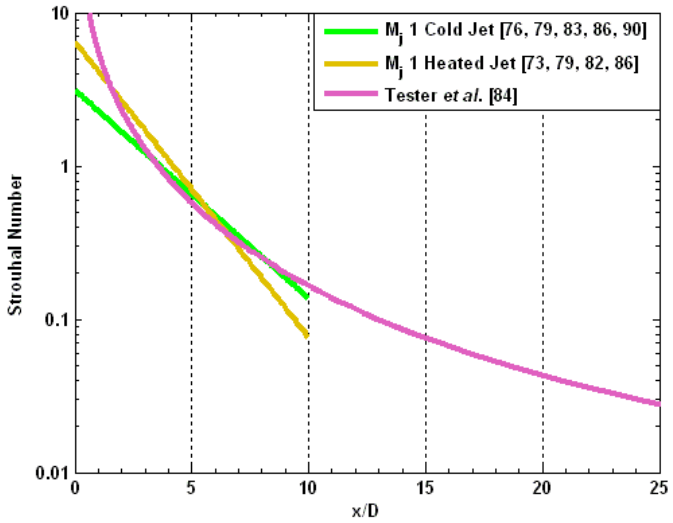

Figure **5-5**: Estimated peak noise emission location as a function of Strouhal number for cold and heated jets operated at $M_j = 1$.

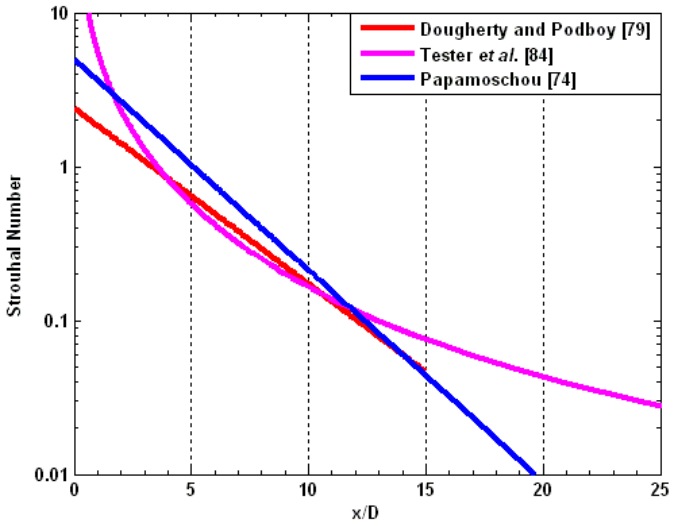

Figure **5-6**: Estimated peak noise emission location as a function of Strouhal number for cold and heated supersonic jets.

Based on the understanding of jet noise source distribution, it is reasonable to see good matching in the high frequency regime of spectrum for measurements conducted at various radial distances with microphones coordinating from the nozzle exit plane as previously shown. During the preliminary study, a specific acoustic measurement was conducted where the coordinate system of microphones was set at x/D = 13 downstream of the nozzle exit plane. This specific acoustic measurement was operated with heat simulated M_j = 1.5 jets for TTR = 3.2 and 3.5 where the phased array measurements [74] had demonstrated that there is a dominant low frequency noise radiating from x/D around 13 nozzle diameters. Since the largest discrepancy (in the acoustic measurements conducted at various radial distances) appears below the peak frequency of spectrum where low frequency noise dominates, this specific measurement should be able to appropriately scale the measured noise for low frequency components. Figure **5-7** shows the results of this specific acoustic measurement with microphones on an arc with an origin at x/D = 13 and measured at R/D = 70, 140, and 280. The experimental results exhibit the expected collapse in the low frequency regime of spectra. The mismatch above the peak frequency was

anticipated due to the downstream shift of the microphone coordinate system. However, based on this preliminary consequence, a more detailed examination was made on how to link the jet noise source distribution to the acoustic far-field measurements.

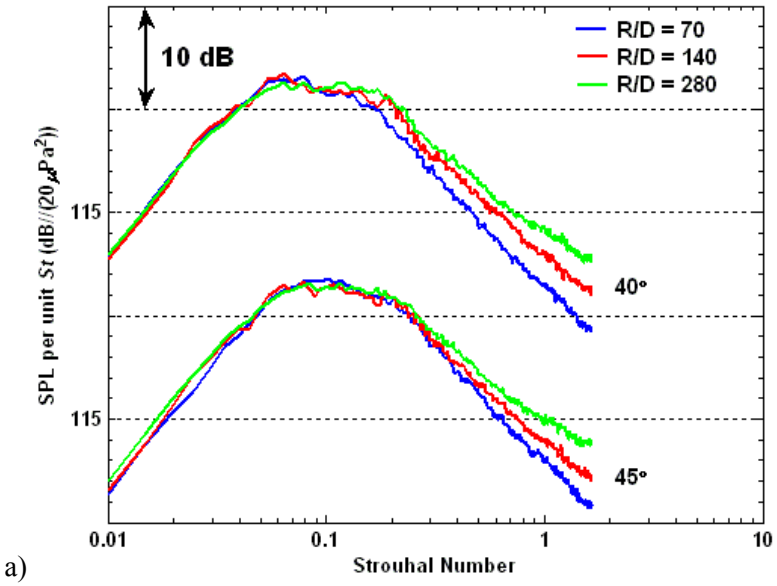

a)

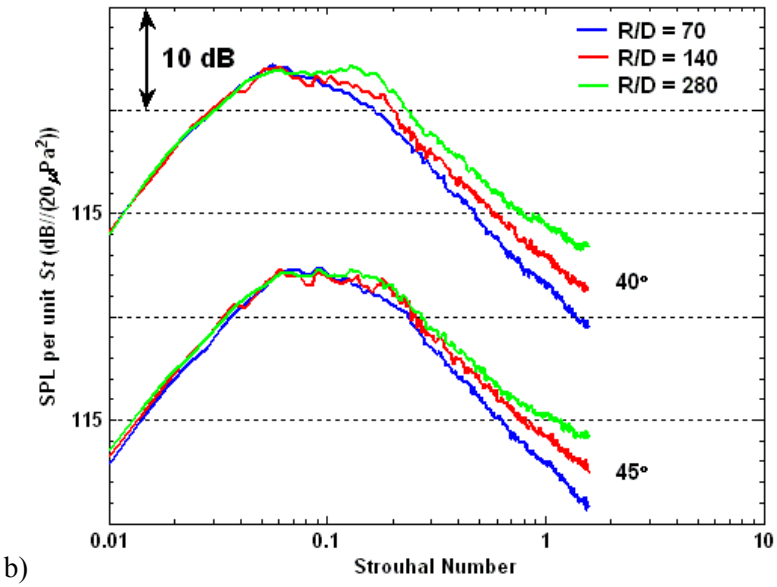

b)

Figure 5-7: Acoustic measurements at polar angle of 40 and 45 degrees conducted with CD nozzle (M_d = 1.5, D = 0.5 in.) operating at M_j = 1.5 where microphones originating at x/D = 13 from nozzle exit plane as measured at R/D = 70, 140, and 280. a) TTR = 3.2. b) TTR = 3.5.

In an effort to produce measurements that can be reliably used by other organizations and propagated to the far-field for noise prediction during an aircraft fly-over, laboratory measurements need to be representative of the true geometric acoustic far-field. The goals of this chapter are to: 1) examine acoustic measurements made in the regions of the acoustic far-field (of supersonic jets) where the true geometric far-field had not yet been reached, 2) examine the details of the noise production regions within these jets in order to better understand the source of the spectral mismatch measured at various radial locations in the acoustic field, and 3) develop a correction methodology with which measurements previously made in the acoustic far-field at ranges shorter than the true geometric far-field could be converted to useful geometric far-field data.

Regarding the third research goal, an advanced processing method has been developed to allow for a more accurate comparison of acoustic measurements from different distances from the nozzle exit plane. The improved acoustic data scaled to the true geometric far-field are referred to as synthesized far-field data. Data produced in this fashion can then be used to obtain better comparisons with measurements from other research groups as well as provide the most accurate data to be used in the acoustic modeling for environmental noise predictions. This advanced processing methodology uses the noise source distribution data that were discussed above. Applying this methodology can also allow one to further identify the nonlinear propagation effects on the spectra that will be demonstrated in the latter section of this chapter.

Regarding the processing methodology, Ahuja *et al.* [92] had proposed something similar in 1987 with the noise source location data provided from the subsonic jets data [93]. It is therefore not an academically innovative idea. Nevertheless, while adopting this methodology, a further step was taken to investigate the measurements of highly heated supersonic jets conducted at various radial distances. The current processing methodology verifies the understanding about the characteristics of jet noise. Therefore it is crucial to demonstrate the capability of this

processing methodology, especially for the measurements of supersonic heated jets, and provide substantial understanding on the application of noise source distribution correction.

5.2 Jet noise directionality and spectra

While first studying the jet noise spectra from the cold jets measurements, which were recorded from a contoured CD nozzle of nominal design Mach number of 1.5, the spectra show reasonable consistency between corresponding sound pressure level and operating jet conditions at each polar angle as shown in Figure **5-8** except for the magnitude and peak frequency of broadband shock associated noise. The peak frequency of turbulent mixing noise is always around $St = 0.2$ among all polar angles within the downstream quadrant. The *OASPL* plot reveals that the peak noise radiation angle is between 25° to 35° for $M_j = 1.22$ to 2.27. This consistent relationship between sound pressure level and operating jet conditions supports the finding that less discrepancy appears in the measurements of cold jets conducted at various radial locations.

Recalling the discrepancy observed in the measurements of heated supersonic jets conducted at various radial locations, there is a downward shift of the non-dimensional peak frequency to lower Strouhal number and a sound pressure level mismatch especially in the dominant noise radiation angle. While investigating the jet noise spectra from the heated jets measurements, which were also conducted with a contoured CD nozzle of nominal Mach number 1.5, the spectra only show reasonable consistency between the corresponding sound pressure level and operating jet conditions at upstream polar angles as shown in Figure **5-9**. At downstream polar angles, there is a downward shift of non-dimensional peak frequency from *St* around 0.2 at 70° to

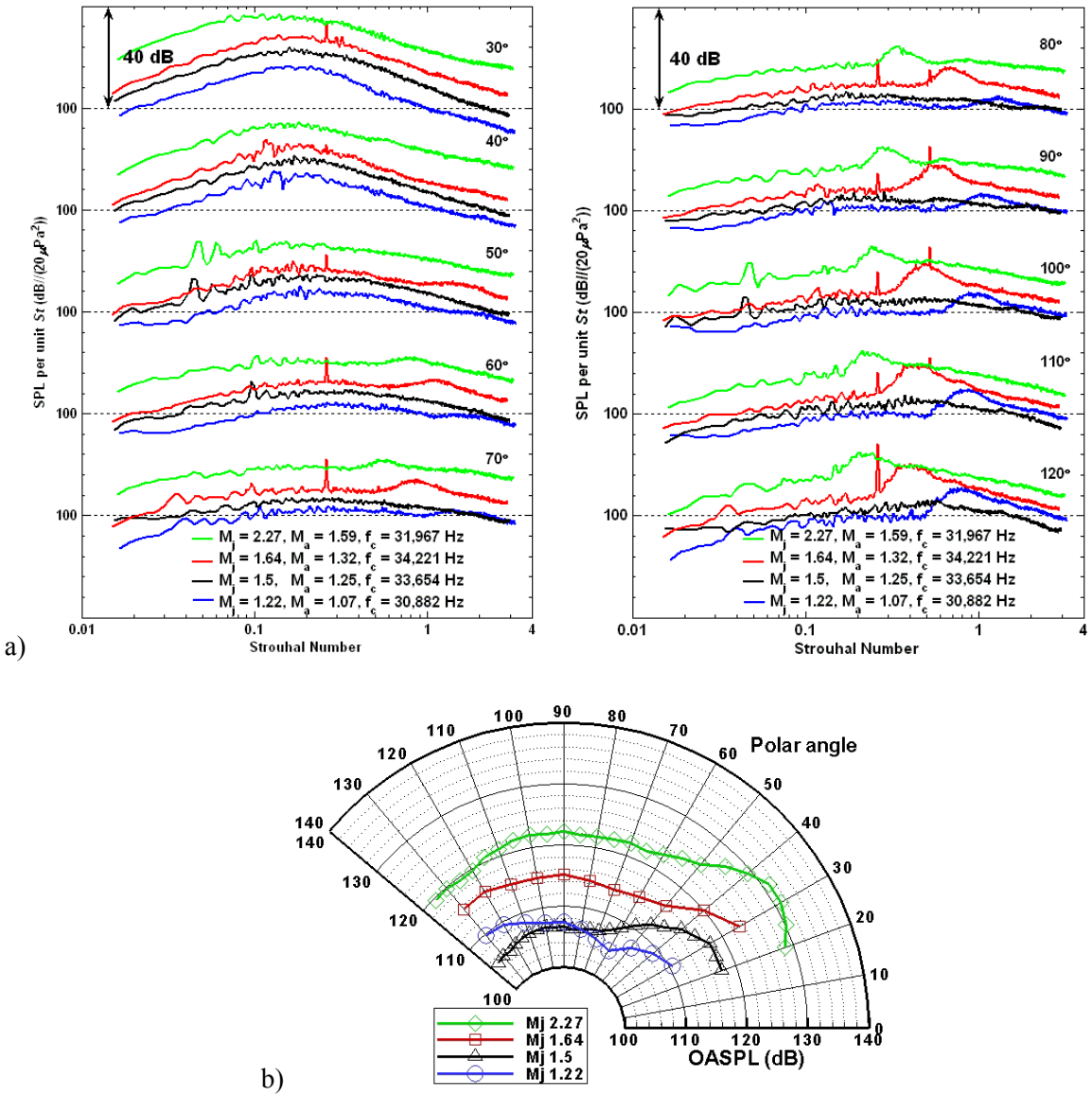

Figure **5-8**: Acoustic measurements from PSU conducted with CD nozzle (M_d = 1.5, D = 0.5 in.) accordingly operated at M_j = 1.22, 1.5, 1.64, and 2.27 with *TTR = 1*, as measured at *R/D* = 140. a) Lossless spectra. b) Overall sound pressure level contour plot.

St around 0.03 at 30°. The trend of downward shift of peak frequency gradually expands in spectra measured at shallow polar angles as a function of jet temperature. This leads to a drastic change in spectrum shape and also reveals that there is more acoustic power gained for low frequency noise radiated from farther downstream locations. Meanwhile, the *OASPL* contour plot

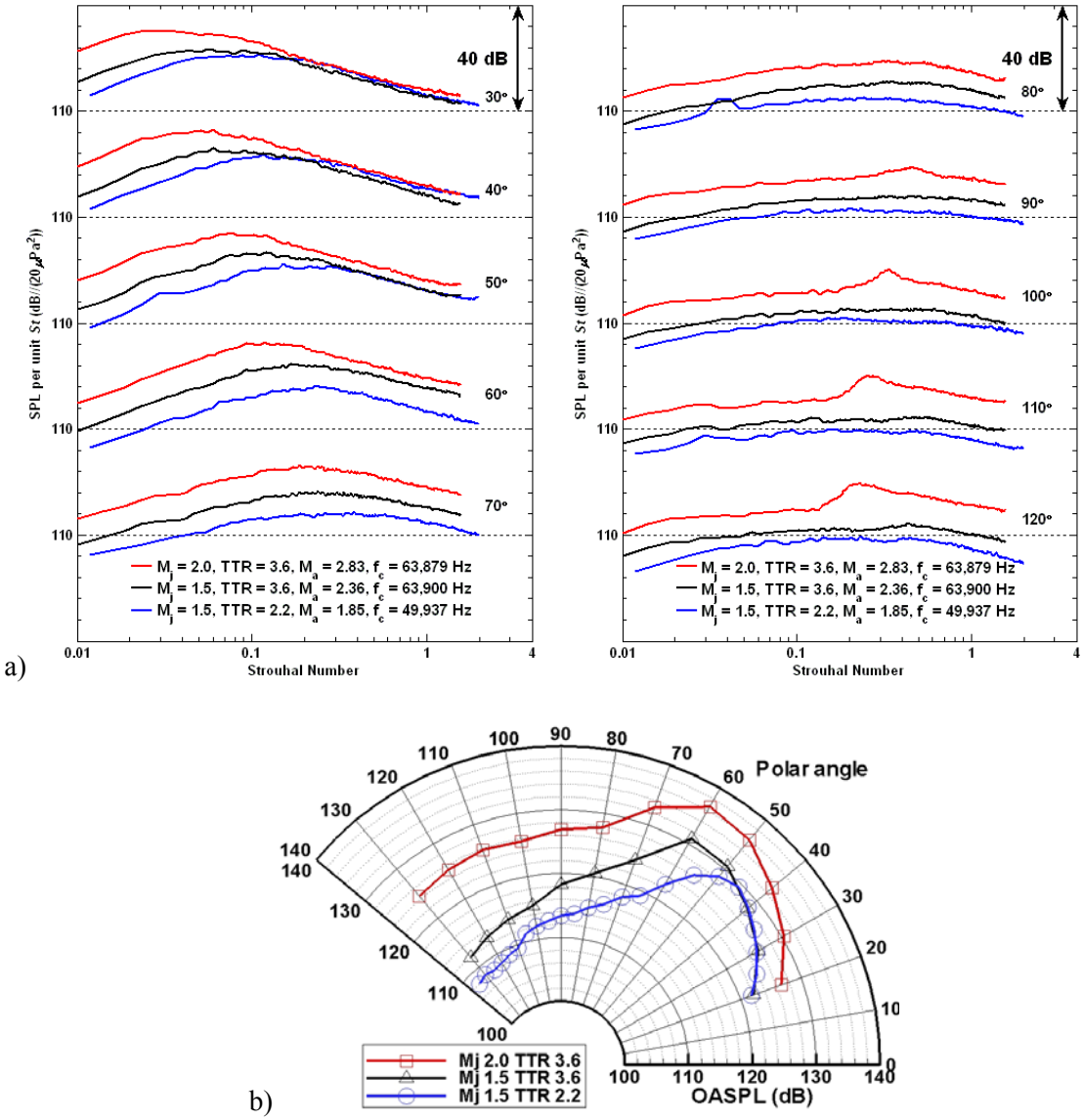

Figure **5-9**: Acoustic measurements from PSU conducted with CD nozzle (M_d = 1.5, D = 0.5 in.) accordingly operated at M_j = 1.5, TTR = 2.2, M_j = 1.5, TTR = 3.6, and M_j = 2, TTR = 3.6, as measured at R/D = 140. a) Lossless spectra. b) Overall sound pressure level contour plot.

presents the peak noise radiation angle that changes from 45° to 60° for these highly heated supersonic jets. By looking at Figures **5-8** and **5-9**, one can see that the jet temperatures enlarge the lobe of the noise generation mechanism and then increase its dominant noise radiation angle. The unclear connection of how the jet temperature raises the low frequency noise in contributing more acoustic power then intrigues the further investigation in this research.

Figure **5-10** presents the spectra and *OASPL* obtained from the acoustic measurements conducted at M_j = 1.5 with *TTR* = 1, and *TTR* = 2.2 respectively. When the jet temperature ratio is raised, the overall sound intensity level is raised and accompanied by a downward shift of non-dimensional peak frequency at shallow polar angle from the jet direction [94] as shown in the spectra. The peak noise emission direction changes from 25° for M_j = 1.5, *TTR* = 1 jets to 45° for M_j = 1.5, *TTR* = 2.2 jets as shown in the *OASPL* polar plot. This is the acoustic trend for jets with higher acoustic Mach number (U_j / a) due to the increased nozzle pressure ratio or total temperature ratio.

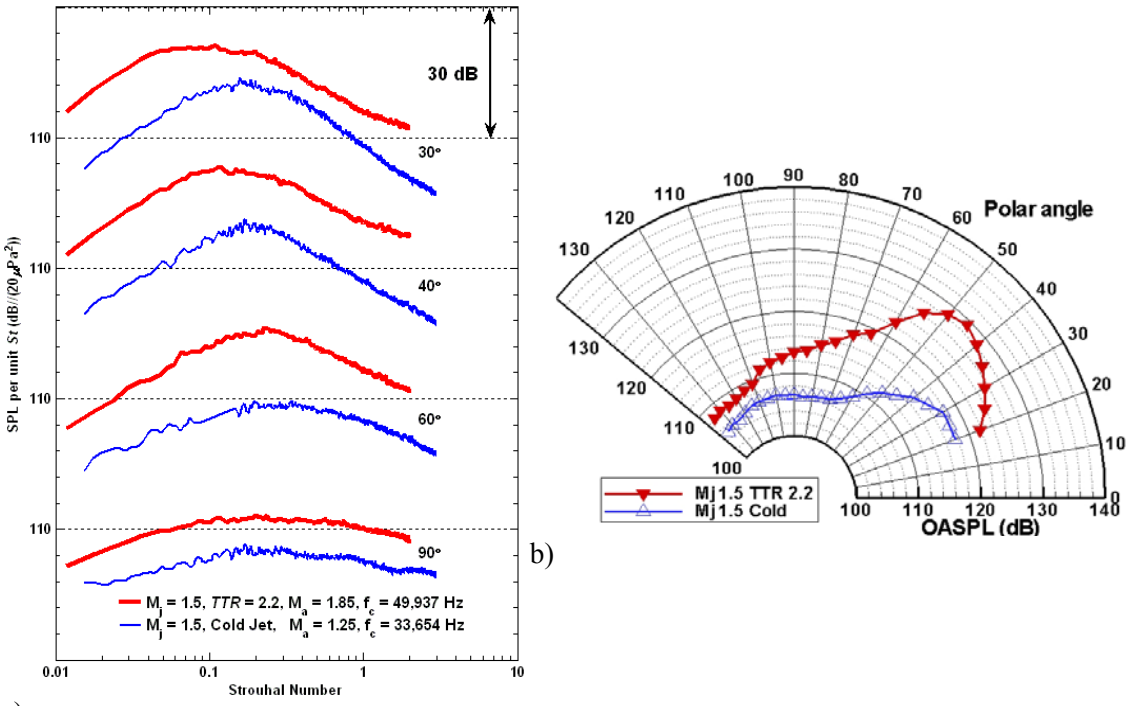

Figure **5-10**: Acoustic measurements from PSU conducted with CD nozzle (M_d = 1.5, D = 0.5 in.) accordingly operated at M_j = 1.5, *TTR* = 1 and 2.2 respectively, as measured at *R/D* = 140. a) Lossless spectra. b) Overall sound pressure level contour plot.

A different illustration is provided in a two dimensional map of the sound intensity field from acoustic measurements with microphones covering available polar angles and various radial locations. Sound intensity contour plots are shown in Figure **5-11** for three specific frequencies

for M_j = 1.5 cold and heated jets. The sound intensity contours are plotted by selecting the *SPL* at a specific frequency measured by the microphones at the locations represented by the black dots. Interpolation between these data points allow for the contours to be extrapolated. The selected representative frequencies correspond to a frequency below, at and above the peak frequency of the acoustic spectra shown in Figure **5-10**. For the heated jet case, the sound intensity contour presents a broad lobe centered around $\theta = 35°$ for $St = 0.08$, and this lobe rotates to larger polar angle with increase in frequency, up until $\theta = 45°$ for $St = 0.2$. The amplitude of that lobe also varies, being highest at the peak noise frequency, as should be expected. While the lobe of sound intensity for $St = 1$ still keeps the same shape, it slightly increases its polar angle of maximum amplitude again with increase in frequency. This means the lobes of these noise radiations display a similar pattern, but the amplitudes and dominant polar angle vary with frequency. Next, the cold jet case presents somewhat similar results, with lobes that do not rotate as much with frequency. The broadening of the peak amplitude lobe of cold jet case is noted for $St = 1$, which is consistent with the more omni-directional nature of the noise produced by fine scale turbulence.

Further, the variances of amplitudes and dominant polar angle of those similar patterns of noise radition can be referred by the acoustic Mach number M_a (U_j / a). The value of acoustic Mach number is strongly influenced by the jet temperature and less responsive to the nozzle pressure ratio. Thus the lobe amplitude is raised by the increasing acoustic Mach number M_a. The noise emission polar angle at a specific frequency component relates positively as a function of acoustic Mach number M_a. Noticeably, when the lobes of low frequency components of noise became more detectable due to the increase of the jet temperature, the low frequency components contribute a significant noise radiation.

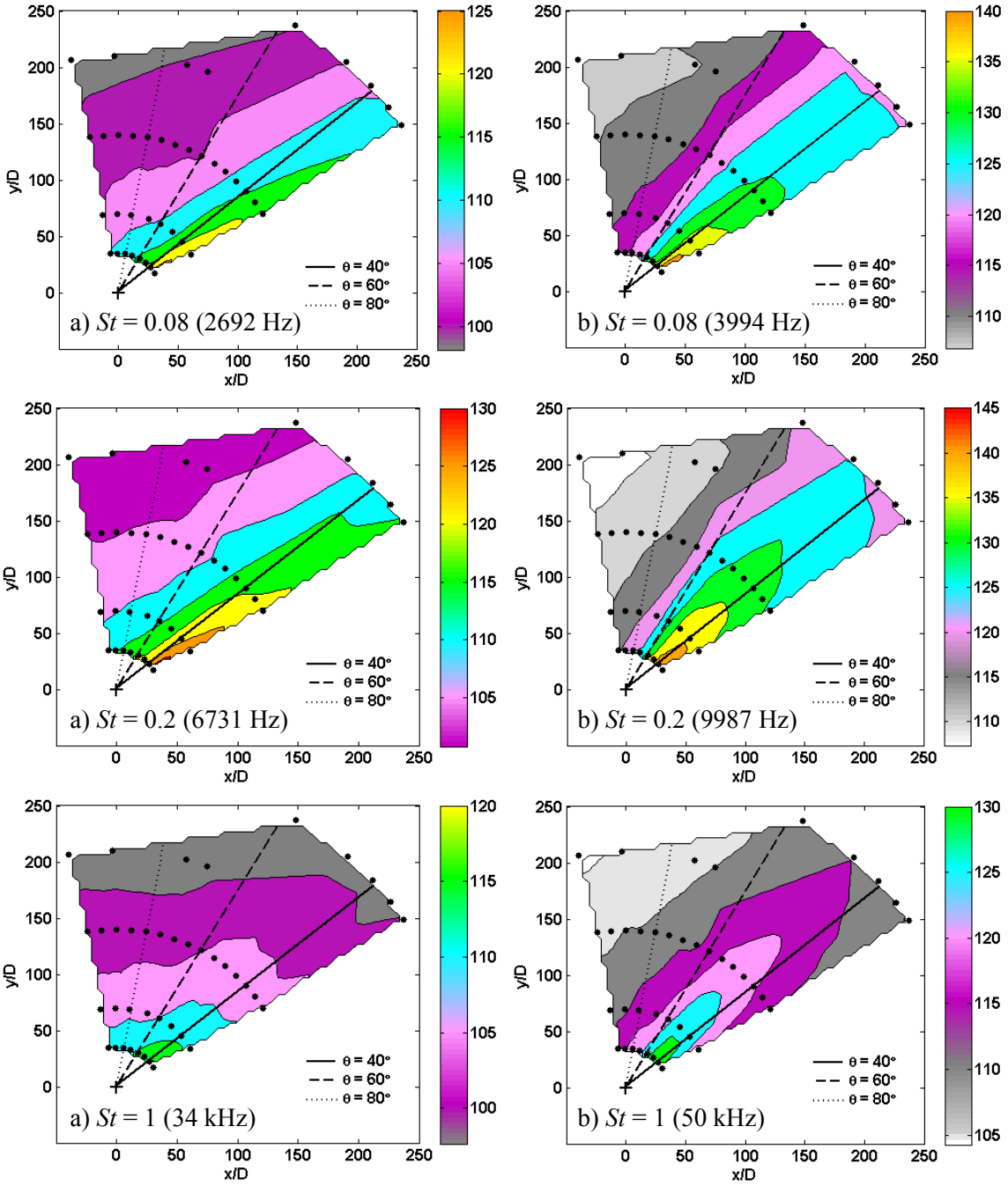

Figure **5-11**: Sound intensity contour plot in specific frequency content extracted from spectra with measurements conducted at M_j = 1.5 jets with a) *TTR* = 1. b) *TTR* = 2.2.

Low frequency noise emitting from farther downstream locations generates the inaccuracy on the measured microphone polar angle and propagation distance originated from the nozzle exit plane, this inaccuracy then leads to the discrepancy generated in the acoustic measurements measured at

various radial locations. Thus, the effect of the jet noise source distribution needs to be considered and involved in the processing methodology of the acoustic far-field measurements for correct interpretation of the measured acoustic spectra.

The observed rotation of the acoustic directivity with frequency can be explained from the turbulence measurements that suggest that the convection velocity of turbulent structures varies with frequency. Such measurements, based on cross-correlations within the jet, have been performed by Harper-Bourne [95], by Kerherve [96] and by Morris and Zaman [97] and demonstrate a relationship between the convection velocity and frequency. Similar experimental results from experiments performed at Penn State with an Optical Deflectometry (OD) setup are shown in Figure **5-12** for the cold M_j = 1.5 jet. Details of the setup are discussed in Veltin *et al.* [19]. The variation of convection velocity with frequency clearly follows the same distribution found by the investigators noted above. The same kind of distribution has been observed in jets of varying speeds (subsonic and supersonic) and temperature ratios. As a result, while the cold jet, of speed U_j = 1400 ft/s, has an overall convective Mach number that is subsonic, the high frequency content that approaches 0.8 times the jet speed has a convection velocity that becomes supersonic and therefore radiates Mach waves. This explains the lobe that appears at larger polar angle for the higher frequencies. For the heated case, most turbulent structures of different length scales travel supersonically, but at different speeds in different frequency regime, causing this rotation of the lobe with frequency observed from the acoustic field measurements. Especially for the low frequency noise radiating from a farther downstream location, since the threshold of sound traveling at supersonic speed reduces, a special method is necessary to carefully treat the low frequency noise component. In full-scale engine testing, people are eager to know the minimum measured radial distance in order to conduct accurate measurements and extrapolate measured data to another location for environmental noise evaluation or far-field noise prediction.

From studying the behavior of jet noise radiation patterns as a function of jets temperature, improved guidance can be provided to the ground-testing personnel.

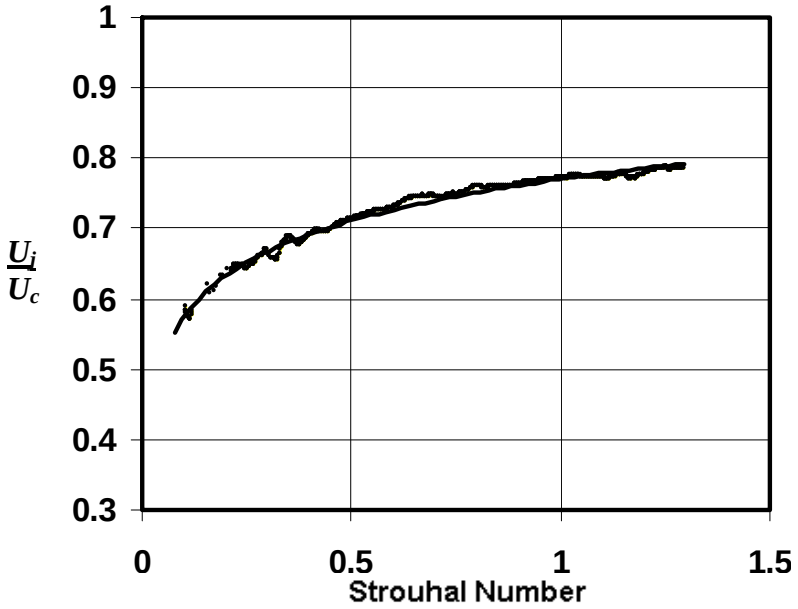

Figure **5-12**: Convection velocity as a function of *St* from the OD measurements conducted with CD nozzle (M_d = 1.5, *D* = 0.5 in.) operated at M_j = 1.5, *TTR* = 1 measured along nozzle lip line from *x/D* = 4 to 9.

In addition, the optical deflectometry turbulence measurements conducted with the cold pure air jet can be used to provide information on the noise generation region as a function of frequency content. Figure **5-13** presents autospectra of the optical signal measured along the lip line of the jet and at varying downstream locations *x*/*D* = 4 to 9 [19]. While these measurements are not sufficient to accurately measure the locus of the noise production region for each frequency component, they do highlight the fact that the highest frequency components are strongest at small downstream locations and the lower frequencies dominate further downstream. The peak of the autospectra shifts from roughly *St* = 0.6 at *x*/*D* = 5 to *St* = 0.1 or below at *x*/*D* = 9. The amplitude also monotonically increases, as is expected within the potential core of such a jet, and as mentioned by Bridges and Wernet [98]. From experimentally derived estimations [8], [99], the length of the potential core for this specific jet is around 7 *D* and the supersonic core length is

around 12 *D*. These measurements therefore conform to the assumption made for the noise source distribution presented earlier, in Figures **5-5** and **5-6**: the high frequency noise is mostly generated close to the nozzle exit and the low frequency noise is predominantly produced farther downstream.

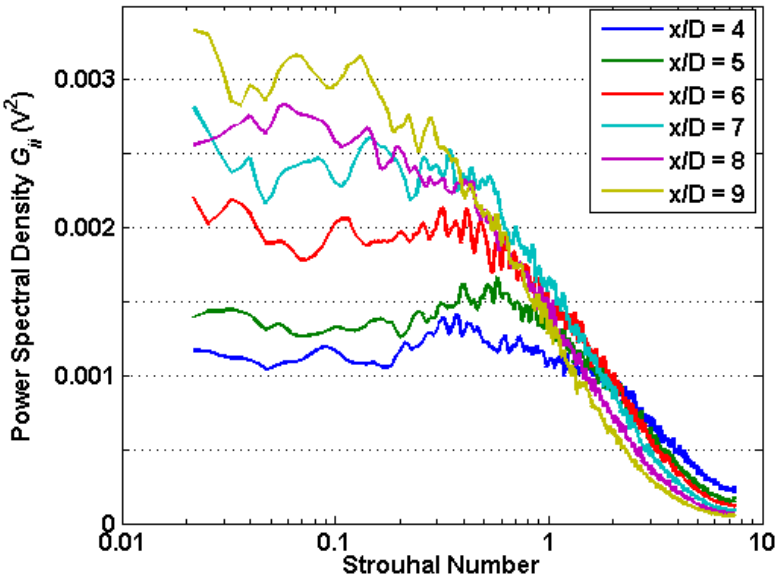

Figure **5-13**: Density fluctuation level as a function of *St* from the OD measurements conducted with CD nozzle (M_d = 1.5, D = 0.5 in.) operated at M_j = 1.5, TTR = 1 measured along nozzle lip line accordingly from x/D = 4 to 9.

5.3 Effect of jet noise source distribution

Following the discussion of jet noise directionality and spectra, attention is now paid to comparisons between measurements performed at different radial distances from the jet. The discrepancy appears when comparisons are made from the measurements conducted at various radial locations. This situation forces one to ask where the threshold distance of the acoustic far-field measurements is. As mentioned earlier, many researchers suggested the appropriate value of the threshold distance for acoustic far-field measurements. However, this scenario does not fit all

cases since the previous discussion has illustrateed that the noise source distribution that causes the comparison discrepancy changes with jet temperature and flow velocity. On the other hand, it is not easy to provide a properly estimated noise source locus as a function of frequency for the jets at specific operating conditions. Albeit under these circumstances, it is crucial to proceed with the jet noise source distribution correction for more accurate experimental results. An example shown below is a representative comparison with the frequency discrepancy that occurs when making comparisons with acoustic measurements conducted at various radial distances. Figure **5-14** presents the *OASPL* polar plot from the measurements acquired at R/D = 35, 70, and 140 for M_j jets with TTR = 1 and 2.2 respectively. As one can see there is almost exactly a 6 dB shift

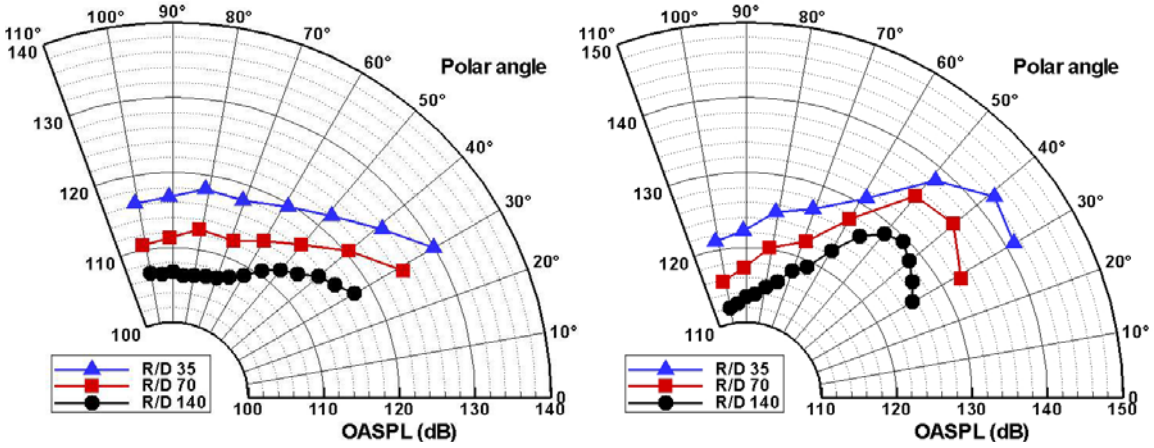

a) b)

Figure **5-14**: *OASPL* plot measured at R/D = 35, 70, and 140 for M_j = 1.5 jets respectively operated at a) TTR = 1. b) TTR = 2.2.

between the R/D = 70 and R/D = 140 measurements for the cold jet, and close to 6 dB between the R/D = 35 and R/D = 70 locations for the same jet. This suggests that the distance of 70 D is already far enough to be considered to be in the geometric far-field, meaning that spectra at any further location can be predicted using spherical spreading. However, for the heated (simulated) case, the linear spherical spreading approximation is inaccurate between R/D = 70 and R/D = 140:

the difference between the measured *OASPL* is not uniformly 6 dB. Particularly, there is an obvious shift in the peak noise emission direction which shifts from 40° at $R/D = 35$ to 45° at $R/D = 140$.

In a more detailed look, the corresponding spectra can be compared between measurements acquired at $R/D = 35$, 70, 140, and 280 for $\theta = 40°$ for the cold jet and $\theta = 50°$ for the heated case, as shown in Figure **5-15**. These polar angles where chosen since they are around the peak noise direction for the jets considered, which is where a small discrepancy in angular location relative to the noise source can induce large changes in the spectra. On the top part of each sub-plot the lossless spectra at each radial location are plotted. On the bottom part of part a) of Figure **5-15** (the cold jet condition) the spectra for $R/D = 35$, 70 and 140 are presented. Data from the two closest positions have been scaled to the distance $R/D = 140$ using linear propagation (assuming spherical spreading). Looking at part a) of Figure **5-15**, the collapse can be seen to be fairly good between all measured distances except the closest one ($R/D = 35$). The latter show some discrepancies as high as 6 dB at low frequencies, but still a good collapse at the high frequencies. This observation is consistent with the *OASPL* plot that suggested that the distance of 70 *D* was far enough to be considered as being in the geometric far-field. The fact that the high frequencies still match, even at the closest location with far-field locations, highlights the fact that these high frequencies are generated very close to the nozzle exit plane. The heat simulated jet spectra in part b) of Figure **5-15** show similar results, except that the best collapse is shown between the two furthest locations ($R/D = 140$ and 280). When these data at are compared they collapse within +/- 1 dB. Spectra measured at $R/D = 70$ or closer and propagated to $R/D = 140$ do not match as well with actual measurements at $R/D = 140$ or further. Discrepancies on the order of +/- 2 dB are found between the data from $R/D = 70$ to 140 and much greater if the data at $R/D = 35$ are compared to the further distances. The peak noise frequency for a given polar angle is also seen to shift to lower values further downstream. This heat simulated jet has a noise

production region which is extended more in the downstream direction of the jet, so it makes sense that the discrepancies are much higher than in the cold case. Once again, the high frequencies match much better, which highlights the fact that these are produced close to the nozzle exit plane.

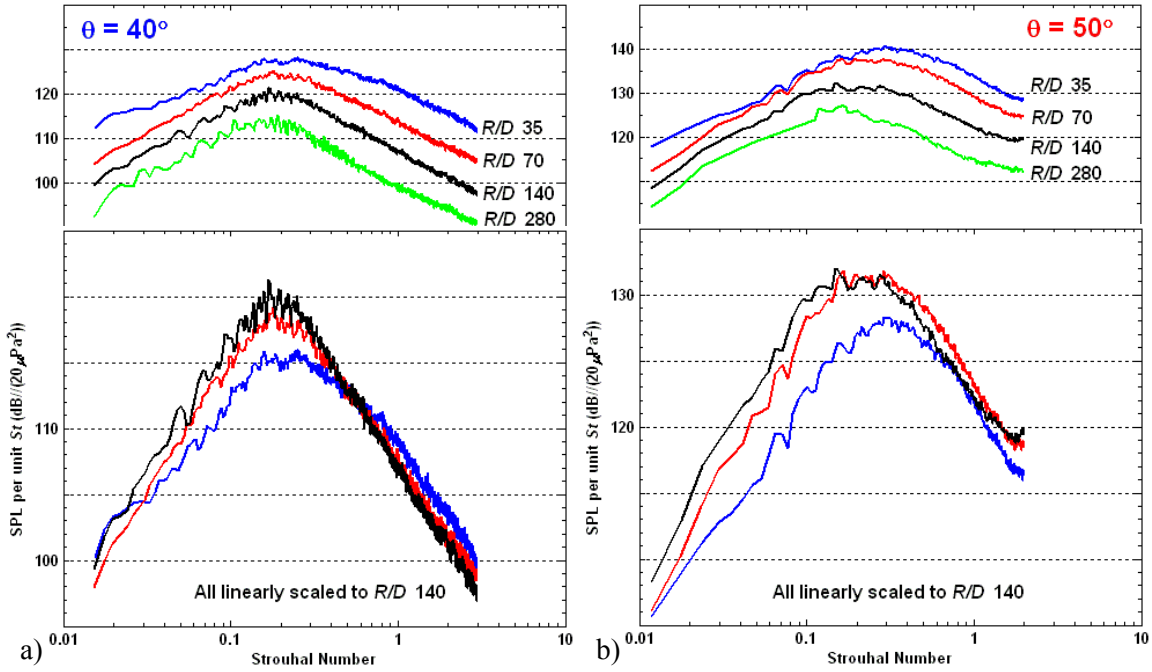

Figure **5-15**: Acoustic measurements conducted with CD nozzle (M_d = 1.5, D = 0.5 in.) as measured at R/D = 35, 70, 140, and 280, for M_j = 1.5 jets respectively operated at a) TTR = 1. b) TTR = 2.2.

5.3.1 Processing methodology on jet noise source distribution

In order to determine the effect of jet noise source distribution on acoustic far-field measurements, the processing methodology with the correction of jet noise source distribution is described below similar to the method proposed by Ahuja *et al.* [92]. The major portion of this processing methodology includes data on the distribution of peak noise emission locations. The first step, therefore, is to acquire a reasonably representative curve of the peak noise source locus

for the specific operating conditions. The experimental results conducted at UCI [74] presented in Figure **5-6** were selected for this purpose. These results were acquired by phased array microphones. There is a numerical estimation of the peak noise locus in Strouhal number for M_j = 1.5 cold and heated jets issuing from a CD nozzle with M_d = 1.5. The experimental conditions for the current study were selected as M_j = 1.5 cold and TTR = 2.2 jets issuing from a CD nozzle with M_d = 1.5. The numerical estimation of the peak noise locus can be described as:

$$x / D(St) = 5.1 - 7.3 \times \log_{10} St \qquad \textbf{5.1}$$

The next step is to choose a target array of microphones in the geometric far-field that will be used to produce estimates of synthesized spectra from the closer measurement array. Figure **5-16** shows how one position in the geometric far-field array relates to the closer acoustic field measurements. The empirical information on the noise source distribution is used to relate the measured spectra to the further distances from the jet. In doing so, there is some change in angular and radial position for the spectrum contents measured from microphones as a function of frequency. For each frequency, the distance and polar angle between each microphone in the acoustic field and the locus of the noise production region can be calculated. Thus for a given frequency band, there is a corrected polar angle θ_f and corrected distance R_f that represents the actual polar location and distance of the microphone with respect to the (estimated) noise source location. The closer the measurement microphones to the jet, the larger the discrepancy between the polar angle measured from the exit plane θ_m and θ_f. The distance of the microphone relative to the noise source also varies similarly. In order to exactly compare measurements performed at two different radial distances, the comparison should therefore be made between the microphone locations relative to the source, not relative to the exit of the jet. In doing so, the discrepancy of sound intensity level mismatch is solved. Obviously, since the source location is a function of frequency, this means that for each frequency band, a different value of θ_f should be matched. By

re-examining the correct sound propagation path for each frequency band, the discrepancy of downward peak frequency shift is solved after comparing the noise following the identical propagation path but measured at various propagation distances. Again, this is schematically represented in Figure **5-16**.

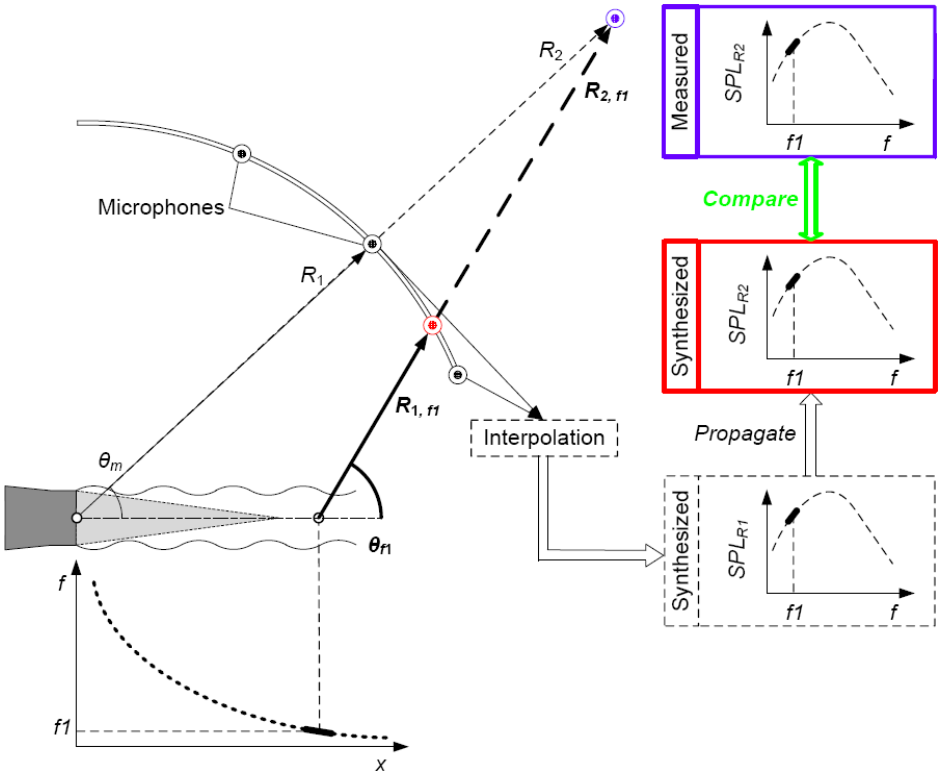

Figure **5-16**: Schematic diagram of the data processing procedure based on the noise source distribution locations for the acoustic measurements conducted at various radial distances.

For example, in order to project measurements conducted at 35 *D* to the geometric far-field position (at 140 *D*), the following steps are followed:

- Choose the geometric far-field radius and polar angle upon which to "project" the spectra from the closer measurement position spectra.
- Obtain for each frequency band the noise source location from the numerical estimation of the locus of peak noise.

- For each frequency band, find the values of $\theta_f = \theta_{f1} = \theta_{f2}$ and R_{1f} and $R_{2f} = R_{140D,f}$ corresponding to the measurement obtained at R_{140D}.
- For each frequency band, find the noise radiation path from the R_{140D} measurement to the R_{35D} measurement, and find the values of $R_{35D,f}$.
- Interpolate between the two closest measurements performed at R_{35D} to obtain a spectrum at the exact θ_f angle, and pick up the corresponding *SPL* for the specific frequency band.
- Assuming spherical propagation, correct the value of the pick-up *SPL* from $R_{35D,f}$ to the $R_{140D,f}$ distance.

This process can obviously be applied to any two radial distances R_1 and R_2, as summarized in Figure **5-16** and Figure **5-17**. Finally, while the whole process is described here with dimensional frequencies for clarity, it can obviously be extended to non-dimensional spectra expressed as a function of Strouhal number.

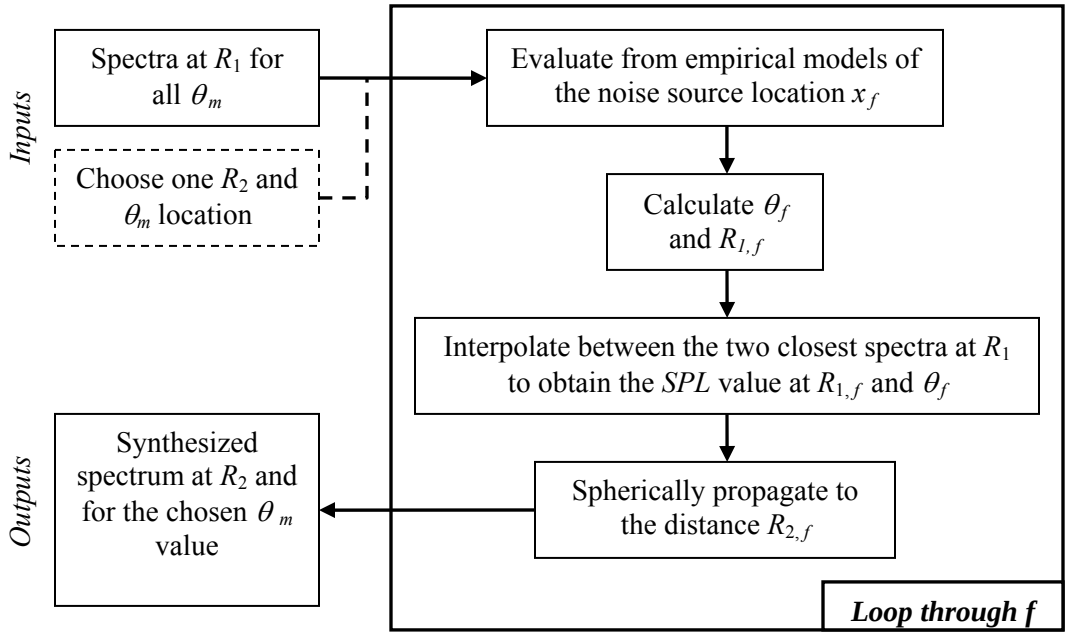

Figure **5-17**: Flow chart of the processing procedure of the jet noise source distribution on the acoustic measurements.

Correction is most useful at polar angles for which the sound pressure level shows large variations for small angular displacements (i.e. around the peak noise direction). In doing so, the spectra comparison across various measured radial distances can provide more accurate and useful results. The concept of this processing methodology is straightforward. The most important of all is still the locus of noise source distribution for certain operating condition. As mentioned earlier, many researchers studied noise source distribution locations via phased array microphone measurements. The following demonstration applied with this processing methodology has proven not only the processing methodology itself, but also the accuracy and fidelity of noise source locus from the experimental results of phased array microphones to be effective. This is quite encouraging since current results were generated under efforts from two different facilities. It also reveals and suggests that one can perform both measurements in a single facility to mutually validate experimental results and contribute to a useful jet noise data base.

5.3.2 Examination of synthesized spectra with noise source distribution correction

The synthesized spectra are now corrected for the distributed nature of the noise source as described in section **5.3.1**. The noise source distribution discussed earlier in Equation **5.1** is used as an underlying assumption for this processing. The measurements at R/D = 70 are first used in order to reproduce synthesized spectra at R/D = 140, and a comparison is made with the actual measurement obtained at R/D = 140. The results are presented in Figure **5-18** parts a) and b) for θ = 40° for the cold jet and θ = 50° for the heated case. These polar angles were chosen as representative cases since they are slightly away from the peak noise direction, which makes them the cases with largest spectral changes with small angular displacement. Similar results were obtained at other polar angles but are not presented here. Subplots a) and b) of the figure represent cases the most relevant to jet noise measurements: comparison between measurements

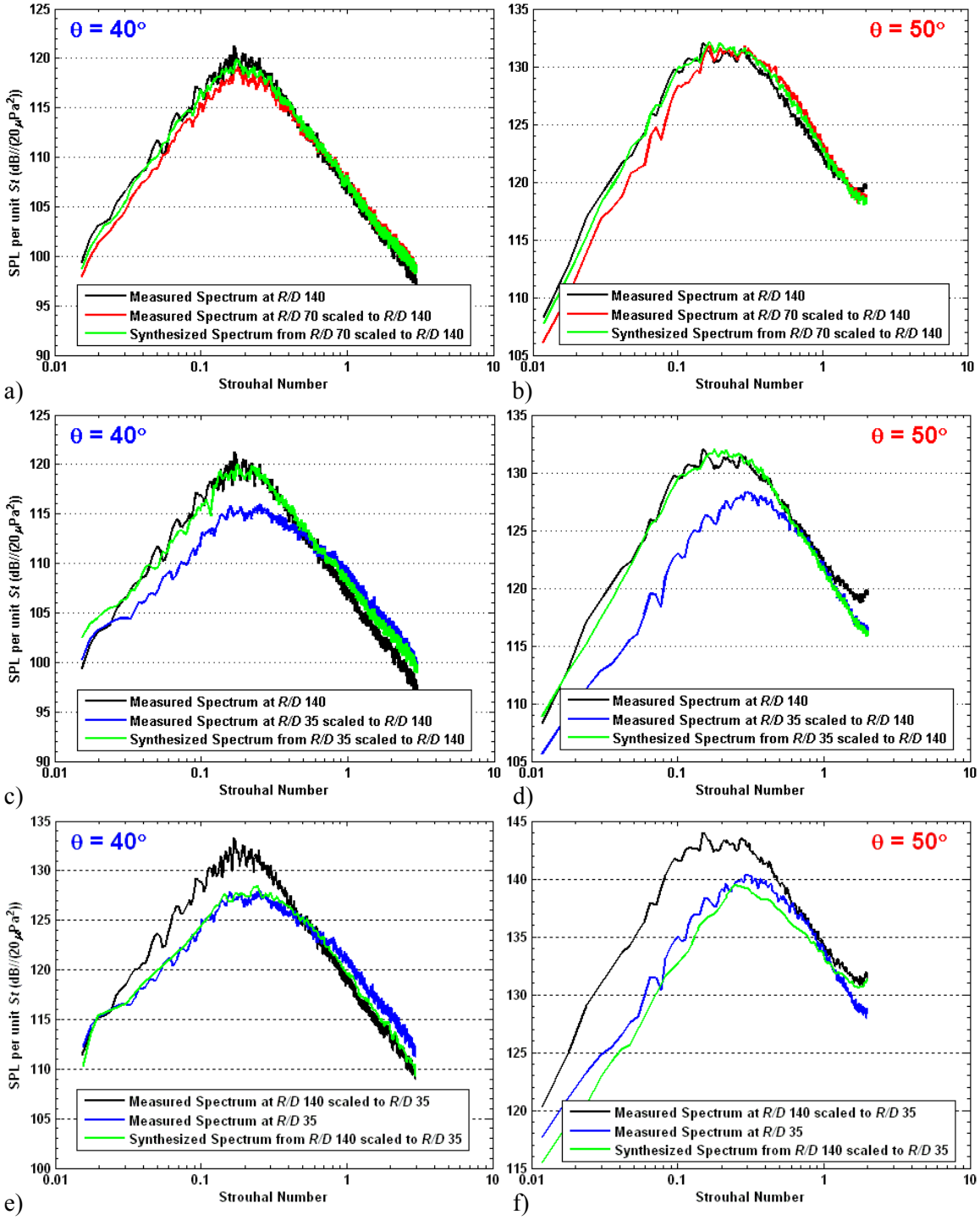

Figure **5-18**: Acoustic measurements conducted with CD nozzle (M_d = 1.5, D = 0.5 in.) operated at M_j = 1.5, TTR = 1 for left column and M_j = 1.5, TTR = 2.2 for right column and corrected with noise source distribution. a) and b) Spectra from R/D = 70 synthesized to R/D = 140. c) and d) Spectra from R/D = 35 synthesized to R/D = 140. e) and f) Spectra from R/D = 140 synthesized to R/D = 35.

obtained at 70 and 140 diameters from the jet exit plane. Its relevance is most important because many groups have published and still publish data measured with microphones located between 50 and 70 diameters. Three spectra are shown in each subplot: the actual spectra measured at R/D = 140 and the spectra measured and synthesized from the measurements at R/D = 70 that is supposedly predicted to represent the spectrum at R/D = 140. As can be seen for both angles and both *TTR* values, the agreement between the two measured spectra is not perfect, with about 1 dB discrepancy at most in the cold case and about 2 dB at low frequencies for the hot case. On the other hand, the synthesized spectra and the actual measurements match almost perfectly (within +/- 1 dB), allowing a much better comparison between measurements that are not quite in the geometric far-field (70 *D*) and others that are far enough to assume spherical spreading of the sound (140 *D*).

As a more extreme case, the same comparison can be made between measurements obtained at 35 and 140 diameters from the jet exit plane, as shown in part c) and d). This time, the discrepancies between the two non-dimensional distances are quite large, especially in the heated case with more than 5 dB differences at low frequencies. The spectra synthesized from the measurements at R/D = 35 in order to predict the spectra at R/D = 140 match with excellent agreement with the actual measurements at R/D = 140. The shift of the peak noise frequency has been completely corrected for, as well as the large discrepancies at the lower frequencies. Similar good results were observed for all polar angles. This provides a very good tool to be able, from measurements that are in the acoustic far-field but not in the geometric far-field, to predict the geometric far-field noise spectra. This kind of accurate projection is enormously useful for proper prediction of the environmental noise on the ground from flying aircraft predicted from propagation models that use the laboratory source measurement data.

Finally, part e) and f) demonstrates that this projection methodology can be applied in both directions: spectra measured at 140 D can be used to reconstruct the spectra that would be measured at R/D = 35. The large discrepancies are once again completely corrected for, providing near-perfect collapse of the spectra. As long as the noise source locus can be acquired accompanying the acoustic measurements covering appropriate polar angles, the spectrum at any selected location inside the acoustic field can be reasonably synthesized.

These results give confidence in both the validity of the methodology used and the accuracy of the noise source distribution used for the calculation. This strengthens the accuracy and understanding of scaling methodology when producing comparisons between measurements acquired at various nozzle diameters or from different facilities with disparate radial distances. It also demonstrates that for a highly heated jet, the beginning of the true geometric acoustic far-field is extended much further than R/D = 50, as previously mentioned.

5.4 Examination of nonlinear propagation effects with noise source distribution correction

Previous efforts made at Penn State [100] showed that there is an energy transfer from mid frequency content to high frequency content, causing the spectrum to lift at the high frequency end when the sound pressure levels in the acoustic field reach levels of approximately 135 dB. Re-examination of this result can be provided using the current methodology to observe the nonlinear propagation effect in a more accurate way. When investigating nonlinear propagation effects, measurements at different radial locations need to be conducted and compared. It typically means that two effects are then causing changes in the spectra: the nonlinear propagation and the effects due to the distributed nature of the noise sources. Gee *et al.* [101] have suggested that due to the effect of the jet noise source distribution these series of measurements may lead to inaccurate spectral comparisons and observations. The methodology

developed in the previous section can therefore be applied to effectively isolate the effects of nonlinear propagation from near-field/far-field effects. Based on the current understanding and demonstration of the jet noise source distribution, the following section proposes a way to assess the nonlinear propagation effect via the methodology developed above.

Figure **5-19** presents the spectra comparison measured at R/D = 35, 70, 140, and 280 for θ = 40°, and 70°. As one can see clearly, there is a trend of curve lifting in the high frequency end at θ = 40° for the measurements at R/D = 280. There are also large differences in the spectral shape at low frequencies, with a shift of the peak, but these are unlikely to be due to the effect of nonlinear propagation but rather to the distributed nature of the noise source. The corresponding values of the Morfey-Howell indicator of nonlinearity, defined in reference [68], were calculated to provide a quick and direct evidence for the appearance of nonlinearity in the frequency domain. (The positive or negative sign of the value of the nonlinearity indicator represents an energy gain or loss at that frequency content.) The nonlinearity indicator shows that there is an energy loss around mid frequencies and significant energy gain in high frequency regions for θ = 40° but not for θ = 70°. It is also noted that this high frequency lift-up is also evident in the hot jet θ = 50° at R/D = 140. The Mach wave radiation angle of the M_j = 1.5, TTR = 2.2 jets is around 40° calculated with $M_c \sim 0.7M_j$. Thus it is reasonable to observe the phenomena of the nonlinear propagation around θ = 40°, where the noise is significantly louder. Figure **5-20** presents the normalized pressure time histories for the measurements at R/D = 35, 70, 140, and 280 for θ = 40°. As one can see the pressure fluctuation time histories gradually show less zero crossings and well-described N shape like waveforms as the measured distances advance. This is evidence of nonlinear propagation in the time domain.

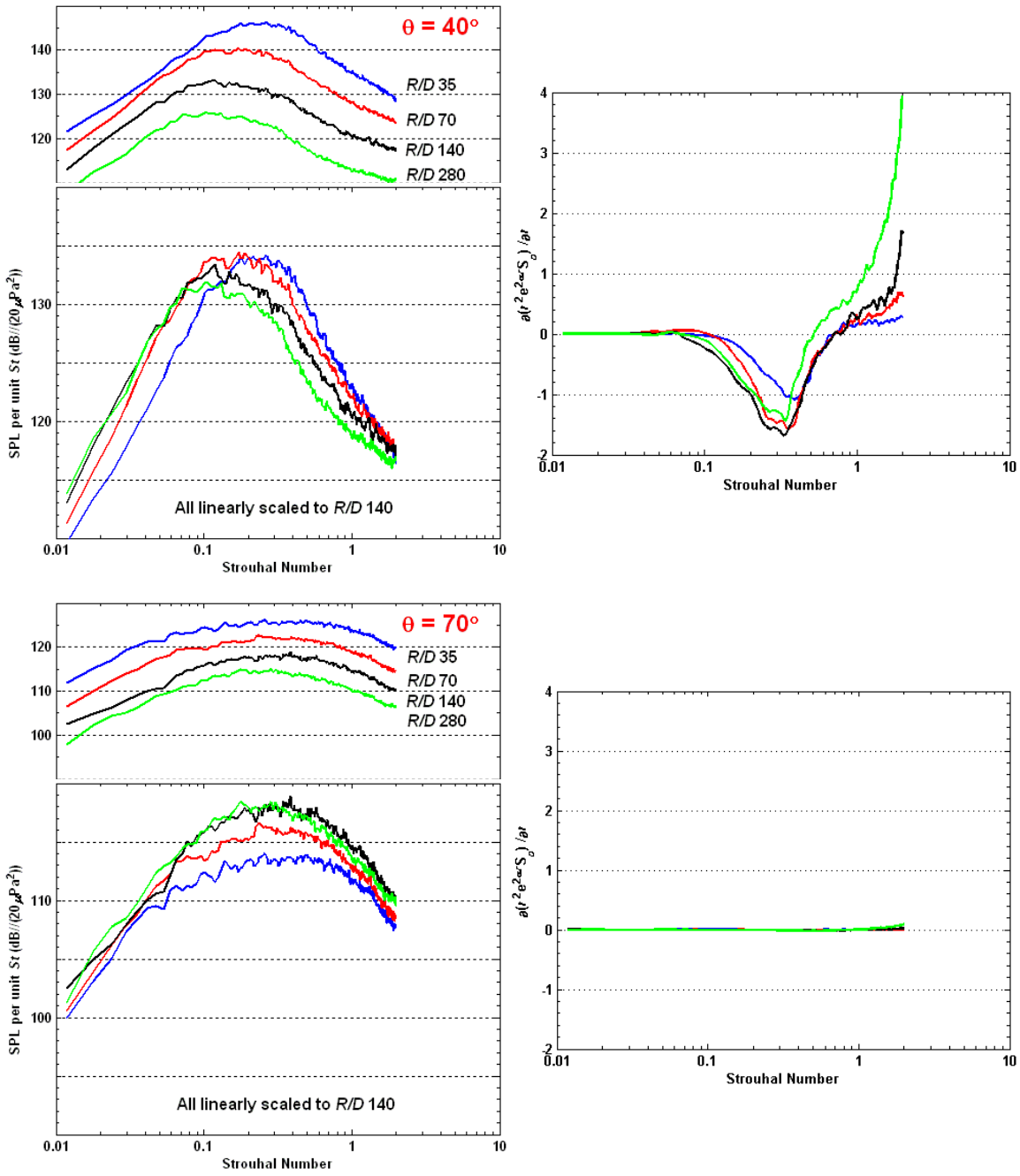

Figure **5-19**: Acoustic measurements conducted with CD nozzle (M_d = 1.5, D = 0.5 in.) operated at M_j = 1.5, TTR = 2.2, as measured at R/D = 35, 70, 140, and 280 for θ = 40°, and 70° and corresponding values of the Morfey-Howell indicator of nonlinearity.

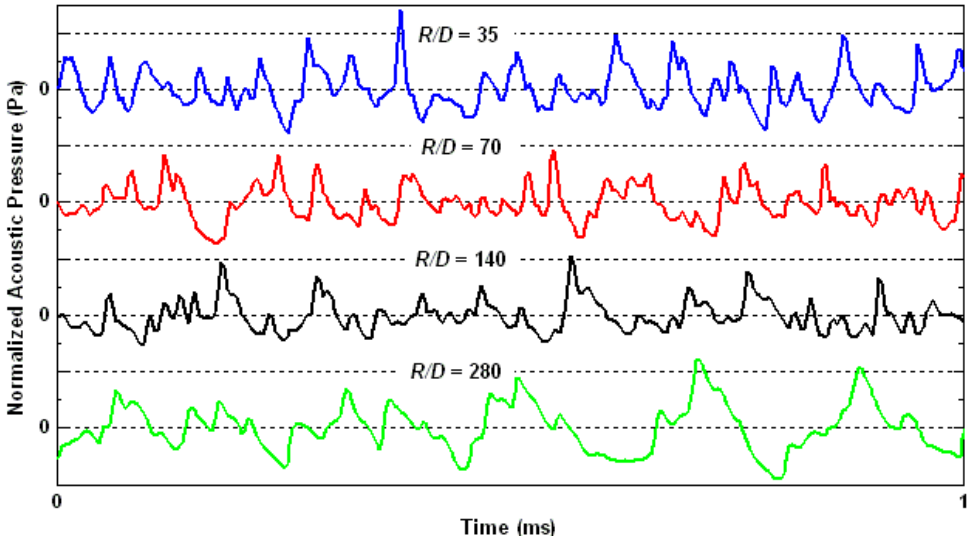

Figure **5-20**: Normalized pressure time histories from acoustic measurements conducted with CD nozzle (M_d = 1.5, D = 0.5 in.) operated at M_j = 1.5, TTR = 2.2, θ = 40°, at R/D = 35, 70, 140, and 280.

The methodology in applying the effect of jet noise source distribution to observe the nonlinear propagation effect is repeated again here. By first selecting one position of measurement at R/D = 280, the noise radiation angle and propagation path are calculated as a function of frequency from the locus of peak noise as shown in Figure **5-6** to this measured position. The corresponding sound intensity levels then can be collected from the identical radiation path across the measurements at R/D = 35, 70, and 140 as a function of frequency. In doing so, the synthesized spectra can be used for comparison as representative of measurements at R/D = 35, 70, and 140. Figure **5-21** presents the resultant spectra at four polar angles. Due to the lack of data at polar angle less than 30 degree for the measurements at R/D = 35 and 70, some synthesized spectra were unable to be generated. As one can see from the spectra comparison at θ = 36° and 41°, there is a close collapse for the spectra from the measurements at R/D = 70 and 140. The spectra from the measurements at R/D = 280 consistently show the energy loss across mid and high frequency content. For the spectra comparison at θ = 47° and 58°, the good collapse at low frequency content is within 1 dB deviation for all measurements. The high frequency end

in the spectra starts to perform a curve lifting as the values of R/D advances. The energy loss at the mid frequency content mostly only appears in the measurements of R/D = 280. These results distinctly present the trends from the Morfey-Howell indicator of nonlinearity where there is an energy loss in the mid frequency content transferred to the energy gain in the high frequency end. It is therefore quite promising in applying this methodology to observe the nonlinear propagation effect for detailed examinations.

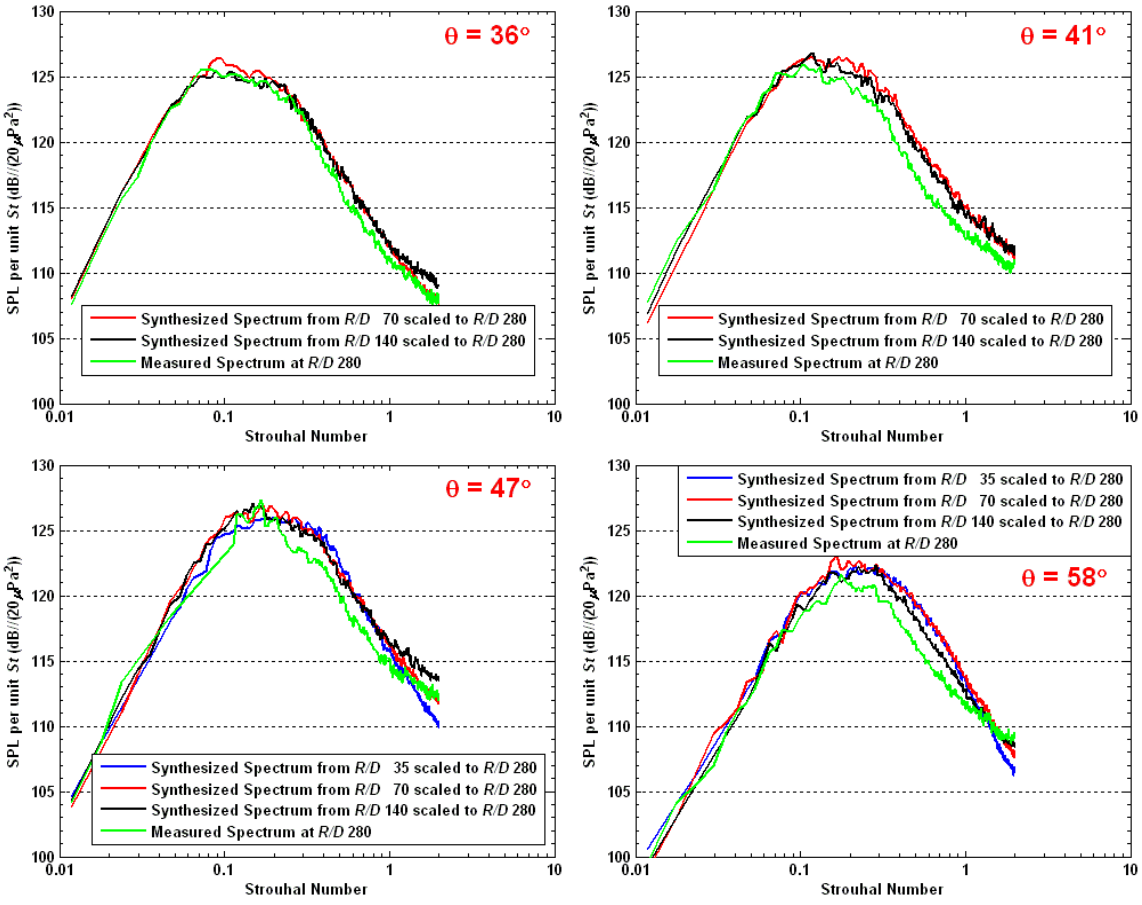

Figure **5-21**: Acoustic measurements conducted with CD nozzle (M_d = 1.5, D = 0.5 in.) operated at M_j = 1.5, TTR = 2.2, as measured R/D = 280. Synthesized spectra were reconstructed respectively from R/D = 35, 70, and 140 and scaled to R/D = 280.

5.5 Summary

In an effort to produce measurements that can be reliably used by other organizations and propagated to the far-field for noise prediction during an aircraft fly-over, laboratory measurements need to be representative of the true geometric far-field. The nature of jet noise is such that the noise source is distributed along the jet, with high frequency components being emitted closer to the nozzle exit and the low frequency components radiating from farther downstream with a dominant sound intensity level. The current study has looked at the details of the noise production regions within supersonic jets in order to better understand the source of the spectral mismatches between measurements conducted at various radial locations. Based on noise source location measurements by several investigators, a processing method with the noise source distribution correction has been developed to allow for a more accurate comparison of spectral measurements from vastly different distances from the nozzle exit plane. This processing methodology is especially critical for the acoustic measurements performed with heated supersonic jets.

Acoustic measurements conducted at four radial distances with fully expanded both cold and simulated hot jets have been used to demonstrate this processing methodology with the noise source distribution correction. Direct comparison of the experimental results demonstrated that measurements at the non-dimensional distance of 70 nozzle diameters do not produce the best accuracy to predict the geometric far-field. Discrepancies among the measurements acquired at various radial locations were observed and documented. By using reliable measurements of the jet noise source distribution [74], synthesized spectra were obtained from acoustic field measurements (35 to 70 diameters) to accurately reproduce measured spectra in the geometric far-field (140 diameters). This methodology strengthens the accuracy and understanding of

scaling methodology when making comparison with the measurements obtained from nozzles of different diameters or from different facilities with disparate radial distances of measured microphones. Moreover, it can be concluded without any doubt from these data that for very hot exhaust jets such as the one used on military aircraft, the threshold distance of the geometric far-field is located much further than the non-dimensional distance $R/D = 50$ used for subsonic cold jets.

The current methodology is extended to examine the nonlinear propagation effect which is another dedicated goal at Penn State. The phenomenon of the nonlinear propagation in the trial case is observed in the frequency domain by the Morfey-Howell nonlinearity indicator and in the time domain with the pressure time histories. For a detailed spectra comparison, the synthesized spectra provide a better accuracy in examining the identical noise radiation path with the appropriate propagation distance as a function of frequency content. The spectra comparison well depicts the energy loss in the mid frequency and the energy gain in the high frequency end of the spectra. It is therefore quite promising in applying this methodology to observe the nonlinear propagation effect for detailed examinations.

For a reasonable application of current proposed methodology, the estimated locus of peak noise emission of the jets at certain operating conditions is necessary. Since the peak emission direction changes with the operating jets conditions, the sound intensity contour depicted by the jet noise source changes as well. Meanwhile, for the jets operated at either over-expanded or under-expanded condition, there is an apprearance of shock-associated noise and this occurance may complicate the currently-adopted methodology. Nevertheless, the proposed methodology still successfully explains the causes of the existing discrepancy for the acoustic measurements acquired at various radial distances. The method can be hypothetically extended to measurements conducted with shock-containing jets. Presently, a single noise source location for each frequency band is the assumption imbedded in the processing methodology. To advance the

methodology, the possibility of adopting multiple noise source locations including turbulent mixing noise and shock-associated noise should be taken into consideration. However, more research is required from phased array microphone measurements on shock-containing jets to acquire the shock associated noise source distribution in jet shear layers depending on over-expanded or under-expanded jets conditions.

At the current development stage, the progress of the effect of jet noise source distribution on acoustic far-field measurements has been able to help on the development of extending acoustic data measured with small scale supersonic model jets to the noise prediction of the practical aircraft exhaust jets.

After demonstrating that the noise source distribution explains the causes of the existing discrepancy for the acoustic measurements acquired at various radial distances, the next chapter provides a noise reduction assessment on the small-scale military-style nozzle with chevrons.

Chapter 6

Advanced Acoustic Assessment of Small-Scale Military-Style Nozzles with Chevrons

6.1 Motivation

As communities pay more attention to the noise levels around airports, there is a strong need to reduce noise generated by military aircraft. Therefore, noise suppression mechanisms are being widely investigated and have led to the recent emergence of new nozzle design concepts such as chevron nozzles, and non-axisymmetric geometries. As new military aircraft are being developed, their enhanced capabilities are usually closely linked to larger noise signatures, rendering them dangerous for ground crews and failing to meet the noise regulations of some countries.

The high-speed jet noise laboratory at The Pennsylvania State University (PSU) has contributed to the studies of jet noise source generation and suppression mechanisms for several years. Recently, studies have concentrated on noise reduction concepts and more accurate representations of military aircraft jets, such as the investigation of the potential benefits of a beveled nozzle [102] or measurements conducted with a rectangular nozzle with thrust vectoring [103]. The current study focuses on another noise reduction application, the addition of chevrons to the nozzle. The testing candidate is a replica of the nozzle installed on F-18 fighter aircraft. This military-style nozzle is composed of multi-facetted straight sections in both the convergent and divergent parts of the nozzle as mentioned previously. The metallic plates forming this inner geometry can slide between each other and allow for control of the area ratio between the throat and the exit plane. Chevrons, with varying degrees of penetration into the flow, attached at the lip

of the nozzle exit, are being designed to reduce the noise production. The present study follows the previously mentioned project on investigating the validity of a scaling methodology that facilitates using small scale experiments to predict aeroacoustic performance of moderate scale supersonic jets. The present investigation extends this first round of measurements by providing advanced acoustic assessment on small-scale military-style nozzles with chevrons.

The first step is to understand the characteristics of the flow field inside a jet before studying the acoustic far-field noise radiated from the turbulence in the noise generation regions of a jet issued from a nozzle. Some efforts [104]-[108] have been made showing the characteristics of turbulence existing in the noise production regions of a jet. The characteristics of turbulence distinguish the noise generation regions of a jet and helps in the methodology of noise source prediction [8]. During a study on the effect of boundary layer thickness on jet spreading, Bradbury and Khadem [109] surprisingly found that inserting a small rectangular tab in the nozzle exit plane can induce a profound effect on jet spreading. This circumferential asymmetry at the nozzle exit plane causes faster decay of the jet centerline velocity, higher turbulent intensity level and entrainment, and gross distortion in the radial jet cross-stream plane. Though the initial flow structure is distorted, the flow development ultimately returns to an axisymmetric self-preserving jet at farther downstream locations. Except for the jet distortion induced by tabs, the pioneering study [46] (stemming from the Concorde project) discusses the jet plumes issued from a notched nozzle which is obtained by cutting V-shaped notches from the nozzle exit edge. The most prominent flow-field modification is the counter-rotating streamwise vortices shed from the notch edge of a nozzle that grow gradually in the downstream direction in a similar fashion to the flow field on the leading edges of delta wings. The jet plume cross-stream section is modified by the lateral jet development in the notch plane for as long as 20 nozzle diameters downstream and this induces lateral momentum transport that results in a faster decay of the jet centerline velocity. It was also demonstrated that there is a tendency to modify the

shock cell structure due to the presence of the notch. Wlezien and Kibens [110] demonstrated the effect of nozzle asymmetry on the acoustic far-field measurements and found that the nozzle asymmetry can lead to asymmetric shock structures which can also suppress screech.

For higher speed (and Mach number) jets, compressibility effects emerge and significantly reduce the growth of the free shear layer causing slower jet spreading [111]. On the other hand, the decay of the jet centerline velocity is a good indicator of the jet spreading. Thus the additionally induced streamwise vortices from the nozzle exit are found to cause a faster decay of jet centerline velocity, higher jet spreading, and enhanced jet mixing [112]-[115]. The vortices entrain more ambient low speed flow than usual into the high speed core-stream causing additional lateral jet development. The lateral jet development significantly alters the axial jet evolution and causes a lateral momentum transfer. Knowles and Saddington [116] provide a review categorizing nozzle varieties for more detailed information on jet mixing enhancement applications for aircraft propulsion.

Since the induced streamwise vortices generated by a chevron nozzle can effectively increase the jet spreading and distort the jet cross-stream development [117], [118], it is necessary to understand the modified flow field and corresponding acoustic benefits. Callender *et al.* [119] presented the observed acoustic far-field trends from measurements conducted with a chevron nozzle: effective low frequency noise reduction and often a high frequency noise penalty. The investigation [120], [121] on flow turbulence intensity shows that chevrons modify the flow turbulence distribution and shift the peak of turbulent kinetic energy upstream. A parametric study on chevrons [48] and a characterization of their performance [122] further provides more detailed information on the effect of chevrons. The amount of penetration of the chevrons in the flow has a major impact on the flow structure and acoustic far-field because it alters the intensity of the streamwise vortices. A direct relation was found between the peak streamwise vorticity intensity and the penetration of the chevrons [123]. Other parameters also have some influences,

such as the number of chevrons that results in a variation of the spacing between neighboring vortices and a sentivity of azimuthal directivity.

The current study focuses on the effects of chevrons of various geometries on the noise produced by military style nozzles under different flow configurations. Measurements performed in the Pennsylvania State University small scale jet noise facility allow for reliable and inexpensive measurements that, early in the design process, can help in the selection of the most promising designs before full-scale production and testing. The following study involves comparisons of chevron nozzle experiments with similar experiments conducted at the NASA Glenn Research Center with nozzles approximately 7 times larger in size. In doing so it is necessary to adopt the convention developed by Henderson and Bridges [51], of characterizing the chevrons by three parameters: width, length, and penetration. This chapter summarizes the results of a series of measurements that demonstrate the effects of chevrons on supersonic jets operating at various conditions of under-expanded, perfectly expanded, and over-expanded pressure ratios. A specific goal is to investigate the conditions, and the chevron designs, at which scaling the results of the experiments to moderate scale (NASA size jets) works well. This study also identifies the conditions for which the scaling to moderate size does not work well and investigates the causes of the discrepancies.

This study presents the experimental results conducted predominantly with military style nozzles representative of the exhaust of aircraft engines of the GE F414 family. (One experiment included here was performed with a contoured, purely converging nozzle with and without chevrons.) The exact inner contours of the military style nozzles were provided by General Electric Aviation Co. under an ongoing contract for the Strategic Environmental Research and Development Program (SERDP) as mentioned earlier. Such military engines possess nozzles with variable geometry, adapting to different flight regimes. However, for this specific research, three nozzles with different exit-to-throat area ratios were used, as specified by GE Aviation. These

nozzles were designed with a multi-faceted (12 segments) inside conical contour. At Penn State, the nozzles were fabricated via rapid prototyping techniques (stereolithography with Accura 50 giving 0.004" (0.102 mm) layer thickness and fused deposition modeling with ABS plastic giving 0.01" (0.254 mm) standard layer thickness). Nozzles of identical inner geometry but seven times larger were tested at NASA GRC for moderate scale experiments. These military style supersonic nozzles (GE nozzles) were built with the identical inner geometry at small and moderate scale to demonstrate the scaling of small heat simulated jets to moderate and full size jets. In general, the diverging portion of the flow contour consists of 12 flat segments that are interleaved to facilitate area adjustment of the operational nozzles. Unlike well designed contoured CD nozzles, pressure differences at the nozzle exit plane result in a plume with weak shock cells, even at pressure conditions that match the area ratio.

The chevron configurations were designed and provided partly by General Electric Aviation and partly by NASA Glenn Research Center [51]. From a large pool of possible chevron choices three designs were chosen, for three different Mach number nozzles, all of which are summarized in Table **6-1** in terms of the non-dimensional chevron parameters: penetration, length and width. Three chevron configurations were selected for the measurements in the current study. The chevrons extend from the nozzle exit plane of the baseline nozzles with one chevron per facet (totaling 12). These are shown schematically in Figure **6-1**. In the study of supersonic jets, the nozzle exit diameter is commonly used to normalize the length of shock cells and jets' downstream locations. As noted earlier and in Table **6-1**, the nozzle referred to as $M_d = 1$ was a purely contoured converging, axisymmetric nozzle whose 8 chevrons had no penetration at all. Table **6-1** also includes the corresponding properties of the NASA nozzles used in their chevron experiments [51], the results of which are used in general comparisons.

Table **6-1**: Nozzle parameters and jet operation conditions for data shown in figures.

	Nozzle Parameters						Jet Operation Conditions		
	M_d	D (inch)	Chevron Counts	Penetration	Length	Width	M_j / TTR	Re X 10^{-6}	Fig. No.
Penn State	1.0	1	8	0	0.25 D	0.4 D	1.5 / 1	1.5	**6-2**
	1.5	0.676	12	0.05 D	0.23 D	0.2 D	1.64 / 1	1.2	**6-7**
							1.64 / 3	0.7	**6-9**
	1.65	0.708	12	0.12 D	0.35 D	0.2 D	1.47 / 1	0.9	**6-10**
							1.47 / 3	0.5	**6-11**
NASA GRC	1.5	4.84	Baseline nozzle				1.64 / 1	8.5	**6-6**
							1.64 / 3	2.1	**6-8**
	1.65	5.07					1.47 / 1	6.6	**6-15** a)
							1.47 / 3	1.7	**6-15** b)
	1.65	5.07	12	0.12 D	0.35 D	0.2 D	1.47 / 3	1.7	**6-12**
	Parameter range of chevrons used at NASA GRC [51]			0.06 D | 0.12 D	0.15 D | 0.35 D	0.12 D | 0.2 D			

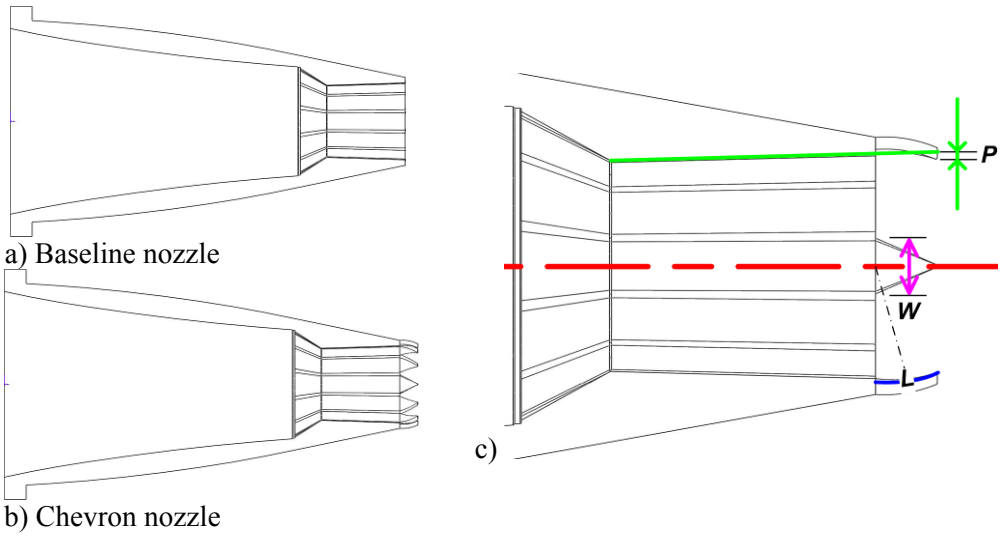

a) Baseline nozzle

b) Chevron nozzle

c)

Figure **6-1**: Schematic of military-style nozzle. a) Baseline nozzle. b) Chevron nozzle. c) Definition of chevron parameters [51].

6.2 Converging chevron nozzle with chevrons possessing no penetration

The major effect of chevrons on a jet flow is the generation of counter-rotating pairs of streamwise vortices. For a chevron nozzle to effectively induce these streamwise vortices, there needs to be a favorable pressure gradient between the core of the jet and the ambient flow. More precisely, it has been shown experimentally [113] that a significant pressure gradient must exist between the outer and inner side of the chevron to effectively produce these streamwise vortices. A series of measurements have been performed at NASA Glenn [48], [122] with a converging nozzle with chevrons designed with various penetration angles. These experimental data show that nozzles with chevrons at no penetration angle fail to generate the desired vortices in subsonic jets, resulting in no substantial difference in the acoustic measurements when compared to the baseline nozzle, with no chevrons. Similar acoustic measurements were conducted at Penn State with two purely converging nozzles of 1 inch exit diameter but differerent nozzle exit geometries (as shown in Figure **2-5**): one with round nozzle exit and another with 8 chevrons shaped in the nozzle exit, resulting in chevrons with no penetration. Acoustic measurements (not shown) performed with cold sonic (M_j = 1.0) jets exhausting from both these nozzles showed no acoustic difference, in agreement with the NASA results [48], [122].

Under-expanded supersonic jets, however, are bound to exhibit a significant pressure gradient at the nozzle exit, which should result in significant production of streamwise vortices, and therefore in noise reduction. Acoustic spectra were therefore measured at a range of polar angles for this nozzle operated in an under-expanded cold jet condition (with M_j = 1.5), with and without zero penetration chevrons. The resulting comparison is shown in Figure **6-2** for a representative number of polar angles. Focusing first on the large scale turbulence mixing noise, there is a very clear noise reduction measured with the chevrons, when compared to the baseline nozzle. As much as 2 dB reduction can be observed in the peak noise direction (around 30°)

across the entire frequency range. This is in accordance with an enhanced mixing of the jet, resulting in a break-up of the largest structures. This mixing noise reduction corresponds to an enhanced mixing with the surrounding air, as can also be observed from the schlieren images in Figure **6-3**. Indeed, the jet spreading angle is clearly enhanced with the chevron nozzle, with obviously some differences between the tip and the notch plane. Since the jets are strongly under-expanded, shock associated noise is also present in the spectra (and the shock cells are clearly visible in the schlieren images).

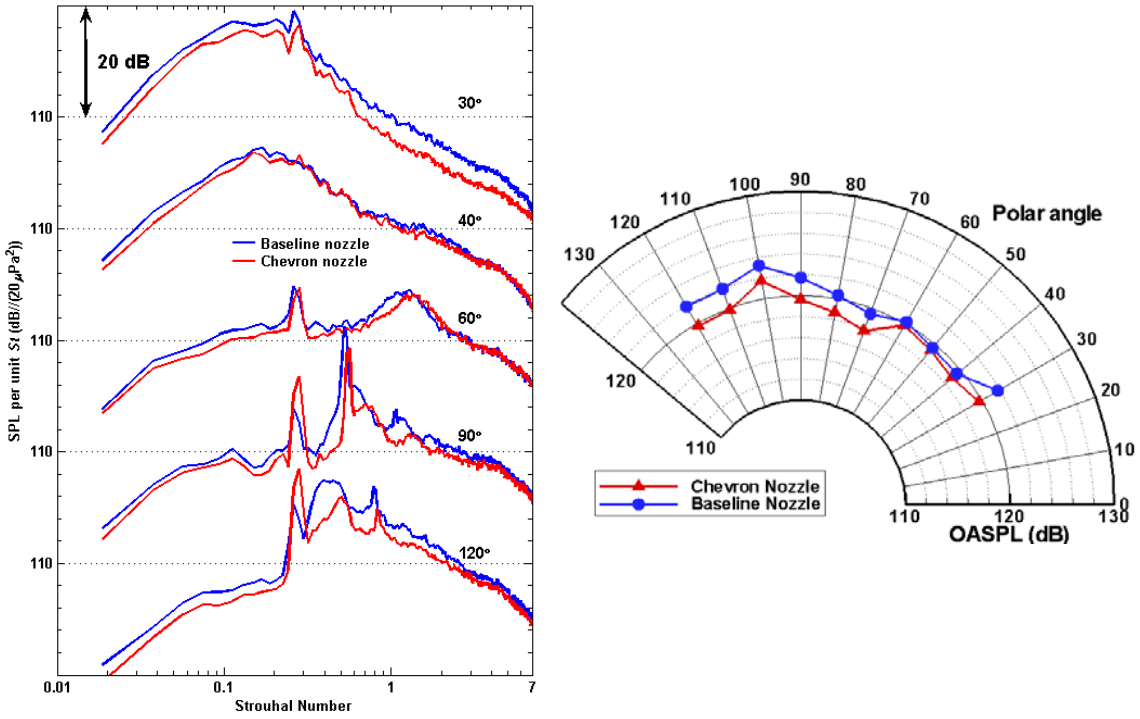

Figure **6-2**: Acoustic spectra conducted with M_d = 1.0 nozzle and chevron nozzle, operating at M_j = 1.5, cold, scaled to *R/D* 100.

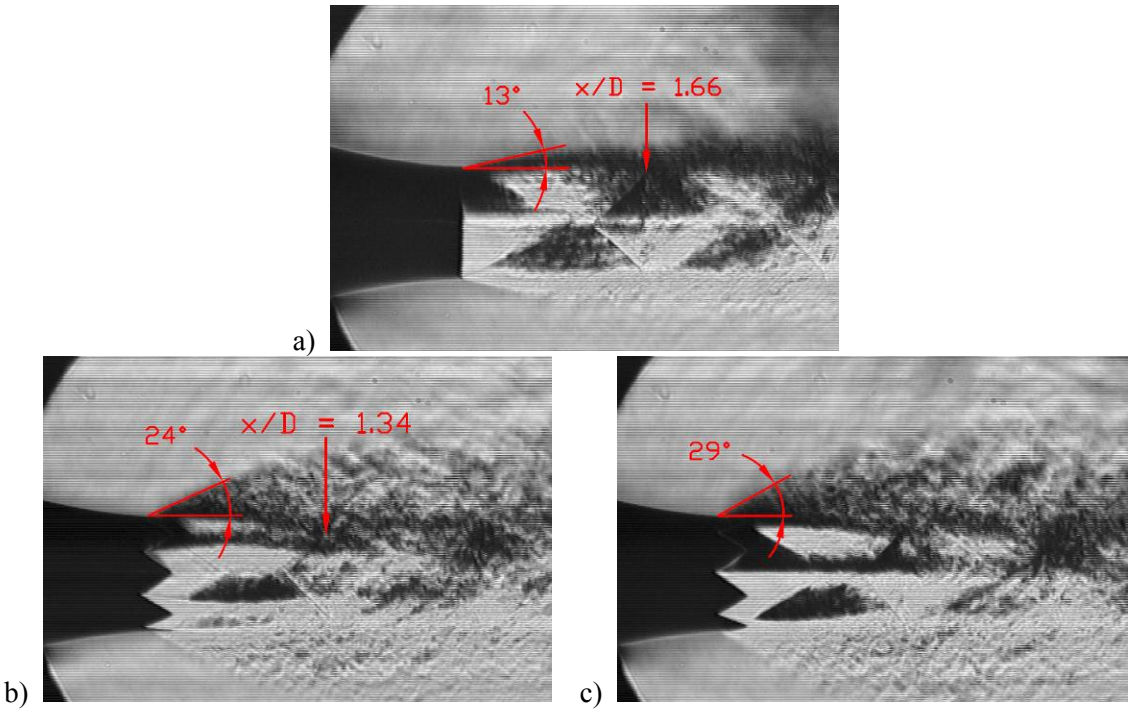

Figure **6-3**: Schlieren visualization from the measurements operated at M_j = 1.5, cold jets respectively conducted with M_d = 1.0 nozzle. a) Baseline nozzle. b) Chevron nozzle measured at tip plane. c) Chevron nozzle measured at notch plane.

Screech tones appear in the acoustic measurements from both nozzles. The second mode of screech, dominates the sideline direction, and the first mode of screech, dominates the upstream direction, with a similar trend in the measurements from both nozzles. The peak screech frequency is slightly higher for the measurements with the chevron nozzle, suggesting a slight shrinking of the shock cells. This can be confirmed by the Schlieren visualization, which shows that the shock length is reduced from 1.66 *D* to 1.34 *D* between the baseline nozzle and the chevron configuration. A similar trend can be observed for the peak frequency of broadband shock-associated noise (BBSAN): it shifts to higher values for the chevron nozzle. The magnitude of BBSAN is also substantially reduced with the chevron nozzle, suggesting that the shock strength has been reduced (which corresponds to shallower angles of the oblique shocks and therefore smaller shock cells). Overall, when examining the *OASPL* values from both of these nozzles, shown in Figure **6-2**, the 2 dB noise reduction already observed at the peak noise

emission on the sound pressure level can be generalized to the *OASPL* reduction across all polar angles. These simple measurements demonstrate that while the penetration angle of the chevrons are indeed important to ensure they result in a reduced emitted noise, the nozzle operating condition is equally important. The outflow from the nozzle lip can have an outward orientation (for under-expanded jets), resulting in an increased effective penetration of the chevron, and therefore enhanced mixing and noise reduction.

6.3 Military-style CD chevron nozzle with chevrons possessing low penetration

Most nozzles are operated off-design, with a Nozzle Pressure Ratio (*NPR*) that leads to a free-jet Mach number M_j different from the nozzle design Mach number M_d. Depending on the off-balanced condition; three classes of jets are defined: over-expanded, under-expanded, and highly under-expanded jets. In practical applications, jets are never fully expanded, even though this condition is achievable in laboratories with careful design of the nozzles and control of the NPR. Unbalanced jets typically exhibit strong pressure gradients at the exit plane of the nozzle, that lead to flow field structures different from a simple conical jet. The appearance of shock cells has a strong influence, not only on the acoustic signature of the jet, but also on the physical shape of the jet flow. Even with a simplified convergent-divergent (CD) nozzle, the shape of the jet mixing layer is significantly altered with varying operating condition, and this can in turn affect the performance of chevrons on the flow. To illustrate this, Figure **6-4** presents Schlieren images visualized with the military-style nozzle possessing a design Mach number of 1.5 operated at M_j = 1.3, 1.5, 1.7, and 1.9, respectively. One can see that the supersonic jet mixing layer at the nozzle exit is slightly altered from inward at M_j = 1.3 to parallel to the jet centerline at M_j = 1.5. The mixing layer exhibits a clear barrel shape as the jet operating condition is raised above the designed nozzle condition. Therefore, for a nozzle with chevrons, of a specific penetration angle,

the effective penetration of the chevrons in the flow will depend on the jet operating condition. A specific chevron design may therefore be more or less efficient at producing the best acoustic benefit during various flight regimes. For a representative visualization of the **over-expanded jets**, Figure **6-5** shows Schlieren visualizations conducted with the military-style baseline nozzle and the chevron nozzle operated at M_j = 1.3 (over-expanded jet condition). The expected effect of excess jets spreading, described in the previous section, is not visible: the chevrons do not provide the enhanced mixing they were designed to. The chevrons on this nozzle are of low penetration in comparison with the range of penetrations defined by Henderson and Bridges [51]. A higher penetration would undoubtedly affect the jet flow and subsequently have a measurable effect on the jet noise. However, this highlights the fact that one chevron design will not provide an optimal noise benefit at all operating conditions. This should be kept in mind before recommending one specific design.

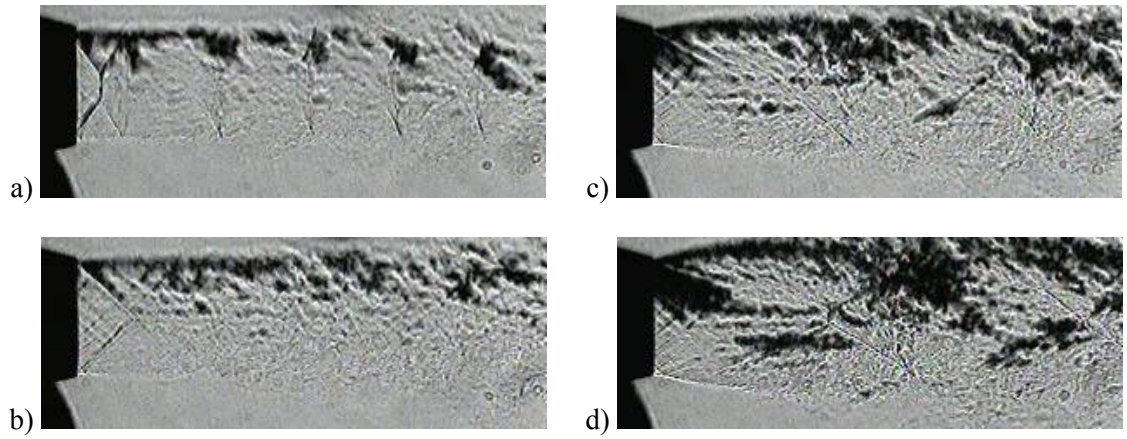

Figure **6-4**: Schlieren images conducted with GE M_d 1.5 baseline nozzles respectively operated at cold jet with M_j at a) 1.3. b) 1.5. c) 1.7. d) 1.9.

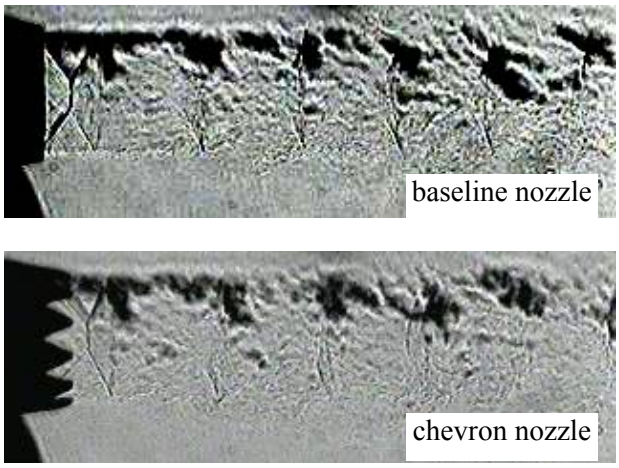

Figure **6-5**: Schlieren images conducted with GE M_d 1.5 baseline nozzle and chevron nozzle operated at M_j = 1.3, cold.

Reasonable success with the chevrons was achieved with the same M_d =1.5 GE nozzle with the chevrons with low penetration angle, this time operating at the **under-expanded** jet Mach number of M_j =1.64. Figure **6-6** first shows the spectral comparison from the measurements conducted with small scale baseline nozzle (D = 0.7 in.) at Penn State and moderate scale baseline nozzle (D = 4.8 in.) at NASA GRC (both with no chevrons). This comparison demonstrates the capability of the acoustic measurements conducted in small scale supersonic jets at Penn State to reasonably well replicate similar measurements at moderate (NASA) scale. How well the small scale jets replicate the moderate-scale jets with chevrons is discussed later. Spectra recorded at a range of polar angles are shown in Figure **6-7**, with direct comparison between the small-scale chevron nozzle jet and the baseline identical nozzle jet (without chevrons). Figure **6-7** presents spectra recorded with pure air cold M_j =1.64 jet and they show substantial levels of noise reduction. Most of the noise reduction is experienced in the downstream arc, in the maximum noise emission direction. That is consistent with the observations from the last section, with noise reductions being dominant for the large scale turbulence noise part of the generated sound. The BBSAN also follows the same trend as previously observed: there is a shift in the peak BBSAN

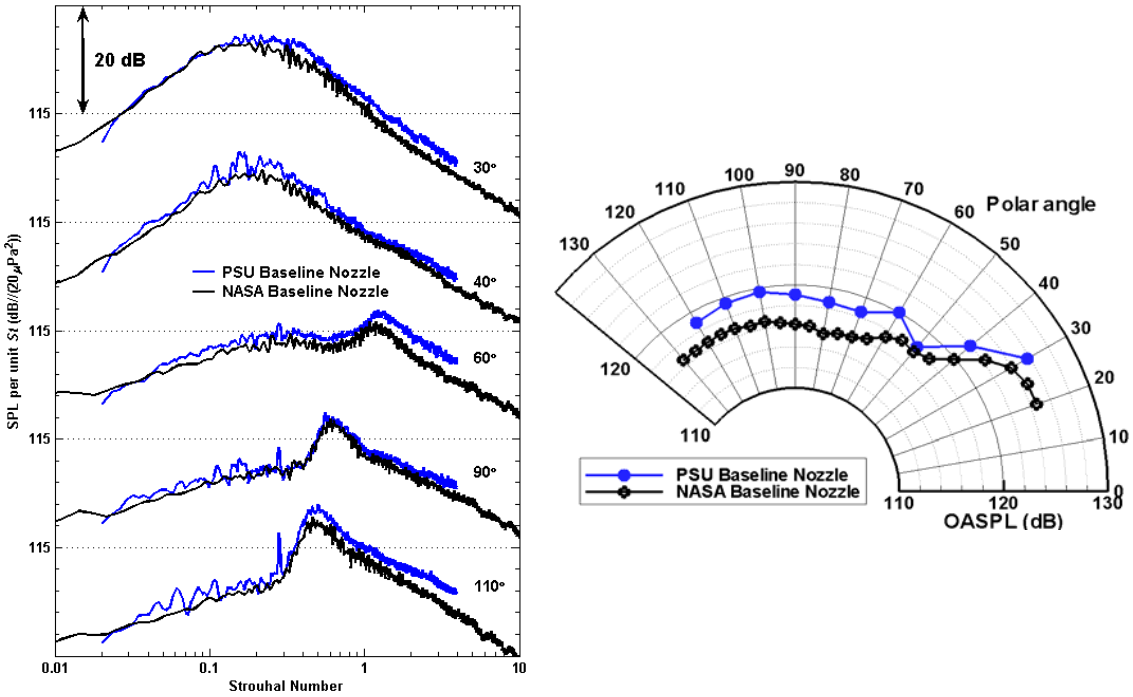

Figure **6-6**: Spectra and *OASPL* comparison from the measurements conducted with GE M_d 1.5 baseline nozzle at Penn State and NASA GRC both operated under-expanded at M_j 1.64, TTR = 1.

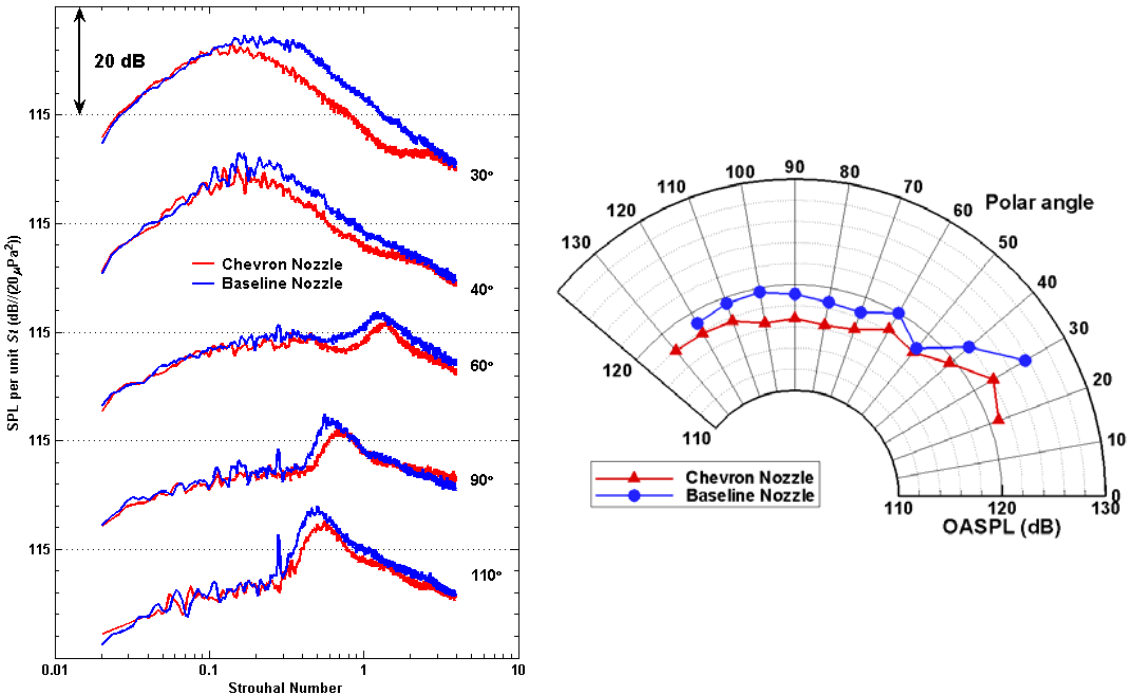

Figure **6-7**: Spectra and *OASPL* comparison from the measurements conducted with GE M_d 1.5 baseline and chevron nozzles operated under-expanded at M_j 1.64, TTR = 1.

frequency to higher frequencies with the chevron configuration, as well as a decrease in amplitude. This suggests smaller shock cells and weaker shocks, and results in a noise reduction on the sideline. Overall, the *OASPL* noise reduction varies from 2 to 4 dB across the polar angle range measured. At this point it appears that the small-scale chevron nozzle experiments produce noise reductions that are comparable to those measured by Henderson and Bridges [51] at NASA. These comparisons were made with cold jets; the focus now turns to the more important hot jet cases.

Figure **6-8** shows a similar spectral comparison of data recorded at the same conditions as the data of Figure **6-6** except the jet is operated with a total temperature ratio of *TTR* = 3.0, where a helium-air mixture was used at Penn Sate and actual heated air was used at NASA GRC. Reasonable agreement is reached between the acoustic measurements obtained from both facilities. There is a systematic discrepancy that the small scale jets are typically two decibels louder in the low frequency range. The discrepancy has been previously identified with a suspected cause attributed to low Reynolds number operation [124]. (A review of this systematic discrepancy is reported in Appendix **B**.) Figure **6-9** shows the spectral comparison of the measurements conducted with the baseline and chevron nozzle in small scale jets. Under this condition, the noise reduction associated with the low penetration chevrons is noticeably less, with maximum levels of about 1.5 dB in the maximum noise emission direction. No perceivable benefit is observed in the sideline direction. Since heat (and helium) affects the jet mixing layer by making it thicker, it is understandable that the increased mixing provided by the chevrons has less effect. Similarly, the BBSAN component is much less dominant in a heated jet on the sideline, due to 1) the increased level of the turbulence mixing noise (caused by a higher jet acoustic Mach number),and 2) the increased mixing layer thickness that weakens the shock cell strength. Therefore, the previously observed shift of the BBSAN frequency and decrease in amplitude is much less apparent and has no effect on the *OASPL*.

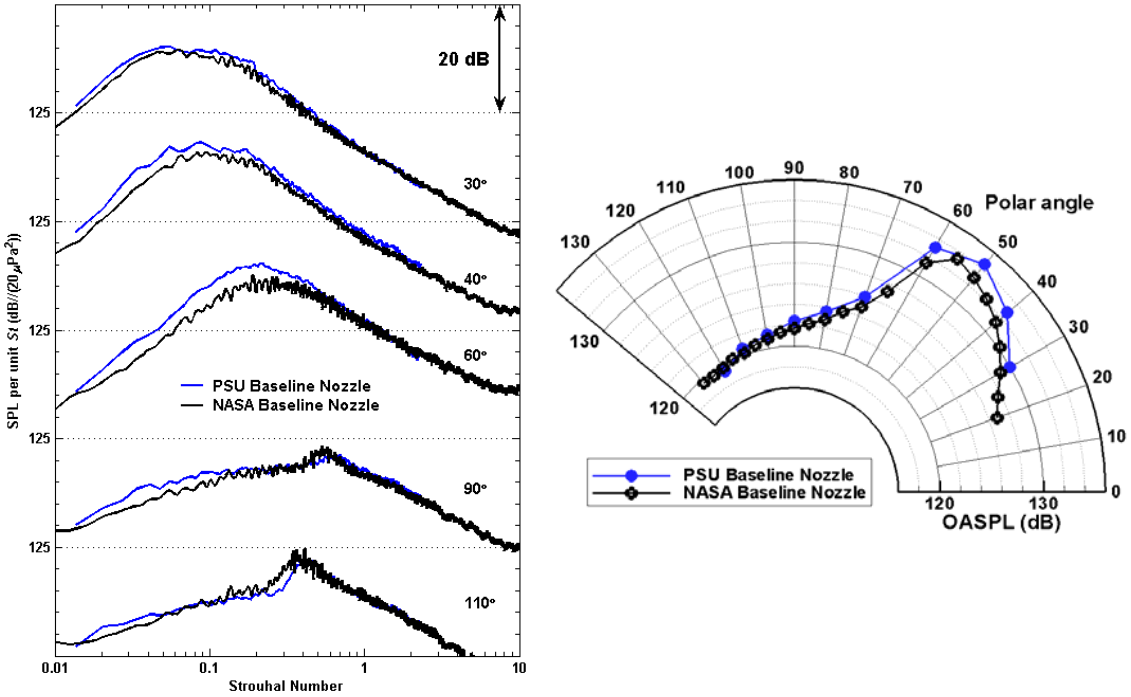

Figure **6-8**: Spectra and *OASPL* comparison from the measurements conducted with GE M_d 1.5 baseline nozzle at Penn State and NASA GRC both operated under-expanded at M_j 1.64, TTR = 3.

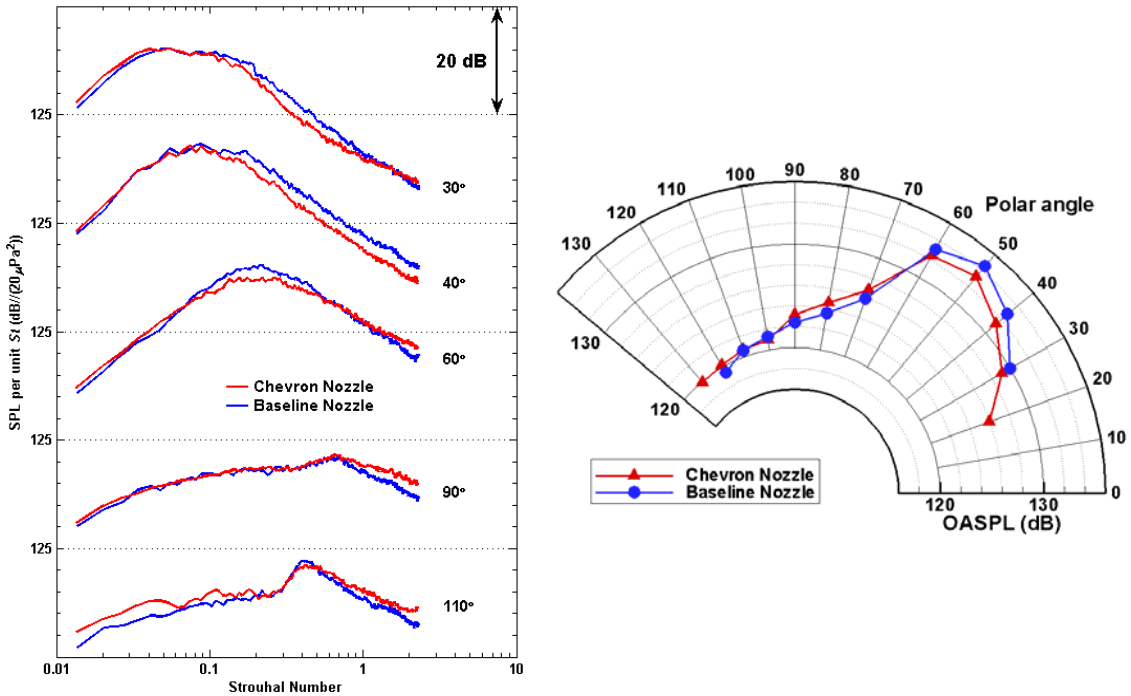

Figure **6-9**: Spectra and *OASPL* comparison from the measurements conducted with GE M_d 1.5 baseline and chevron nozzles operated under-expanded at M_j 1.64, TTR = 3.

6.4 Military-style CD chevron nozzle with chevrons possessing high penetration

Following the experience obtained with the two chevron jet experiments described in the previous sections, a new nozzle was designed and fabricated with chevrons whose parameters matched the highest values used in the NASA GRC experiments [51]. The intention was to operate this M_d = 1.65 nozzle in an over-expanded condition, with a jet exit Mach number M_j = 1.47 and an effective jet diameter smaller than the nozzle exit diameter. This operating condition is of particular interest since it is representative of take-off conditions (at sea level pressures), during which the jet flow experiences its highest back pressure. Hence in order to affect the flow, long high penetration chevrons are required. The goal of this measurement is to demonstrate the capability of chevrons to provide noise reduction in small scale heat simulated supersonic jets operating in **over-expanded conditions**. As a first step, spectra measured from cold jets issuing from this chevron nozzle and the baseline nozzle are presented in Figure **6-10**. From this figure, there is a noise reduction of about 2 dB in the maximum noise emission direction, confirming the ability of the chevrons to affect the jet flow. These values are *approximately* comparable to levels obtained in moderate (NASA) size jet facility experiments. While there is noise reduction of large scale mixing noise, no reduction in the sideline direction is visible. However, the BBSAN component of the spectra shifts to higher frequency values, suggesting a similar shortening of the shock cell structures as previously observed.

Turning to the simulated hot jet experiments, Figure **6-11** presents a group of spectral data recorded with the helium-air jets at the otherwise same conditions as the data in Figure **6-10**. This time the effects of the chevrons on the noise spectra are **imperceptible**, and this is the most important operating condition in this study. For comparison, data measured by NASA GRC with an "identical" M_d = 1.65 chevron nozzle (with an exit diameter of D_e = 12.88 cm, 5.07 in.) are presented in Figure **6-12**. These larger scale data show a significant effect of the chevrons, with

reduction of the peak noise amplitude by about 3 dB, a shift of the BBSAN peak to higher frequencies. Even though these moderate-scale data were obtained with a surrounding flow simulating the plane forward flight, similar effects of the chevrons are expected without the forward flight. This result is contradictory to the observations from the small-scale experiments. The cause can not be attributed to the heat simulation with helium-air, which has previously been validated; therefore more attention needs to be paid to the details of the experimental conditions.

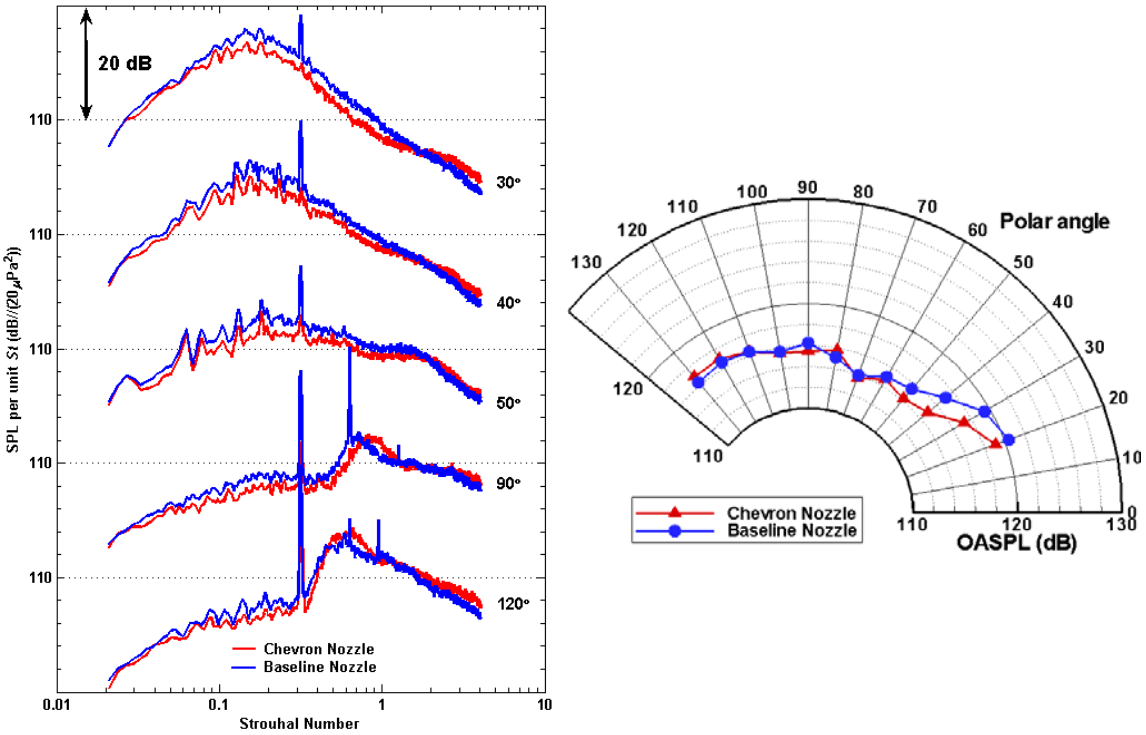

Figure **6-10**: Acoustic spectra and *OASPL* from the measurements conducted with GE M_d 1.65 baseline and chevron nozzles operated at M_j = 1.47, *TTR* = 1.

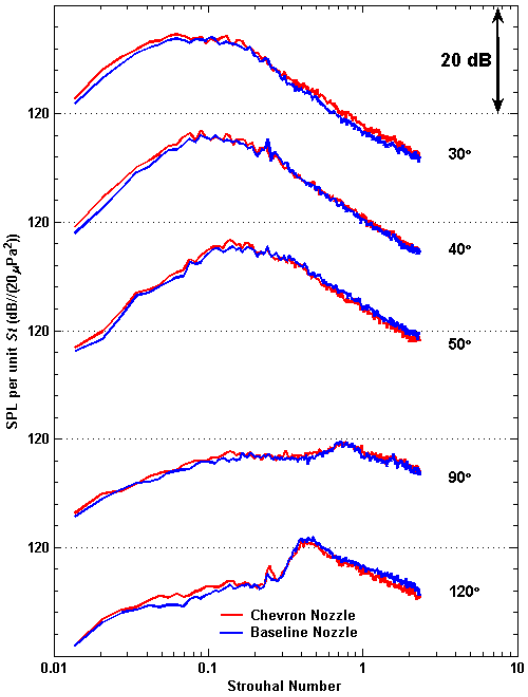

Figure **6-11**: Acoustic measurements conducted with GE M_d 1.65 baseline and chevron nozzles operated at M_j = 1.47, TTR = 3.

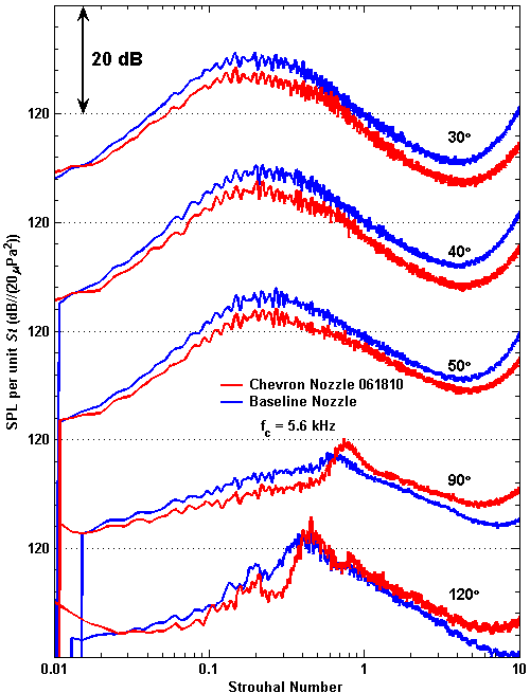

Figure **6-12**: Acoustic measurements conducted with GE M_d 1.65 baseline and chevron nozzles under forward flight simulation with M_f = 0.3 operated at *same conditions as Figure* ***6-11*** *by NASA GRC with a jet of exit diameter 5.07 inch*.

The Reynolds number of the jet operating at the simulated heated jet condition of the data of Figure **6-11** is approximately 539,000 which compares to the value *Re* = 1,677,000 for the NASA experiment and to *Re* = 922,000 of the cold jet experiment (Figure **6-10**). It is hypothesized that this value is low enough to sustain an annular laminar boundary layer in the nozzle that is more sensitive to separation than a turbulent boundary layer. In the over-expanded condition it is likely that the adverse pressure gradient at the exit is separating the boundary layer to the point that the chevrons have an imperceptible effect on the flow, and the subsequent noise reduction. Papamoschou and Zill [125] have clarified the shock formation inside the nozzle when the boundary layer separates from the nozzle surface when the supersonic nozzle is operating in the over-expanded condition. Romine [126] discussed that during the sea-level operation of a rocket, the nozzle is subjected to an over-expanded condition causing high side loads on the nozzle wall. The flow separation incurred inside the nozzle wall is the reason responsible for these consequences. While there is an issue of the Reynolds number, the location of the flow separation inside the nozzle therefore affects the efficiency of the chevrons.

Fortunately there is a quite easy test of the hypothesis discussed above. An alternate method of rapid prototyping uses fused deposition modeling with ABS plastic. This method produces a nozzle that meets the geometric requirements but has a noticeably rougher surface. The disturbances introduced into the boundary layer flow have the potential to trip the flow to transition to turbulence, or at least introduce enough disturbances to delay separation. In the case of the chevron nozzle this would permit the chevrons to penetrate enough of the high speed flow to alter the downstream flow and provide some noise reduction. A schematic of the flow separation with the laminar and turbulent boundary layers respectively is shown in Figure **6-13** to help visualize the situation occurring in the small scale jets. Figure **6-14** first presents acoustic data measured with both the ABS rough baseline nozzle and the SLA smooth baseline nozzle.

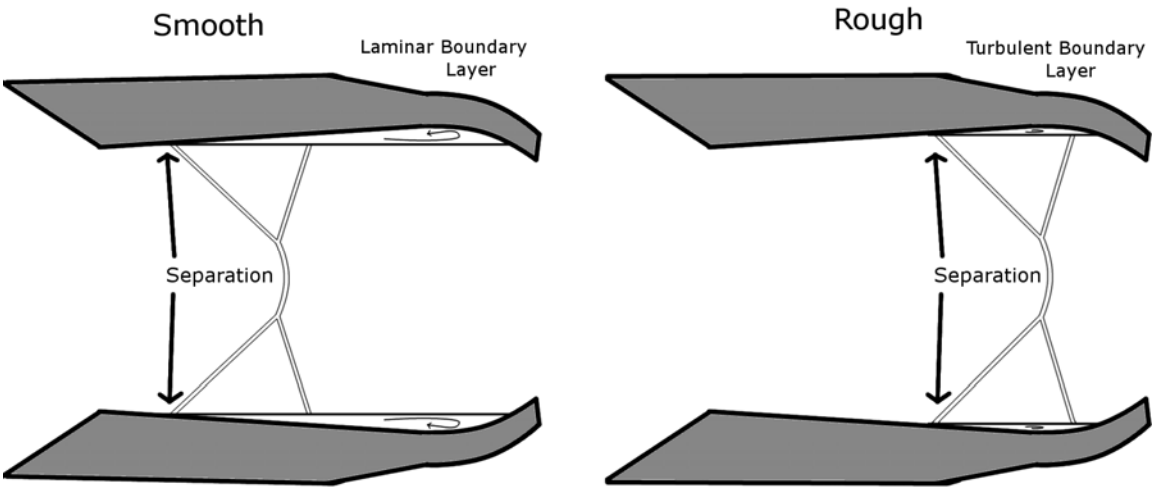

Figure **6-13**: Schematic of the hypothesized flow separation respectively in the laminar boundary layer given by the smooth nozzle and turbulent boundary layer given by the rough nozzle in the small scale jets.

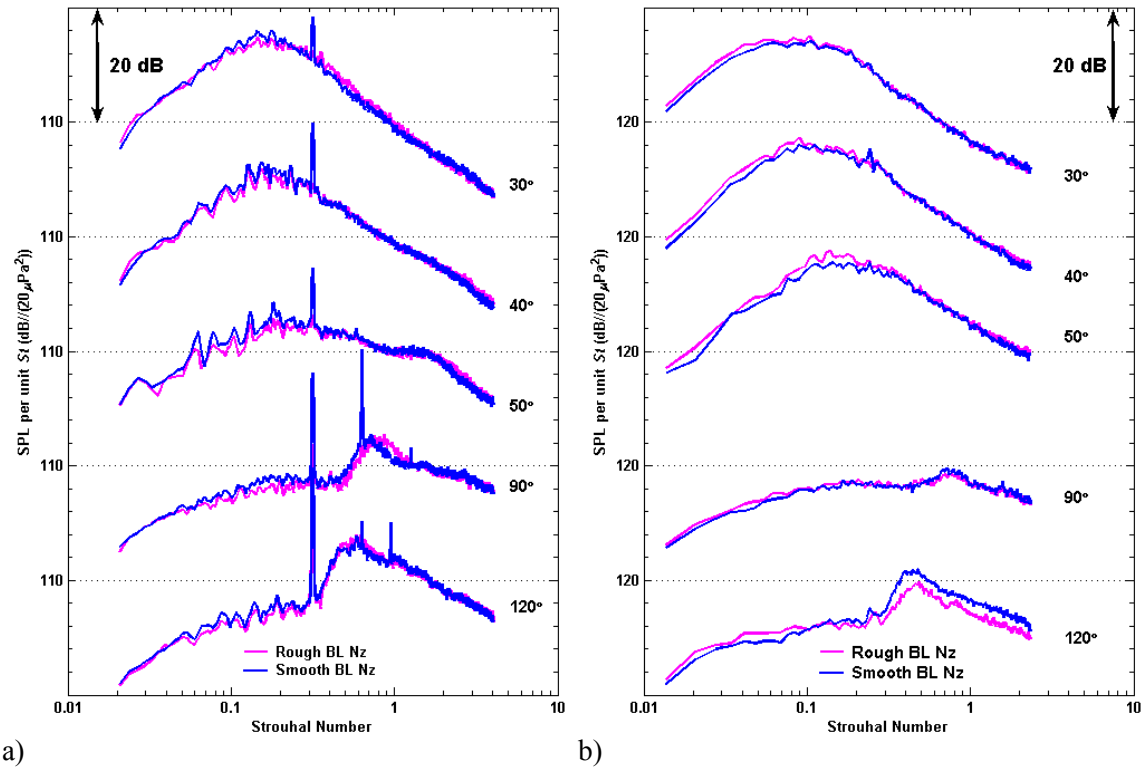

Figure **6-14**: Acoustic spectra from the measurements conducted with GE M_d 1.65 baseline nozzles (rough and smooth) operated at M_j = 1.47 with a) *TTR* = 1. b) *TTR* = 3.

The nozzle designs were both the GE M_d = 1.65 type, and the operating condition for both was M_j = 1.47, *TTR* = 1.0 and 3.0. It is clearly seen that the roughness effect does not significantly alter the measurements in the cold and heated jets with no chevrons. This is in line with results from Bradbury and Khadem [109] who have demonstrated that there is no significant effect in the round jet acoustic measurements due to the boundary layer thickness variation. The variation of the turbulence intensity level at the nozzle exit needs to be at least 20 % of the amount at the end of the potential core to significantly affect the experimental results. Figure **6-15** presents the spectral comparison between the **small-scale and moderate-scale jets** at the same operating condition shown in Figure **6-14**. A good match is shown in the cold jet case and reasonable agreement is reached in heated jet case. This again validates the capability and accuracy of the acoustic measurements operated in the small scale supersonic jets at Penn State.

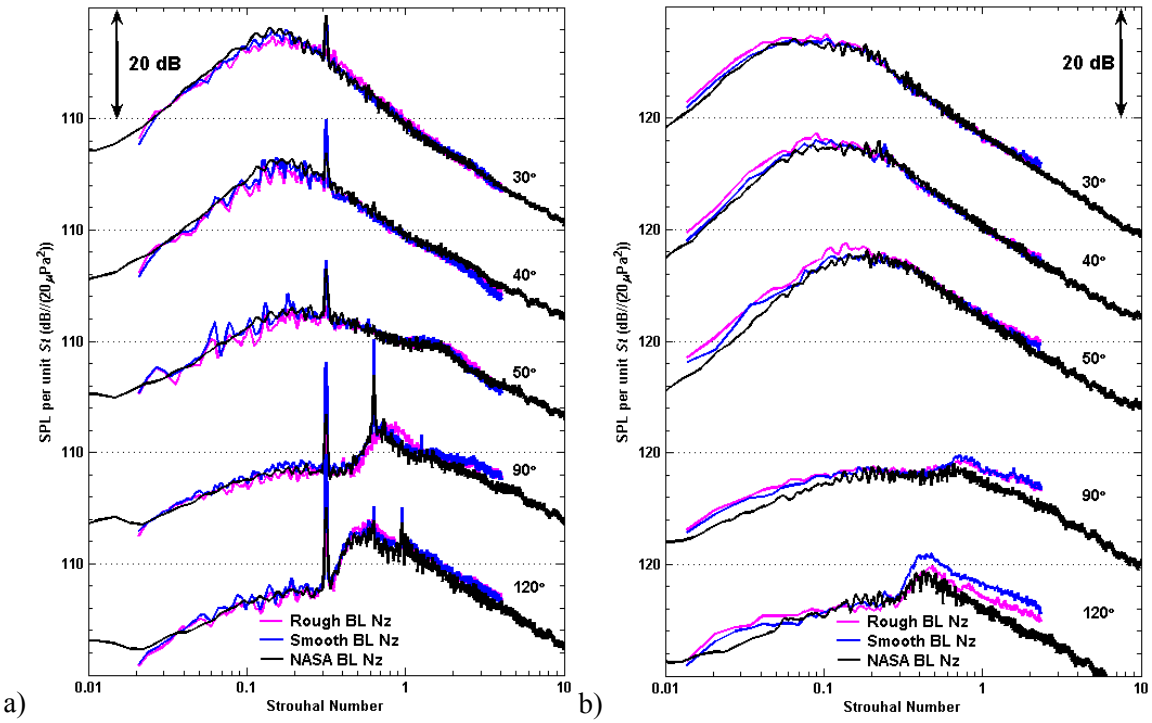

Figure **6-15**: Acoustic spectra from the measurements conducted with GE M_d 1.65 baseline nozzles at NASA GRC and PSU with rough and smooth baseline nozzles operated at M_j = 1.47 with a) *TTR* = 1. b) *TTR* = 3.

Figure **6-16** then presents acoustic data measured with both the ABS rough nozzle and the SLA smooth nozzle both with the high penetration chevrons. In the cold jet case, where the Reynolds number is around 922,000, it can be seen that both nozzles result in the same amount of noise reduction. However, in the heated jet case, where the Reynolds number is reduced to around 539,000, discrepancies emerge in the noise benefits of the chevrons. The hypothesis mentioned earlier is that in the low Reynolds numbers the boundary layer inside the nozzle stays laminar, causing a larger flow separation region. This makes the chevrons ineffective in the over-expanded jets, hence producing negligible noise reduction. When the nozzle surface has some amount of roughness, Zapryagaev and Solotchin [36] showed that it can affect the generation and development of streamwise vortex structures at the nozzle exit plane. These pressure variations have the ability to induce an amplification of the vortices intensity, resulting in an increase of the mixing layer thickness. In doing so a turbulent boundary layer might appear inside the nozzle surface and delay the flow separation. In addition, Gutmark and Ho [127] have demonstrated that an extremely low-level spatially coherent disturbance may alter the initial conditions of the jet shear layer. Since the effect of chevrons is to modify the flow field in the downstream ranges of the first several nozzle diameters, the initial development of the jet mixing layer becomes critical especially for the jets operating in the over-expanded condition. As shown in Figure **6-16** the chevrons now become effective in the over-expanded jets and cause small amounts noise reduction. It is quite important to demonstrate this effect and consequence. Since very good agreement was observed in the acoustics of the baseline nozzles between the small-scale and moderate-scale jets, it was expected to observe similar noise reduction by the chevron nozzle in the small-scale jets. However, as discussed above, in the small-scale jets the flow condition at the nozzle exit at low Reynolds number may not adequately mimic the phenomena of the noise reduction mechanism observed in the moderate-scale jets or even the full scale engine exhausts.

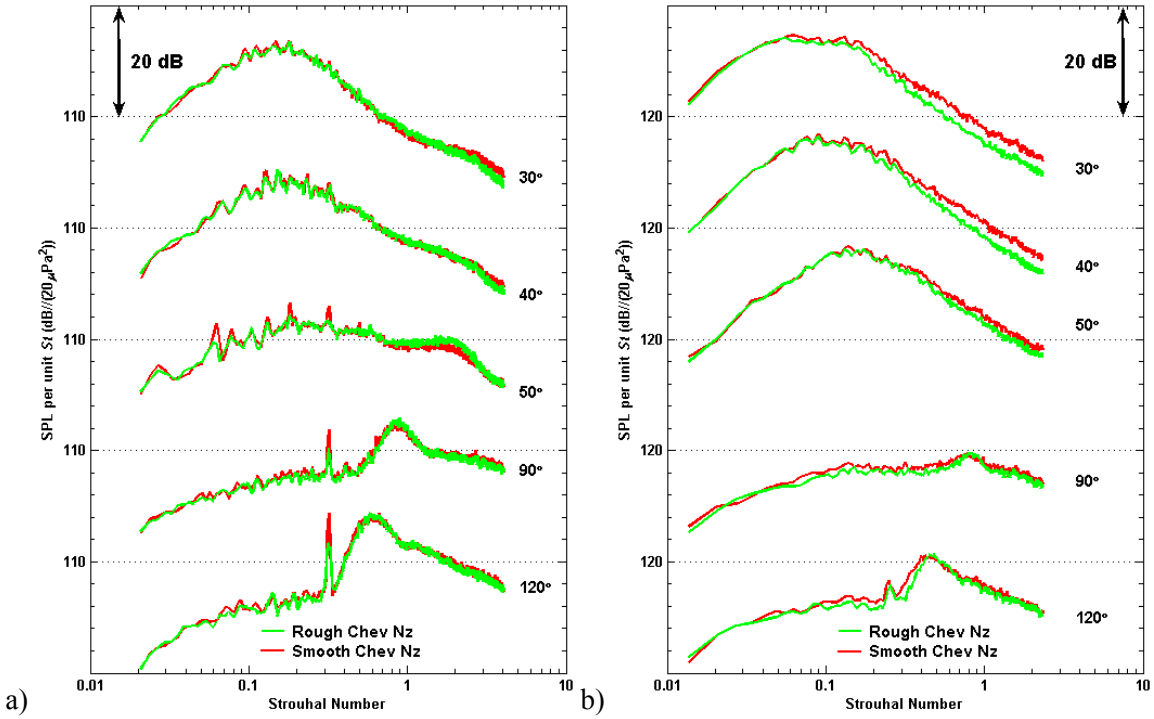

Figure **6-16**: Acoustic spectra from the measurements conducted with GE M_d 1.65 chevron nozzles (rough and smooth) operated at M_j = 1.47 with a) *TTR* = 1. b) *TTR* = 3.

Figure **6-17** shows the noise reduction level from the measurements conducted with the rough baseline nozzle and the rough chevron nozzle both operated at M_j = 1.47, *TTR* = 3.0. The observed noise reduction level is somewhat less than the one observed in the moderate scale jets but it is definitely present. More detailed examination is necessary to exactly evaluate the noise reduction level from the measurements conducted with small scale jets and moderate scale jets, including some direct comparisons with moderate scale chevron nozzles. However, a preliminary conclusion is that small-scale chevron nozzle experiments with high temperature ratio jets may fail to accurately represent the noise reduction potential of jets of practical size.

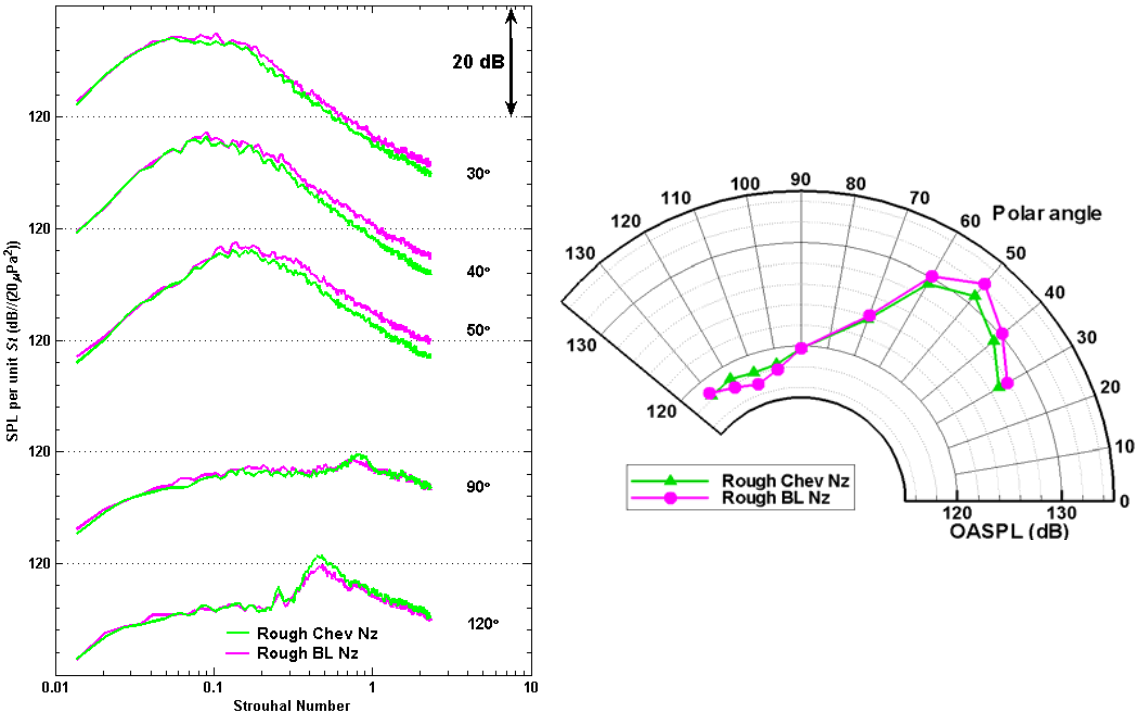

Figure **6-17**: Acoustic spectra and *OASPL* from the measurements conducted with GE M_d 1.65 baseline and chevron nozzles (both rough) operated at M_j = 1.47 with *TTR* = 3.

A preliminary study of the numerical calculation prediction of the flow field issuing respectively from the laminar and turbulent flow nozzle also reveals similar trends observed in the experiments. Computations performed by Miller [128] are shown in Figure **6-18** that presents the numerical results of the flow field predictions individually calculated with the laminar or turbulent flow emerging on the inner nozzle wall. The test case is a round CD M_d 1.5 nozzle with D = 0.5 in. operating at M_j = 1.3, *TTR* = 2.2 giving *Re* = 337,000. These test parameters—small-scale jet operating at an over-expanded condition possessing a critical low Reynolds number—are very similar to our experimental jet conditions and nozzle size. Figure **6-18** a) first shows the calculation with the fully turbulent flow and the oblique shock emerges slightly downstream nozzle exit. On the contrary, as shown in Figure **6-18** b) the oblique shock emerges early causing a flow separation or re-circulating region when the calculation involves the laminar flow inside the nozzle and the turbulent flow outside the nozzle. These findings closely match our hypothesis

as shown in Figure **6-13** and the corresponding experimental results. At the current stage, therefore, it is appropriate to make the following summary statements. From the flow visualizations [125] and practical rocket operations [126] of supersonic jets operating at over-expanded conditions, it was found that there is a flow separation or re-circulating region occuring inside the nozzle wall. Supported from the numerical calculations [128], while the laminar flow appears inside the nozzle, the earlier presence of the oblique shocks inside the nozzle might aggravate the flow separation. Concluded from these findings and the experimental results from the small-scale (low Reynolds no.) heat-simulated jets, it seems reasonable that at over-expanded condition chevrons are ineffective.

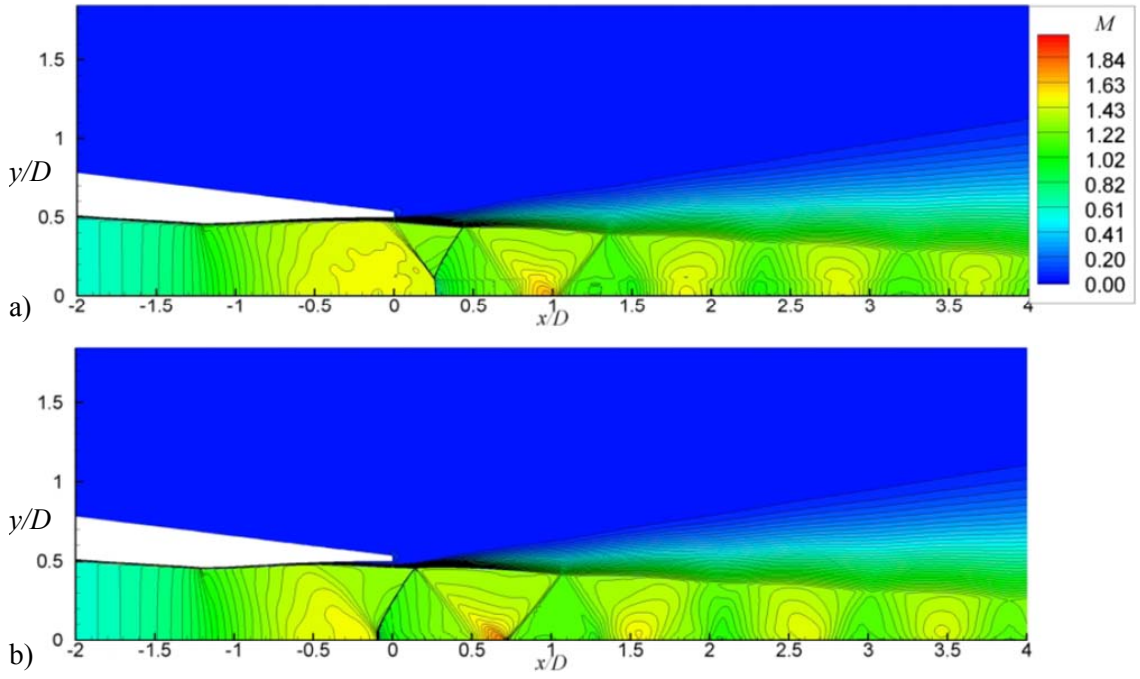

Figure **6-18**: Mach number contours from the calculations with round CD M_d 1.5 nozzle (D = 0.5 in.) operated at M_j = 1.3, TTR = 2.2 with Re = 337,000. a) Fully turbulent flow. b) Laminar flow inside the nozzle and turbulent flow everywhere outside the nozzle. From Miller [128].

6.5 Flow-field analysis of supersonic jets exhausted from the nozzle with chevrons

During the previous discussion of far-field acoustic measurements and schlieren visualization, the effect of chevrons has been demonstrated. This section advances the discussion and provides the physical mechanism for the noise suppression given by chevrons. First, the imbalance of the (favorable) pressure gradient existing between the inner and outer side of chevrons induces the counter-rotating pairs of streamwise vortices. These streamwise vortices possess a comparatively larger length scale than the one in the initial shear layer growing from the lip of the round nozzle. The improved jet spreading, mixing, and entrainment facilitate the decay of the jet centerline velocity and redistribute the turbulent kinetic energy with an upstream shift of the peak turbulence intensity level. schlieren visualization has exhibited the amplified jet spreading due to the presence of chevrons. Most of the far-field acoustic spectra (in other researchers' studies) measured with a chevron nozzle exhibit the acoustic benefit with lower sound intensity level in the frequency content below the peak frequency of the spectra and an acoustic penalty of the excess high frequency noise appearing in the high frequency end of spectra when compared to the round nozzle measurements. Also, from the previously presented spectra, the spectrum shape at the dominant peak emission angle is slightly modified with a broad peak due to the presence of the chevrons. Meanwhile, it is reasonable to believe that there is a noise suppression of the Mach wave radiation in the proximity of the nozzle exit due to the streamwise vortices rolling up in the nozzle exit plane.

To support these observations, a detailed examination of the flow field and corresponding statistics are given below. This section is mainly comprised of flow property measurements performed with a five probe pitot rake. One baseline nozzle and two chevron nozzles (all possessing $M_d = 1.5$) were considered. The detailed chevron parameters and corresponding jet

operation conditions are listed in Table **6-2**. Two chevron nozzles are referred to as "short chevron" and "long chevron" for convenience in the following discussion.

Table **6-2**: Nozzle parameters and jet operation conditions for data of flow-field analysis.

Nozzle Parameters						Jet Operation Conditions	
M_d	D (inch)	Chevron Counts	Penetration	Length	Width	M_j / TTR	Re X 10^{-6}
1.5	0.676	12	0.04 D	0.16 D	0.2 D	1.47 / 1	0.9
			0.05 D	0.23 D	0.2 D	1.64 / 1	1.2
		Baseline					

Figure **6-19** presents the centerline variations of jet velocity from the measurements conducted with the baseline and chevron nozzles both operated at M_j 1.64 and unheated. The modulation of the centerline variations of jet velocity is due to the presence of shock cells. The measurements from the chevron nozzle exhibit a faster decay of the centerline variation of jet velocity than the baseline nozzle. It is evident to see that the end of the potential core is around 7.2 nozzle diameters (similar to the empirical calculation [99]) for the jets issuing from the

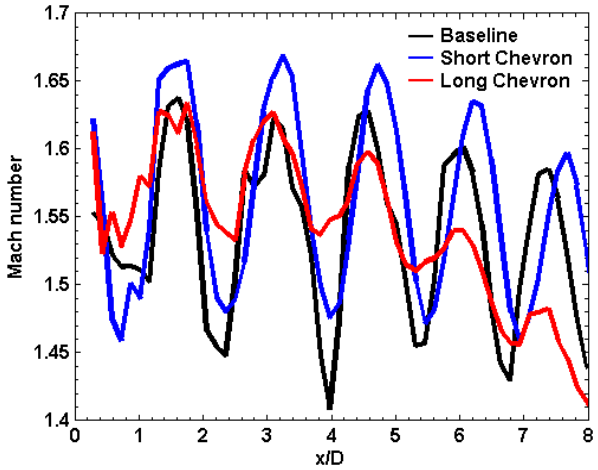

Figure **6-19**: Centerline variations of the jet velocity from the flow field measurements conducted with GE M_d 1.5 nozzles (baseline, short chevron, long chevron) operated at M_j = 1.64, cold.

baseline nozzle and around 4.4 nozzle diameters for the jets issued from the nozzle with long chevrons. The magnitude variations of the shock cell strength also match the observation from the far-field acoustic spectra where a lower magnitude of broadband shock-associated noise is seen in the measurements from the nozzle with long chevrons than the one from the baseline nozzle.

The shortening of the jet potential core is a good indicator of the improved jet spreading. The jet spreading is evaluated by the value of the vorticity thickness (δ) measured across the jet shear layer and is calculated as follows, where U represents the jet velocity on the jet centerline axis and r is the distance in the jet radial direction.

$$\delta = \frac{U_{\max}}{\left|\frac{dU}{dr}\right|_{\max}} \qquad \textbf{6.1}$$

Figure **6-20** shows an improved jet spreading with jet downstream distance due to the presence of chevrons as evidence of improved lateral jet development. The slope of the abrupt increases of the jet spreading from the measurements conducted with the chevron nozzles appears within the first 2 nozzle diameters with a subsequent jet spreading slope similar to the one from the baseline nozzle. Meanwhile, the initial jet spreading is higher in the notch plane than the tip plane with a cross-over in the downstream location similar to the observation from Longmire *et al.*

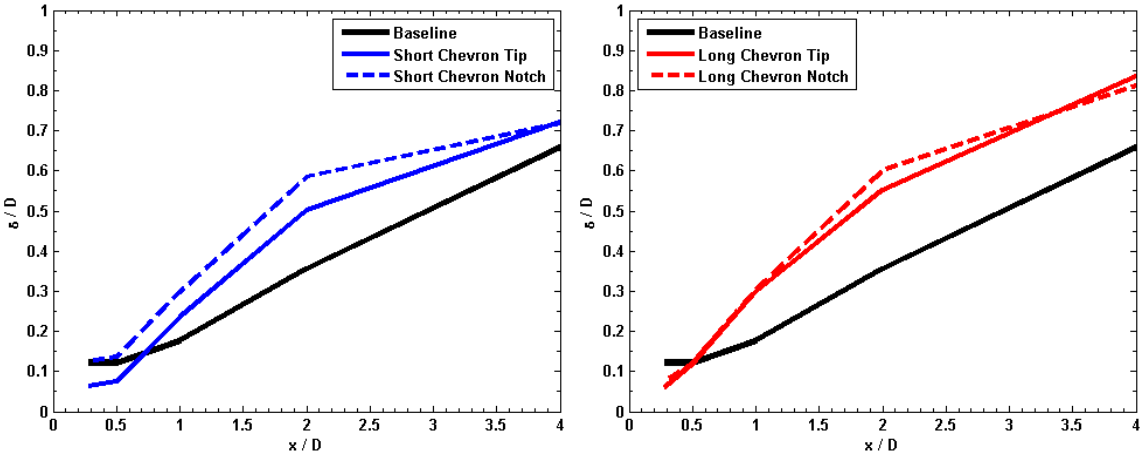

Figure **6-20**: Normalized vorticity thickness from the flow field measurements conducted with GE M_d 1.5 nozzles (baseline, short chevron, long chevron) operated at M_j = 1.64, cold.

[117]. The abrupt increase of the jet spreading makes the jets issuing from the chevron nozzle reach a shear layer thickness of 0.6 nozzle diameters at around two nozzle diameters downstream. In comparison, jets issuing from the baseline nozzle take 4 nozzle diameters to develop the shear layer reaching similar thickness. The current pitot measurements only provide the experimental data from the test nozzles with two chevron configurations. More detailed examination and discussion will be necessary to fully understand the physical mechanism of the improved jet spreading caused by chevrons.

To understand the improved jet spreading caused by chevrons, it is helpful to examine the streamwise vortices induced by the chevrons from the cross-stream contour plot. Figure **6-21** to Figure **6-24** present the Mach number contour plots along the radial cross-stream plane at various axial locations from the pitot measurements conducted with baseline and chevron nozzles respectively shown in the figure order from left to right. Figure **6-21** b) shows that the axis of the abscissa and ordinate both represents the tip plane of the chevron nozzle and the middle point of facet of the baseline nozzle. As shown in Figure **6-21** a) there is a trend of the lateral jet development in the radial outward direction at the notch location of chevrons. The perimeter of the jets is modified due to chevrons. Instead of round shape, the jets exhibit a dendritic or gear-like shape. The jets seem to be squeezed inward in the tip of chevrons because of the collateral jets relationships with the jets poking outward in the notch of chevrons. Moreover, the radial outgoing jets increase the jet spreading that generates excess jet development in the notch of chevrons.

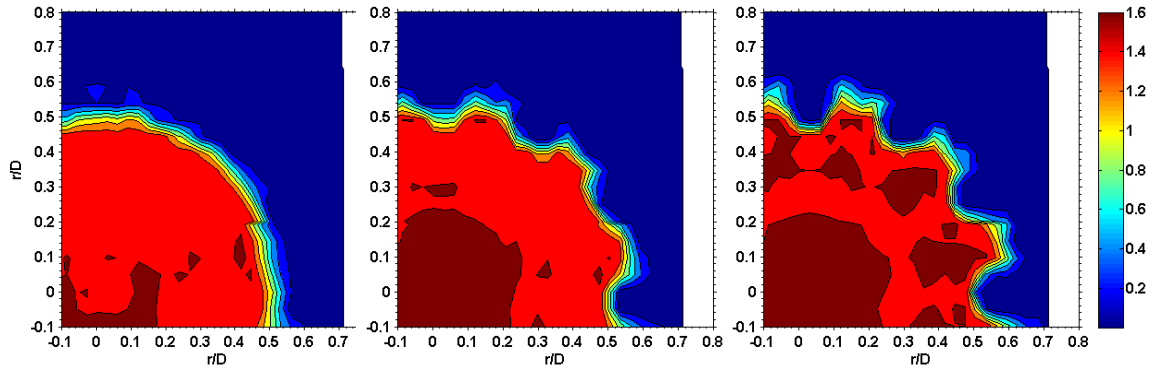

a)

b) baseline nozzle chevron nozzle

Figure **6-21**: a) Cross-stream Mach number contour plot from the flow field measurements acquired at x/D = 0.28 conducted with GE M_d 1.5 nozzles (baseline, short chevron, long chevron respectively in the figure order from left to right) operated at M_j = 1.64, cold. b) Axis of the abscissa and ordinate in the contour plot relative to baseline and chevron nozzles.

As the jets evolve axially from x/D of 0.28 to x/D of 0.5 as shown in Figure **6-22**, the high speed jets still dominate the jet development in the notch of the chevrons. While the streamwise vortices shed the high speed core-stream outward at the notch of chevrons, it also entrains the ambient low speed flow causing improved jet spreading, mixing, and entrainment. Though the current pitot measurements only provide the mean flow properties, it is still reasonable to state that there is a trend of the energy transport in the radial outgoing direction. Thus the chevrons seem to make the peak turbulent kinetic energy move radially outward.

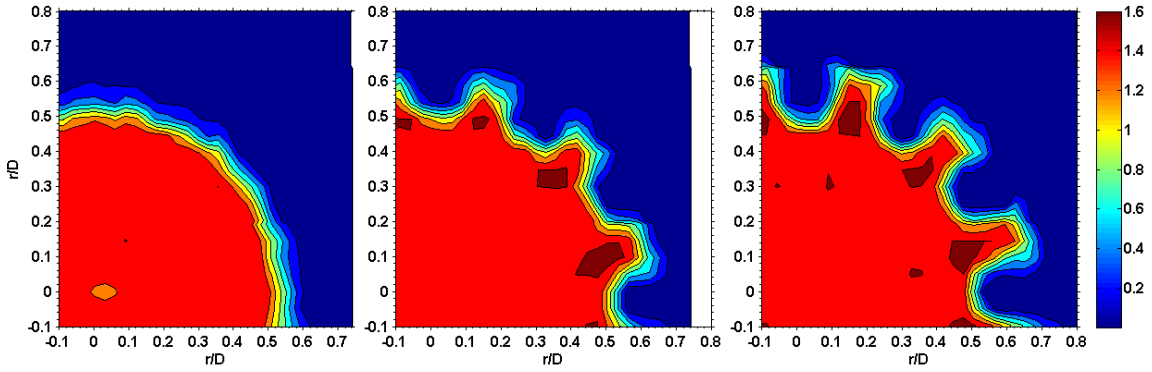

Figure **6-22**: Cross-stream Mach number contour plot from the flow field measurements acquired at x/D = 0.5 conducted with GE M_d 1.5 nozzles (baseline, short chevron, long chevron respectively in the figure order from left to right) operated at M_j = 1.64, cold.

As jets axially evolve from x/D of 0.5 to x/D of 1 as shown in Figure **6-23,** the dendritic shape in the core high speed stream gradually became less spiky in the measurements conducted with chevron nozzles. In these dendritic shaped regions, instead of the core high speed flow, a thin, slim, radially-stretched secondary high speed flow emerges. The neighboring regions between two radially-stretched flows start to be gradually filled with the low speed entrained flow. The jet Mach number contour plot is hence similar to the jetlets model described by Tam and Zaman [23]. The essential core high speed jet momentum is disspated and then diminished by the individual and independent jetlet induced by chevrons. In such way, the jet centerline velocity

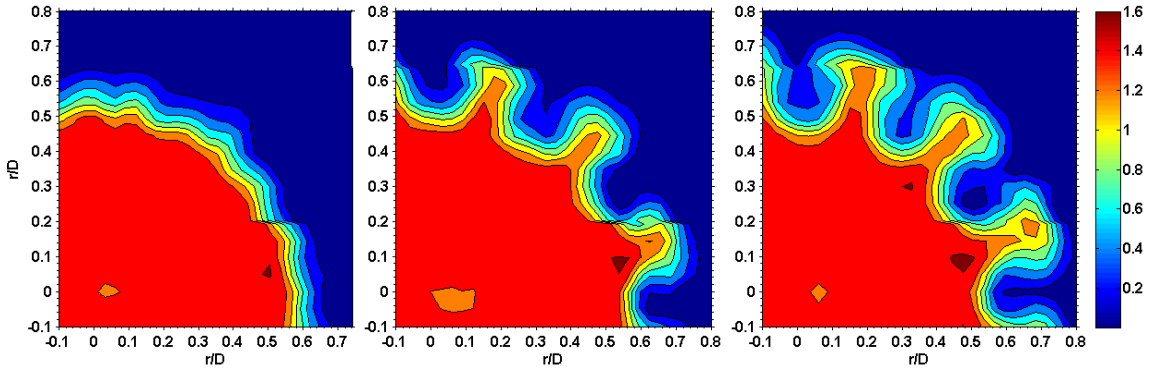

Figure **6-23**: Cross-stream Mach number contour plot from the flow field measurements acquired at x/D = 1 conducted with GE M_d 1.5 nozzles (baseline, short chevron, long chevron respectively in the figure order from left to right) operated at M_j = 1.64, cold.

exhibits a faster decay since the jet momentum is dissipated due to these jetlets generated by chevrons. As seen here and suggested by Opalski *et al.* [122] the variance of the chevron penetration angles elongates the effective flow region of the pre-described secondary flow rather than creates a more compact vortex structure with higher intensity. Since there is no change in the chevron counts, no substantial space can be adjusted between the neighboring jetlets. The higher penetration angle also represents higher pressure gradient between the inner and outer side of chevrons so that the induced jetlets could only amplify the effective flow development in the radial direction causing a further stretching of the lateral flow.

Figure **6-24** shows the jet development respectively at *x/D* of 2 and 4. First, the jet perimeter of the core high speed stream resumes to round shape without specific azimuthal

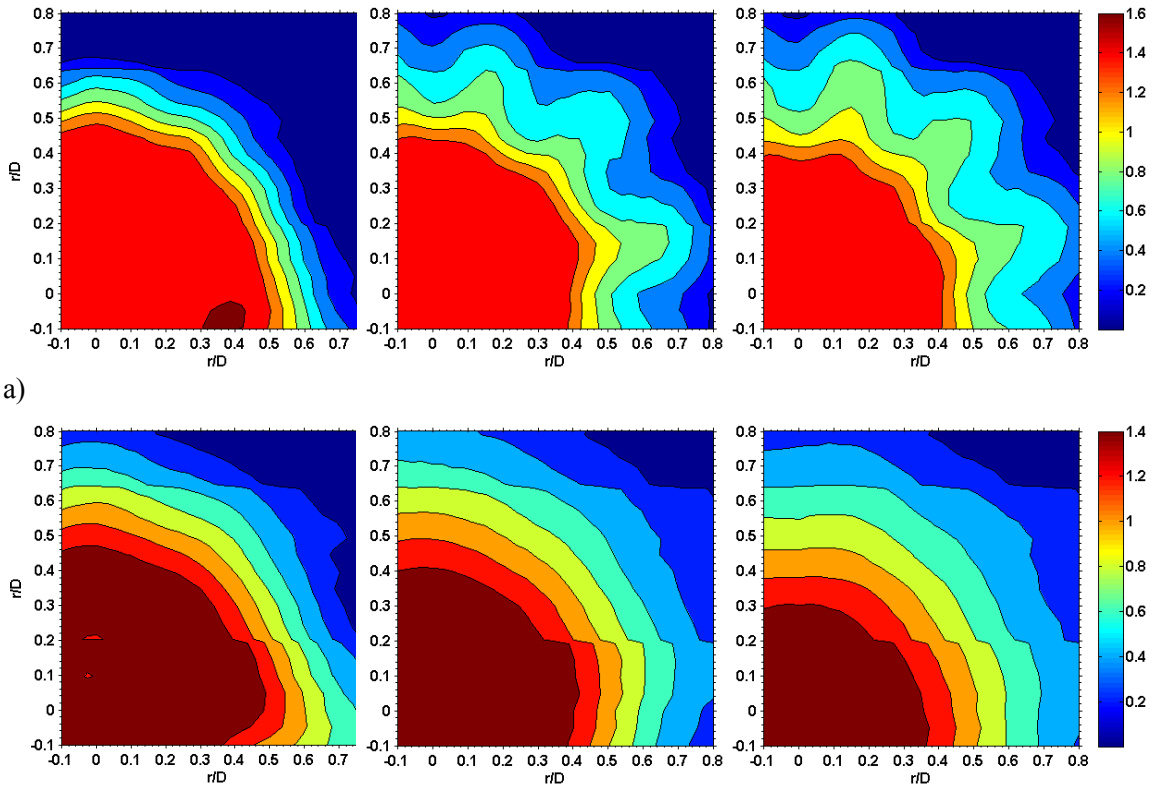

Figure **6-24**: Cross-stream Mach number contour plot from the flow field measurements conducted with GE M_d 1.5 nozzles (baseline, short chevron, long chevron respectively in the figure order from left to right) operated at M_j = 1.64, cold and acquired at a) x/D = 2. b) x/D = 4.

modulation in the measurements conducted with chevron nozzles. Secondly, the effective region of the core high speed flow is now largely reduced but the overall cross-stream flow region is greatly expanded due to the presence of chevrons. The perimeter of the outer flow ultimately recovers to the round shape as the jets axially evolve to *x/D* of 4 shown in Figure **6-24** b). This demonstration of the cross-stream jet development distinctly unveils that the jets are dramatically modified within the first 2 nozzle diameters. Though the jets are naturally induced by the presence of chevrons at the nozzle exit plane, ultimately they quickly recover to the axisymmetric flow.

To quantify the corresponding statistics from the Mach number contour plot at the cross-stream plane, Figure **6-25** presents the corresponding normalized radial velocity at various downstream locations. The normalized velocity is plotted versus the normalized radial distance η defined as following where *r* represents the distance in the jet radial axis. The value of $r_{0.5}$ is equal to the distance to the radial location where the local jet velocity is half of the maximum jet velocity.

$$\eta = \frac{r - r_{0.5}}{\delta} \qquad \textbf{6.2}$$

Due to the thin shear layer thickness and not many data points acquired within the first nozzle diameter, only normalized radial velocity profiles at *x/D* = 1, 2, and 4 are available in Figure **6-25**. The curves show a similar trend on the one studied by Alkislar *et al.* [118] where a subsonic Mach 0.9 cold jet was investigated. One who is interested in the generation and development of the counter-rotating streamwise vortices can review their work. The normalized velocity profile provides a way to clarify the flow development by the velocity gradient. As mentioned previously, the jets spike out in the notch of chevrons making the jets slightly squeezing in the tip of chevrons. Therefore it can be seen that a steep slope appears in the tip of

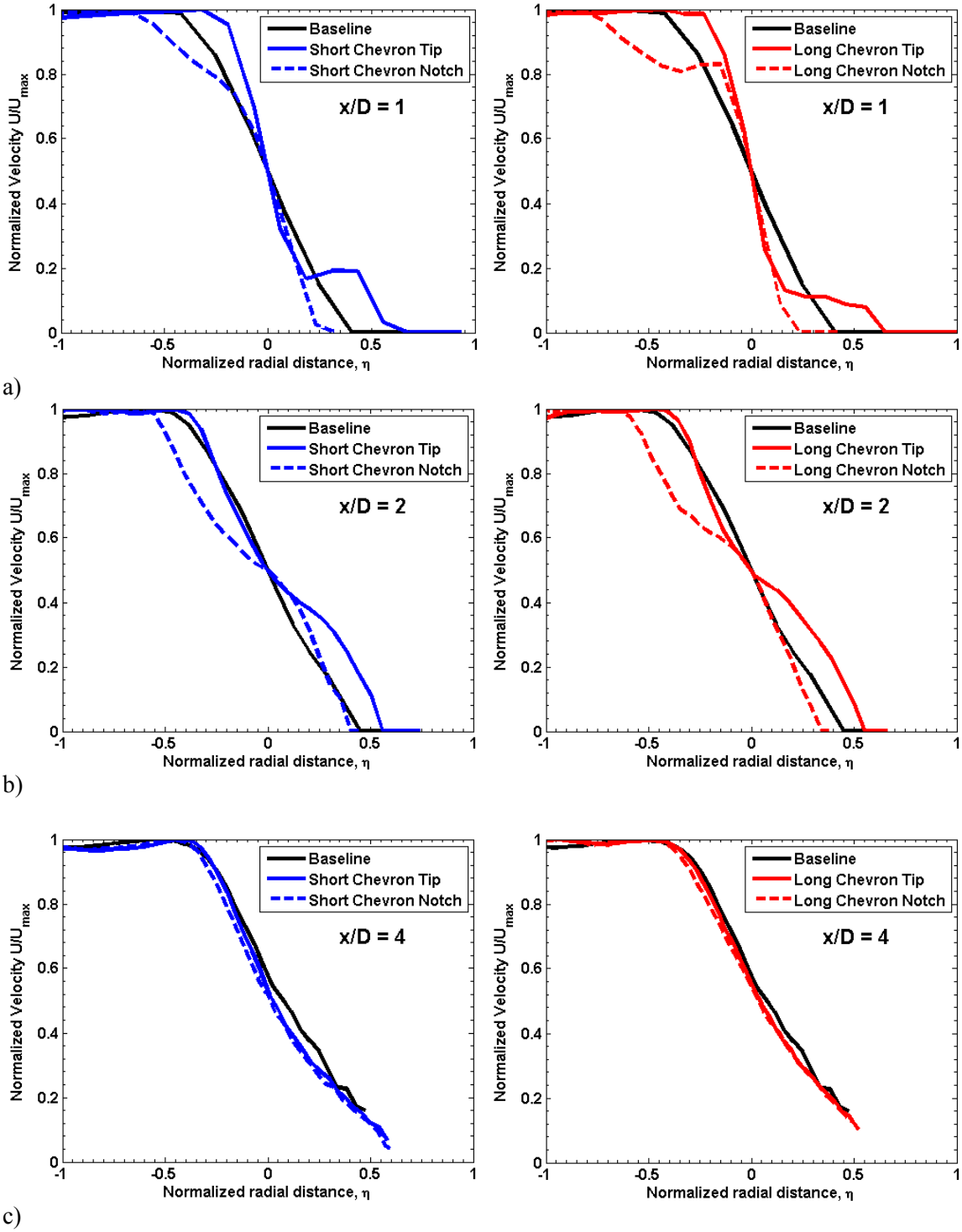

Figure **6-25**: **N**ormalized radial velocity profile from the flow field measurements conducted with GE M_d 1.5 nozzles (baseline, short chevron, long chevron) operated at M_j = 1.64, cold respectively acquired at a) x/D = 1. b) x/D = 2. c) x/D = 4.

chevrons at x/D = 1 as shown in Figure **6-25** a). The small bulge in the root of the zigzag shape of the velocity profile comes from the entrained ambient low-speed flow. While the jets in the notch of chevrons exhibit a radial-stretched secondary high speed flow, the velocity profile shows a gradual plateau containing 80 percent of the mean flow velocity up to the location of the half velocity point (η = 0) following a precipitate drop to the outer edge of the shear layer. This scenario reveals that the jet swiftly breaks outward accompanying 80 percent of the mean core flow velocity. This also supports that small amount of jet momentum is transported radially outward facilitating the jet mixing between the core high speed stream and the ambient low speed flow. As the jet axially evolve from x/D of 1 to x/D of 2 as shown in Figure **6-25** b)**,** at the tip of chevrons the high speed side of the jet (η < 0) starts to evolve with a slope similar to the one issued from the baseline nozzle. However, in the low speed side of the jet, the entrained flow gradually grows with increased flow speed contributed by the outgoing high speed core-stream from the notch of chevrons. At the notch of chevrons, on the contrary, the low speed side of jets (η > 0) starts to evolve with a slope similar to the one issued from the baseline nozzle. The high speed side of the jet still possesses non-uniform distribution of the flow velocity waiting for the gradual momentum transport (initially carried out from outgoing high speed core-stream) into the entrained flow. As the jet axially evolve from x/D of 2 to x/D of 4 as shown in Figure **6-25** c)**,** the flow ultimately reaches the axisymmetric condition with all curves closely overlapping. Though there are not enough points acquired in the outer edge of the shear layer, it is reasonable to believe that the jet has become axisymmetric.

For the completeness of the experimental results, Figure **6-26** and Figure **6-27** respectively present the Mach number contour plots along the radial cross-stream plane and its corresponding normalized radial velocity from the measurements conducted with the baseline and chevron nozzles operated at M_j 1.47 cold jets. Since the jet is operated at over-expanded condition

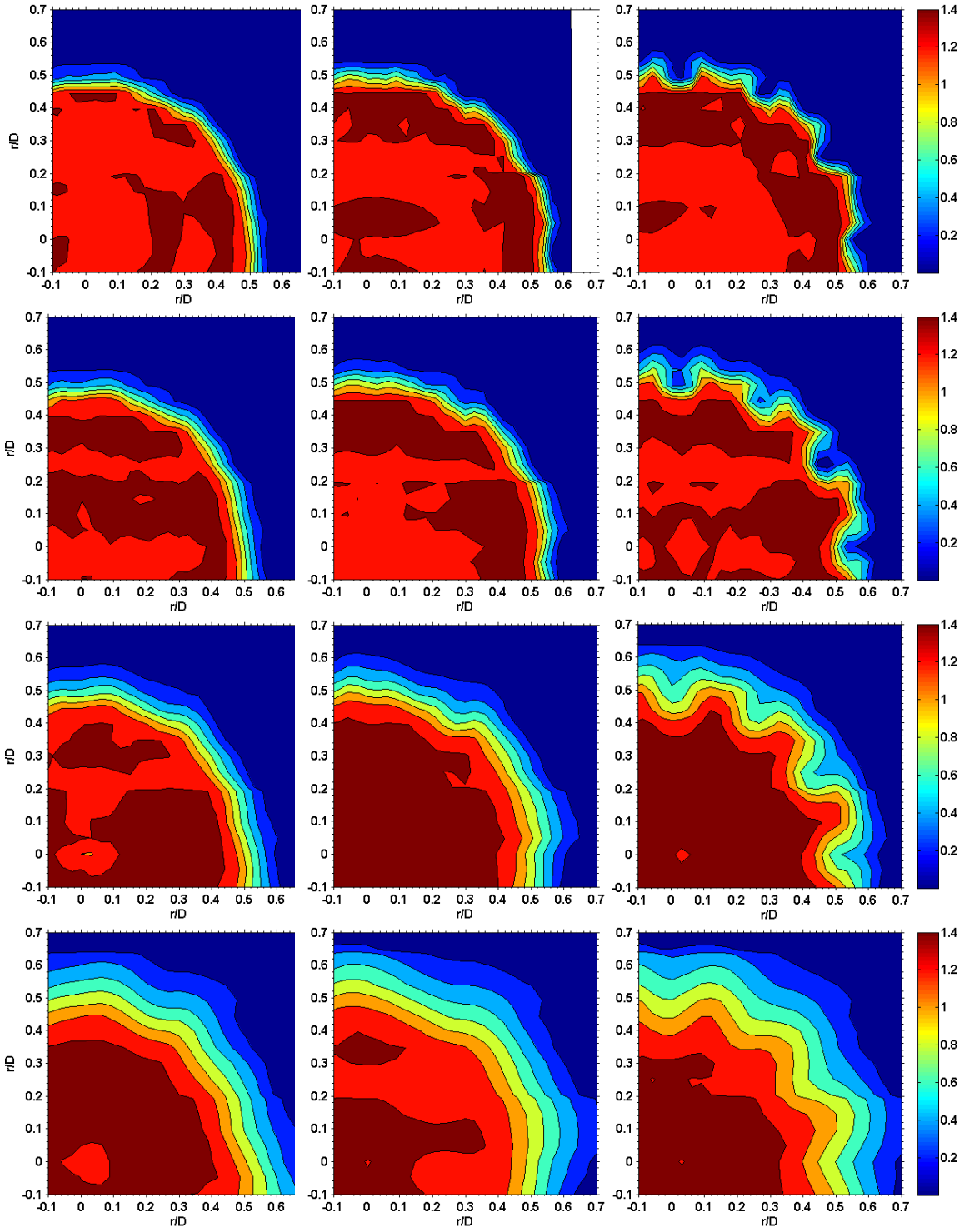

Figure **6-26**: Cross-stream Mach number contour plot from the flow field measurements conducted with GE M_d 1.5 nozzles (baseline, short chevron, long chevron respectively in the figure order from left to right) operated at M_j = 1.47, cold acquired respectively at x/D = 0.28, 0.5, 1, and 2 from the first row to the fourth row.

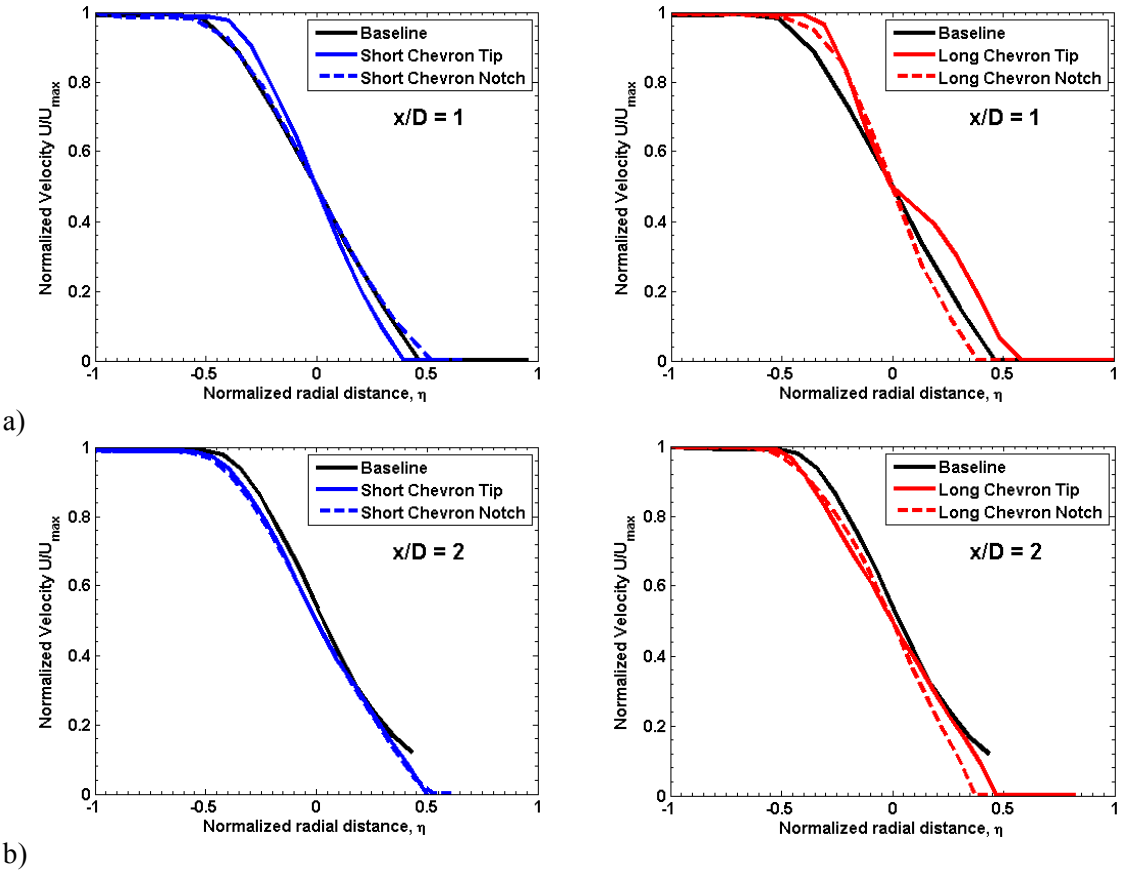

Figure **6-27**: **N**ormalized radial velocity profile from the flow field measurements conducted with GE M_d 1.5 nozzles (baseline, short chevron, long chevron) operated at M_j = 1.47, cold acquired respectively at a) x/D = 1. b) x/D = 2.

accompanying with an adverse pressure gradient at the nozzle exit plane, acoustic spectra have revealed no substantial acoustic benefit due to chevrons (therefore not shown here). The Mach number contour plot along the radial cross-stream plane as shown in Figure **6-26** then barely exhibits similar gear-like shape in the measurements conducted with the long chevron nozzle. The extruded region of the gear-like shape is seen clearly to be flatten and limited, implying the implicit effect of chevrons. The normalized radial velocity as shown in Figure **6-27** also barely presents the slope modulation distinguishing the tip and notch plane of chevrons. Only the small bulge in the root of the zigzag shape reveals the amplification of the ambient entrained low-speed

flow. The flow ultimately reaches the axisymmetric condition with all curves closely overlapping at $x/D = 2$.

6.6 Evaluation on forward flight simulation

Since the most important purpose of noise reduction concepts is to provide reduction of the emitted sound during take-off, measurements under forward flight conditions are crucial for full qualification of the efficiency of chevrons. Forward flight simulation can be performed in the Penn State facility, as mentioned earlier and described in detail by Veltin *et al.* [129]. Preliminary measurements with forward flight were conducted with a baseline nozzle and a chevron nozzle. The forward flight Mach number M_f was set to 0.17, which is close to a take-off Mach number for a typical fighter aircraft. Since the forward flight flow consists of a limited-width low-speed free jet, refraction of the sound through the mixing layer needs to be compensated for. These corrections are described in detail in Veltin *et al.* [129] for this facility. Figure **6-28** shows the preliminary experimental results from the baseline nozzles operated at $M_j = 1.64$ cold jets with $M_f = 0$, 0.1, and 0.17 respectively. One can see that there is a general decrease of the turbulent mixing noise and a downward shift of the peak frequency of the broadband shock-associated noise, accompanied with a decrease in its amplitude. These observations are similar to the studies reported by Norum and Shearin [130], [131]. The effect of the chevrons on the acoustic spectra under the effect of forward flight is shown in Figure **6-29**. The acoustic benefit due to chevrons is very similar to what was previously observed without the forward flight as shown in Figure **6-7**. The effect of chevrons under the effect of the forward flight makes the noise reduction of the broadband shock-associated noise more marginal. However, these preliminary results reveal that the noise reduction seen in the static test is still observable in the forward flight simulation. This is quite encouraging although only limited experimental data can support this conclusion at the

current stage. More detailed study on the actual efficient noise reduction of chevron under the effect of the forward flight is ongoing to further reach a solid conclusion.

Figure **6-30** presents the schlieren images from the measurements conducted with the baseline and chevron nozzles operated at M_j 1.64 cold jets with M_f = 0 and 0.17 respectively. It has been shown that there is no substantial modification on the shock cell structures of the jet. Currently schlieren images only have resolution up to around 3 nozzle diameters downstream where the images start to blur farther downstream. Norum and Shearin [130] had demonstrated that the stretching of the shock cell structures due to the forward flight effect emerges approximately after 5 nozzle diameters downstream. Our current positioning of schlieren visualizations therefore does not include this position.

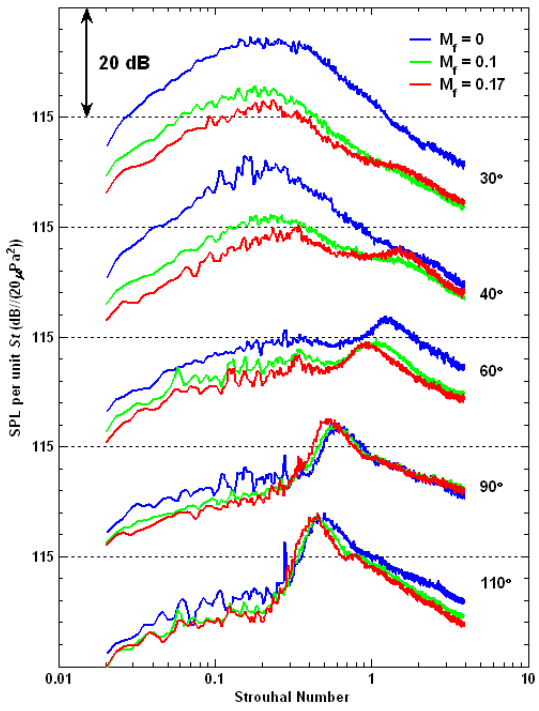

Figure **6-28**: Acoustic measurements conducted with GE M_d 1.5 baseline nozzles operated at M_j = 1.64, cold, accompanying with M_f = 0, 0.1, and 0.17 respectively.

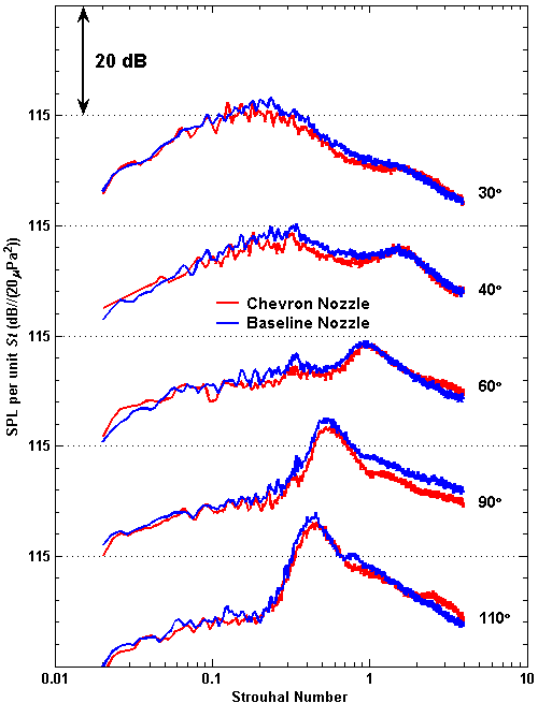

Figure **6-29**: Acoustic measurements conducted with GE M_d 1.5 baseline and chevron nozzles operated at M_j = 1.64, cold, accompanying with M_f = 0.17.

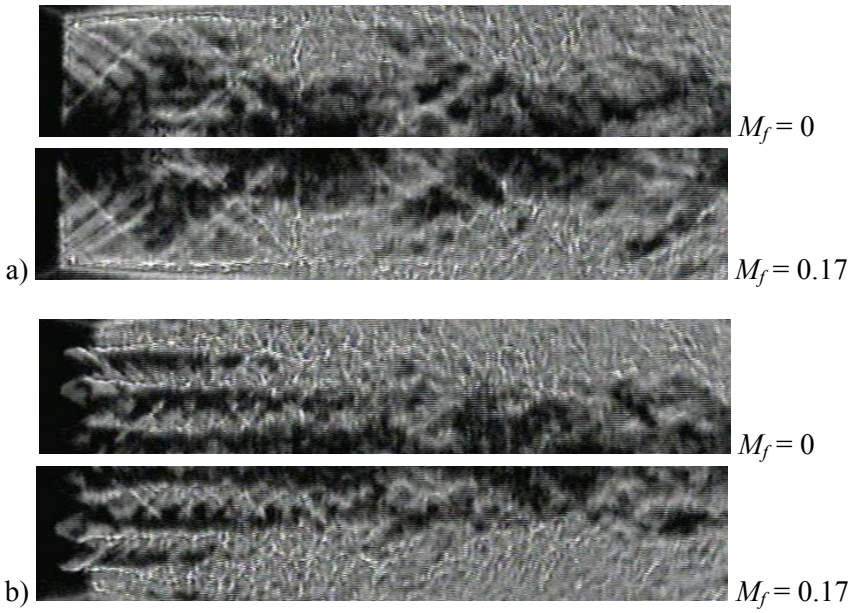

Figure **6-30**: Schlieren images from measurements conducted with GE M_d 1.5 nozzle operated at M_j = 1.64, cold, accompanying with M_f = 0 and 0.17 respectively with images locally zoom in. a) Baseline nozzle. b) Chevron nozzle.

6.7 Effect of the empennage on the radiated noise

In order to fully validate the measurements made at Penn State with full scale measurements, integration of the military-design nozzles into an accurate representation of a F35 empennage was performed. The empennage is expected to affect the acoustic spectra by reflecting and scattering some of the acoustic waves, in a way similar to what was observed by Papamoschou and Mayoral [132]. It may also affect the entrained flow field, with possibly more or less effect with the presence of forward flight. Figure **6-31** a) shows a picture of the 1/48 empennage model mounted on the baseline nozzle. The empennage and nozzle scales were evaluated to be dimensionally accurate within 10% error with the published specifications of the JSF from the website of Lockheed Martin.

A series of measurements were conducted with military-style nozzle of design Mach number 1.5 for a variety of cold jet conditions with M_j varying from 1.3 to 1.7, with and without the empennage model. The experiments include three various azimuthal angles for the empennage model, as defined from the picture of Figure **6-31** a). For all values of M_j tested and all azimuthal angles, no effect was observed due to the presence of the empennage. Figure **6-31** b) shows sample spectra, acquired at M_j = 1.36 where this jet condition at least shows the subtle modification on the screech intensity level. The spectra present a perfect overlap among all different values of ϕ. Extension of these measurements with the addition of a surrounding forward flight simulating flow also presented no acoustic effects of the empennage model.

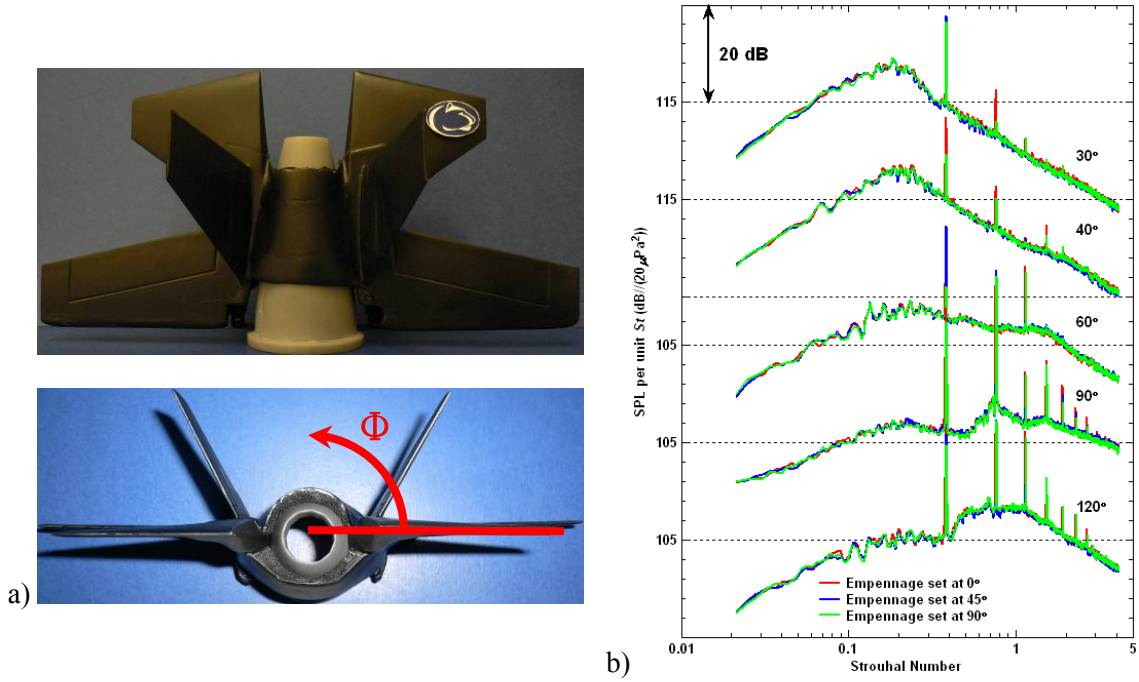

Figure **6-31**: a) 1/48 scale aircraft model end view with model rotating azimuthal angle, φ, where red line represents the measured plane of microphone array. b) Spectra comparison from measurements conducted with GE M_d 1.5 baseline nozzle operated at M_j = 1.36, cold accompanied with empennage set at φ = 0°, 45°, and 90° respectively.

6.8 Summary

Preliminary baseline jet acoustic measurements performed earlier have demonstrated very good agreement between the small scale experiments performed at Penn State and moderate scale data acquired at NASA Glenn Research Center. This demonstrates the supersonic jet acoustic scaling methodology used. This chapter hence continues from the previous chapters by providing an acoustic assessment of small-scale military-style nozzles with chevrons. Three chevron configurations were selected for the acoustic measurements. In studying the effect of chevrons in the supersonic jets, the jet operating conditions reveal that there is a need to adequately adjust the penetration angle of the chevrons for the optimization of the acoustic benefit with consideration given to anticipated propulsion efficiency penalties. The acoustic benefit of the converging chevron nozzle with chevrons possessing no penetration angle operated at M_j = 1.5 cold jets shows an average 2 dB noise reduction observed in the peak noise direction (around 30°) across the entire frequency range. The effect of chevrons, shrinking the shock cell structures and improved jet spreading, is clearly evident, similar to the observation in moderate scale jets.

The subsequent experiments, with the military-style CD nozzle with chevrons possessing low penetration angle, fail to show any acoustic benefit for the over-expanded conditions. However, significant noise reduction is seen for nozzle operated at under-expanded conditions. This demonstrates the importance of both the jet operating condition and the penetration angle of the chevrons.

While a good match was demonstrated between measurements conducted with baseline nozzles in small- and moderate-scale jets, it was unproven for small-scale jets with chevrons. In the current study, identical CD chevron nozzles with chevrons possessing a large penetration

angle were individually built at Penn State and NASA GRC (with a scaling factor of 7). This study tried to assess the scaling issue with chevron nozzles and the best acoustic benefit of jets operated at a similar condition to that of military aircraft at take-off. In the cold jet case, there is a noise reduction of about 2 dB in the maximum noise emission direction, confirming the ability of the chevrons to affect the over-expanded jets. However, in the heated jet case, there is no perceptible noise reduction due to chevrons observed in the small-scale measurements, while the larger-scale ones do show a significant effect. The hypothesis advanced is that the Reynolds number in the heat-simulated small scale measurements is low enough to sustain an annular laminar boundary layer in the nozzle that is more sensitive to separation than is a turbulent boundary layer. In the over-expanded condition it is likely that the adverse pressure gradient at the exit is separating the boundary layer to the point that the chevrons have an imperceptible effect on the flow, and the subsequent noise reduction. In further explaining this hypothesis, a rougher chevron nozzle was fabricated in order to trip the flow to transition to turbulence, or at least introduce enough disturbances to delay separation. In doing so, the small-scale experiments show similar effects of the chevrons on heated jets as the moderate-scale measurements. However, the noise reduction levels are still not as high as the one observed in the moderate-scale jets.

Based on the demonstration of the scaling methodology from the measurements of the baseline nozzle individually conducted in the small scale jets at Penn State and the moderate scale jets at NASA GRC, one can confidently state that the acoustics issued from the small scale supersonic jets can appropriately predict the acoustics issued from the moderate-scale supersonic jets or even the full-scale engine exhausts. However, some of the flow field phenomena may be limited in the small-scale jets, which can not adequately mimic some details of the actual flow field appearing in the larger-scale jets. As a result, while the expected noise reduction (at over-expanded condition) from the chevron nozzle is observed with cold small scale jets, it is absent from small scale heat simulated jets with low Reynolds number. Further studies will focus on the

corresponding noise reduction level between small and moderate scale jets to deliberately assess the capability of the noise reduction in non-actual engine scale measurements and the potential effect of the Reynolds number.

Lastly the flow field measurements performed with a pitot rake set up with chevron nozzles further distinguish the flow field of the supersonic cold jets due to chevrons. It was shown that the jet spreading and entrainment are largely improved in the measurements conducted with chevron nozzles operated at under-expanded condition especially within the range of the first 2 nozzle diameters. The induced flow-field changes appear to recover to the same flow field as the one issued from the round nozzle.

Chapter 7

Conclusions and Future Work

7.1 Summary of objectives

The goals of this thesis were to:

- Perform extensive acoustic measurements with several supersonic nozzles operating at various pressure and simulated temperature ratios to create a database with which to develop improved understanding of supersonic jet noise relevant to military (fighter) aircraft.
- Through extensive comparison with moderate-scale (NASA) supersonic jet acoustic measurements, develop a methodology for using small-scale data to reliably predict the noise at moderate scale. (Ultimately this will be used to carry the predictions to full-scale engine noise).
- Investigate the ability of the newly developed scaling methodology to accurately predict the ability of chevron nozzles to accomplish noise reduction in a series of representative chevron designs and jet operating conditions.

7.2 Major results

The acoustic measurements of small-scale models of a military style supersonic nozzle were conducted in unheated and heat simulated jets in the jet noise laboratory at Penn State. The scaling methodology was developed to produce spectral comparisons between the small scale measurements made at Penn State and the moderate scale measurements from NASA Glenn Research Center. The comparisons of various scales of supersonic jets operating at the same condition (same pressure and temperature ratios) closely match each other. These comparisons

also partially include the experimental data acquired at NASA Langley Research Center and the Boeing Low Speed Aeroacoustic Facility conducted with similar but not identical round CD nozzle. These extensive spectral comparisons verify the data processing methodology and validate the experimental accuracy for the acoustic measurements conducted in the small-scale jet noise facility at Penn State.

The major results, in more detail, are categorized and described below.

- Baseline round nozzle experiments

A series of experiments have been conducted with the baseline round nozzles at Penn State. These measurements replicate the same operating conditions (cold and hot jets) of the moderate-scale measurements conducted at NASA. The scaling methodology from those high quality experimental data has been developed and shows that the acoustic spectra and *OASPL* of the NASA data are closely replicated by the small-scale Penn State experiments.

- Near-field / Far-field acoustic measurements

A series of acoustic measurements were conducted to first evaluate the impact of the measured microphone locations at the same polar angle originating from the nozzle exit plane. An empirical approximation of the noise source distribution of a supersonic M_j 1.5 heated jet concluded from the phased array microphone measurements is used to represent the noise source locations in developing an accurate scaling routine to develop true geometric far-field spectra at specific polar angles. The effect of the jet noise source distribution was examined while performing this scaling methodology. At the current stage, the observed discrepancies on the near-field / far-field acoustic measurements are well interpreted as the impact of the jet noise source distribution on the measured microphone array. These observed discrepancies among the measurements acquired at various radial locations were documented. An advanced processing method was developed to allow for more accurate comparisons of spectral measurements from vastly different distancesfrom the nozzle exit plane. By using reliable measurements of the jet noise source

distribution [74], synthesized spectra were obtained from acoustic field measurements (at 35 to 70 jet diameters) to accurately reproduce measured spectra in the geometric far-field (140 diameters). This part of data processing strengthens the accuracy and understanding of the overall scaling methodology.

- Baseline round nozzle with chevrons experiments

The baseline jet acoustic measurements performed have demonstrated very good agreement between the small scale experiments performed at Penn State and moderate scale data acquired at NASA Glenn Research Center. While good matching was demonstrated between measurements conducted with baseline nozzles in small- and moderate-scale jets, the consecutive task was to evaluate the small-scale jets with chevrons. The identical CD chevron nozzles with chevrons possessing a large penetration angle were individually built at Penn State and NASA GRC (with a scaling factor of 7). In the cold jet case, there is a noise reduction of about 2 dB in the maximum noise emission direction, confirming the ability of the chevrons to affect the over-expanded jets. However, in the heated jet case, there is no perceptible noise reduction due to chevrons observed in the small-scale measurements, while the larger scale ones do show a significant effect (with reduction of the peak noise amplitude by about 3 dB). The hypothesis advanced is that the Reynolds number in the heat-simulated small scale measurements is low enough to sustain an annular laminar boundary layer in the nozzle that is more sensitive to separation than is a turbulent boundary layer. In the over-expanded condition it is likely that the adverse pressure gradient at the exit is separating the boundary layer to the point that the chevrons have an imperceptible effect on the flow, and the subsequent noise reduction. To further investigate this hypothesis, a rougher chevron nozzle was fabricated in order to trip the flow to transition to turbulence, or at least introduce enough disturbances to delay separation. In doing so, the small scale experiments show similar effects of the chevrons on heated jets as the moderate-scale

measurements. However, the noise reduction levels are still not as high as the one observed in the moderate scale jets.

- Schlieren visualization experiments

The schlieren flow visualizations were undertaken with various chevron configurations and flow conditions to provide an extensive database of schlieren flow visualization and enable the validation of the location of the shock cells. The schlieren photographs reveal the flow-field modifications due to various chevron configurations and different jet operating conditions. The combined benefit was to collect an extensive database of schlieren visualization.

- Pitot probe experiments

Pitot probe measurements were conducted to study the noise reduction mechanisms of chevrons. The flow-field modifications, physically caused by chevrons, were documented with radial and axial distributions. The statistics of these flow-field modifications were examined and correlated with the chevron configurations and jet operation conditions. These sets of measurements accompanying the schlieren visualization are used to interpret the effect of chevrons on the noise reduction mechanisms.

- Combined forward flight experiments

The simulated forward flight condition was included in the above experiments to provide an extensive database of various nozzle configurations, jet flow conditions, and forward flight conditions. The experimental data of small-scale jets in forward flight further advance the experimental feasilibity of small-scale model jets.

7.3 Summary of the scaling methodology

The methodology developed to scale small jet experiments to moderate and full scale jet measurements is summarized below.

- Develop a data base of comparative experiments all using common nozzle geometries, flow conditions (pressure and temperature ratios), and microphone measurements locations.
- Use the newly developed microphone free-field correction for microphone measurements performed at grazing incidence. Such an orientation is used to minimize the effect of varying acoustic incidence on microphones.
- Nondimensionalize all data and present with common amounts of atmospheric attenuation correction (prefer "lossless") and at common microphone non-dimensional positions.
- When data base for comparisons includes unequal microphone range positioning (*R/D*), using spherical spreading of noise radiation to scale to common range if all data are in the true geometric far-field.
- When using acoustic data that have not been performed with microphones in the true geometric far-field, correct said data based on the method developed by Kuo, Veltin, and McLaughlin [133] that extrapolates (and corrects) the acquired acoustic data base to a true geometric far-field condition for use in the analysis.

7.4 Future work

Inspired by the current work, some issues that can potentially expand the scale of the research are summarized below.

Since the military-style supersonic nozzle is mostly operated at off-design conditions, the dominant noise source of the broadband shock-associated noise (BBSAN) emerging in the jet upstream direction becomes critical to the jet noise radiation. Future study should focus on the effects of supersonic jets' operating conditions on the noise emission of BBSAN. It has been shown that the effect of jet temperature is to gradually increase the magnitude of BBSAN. However, it seems that the magnitude of BBSAN saturates (reaches the maximum) at $TTR = 1.6$

from current experimental data acquired at Penn State. The effect of jet temperature also slightly modifies the peak frequency of BBSAN. Bridges and Wernet [134] have demonstrated that the jet temperature does not alter the shock cell structure, and the shock cell structure is only dependent on the jet Mach number. When the jets become heated, it was found that there is a trend of thickening the jet mixing layer and shortening the jet potential core. These alter the turbulence intensity level of jets as compared to the one from the unheated jets. Then, the interaction between the jet shear layer (with redistributed turbulent structures) and the shock cell structures leads to the peak frequency of BBSAN dissimilar to the one obtained from the cold jets measurements. A more thorough understanding involved the effect of jet temperature on the jet noise radiation, therefore, is expected.

To extend the understanding of the jet noise source distribution, the directional noise emission generated by the large scale turbulent structure dominating in the jet downstream direction can be further examined by the potential capability of the phased array microphone and the near-field OD measurements. To proceed with the phased array microphone measurements, it is crucial to firstly establish a data processing program to process the experimental results. Besides, the near-field jets investigation via the OD measurements might potentially present the noise radiation contours in the near field of jets. The goal of these two measurements is to look at the noise emission pattern in the acoustic near field.

Based on the encouraging demonstration of the scaling methodology from the measurements of the baseline nozzle individually conducted in the small scale jets at Penn State and the moderate scale jets at NASA GRC, it is quite promising to conduct the acoustic measurements with the potential candidate of the noise suppression devices, the beveled CD nozzle, for example. The previous experience on the measurements conducted with the converging beveled nozzle has shown the acoustic benefit of beveled nozzles. To extend the

understanding of these physical phenomena, a further investigation of the beveled CD nozzle should be conducted by establishing the experimental database of the acoustic measurements.

Lastly the capability of the forward flight simulation established in the small-scale jet facility at Penn State has demonstrated reasonable experimental results. The advanced evaluation of the accuracy of the forward flight simulation needs spectral comparisons from the measurements conducted at other facilities possessing similar forward flight capability. This ability will advance the small-scale jet noise facility at Penn State as a premier multi-functional university facility in the United States.

Appendix A

An Empirical Free-field Response of High-frequency Accuracy Improvement for 1/8 inch Microphone Performed under Small-Scale Supersonic Jets

A.1 Motivation

Since the early 1990's, supersonic jet noise research has seen renewed interest, largely due to the High Speed Civil Transport program carried on by NASA during that decade. Mixing of high speed jets with ejector flows was then envisioned as a very promising way to reduce the flow speed, and hence the acoustic signature. With the discontinuation of the project in 1999, jet noise research groups have shifted their work toward military jets, since these are still the (largely) dominant noise source during military aircraft operations. The high noise levels induced by these hot supersonic jets are a health threat to military personnel during take-off, and an annoyance to communities in areas surrounding airports. However, the very low bypass ratio of such jets does not allow the use of ejectors as a noise reduction mechanism. Efforts to modify the jet flow in more subtle ways in order to reduce the emitted noise have reached sound reductions of the order of 3 decibels (dB). Acoustic measurements of great accuracy are therefore needed in order to properly assess the efficiency of noise reduction concepts.

To contribute to research efforts, the jet noise laboratory at the Pennsylvania State University (PSU) has been conducting small-scale measurements for the past 15 years. These experiments have produced data with reasonable accuracy compared to moderate scale or full-scale measurements made at NASA or in industrial laboratories. Acoustic measurements are made in the Penn State facility with single-stream supersonic jets of diameters between 0.5 in. and 1 in., which correspond to a 1/40 to 1/20 ratio with full scale engine exhaust jets.

Comparisons between data measured at Penn State and those acquired in larger facilities were first made by Doty and McLaughlin [49] and showed reasonably good agreement. However, efforts to develop improved accuracy have become more important as some of the proposed methods to reduce jet noise do significantly decrease the peak noise in the dominant noise propagation direction but often increase the high frequency noise (that has less directional character). It is therefore important to be able to determine these high frequency components more accurately than in prior years. A major goal of the Penn State high speed jet noise experiments has been to assess the accuracy of using acoustic data measured with small-scale jets to predict the noise generated by moderate-scale and full size exhaust jets. Examples of moderate-scale jet acoustic experiments include those currently being conducted by Boeing [45], [54], GE Aircraft Engines and NASA [52], [53].

The fundamental basis of scaling data from small jet experiments to moderate-scale jets is to properly non-dimensionalize the data. [Industrial practice often incorporates the subsequent step of re-dimensionalizing the resulting data to larger-scale sizes (often actual engine).] In any event, initial non-dimensionalization is the proper fundamental first step. To establish the reliability of any such scaling effort, it is important to compare small-scale acoustic spectral data recorded at identical non-dimensional positions as those made with larger (either moderate-scale or full size) jet experiments. These spectral data are plotted as a function of non-dimensional frequency (Strouhal number). In this conversion process it is important to adjust the spectral levels so that the non-dimensional spectral levels integrate to the correct level of overall sound pressure level (*OASPL*). This is not enough, however. As noted by Doty and McLaughlin [49], Viswanathan [45] and Ahuja [135] among many others, appropriate accounting (with corrections) must be made of the effects of non-uniform response of the microphones with frequency, particularly at high frequencies where the acoustic wavelengths become smaller, and approximately the size of the microphone diaphragms.

In addition to the microphone corrections, the atmospheric attenuation correction become increasingly important as this attenuation scales with the square of the frequency, which itself is proportional to the inverse of the size scale. Therefore, the high frequency end of jet noise spectra suffers severe attenuation during propagation. This must be accounted for in any accurate jet noise scaling prediction method. The method described by Bass *et al*. [136], [137] for correction of atmospheric attenuation effects has gained widespread acceptance in the jet noise community for its accuracy. The microphone responses on the other hand normally rely almost completely on manufacturers' specifications. These have, for the most part, worked well, with very few investigators questioning the final results. Such is not the case for all experiments, in particular for those performed with the current set-up in the jet noise research laboratory at Penn State.

As part of the Penn State jet noise research, numerous comparisons were produced between acoustic measurements obtained from specific jet flows at Penn State and in larger facilities using virtually identical nozzle geometries (except for the scale size). After careful examination of such acoustic spectral comparisons, discrepancies were identified in the highest frequency range. An example of such a comparison is shown in Figure **A-1**, where acoustic spectra from measurements acquired at Penn State were processed following the microphone and atmosphere attenuation correction methodology used in numerous past experiments [62], [71]. These spectra are plotted together with spectra acquired at NASA using a supersonic nozzle of identical internal geometry (and area ratio of AR = 1.18), but an exit diameter 7 times larger. There is a hump in the PSU spectra at non-dimensional frequency (Strouhal number) between (approximately) 2 and 4. These measurements were obtained with 1/8 in. diameter condenser microphones and correspond to a rise of the spectra occurring around 50 to 80 kHz and attenuation at frequencies approaching and above 100 kHz. It is noted that the data plotted in Figure **A-1** have been fully corrected for conventional microphone and atmospheric attenuation

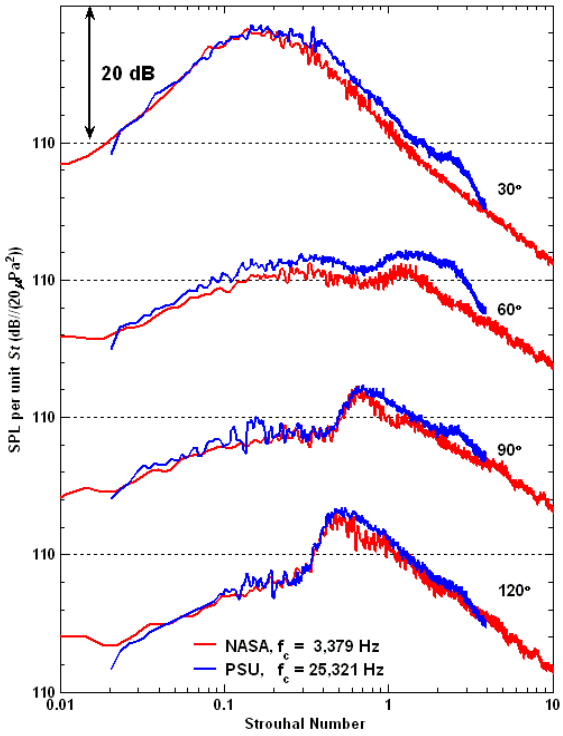

Figure **A-1**: Lossless spectra comparison from PSU (processed with the published free-field response) and NASA both issuing from $M_d = 1.5$ ($AR = 1.18$) GE nozzle operated at $NPR = 4$, $M_j = 1.56$, and scaled to $R/D = 100$.

response [136], [137]. These discrepancies occur across all polar angles and similar observations were made across a large range of jet conditions. Comparisons made between measurements performed at the Penn State facility with nozzles of two different sizes (0.5 in. and 1 in.) also showed similar discrepancies, as can be seen in Figure **A-2**. Though the spectra were plotted in terms of the non-dimensional frequency (Strouhal number), a consistent discrepancy was still observed within the same dimensional frequency range. The fact that these mismatches appeared between measurements performed on the same day and in the same facility tends to cast some doubt either on the reliability of the microphones or on the accuracy of the corrections applied to the measurements at high frequency. It is noted that the microphones used for these measurements were placed at a grazing incidence. Justifications for this setup are detailed in the

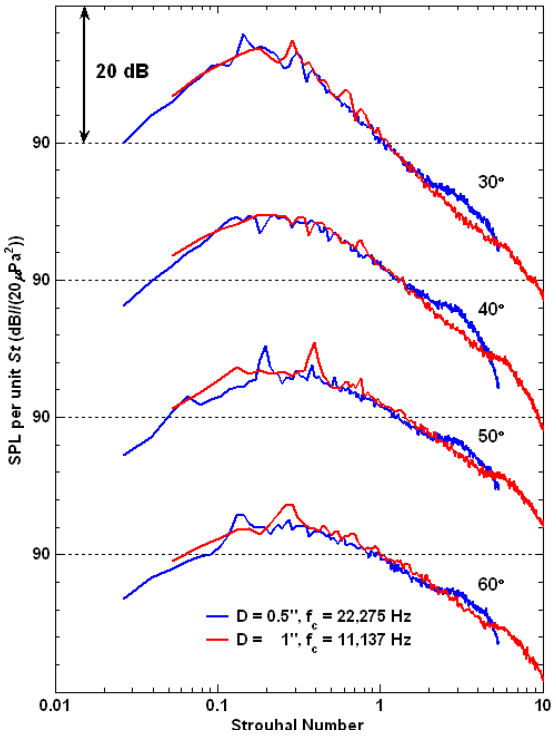

Figure **A-2**: Lossless spectra comparison from PSU (processed with the published free-field response) issuing from two converging nozzles with a ratio of two in the nozzle exit diameter operated at $NPR = 1.69$, $M_j = 0.9$, and scaled to $R/D = 100$.

result part of this Appendix. It should also be mentioned that Viswanathan [45] clearly showed a small discrepancy within this specific non-dimensional frequency range (after accounting for the scale size of his ¼ in. microphones) when comparing measurements from microphones in normal and grazing incidences. Some investigation work was thus carried out in order to assess whether the microphone responses provided by the manufacturer [138] (and in numerous subsequent publications [139]) are accurate enough to provide reliable high frequency data.

The systematic discrepancies that are present in the high frequency portion of the data shown in Figure **A-1** and Figure **A-2** are found in almost all of the Penn State acoustic spectra recorded and processed within the past 5 years. It is noted that within that time frame two changes were made to the microphone array.

1) In an effort to reduce the sensitivity of the microphone to directional variations that are part of measuring noise from distributed (non point) acoustic sources, an array of microphones, *all at grazing incidence* was developed. (The microphone diaphragms are all arranged in a plane that intersects the centerline of the jet, thus assuring that the acoustic waves propagation direction is at a grazing incidence to the microphone.)

2) Several of the new microphones that were added (or replaced) were manufactured by *GRAS* (model 40 DP). These microphones have excellent dynamic range and signal to noise ratio but they have different actuator responses from their Brüel and Kjaer (*B&K*) model 4138 counterparts. It is also noted that *GRAS* does not provide full free-field frequency response data as does *B&K*. Anticipating that the free-field response is predominantly due to acoustic refraction, prior practice in the laboratory of Penn State was to use the *B&K* data for this specific correction. Initially this procedure was not verified

At the initiation of the present study, the suspect sources of uncertainty were attributed to: 1) locating the microphones at a distance not quite in the true geometric far-field of the jet, 2) not accounting for the effects of the angle of incidence of the sound waves onto the microphone diaphragm, due to the distributed nature of the noise source, 3) inaccuracy of the non uniform microphone response with frequency for microphones with grazing incidence (and protective grid caps), particularly for *GRAS* microphones, 4) inadequacy of the atmospheric attenuation correction.

Focusing back on the discrepancies seen in Figure **A-1** and Figure **A-2**, the goal of the present study was to conduct numerous microphone measurements in a repeatable acoustic field (produced by supersonic jets) to examine the sensitivity to the aforementioned parameters and develop an improved processing methodology to provide improved accuracy.

A.2 1/8 in. microphone response

Almost all laboratory measurements obtained from small to moderate high speed jets apply microphone and atmospheric attenuation corrections to the acoustic data. At Penn State the condenser microphones of the type manufactured by *B&K* and *GRAS* that have the high frequency response needed for air jet noise experiments are specifically referred. The first correction to be applied results from the non-uniform actuator pressure response (also referred to as electrostatic actuator pressure response). This response relates the ratio of the *RMS* output voltage to the *RMS* of a sound pressure uniformly applied to the diaphragm, as a function of frequency. This frequency response is dependent on the details of the microphone diaphragm dynamics and the preamplifier circuit that is connected directly (through an adaptor) to the microphone. These responses are normally quite similar, but are provided by the manufacturer for each microphone. Figure **A-3** is an example of manufacturer's supplied data for *B&K* 1/8 in. microphones.

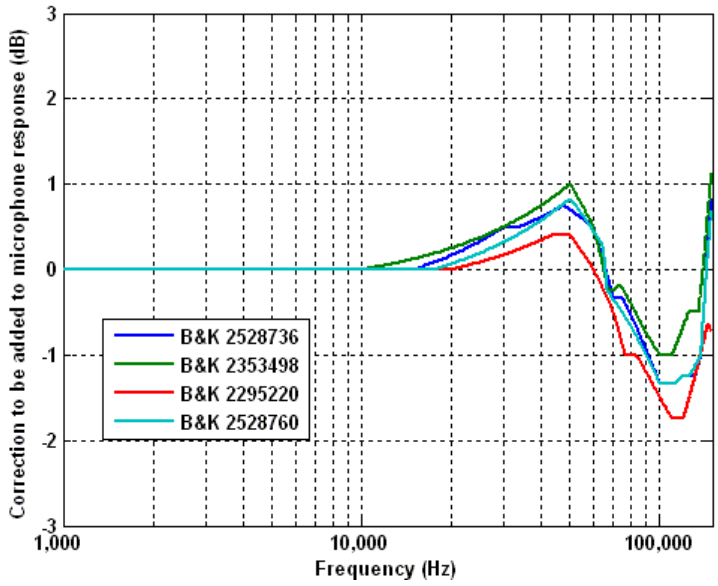

Figure **A-3**: The magnitude of actuator response for microphones fabricated by *B&K*.

The second type of non-uniform frequency dependence of a condenser microphone is referred to as free-field response, an example of which is shown in Figure **A-4**. These data are provided by *B&K* [138], [139] for a 1/8 in. diameter microphone that is at either normal or grazing incidence to the direction of propagation of the acoustic field. It is noted that all experiments at Penn State are made with the grid caps on to prevent accidental damage, and the data of Figure **A-4** are provided for that configuration.

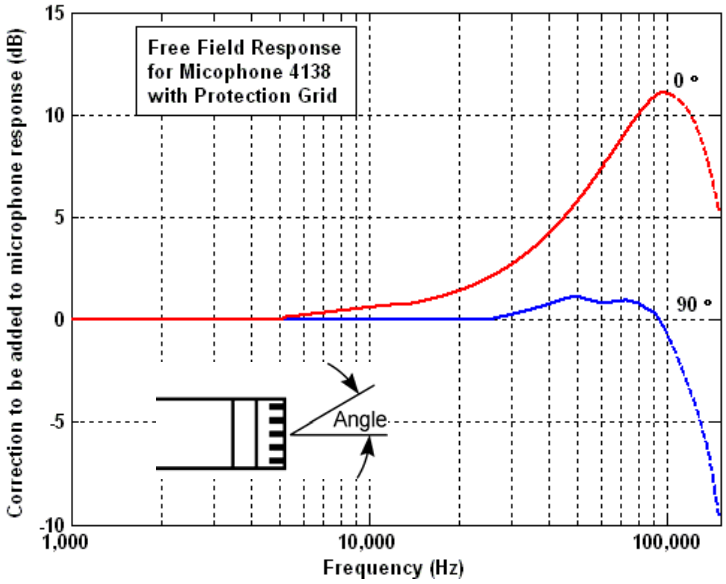

Figure **A-4**: Published *B&K* free-field response [138], [139] provided by the manufacturer for two microphone incidences.

For best accuracy of any jet noise acoustic (microphone) measurement, it is standard practice to correct the spectral data for these two aspects of non-uniform frequency response. This was mentioned earlier when introducing Equation **3.3**.

A.3 Examination on data processing procedure

A key component of the work to establish new response data to use in an appropriate compensation or correction routine is to have a standard of reliable and accurately measured data. As can be seen in Figure **A-1** and Figure **A-2**, two such possibilities are used involving a larger jet nozzle at Penn State, and data measured at NASA with larger jets and facilities.

To reiterate, in performing microphone experiments, three physical corrections and two dimensional conversions are applied to the raw data to compute the lossless spectra. Those dimensional conversions are applied to all frequency components with identical magnitude. The values of spectrum as a function of frequency after the dimensional conversions thus exhibit consistent magnitude shift across whole frequency range. On the other hand, three physical corrections are all functions of frequency and their magnitudes increase with the frequency. Figure **A-5** shows an example of spectra with raw data applied the dimensional conversions only. Figure **A-6** shows their lossless spectra (included three physical corrections). As one can see, the discrepancy emerges after the applications of physical corrections. To spot potential errors during data processing procedure an effort was made to examine individual components of the microphone corrections one by one. These individual examinations are presented in the following sections.

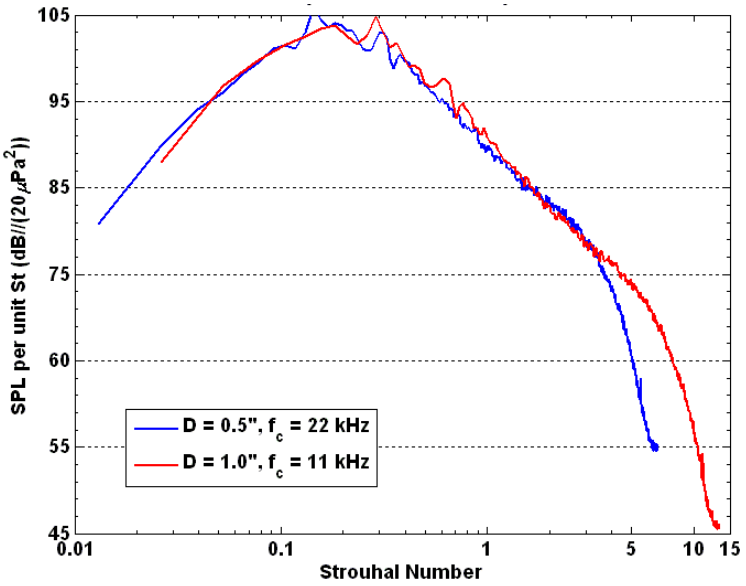

Figure **A-5**: Raw data comparison from PSU issuing from two converging nozzles with a ratio of two in the nozzle exit diameter operated at $NPR = 1.69$, $M_j = 0.9$, scaled to $R/D = 100$, $\theta = 30°$.

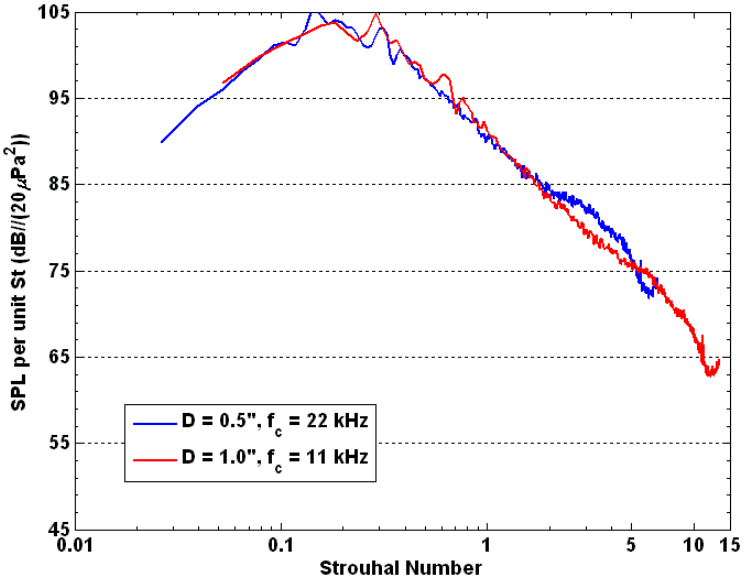

Figure **A-6**: Lossless spectra comparison from PSU issuing from two converging nozzles operated at $NPR = 1.69$, $M_j = 0.9$, scaled to $R/D = 100$, $\theta = 30°$.

A.3.1 Effect of the atmospheric attenuation correction

While sound waves travel in the air, its amplitude reduces due to the energy loss on the molecular vibrational relaxation related to the atmospheric humidity and traveling distance. The corresponding loss as a function of relative humidity, temperature, and pressure has been examined by many researchers [136], [137], [140]. The expression and calculation also can be found in the Standard [141] published by American National Standards Institute as shown in Figure **A-7**. The sound attenuation level exponentially increases with frequency causing a rapid drop in the high frequency end of measured raw spectra as shown in Figure **A-5**.

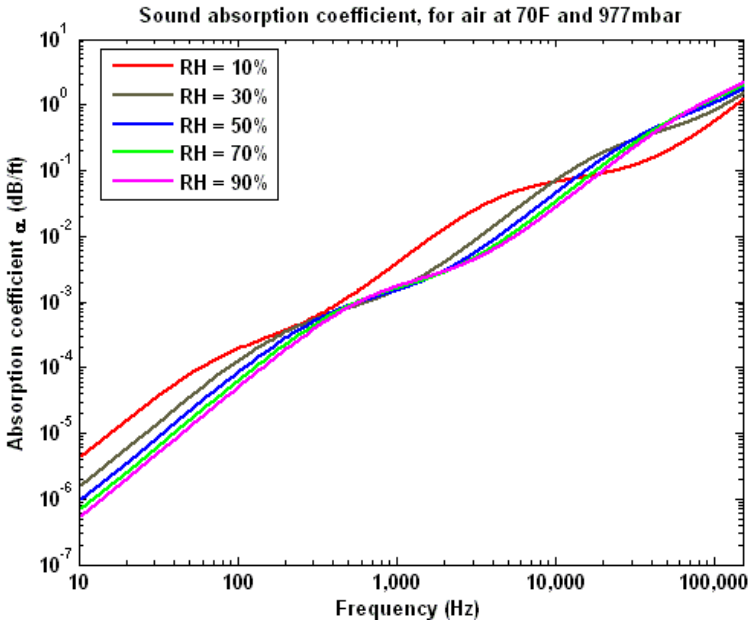

Figure **A-7**: Effect of the relative humidity on the sound absorption coefficient of air at averaged ambient condition (T = 70 F, P = 977 mbar).

Because experiments are typically conducted under different atmospheric (humidity and temperature) conditions, the application of the atmospheric attenuation correction was first examined for a potential source of error. Experiments were first conducted with various humidity levels and temperatures to assess the exact influence of these on the atmospheric attenuation

correction and on the resulting corrected spectra. It was determined that one could gain some control of the humidity in the anechoic chamber by running the dried air jet for an extended period of time without using the exhaust fan, thus lowering the room humidity quite substantially.

Figure **A-8** a) shows an enlarged view of the highest frequencies of the spectra processed via the formula shown in Equation **3.3** and obtained for two humidity conditions. Although it is a lossless spectrum, the comparison still exhibits a constant discrepancy in the frequency range from 50 to 120 kHz, after correcting for the atmospheric attenuation. The corrections for atmospheric attenuation for the two humidity conditions of the data in Figure **A-8** a) are shown in Figure **A-8** b). The shape of such corrections is such that they cannot cause the bulge that remains in the data of Figure **A-8** a) following data processing. It is noted that, for these extreme humidity conditions, the spectra collapse within an accuracy of ± 1 dB across the frequency range. The next individual effect to examine was the actuator response.

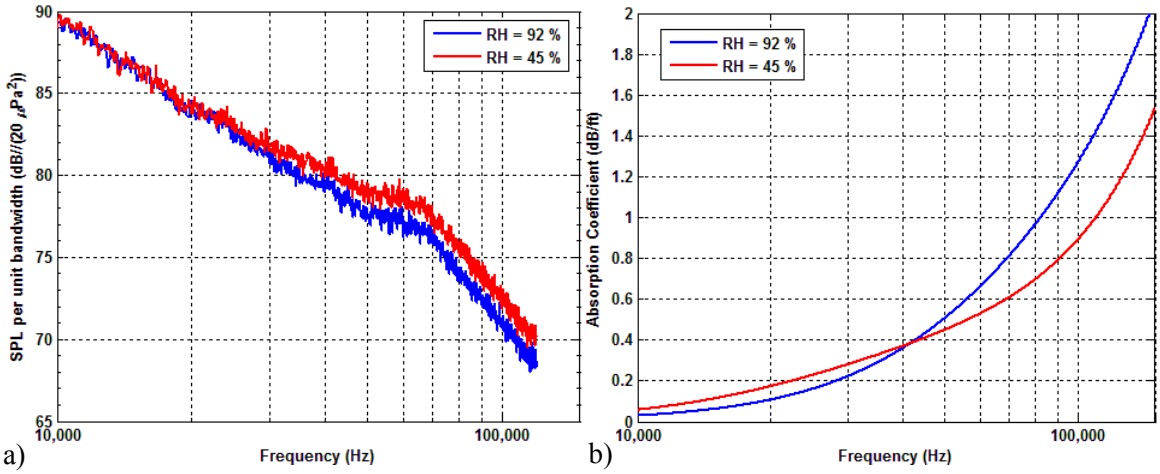

a) b)

Figure **A-8**: a) Lossless spectra from PSU (processed with the published free-field response) issuing from M_d = 1.5 (AR = 1.18) GE nozzle at relative humidity of 92% and 45% operated at NPR = 4, M_j = 1.56, scaled to R/D = 100. b) Atmospheric absorption coefficient (based on the method of Bass *et al.* [136], [137]) according to the relative humidity of 92% and 45% in response with frequency.

A.3.2 Effect of the actuator response

The second effect to be presented is the actuator response that is specific to each microphone and results from a pure electronic calibration by the microphone manufacturer. Figure **A-3** and Figure **A-9** show the magnitude of the actuator responses for each microphone used in the current measurements from two manufacturers. As can be seen, their value is within ± 0.5 dB for the *B&K* microphones and within ± 2 dB for the *GRAS* microphones (for frequencies below 100 kHz). Since these given values are recorded from an electronic calibration with the response from the microphone diaphragm, the fidelity and precision of the actuator response is reliable. A large body of experimental spectra has been measured using a number of microphones and no consistent pattern appeared, apart from the "bulge" evident in the high frequency part of the spectra in Figures **A-1**, **A-2**, and **A-8**. Thus it was concluded that the actuator response is not responsible for any processing errors in the present experiments.

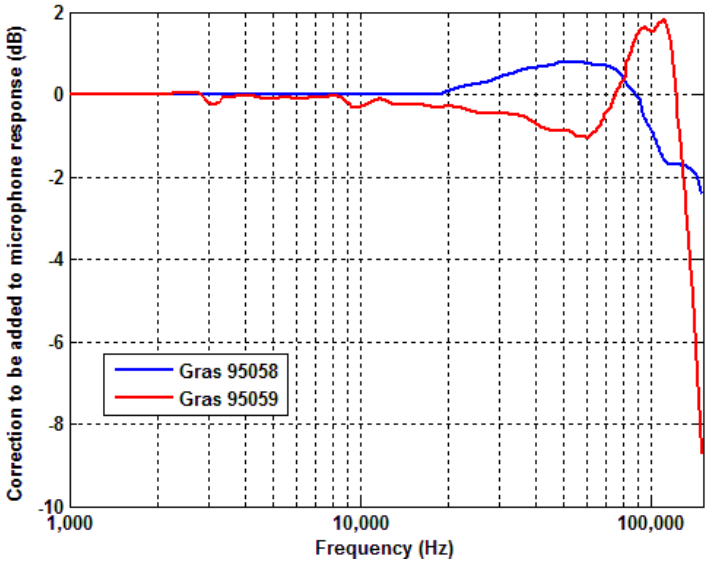

Figure **A-9**: The magnitude of actuator response for microphones fabricated by *GRAS*.

A.3.3 Effect of the free-field response

The last physical correction notably affecting the spectral features is due to the free-field response of the microphone, which also varies with the incidence of the microphone to the sound field. During typical measurements in the high speed jet noise facility at Penn State (as mentioned earlier), the microphones are all oriented at a grazing incidence, meaning that rather than facing the jet exit (normal incidence), the diaphragm plane is oriented such that it contains the jet axis. This incidence was originally chosen for two reasons: 1) the ease of fabrication of a moving (rotating) microphone boom in order to cover all jet polar angles with the limited number of microphones that are affordable on a university budget, 2) in studies on non-linear propagation, reliable estimates of the signal skewness were sought, typically calculated from the time traces before microphone corrections. Since microphones at grazing incidence have lower corrections as a function of frequency, this orientation was judged as preferable in the scope of non-linear propagation studies. It however became obvious that the grazing incidence has a third, equally important advantage: the great majority of the measured sound intersects the microphone at the grazing incidence (90˚) within a very close tolerance. In a typical normal incidence setting, angles as high as 8 degrees can be observed due to the length of the distributed source of the highest speed supersonic jets being measured as mentioned in chapter **5**. Such uncertainty in the incidence angle is undesirable since the free-field correction varies largely with wave incidence.

In order to investigate the validity of the free-field response, microphones were set up in pairs in the far-field of both transonic and supersonic jets at the same polar and radial positions but different azimuthal locations to avoid noise reflection from one sensor to another. In each pair one microphone was set to normal incidence and the other to grazing incidence. The measured data were processed with the free-field response corresponding to either the grazing incidence or the normal incidence from prior manufacturer's data [138], [139]. An example of the high end

portion of the resulting spectra is shown in Figure **A-10**, in which the top two traces show raw spectra as measured and the bottom two show lossless spectra following Equation **3.3**. As one can see, the raw spectrum generated from the microphone at normal incidence clearly shows a higher response of the microphone at high frequencies (by as much as 2.5 dB). However, the lossless spectra, processed using the free-field response published by *B&K* and shown in Figure **A-4**, do not collapse to the accuracy set as a goal for the current study. For such an experiment the goal for accuracy/repeatability is ±0.5dB. Numerous such comparisons showed the same effect: the small hump persists in the spectra given by the microphone with grazing incidence. It is quite

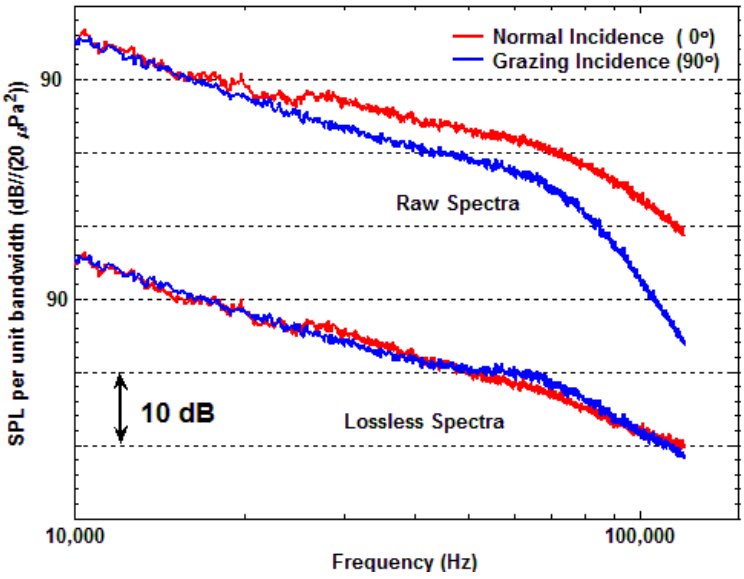

Figure **A-10**: Measurements made with two microphones, one grazing and the other facing the jet exit plane. Raw spectra as measured at the top, and the lossless spectra as calculated via Eq. **3.3** (process with the published free-field response) clearly present the sensitivity of the microphone incidence.

apparent that the difference in the free-field response, which is up to 10 dB from normal (0°) to grazing (90°) incidence, is located at the same frequency range as the bulge. Therefore, the free-field response is highly susceptible to be the source of the observed discrepancy in the high frequency portion of the spectra. Firstly, it is noted that the assumption that the *B&K* free-field microphone correction could be applied to the *GRAS* microphone data with reasonable accuracy

was not substantiated by the data. Secondly, the data of Figure **A-10** showed that the 40 years old *B&K* data [138], [139] do not appear to have the precision that is desired for the current study. The combined evidence leads to the conclusion that the discrepancy in the processed data can be attributed to the application of *B&K* free-field response data to both *B&K* and *GRAS* microphone measurements in the manner previously followed.

Therefore, the data of Figure **A-10** demonstrates the need for a revised free-field response for accurate measurements at the highest frequencies.

A.4 Development of an empirical free-field response

A direct way to produce a new free-field response is to build it empirically from a representative matrix of measurements. For this purpose, an extensive matrix of operating conditions is necessary to provide a diversified data base. The experimental results used for the construction of the empirical free-field response were conducted at Penn State with a 0.5 in. converging-diverging nozzle, operated with different Nozzle Pressure Ratios (NPR's). Six microphones were used, located at polar angles $\theta = 30°$ to $80°$ with $10°$ angular separation and the time records were acquired for numerous jet conditions. The signal path of the connections for the instruments is crucial and was carefully documented. The method followed to establish the new (PSU empirical) free-field correction was to make the numerous measurements described above and make all microphone (and atmospheric attenuation) corrections using the previous method. (The previous method (hereon referred to as method 1) uses the free-field correction shown in Figure **A-4** for grazing (90°) incidence). A large matrix of such data was assembled, examples of which are shown in Figure **A-11**. A straight line (in red) was added on the figure and manually aligned with the spectra. This line of constant slope essentially follows the spectral data measured by NASA (Figure **A-1**) and data measured in the laboratory of Penn State with the

larger 1 in. diameter nozzle (Figure **A-2**). These spectra are referred to as the "standard spectra" to which new data should be corrected to. The discrepancies between the data produced by method 1, and the accepted standard spectra (from NASA e.g. Figure **A-1**) were all documented and sorted into two categories (*GRAS* microphones and *B&K* microphones). These data were all averaged at an appropriate number of frequencies from which new PSU empirical free-field response functions were derived. Such improved response functions are subsequently used for the free-field portion of the corrections (as first summarized in Equation **3.3**). A plot of the new free-field corrections (one each for *B&K* and *GRAS* microphones) is show in Figure **A-12**. The previously published *B&K* correction for this specific microphone condition is shown on the same graph.

To reiterate, this free-field response has been developed using a large amount of experimental data to optimize the accuracy of grazing incidence microphone measurements. At this point it is important to point out that all of measurements made to date indicate that the *B&K* published data for normal incidence is very accurate, both with and without the grid cap.

A final comment is appropriate regarding Figure **A-12**. Included are two photographs of the grid caps of the *B&K* and *GRAS* 1/8 in. microphones. The slight difference in the details of these grid caps could account for the small differences in the frequency response of the two microphones. Additionally, it is important to continue to apply the individual actuator response correction for each microphone, particularly if both *B&K* and *GRAS* microphones are used in the experiments. Additional attention must be paid at these high frequencies to the characteristic of the response of the drive amplifiers in the frequency range near 100 kHz.

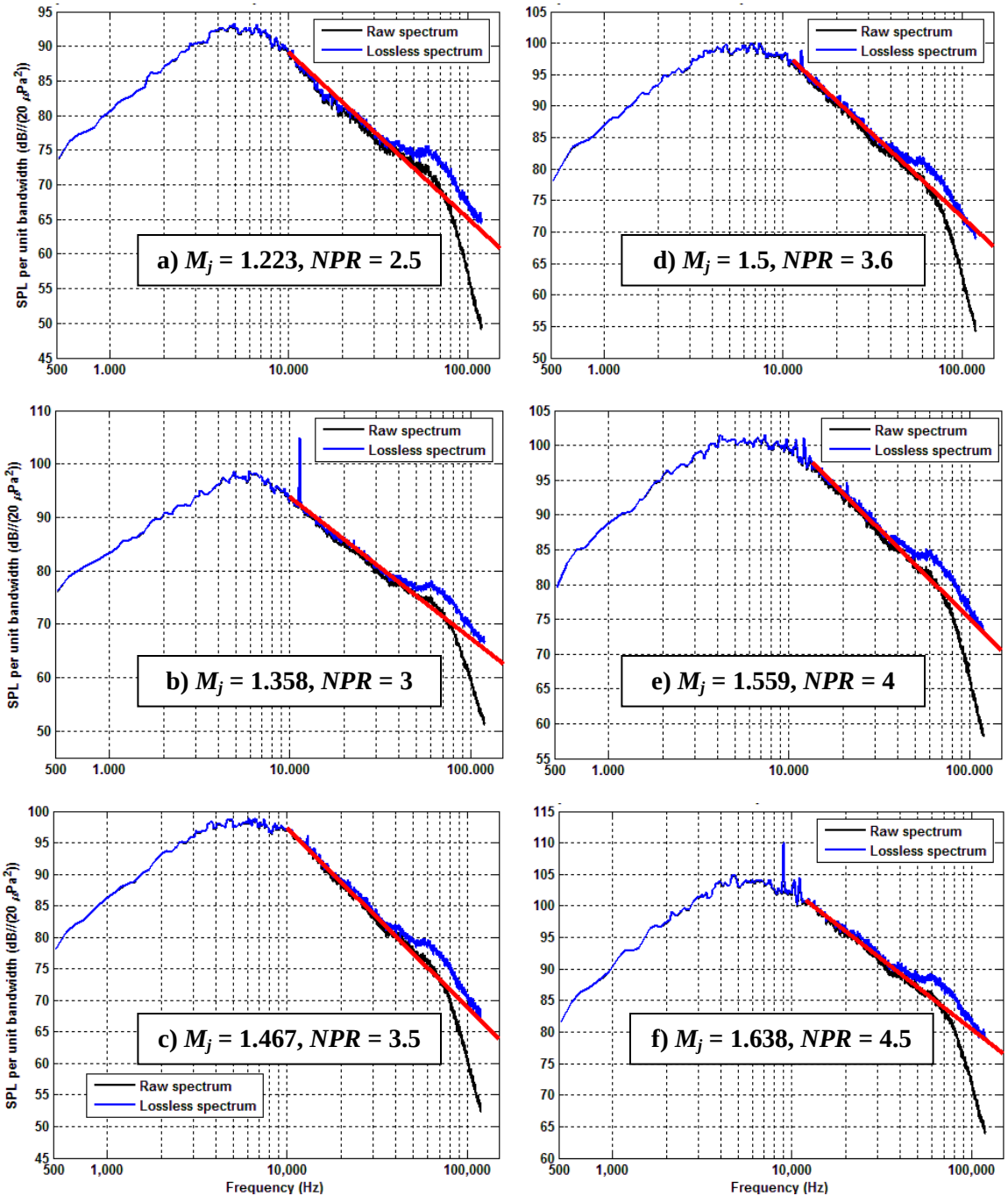

Figure **A-11**: Raw spectrum as measured and the lossless spectrum as calculated from Eq. **3.3** are conducted with the converging-diverging nozzle (M_d = 1.5, D = 0.5 in.) at 30°. The red lines correspond to the expected roll-off slope of the spectra at high frequency and a consistent discrepancy is observed in comparison with the lossless spectrum (blue).

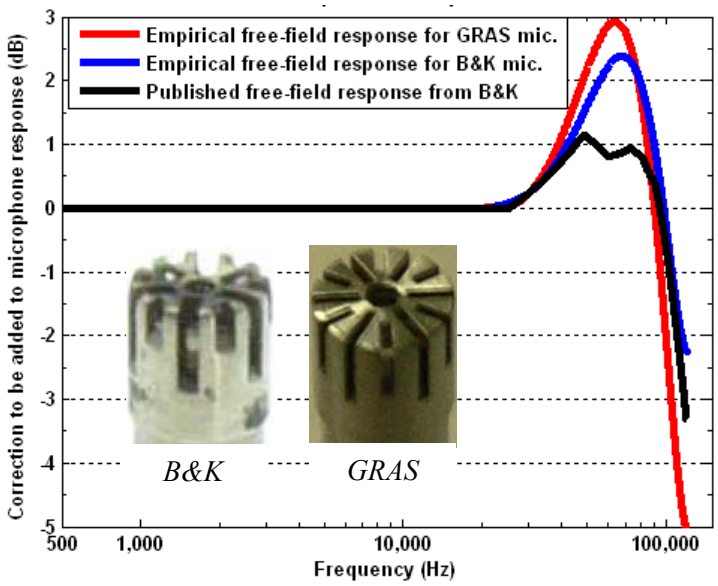

Figure **A-12**: The empirical free-field response obtained from current method compared with the published free-field response from *B&K* [138], [139].

A.5 Validation of the empirical free-field response

In order to validate the empirical free-field response, the responses published by the manufacturers are replaced by the newly developed ones and used for processing of another set of data acquired at Penn State. The resulting spectra were then compared to three groups of data all acquired at NASA Glenn Research Center and referred to as medium-scale data all provided by Dr. J. E. Bridges [58]. Before performing the comparison between the acoustic measurements from the two facilities, the received data from NASA were transformed to non-dimensionalized frequency and propagated back to $R_{prop} = 100\ D_j$.

The validation comparisons with NASA data were performed with data obtained from experiments conducted with two sizes and types of jets. The first were conducted with nozzles designed and provided by GE Aviation corresponding to nozzles of the F414 engine family. Figure **A-13** and Figure **A-14** show comparisons of the Penn State acoustic data using the new

microphone correction method with NASA data performed with jets issuing from a nozzle of matching internal contour, but 7 times larger.

A comparison of data measured at Penn State with those at NASA Glenn Research Center for this GE nozzle operated at under-expanded condition was shown in Figure **A-1**, using the previously published free-field response correction. Figure **A-13** now shows the same comparison with the new empirical free-field response. As can be seen, the high frequency content of the two spectra now matches very closely over all polar angles. The data in Figure **A-13** are recorded with a slightly underexpanded jet. Figure **A-14** presents a similar comparison with jets issuing from the same nozzle in an over-expanded condition. A good agreement of the high frequency content of the two spectra is reached again, with less than 2 dB deviation between the two experiments. In both cases the measurements of the broadband shock associated noise is replicated with excellent accuracy.

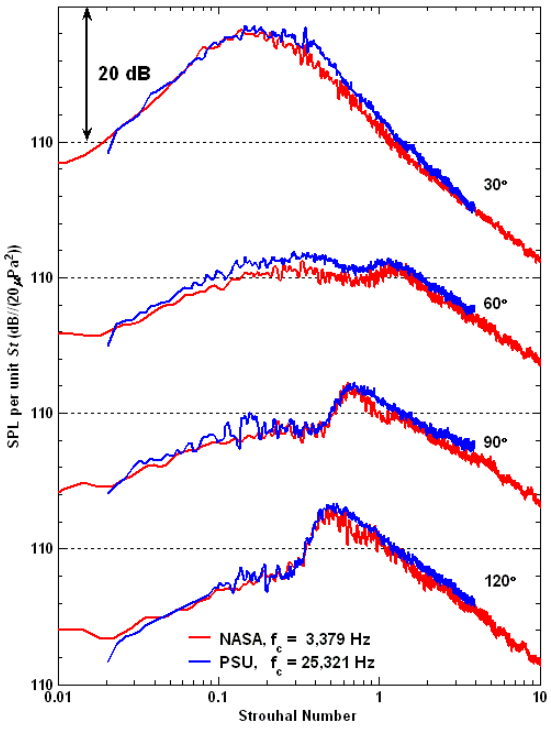

Figure **A-13**: Lossless spectra comparison same as Figure **A-1** with the experimental data from PSU processed with the empirical free-field response.

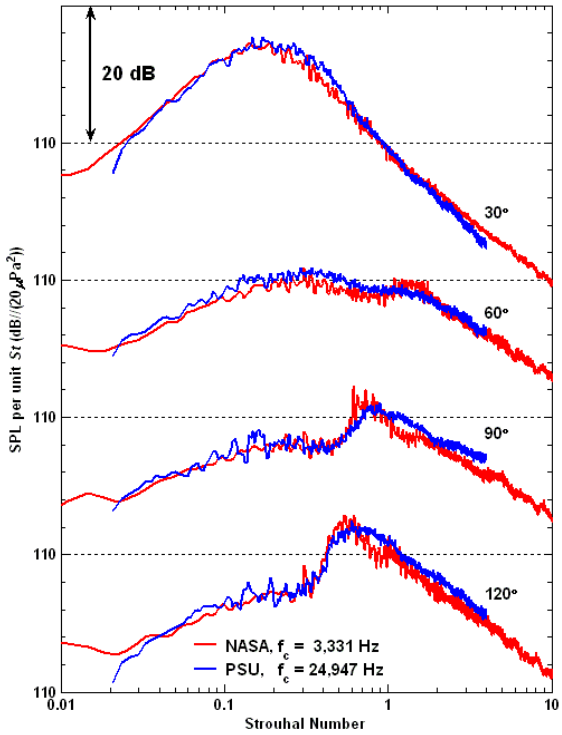

Figure **A-14**: Lossless spectra comparison from PSU (processed with the empirical free-field response) and NASA issuing from M_d = 1.5 (AR = 1.18) GE nozzle operated at NPR = 3.5, M_j = 1.47, and scaled to R/D = 100.

An additional comparison was made also with jets issuing from a contoured CD nozzle shown in Figure **A-15**. In this case, jets are operating at close to perfectly expanded pressure ratios. The data, measured in jets whose diameters differ by a factor of 8, agree across the spectra within about 1 dB. This is the strongest evidence that the newly developed microphone measurement correction method is very accurate.

As a final comment, while explanations were given behind the choice of keeping the grid caps and using the grazing orientation, it is acknowledged that a large majority of high speed jet noise experiments are performed with microphones that are oriented at normal incidence to the oncoming acoustic waves. It is noted however, that a draft standard [142] for "Methods for the Measurement of Noise Emissions from High Performance Military Jet Aircraft" is presently being developed by a group of Department of Defense, NASA and academic contributors. The

standard for flyover measurements specifies microphone placement at grazing incidence with grid caps in place. The correction methodology described in this paper is directly applicable to measurements following such specification.

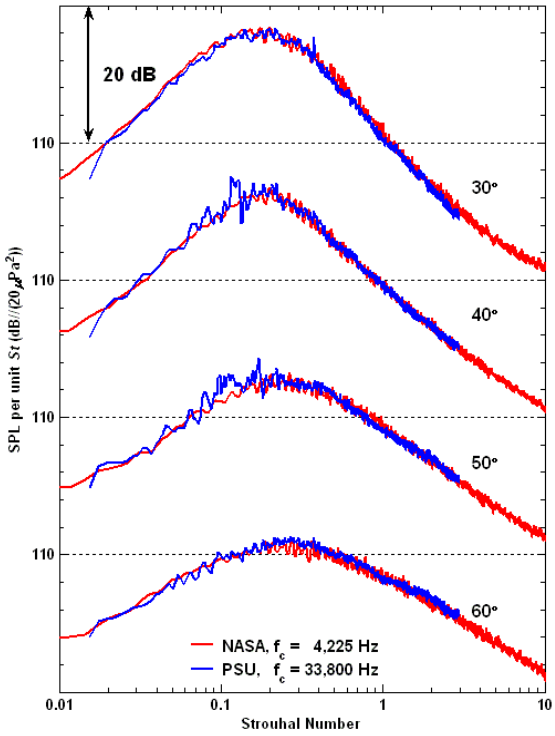

Figure **A-15**: Lossless spectra comparison from PSU (processed with the empirical free-field response) and NASA issuing from $M_d = 1.5$ ($AR = 1.18$) CD nozzle operated at $NPR = 3.67$, $M_j = 1.5$, and scaled to $R/D = 100$.

A.6 Summary

The jet noise research laboratory at the Pennsylvania State University has been conducting small-scale measurements for the past 15 years with reasonable accuracy compared to moderate-scale or full-scale measurements made in NASA or industrial laboratories. However, as more noise reduction concepts have been proposed, the need to produce more accurate data increases. Therefore the current study focused on methods to improve the precision of acoustic measurements at the high frequency range in small-scale high speed jet experiments. In such experiments the acoustic spectra contain significant energy up to 100 kHz which challenges the accuracy of present methods. An extensive series of measurements in the acoustic field of transonic and supersonic jets has demonstrated that for improved accuracy, the published free-field response of the microphones needs to be substantially altered to provide (significantly) improved accuracy of the measurements. Thus a method is proposed to replace the published free-field response by an empirical free-field response calculated specifically for microphones operated with grazing incidence orientation. It is noted that such a positioning of the microphones can provide an additional advantage, with less sensitivity to acoustic directionality, in some situations. Due to differences in the details of the geometry of their grid caps, two different empirical free-field responses are developed: one for *B&K* and one for *GRAS* microphones. Several comparisons using this new response demonstrated the significantly improved accuracy of high frequency components of the acoustic spectra, as high as 100 kHz. Thus the usable range of acoustic measurements of the spectra of the Penn State high speed small-scale jets has been extended. Such an improvement is particularly important in experiments that quantify the phenomenon of non-linear propagation distortion, a topic of increased importance with studies of very high speed exhaust jets of military aircraft.

Appendix B

The Low Reynolds Number Effect on Excessive Noise Contribution to Low Freqeuency Components of Spectra Measured with Heated Jet Simulation

Figure **B-1** shows the spectral comparison between the heat simulated jet and heated jet measurements. These measurements were both conducted at far-field, but in different non-dimensional locations. A systematic discrepancy was observed across all observation angles presented in the figures. There is excessive noise contribution to the low frequency components of spectra from the measurements conducted with the heat simulated jets (PSU data). The Reynolds number remained low while measuring the heated jet simulation. It is, therefore, speculated that low Reynolds number effect may contribute to this discrepancy. Although the discrepancy is similar to the effect caused by the noise source distribution (i.e. the observed discrepancy in the spectral comparison from the measurements conducted at different non-dimensional locations), the noise source distribution will not cause the discrepancy observed in the spectral comparison from the measurement conducted at the far-field (the measured locations conducted in this study) but not identical non-diementional locations. Figure **B-2** shows there is still a systematic discrepancy observed in the the spectral comparison from the measurements both conducted at R/D = 140; this example demonstrates the possibility that the low Reynolds numbers causes the discrepancy.

Furthermore, to prove the discrepancy is not caused by the noise source distribution, we compared the spectra synthesized at R/D = 80, 100, and 120 and found the discrency caused by the noise source distribution is smaller than the observed one in Figure **B-1**. Figure **B-3** extracted from Figure **5-18** demonstrates that the synthesized spectrum can represent the measured spectrum. Similar to Figure **B-3**, three spectra were generated via similar procedures synthesized

to *R/D* = 80, 100, and 120. Figure **B-4** shows the spectral comparison with all spectra scaling to *R/D* = 140. The discrepancy measured between *R/D* = 80 and 140 is around 1 dB across the low frequency contents; therefore, the discrepancies between R/D 140 and the synthesized spectra at *R/D* = 100 or 120 are then less than 1 dB. This demonstrates that the effect of the noise source distribution becomes insignificant (less than 1 dB discrepancy at this jet operating condition) when the measurements are conducted at far-field. For all actual measurements conducted at the Penn State, the values of *R/D* have been carefully kept to be larger than 100, so the discrepancy due to the R/D differences should be less than 1dB. However, the observed discrepancy in Figure **B-1** is around 3 dB, which can only leads a conclusion that the cause is the low Reynolds number.

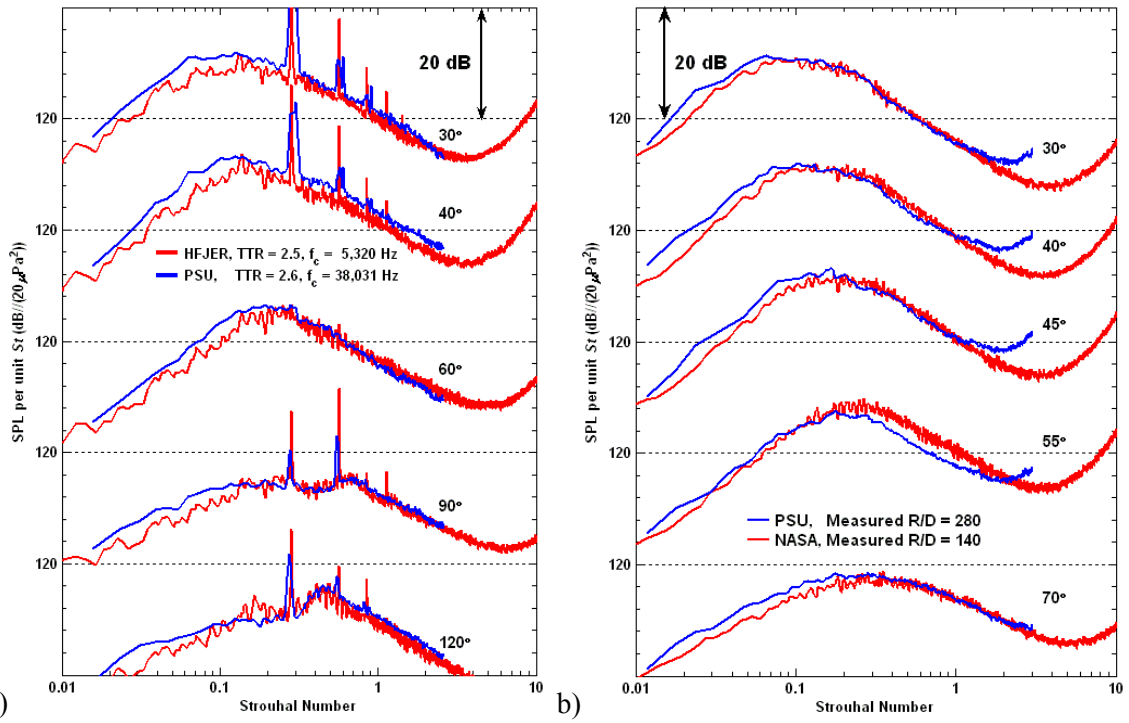

Figure **B-1**: a) Spectral comparison of heat simulated jet (*TTR* = 2.6) from PSU and heated jet (*TTR* = 2.5) from HFJER both issuing from GE nozzle with M_d = 1.65, M_j = 1.36, and scaled to *R/D* = 100. b) Spectral comparison from the measurements between PSU (*D* = 0.5 in.) and NASA HFJER (*D* = 4 in.) both conducted with CD M_d 1.5 nozzle operated at M_j = 1.5 for *TTR* = 2.2 with measured *R/D* = 280 and 140 respectively.

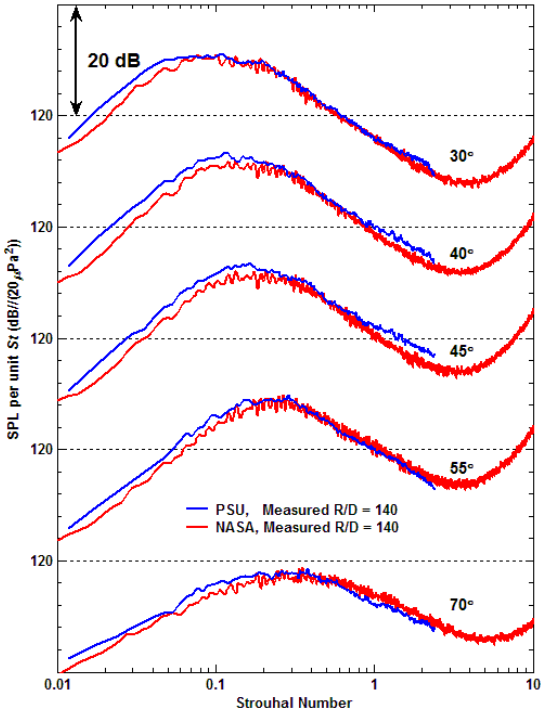

Figure **B-2**: Spectral comparison from the measurements between PSU (D = 0.5 in.) and NASA HFJER (D = 4 in.) both conducted with CD M_d 1.5 nozzle operated at M_j = 1.5 for TTR = 2.2 with measured R/D = 140.

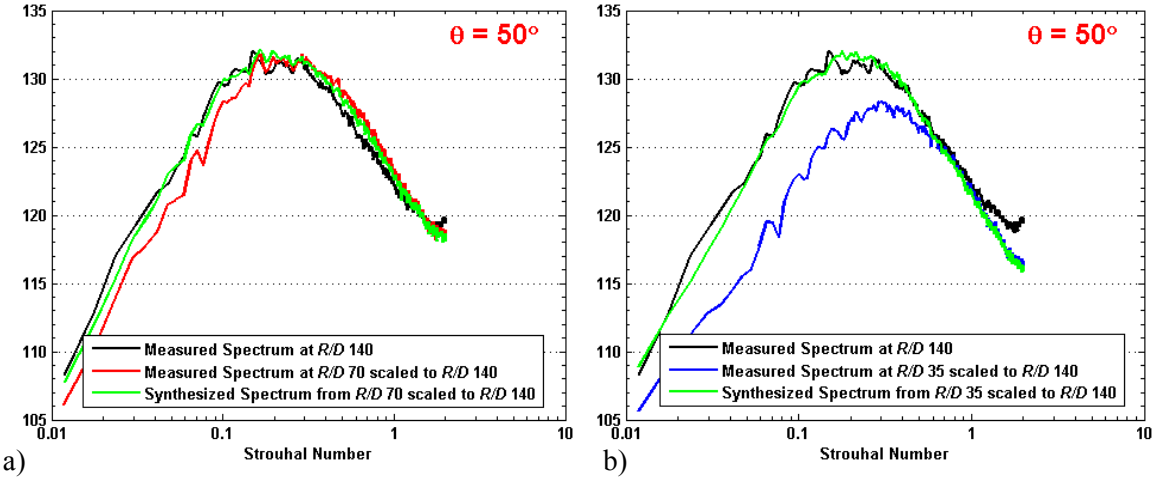

Figure **B-3**: Acoustic measurements conducted with CD nozzle (M_d = 1.5, D = 0.5 in.) operated at M_j = 1.5, TTR = 2.2 and corrected with noise source distribution. a) Spectra from R/D = 70 synthesized to R/D = 140. b) Spectra from R/D = 35 synthesized to R/D = 140.

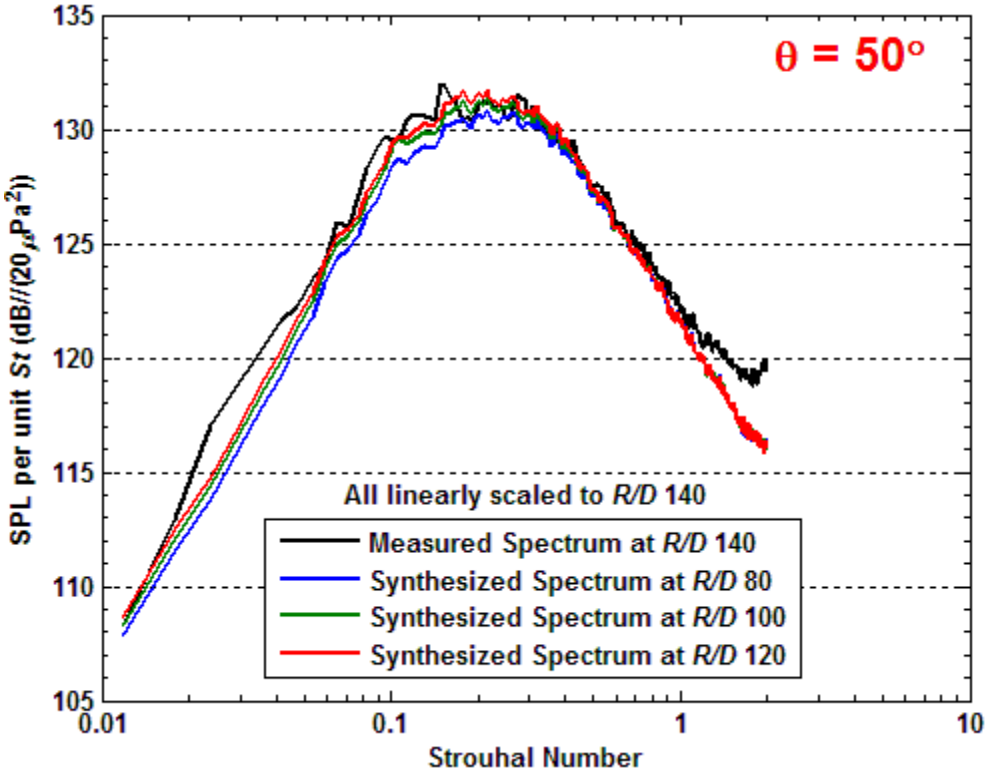

Figure **B-4**: Acoustic measurements conducted with CD nozzle (M_d = 1.5, D = 0.5 in.) operated at M_j = 1.5, TTR = 2.2. Spectrum as measured at R/D 140 and synthesized spectra at R/D = 80, 100, and 120 (from measurements acquired at R/D = 35). All spectra are linearly scaled to R/D = 140.

Bibliography

[1] Lighthill, M. J., "On sound generated aerodynamically. I. General theory," *Proceedings of the Royal Society of London. Series A, Mathematical and Physical Sciences*, Vol. 211, No. 1107, 1952, pp. 564-587.

[2] Lighthill, M. J., "On sound generated aerodynamically. II. Turbulence as a source of sound," *Proceedings of the Royal Society of London. Series A, Mathematical and Physical Sciences*, Vol. 222, No. 1148, 1954, pp. 1-32.

[3] Ffowcs-Williams, J. E., "The noise from turbulence convected at a high-speed," *Philos. Trans. Roy. Soc. London Ser. A*, Vol. 255, 1963, pp. 469-503.

[4] Atvars, J., Schubert, L. K, and Ribner, H. S., "Refraction of sound from a point source placed in an air jet," *J. Acoust. Soc. Amer.,* Vol. 37, 1965, pp. 168-170.

[5] Lilley, G. M., "On the noise from jets. Noise mechanisms," AGARD-CP-131, 1974, pp. 13.1–13.12.

[6] Ribner, H. S., "Strength distribution of noise source along a jet," *J. Acoust. Soc. Amer.*, Vol. 30, No. 9, 1958, pp. 876.

[7] Powell, A., "Similarity and turbulent jet noise," *J. Acoust. Soc. Amer.*, Vol. 31, No. 6, 1959, pp. 812-813.

[8] Nagamatsu, H. T., Sheer, R. E., and Horvay, G., "Supersonic jet noise theory and experiments," Basic aerodynamic noise research NASA SP-207, Washington, D. C., July 14-15,1969.

[9] Philips, O. M., "On the generation of sound by supersonic turbulent shear layers," *Journal of Fluid Mechanics*, Vol. 9, 1960, pp. 1–28.

[10] Tam, C. K. W. and Morris, P. J., "The radiation of sound by the instability waves of a compressible plane turbulent shear layer," *Journal of Fluid Mechanics*, Vol. 98, 1980, pp. 349–381.

[11] Morris, P. J. and Tam, C. K. W., "Near and far field noise from large-scale instabilities of axisymmetric jets," AIAA Paper No. 77-1351, 1977.

[12] Morris, P. J. and Tam, C. K. W., "On the radiation of sound by the instability waves of a compressible axisymmetric Jet," Mechanisms of Sound Generation in Flows, E.A. Muller, Editor, Springer-Verlag, 1979.

[13] Tam, C. K. W. and Burton, D. E., "Sound generated by instability waves of supersonic flows. Part 2. Axisymmetric jets," *Journal of Fluid Mechanics*, Vol. 138, 1984, pp. 273–295.

[14] McLaughlin, D. K., Morrison, G. L., and Troutt, T. R., "Experiments on the instability waves in a supersonic jet and their acoustic radiation," *Journal of Fluid Mechanics*, Vol. 69, 1975, pp. 73–95.

[15] Morrison, G. L. and McLaughlin, D. K., "The noise generation by instabilities in low Reynolds number supersonic jets," *Journal of Sound and Vibration*, Vol. 65, No. 2, 1979, pp. 177–191.

[16] Troutt, T. R. and McLaughlin, D. K., "Experiments on the flow and acoustic properties of a moderate-Reynolds-number supersonic jet," *Journal of Fluid Mechanics*, Vol. 116, 1982, pp. 123–156.

[17] Tam, C. K. W., Chen, P., and Seiner, J. M., "Relationship between the instability waves and noise of high-speed jets," *AIAA Journal*, Vol. 30, No. 7, 1992, pp. 1747-1752.

[18] Seiner, J. M., Bhat, T. R. S., and Ponton, M. K., "Mach wave emission from a high-temperature supersonic jet," *AIAA Journal*, Vol. 32, No. 12, 1994, pp. 2345-2350.

[19] Veltin, J., Day, B. J., and McLaughlin, D. K., "Correlation of flow and acoustic field measurements in high speed jets," AIAA Paper No. 2009-3250, 2009. Submitted for publication to the AIAA Journal 2010.

[20] Veltin, J., "On the characterization of noise sources in supersonic shock containing jets," PhD Thesis, 2008, The Pennsylvania State University.

[21] Day, B. J., "Turbulence measurements in supersonic jets with optical deflectometry," Master Thesis, 2010, The Pennsylvania State University.

[22] Tam, C. K. W., Golebiowski M., and Seiner J. M., "On the two components of turbulent mixing noise from supersonic jets," AIAA Paper No. 96-1716, 1996.

[23] Tam, C. K. W. and Zaman, K. B. M. Q., "Subsonic jet noise from nonaxisymmetric and tabbed nozzles," *AIAA Journal*, Vol. 38, No. 4, 2000, pp. 592-599.

[24] Harper-Bourne, M. and Fisher, M. J., "The noise from shockwaves in supersonic jets," AGARD-CP-131, 1974, pp. 11.1-11.13.

[25] Powell A., "On the mechanism of choked jet noise," *Proceedings of the Royal Society of London. Series B*, Vol. 66, 1953, pp. 1039-1056.

[26] Poldervarrt, L. J., Vink, A. T., and Wijnands, A. P. J., "The photographic evidence of the feedback loop of a two dimensional screeching supersonic jet of air," *Proceedings of the International Congress on Acoustics*, Tokyo, Japan, Aug 21-28, 1968.

[27] Norum, T. D., "Screech suppression in supersonic jets," *AIAA Journal*, Vol. 21, No. 2, 1983, pp. 235-240.

[28] Tam, C. K. W., Seiner, J. M., and Yu, J. C., "Proposed relationship between broadband shock associated noise and screech tones," *Journal of Sound and Vibration*, Vol. 110, No. 2, 1986, pp. 309-321.

[29] Pao, S.P., Wenzel, A.R., and Oncley, P.B., "Prediction of ground effects on aircraft noise," NASA Technical Paper 1104, 1978.

[30] Lassiter, L. W. and Hubbard, H. H., "The near noise field of static jets and some model studies of devices for noise reduction," National Advisory Committee for Aeronautics, Report 1261, 1956.

[31] Viswanathan, K., "Does a model scale nozzle emit the same jet noise as a jet engine," *AIAA Journal*, Vol. 46, No. 2, 2008, pp. 336-355.

[32] Olsen, W. A., Gutierrez, O. A., and Dorsch, R. G., "The effect of nozzle inlet shape lip thickness and exit shape and size on subsonic jet noise," AIAA 11th Aerospace Sciences Meeting, Washington D. C., Jan 10-12, 1973.

[33] Seiner, J. M., Norum, T. D., and Maestrello, L., "Effects of nozzle design on the noise from supersonic jets," NASA Technical Reports Server, 1980.

[34] Viswanathan, K. and Clark, L. T., "Effect of nozzle internal contour on jet aeroacoustics," *International Journal of Aeroacoustics*, Vol. 3, No. 2, 2004, pp. 103–135.

[35] Bridges, J. and Hussain, F., "Effects of nozzle body on jet noise," *Journal of Sound and Vibration*, Vol. 188, No. 3, 1995, pp. 407–418.

[36] Zapryagaev, V. I. and Solotchin, A. V., "An experimental investigation of the nozzle roughness effect on streamwise vortices in a supersonic jet," *Journal of Applied Mechanics and Technical Physics*, Vol. 38, No. 1, 1997, pp. 78-86.

[37] Ponton, M. K. and Seiner, J. M., "The effects of nozzle exit lip thickness on plume resonance," *Journal of Sound and Vibration*, Vol. 154, No. 3, 1992, pp. 531–549.

[38] McLaughlin, D. K., Morrison, G. L., and Troutt, T. R., "Reynolds number dependence in supersonic jet noise," *AIAA Journal*, Vol. 15, No. 4, 1977, pp. 526-532.

[39] Stromberg, J. L., McLaughlin, D. K., and Troutt, T. R., "Flow field and acoustic properties of a Mach number 0.9 jet at a low Reynolds number," *Journal of Sound and Vibration*, Vol. 72, No. 2, 1980, pp. 159–176.

[40] Hu, T.-F. and McLaughlin, D. K., "Flow and acoustic properties of low Reynolds number underexpanded supersonic jets," *Journal of Sound and Vibration*, Vol. 141, No. 3, 1990, pp. 485–505.

[41] Viswanathan, K. "Aeroacoustics of hot jets," *Journal of Fluid Mechanics*, Vol. 516, 2004, pp. 39–82.

[42] Zaman, K. B. M. Q., "Flow field and near and far sound field of a subsonic jet," *Journal of Sound and Vibration*, Vol. 106, No. 1, 1986, pp. 1–16.

[43] Papamoschou, D. and Debiasi, M., "Noise measurements in supersonic jets treated with the Mach wave elimination method," *AIAA Journal*, Vol. 37, No. 2, 1999, pp. 154-160.

[44] Koch, L. D., Bridges, J., Brown, C., and Khavaran, A., "Experimental and analytical determination of the geometric far field for round jets," *Noise Control Engineering Journal*, Vol. 53, No. 1, 2005, pp.20–28.

[45] Viswanathan, K., "Instrumentation considerations for accurate jet noise measurements," *AIAA Journal*, Vol. 44, No. 6, 2006, pp. 1137-1149.

[46] Pannu, S. S. and Johannesen, N. H., "The structure of jets from notched nozzles," *Journal of Fluid Mechanics*, Vol. 74, 1976, pp. 515–528.

[47] Zaman, K. B. M. Q., Reeder, M. F., and Samimy, M., "Supersonic jet mixing enhancement by delta tabs," AIAA Paper No. 92-3548, 1992.

[48] Bridges, J. and Brown, C., "Parametric testing of chevrons on single flow hot jets," AIAA Paper No. 2004-2824, 2004.

[49] Doty, M. J. and McLaughlin, D. K., "Acoustic and mean flow measurements of high-speed, helium-air mixture jets," *International Journal of Aeroacoustics*, Vol. 2, No. 2, 2003, pp. 293–334.

[50] Doty, M., "An experimental investigation of the aeroacoustic properties of high-speed, helium/air mixture axisymmetric jets", PhD Thesis, 2002, The Pennsylvania State University.

[51] Henderson, B. and Bridges, J., "An MDOE investigation of chevrons for supersonic jet noise reduction," AIAA Paper No. 2010-3926, 2010.

[52] Bridges, J., "Measurements of turbulent flow field in separate flow nozzles with enhanced mixing devices—Test Report," NASA TM—2002-211366, 2002.

[53] Bridges, J. and Brown, C. A., "Validation of the small hot jet acoustic rig for aeroacoustic research," AIAA Paper No. 2005-2846, 2005.

[54] Viswanathan, K., "Jet aeroacoustic testing: Issues and implications," *AIAA Journal*, Vol. 41, No. 9, 2003, pp. 1674-1689.

[55] Kinzie, K. W. and McLaughlin, D. K., "Measurements of supersonic Helium/Air mixture jets," *AIAA Journal*, Vol. 37, No. 11, 1999, pp. 1363-1369.

[56] Papamoschou, D., "Acoustic simulation of coaxial hot air jets using cold Helium–Air mixture jets," *Journal of Propulsion and Power*, Vol. 23, No. 2, 2007, pp. 375–381.

[57] Miller, S. and Veltin, J., "Experimental and numerical investigation of flow properties of supersonic helium-air jets," AIAA Paper No. 2010-471, 2010.

[58] Bridges, J., Jet noise data provided by personal communication, 2008.

[59] Blackstock, D. T., "Nonlinear propagation distortion of jet noise," Applied research laboratories, Univ. Texas at Austin, 1975.

[60] Webster, D. A. and Blackstock, D. T., "Experimental investigation of outdoor propagation of finite-amplitude noise," CR 2992, NASA, 1975.

[61] Lowson, M. V. and Ollerhead, J. B., "Visualization of noise from cold supersonic jets," *J. Acoust. Soc. Amer.*, Vol. 44, No. 2, 1968, pp. 624–630.

[62] Petitjean, B. P. and McLaughlin, D. K., "Experiments on the nonlinear propagation of noise from supersonic jets," AIAA Paper No. 2003-3127, 2003.

[63] Petitjean, B. P. and McLaughlin, D. K., "Characterizing acoustic pressure waveforms in jet noise experiencing nonlinear propagation," AIAA Paper No. 2004-3017, 2004.

[64] Viswanathan, K., Alkislar, M. B., and Czech, M. J., "Characteristics of the shock noise component of jet noise," AIAA Paper No. 2008-2835, 2008.

[65] Pernet, D.F. and Payne, R.C., "Nonlinear propagation of signals in air," *J. Sound Vib.*, Vol. 17, No. 3, 1971, pp. 383–396.

[66] Crighton, D. G., "Model equations of nonlinear acoustics," *Annual Review of Fluid Mechanics*, Vol. 11, 1979, pp. 11-33.

[67] Morfey, C. L. and Howell, G. P., "Nonlinear propagation of aircraft noise in the atmosphere," *AIAA Journal*, Vol. 19, No. 8, 1981, pp. 986-992.

[68] Howell, G. P. and Morfey, C. L., "Nonlinear propagation of broadband noise signals," *J. Sound Vib.*, Vol. 114, No. 2, 1987, pp. 189–201.

[69] Brouwer, H. H., "Numerical simulation of nonlinear jet noise propagation," AIAA Paper No. 2005-3088, 2005.

[70] Saxena, S., Morris, P. J., and Viswanathan, K., "Algorithm for the nonlinear propagation of broadband jet noise," *AIAA Journal*, Vol. 47, No. 1, 2009, pp. 186-194.

[71] Petitjean, B. P., Morris, P. J., and McLaughlin, D. K., "On the nonlinear propagation of shock-associated jet noise," AIAA Paper No. 2005-2930, 2005.

[72] Seiner, J. M. and Norum, T. D., Jet noise data provided by private communication, 2001.

[73] Lee, S. S. and Bridges, J., "Phased-array measurements of single flow hot jets," AIAA Paper No. 2005-2842, 2005.

[74] McLaughlin, D. K., Kuo, C.-W., and Papamoschou, D., "Experiments on the effect of ground reflections on supersonic jet noise," AIAA Paper No. 2008-22, 2008.

[75] Chu, W. T., Laufer, J., and Kao, K., "Noise source distribution in subsonic jets," International Conference on Noise Control Engineering, Washington D.C., Oct 4-6, 1972.

[76] Grosche, F. -R., "Distributions of sound source in intensities in subsonic and supersonic jets," AGARD-CP-131, 1974, pp. 4.1–4.10.

[77] Laufer, J., Schlinker, R., and Kaplan, R. E. "Experiments on supersonic jet noise," *AIAA Journal*, Vol. 4, No. 4, 1976, pp. 489-497.

[78] Papamoschou, D. and Dadvar, A., "Localization of multiple types of jet noise sources," AIAA Paper No. 2006-2644, 2006.

[79] Dougherty, R. P. and Podboy, G. G., "Improved phased array imaging of a model jet," AIAA Paper No. 2009-3186, 2009.

[80] Potter, R. C., "Jet-orifice-surface interaction noise," Basic aerodynamic noise research NASA SP-207, Washington, D. C., July 14-15, 1969.

[81] Bishop, K. A., Ffowcs Williams, J. E., and Smith, W., "On the noise source of the unsuppressed high-speed jet," *J. Fluid Mech.*, Vol. 50, 1971, pp. 21–31.

[82] MacGregor, G. R. and Simcox, C. D., "The location of acoustic sources in jet flows by means of the 'wall isolation' technique," AIAA Paper No. 73-1041, 1973.

[83] Petersen, R. A., Kaplan, R. E., and Laufer, J., "Ordered structures and jet noise," CR-134733, NASA, 1974.

[84] Tester, B. J., Morris, P. J., Lau, J. C., and Tanna, H. K., "The generation, radiation, and prediction of supersonic jets noise," AFAPL-TR-78-85, Vol. 1, 1978.

[85] Seiner, J. M. and Ponton, M. K., "Aeroacoustic data for high Reynolds number supersonic axisymmetric jets," TM 86296, NASA, 1985.

[86] Narayanan, S., Barber, T. J., and Polak, D. R., "High subsonic jet experiments turbulence and noise generation studies," *AIAA Journal*, Vol. 40, No. 3, 2002, pp. 430-437.

[87] Panda, J., and Seasholtz, R. G., "Experimental investigation of density fluctuations in high-speed jets and correlation with generated noise," *J. Fluid Mech.*, Vol. 450, 2002, pp. 97–130.

[88] Ukeiley, L. S. and Ponton. M. K., "On the near field pressure of a transonic axisymmetric jet," *International Journal of Aeroacoustics*, Vol. 3, No. 1, 2004, pp. 43–66.

[89] Tam, C. K. W., Pastouchenkoa, N. N., and Schlinker, R. H., "Noise source distribution in supersonic jets," *J. Sound Vib.,* Vol. 291, 2006, pp. 192–201.

[90] Bogey, C., Barre, S., Fleury, V., Bailly, C., and Juve, D., "Experimental study of the spectral properties of near-field and far-field jet noise," *International Journal of Aeroacoustics*, Vol. 6, No. 2, 2007, pp. 73–92.

[91] Papamoschou, D., Morris, P. J., and McLaughlin, D. K., "Beamformed flow-acoustic correlations in high-speed jets," AIAA Paper No. 2009-3212, 2009.

[92] Ahuja, K. K., Tester, B. J., and Tanna, H. K., "Calculation of far field jet noise spectra from near field measurements with true source location," *J. Sound Vib.,* Vol. 116, 1987, pp. 415–426.

[93] Laufer, J., Kaplan, R. E., and Chu, W.T., "On noise produced by subsonic jets," Proceedings of the Second Interagency Symposium on University Research in Transportation Noise, Vol. I, 1974, pp. 50-58.

[94] Tanna, H. K., "An experimental study of jet noise Part I: Turbulent mixing noise," *J. Sound Vib.*, Vol. 50, No. 3, 1977, pp. 405–428.

[95] Harper-Bourne, M., "Jet noise turbulence measurements," AIAA Paper No. 2003-3214, 2003.

[96] Kerhervé, F., Fitzpatrick, J., and Jordan, P., "The frequency dependence of jet turbulence for noise source modeling," *J. Sound Vib.*, Vol. 296, 2006, pp. 209-225.

[97] Morris P. J. and Zaman, K. B. M. Q., "Velocity measurements in jets with application to noise source modeling," *J. Sound Vib.*, Vol. 329, 2010, pp. 394-414.

[98] Bridges, J. and Wernet, M. P., "Effect of temperature on jet velocity spectra," AIAA Paper No. 2007-3628, 2007.

[99] Lau, J. C., Morris, P. J., and Fisher, M. J., "Measurements in subsonic and supersonic free jets using a laser velocimeter," *Journal of Fluid Mechanics*, Vol. 93, 1979, pp. 1–27.

[100] Petitjean, B. P., "On the nonlinearities in the noise radiated from high-speed model jets", PhD Thesis, 2006, The Pennsylvania State University.

[101] Gee, K. L., Shepherd, M. R., Falco, L. E., Atchley, A. A., Ukeiley, L. S., Jansen, B. J., and Seiner, J. M., "Identification of nonlinear and near-field effects in jet noise using nonlinearity indicators," AIAA Paper No. 2007-3653, 2007.

[102] Petitjean, B. P., Viswanathan, K., McLaughlin, D. K., and Morris, P. J., "Space-time correlation measurements in subsonic and supersonic jets using optical deflectometry," AIAA Paper No. 2007-3613, 2007.

[103] Goss, A. E., Veltin, J., Jaehyung, L., and McLaughlin, D. K., "Acoustic measurements of high-speed jets from rectangular nozzle with thrust vectoring," *AIAA Journal*, Vol. 47, No. 9, 2009, pp. 1482-1490.

[104] Davies, P. O. A. L., Fisher, M. J., and Barratt, M. J., "The characteristics of the turbulence in the mixing region of a round jet," *Journal of Fluid Mechanics*, Vol. 15, 1963, pp. 337–367.

[105] Bradshaw, P., Ferris, D. H., and Johnson, R. F., "Turbulence in the noise-producing region of a circular jet," *Journal of Fluid Mechanics*, Vol. 19, 1964, pp. 591–624.

[106] Wygnanski, I. and Fiedler, H., "Some measurements in the self-preserving jet," *Journal of Fluid Mechanics*, Vol. 38, 1969, pp. 577–612.

[107] Crow, S. C. and Champagne, F. H., "Orderly structure in jet turbulence," *Journal of Fluid Mechanics*, Vol. 48, 1971, pp. 547–591.

[108] Yule, A. J., "Large-scale structure in the mixing layer of a round jet," *Journal of Fluid Mechanics*, Vol. 89, 1978, pp. 413–432.

[109] Bradbury, L. J. S. and Khadem, A. H., "The distortion of a jet by tabs," *Journal of Fluid Mechanics*, Vol. 70, 1975, pp. 801–813.

[110] Wlezien, R. W. and Kibens, V., "Influence of nozzle asymmetry on supersonic jets," *AIAA Journal*, Vol. 26, No. 1, 1988, pp. 27-33.

[111] Elliott, G. S. and Samimy M., "Compressibility effects in free shear layers," *Physics of Fluids A*, Vol. 2, No. 7, 1990, pp. 1231-1240.

[112] Tillman, T. G., Patrick, W. P., and Paterson, R. W., "Enhanced mixing of supersonic jets," *Journal of Propulsion and Power*, Vol. 7, No. 6, 1991, pp. 1006–1014.

[113] Samimy, M., Zaman, K. B. M. Q., and Reeder, M. F., "Effect of tabs on the flow and noise field of an axisymmetric jet," *AIAA Journal*, Vol. 31, No. 4, 1993, pp. 609-619.

[114] Krothapalli, A., King, C. J., and Strykowski, P. J., "The role of streamwise vortices on the sound generation of supersonic jets," AIAA Paper No. 93-4320, 1993.

[115] Carletti, M. J., Rogers, C. B., and Parekh, D. E., "Use of streamwise vorticity to increase mass entrainment in a cylindrical ejector," *AIAA Journal*, Vol. 33, No. 9, 1995, pp. 1641-1645.

[116] Knowles, K. and Saddington, A. J., "A review of jet mixing enhancement for aircraft propulsion applications," *Proc. IMechE Part G: J. Aerospace Engineering*, Vol. 220, 2006, pp. 103–127.

[117] Longmire, E. K., Eaton, J. K., and Elkins, C. J., "Control of jet structure by crown-shaped nozzles," *AIAA Journal*, Vol. 30, No. 2, 1992, pp. 505-512.

[118] Alkislar, M. B., Krothapalli, A., and Butler, G. W., "The effect of streamwise vortices on the aeroacoustics of a Mach 0.9 jet," *Journal of Fluid Mechanics*, Vol. 578, 2007, pp. 139–169.

[119] Callender, B., Gutmark, E., and Martens, S., "Far-field acoustic investigation into chevron nozzle mechanisms and trends," *AIAA Journal*, Vol. 43, No. 1, 2005, pp. 87-95.

[120] Bridges, J. and Wernet, M. P., "Turbulence measurements of separate flow nozzle with mixing enhancement features," AIAA Paper No. 2002-2484, 2002.

[121] Gutmark, E., Callender, B. W., and Martens, S., "Aeroacoustics of turbulent jets: Flow structure, noise sources, and control," *JSME International Journal Series B*, Vol. 49, No. 4, 2006, pp. 1078-1085.

[122] Opalski, A. B., Wernet, M. P., and Bridges, J., "Chevron nozzle performance characterization using stereoscopic DPIV," AIAA Paper No. 2005-444, 2005.

[123] Foss, J. K. and Zaman, K. B. M. Q., "Large- and small-scale vortical motions in a shear layer perturbed by tabs," *Journal of Fluid Mechanics*, Vol. 382, 1999, pp. 307-329.

[124] McLaughlin, D. K., Bridges, J., and Kuo, C.-W., "On the scaling of small, heat simulated jet noise measurements to moderate size exhaust jets," *International Journal of Aeroacoustics,* Vol. 9, No. 4&5, 2010, pp. 627–654.

[125] Papamoschou, D. and Zill, A., "Fundamental investigation of supersonic nozzle flow separation," AIAA Paper No. 2004-1111, 2004.

[126] Romine, G. L., "Nozzle flow separation," *AIAA Journal*, Vol. 36, No. 9, 1998, pp. 1618-1625.

[127] Gutmark, E. and Ho, C.-M., "Preferred modes and the spreading rates of jets," *Physics of Fluids*, Vol. 26, No. 10, 1983, pp. 2932-2938.

[128] Miller, S. A. E., "The prediction of broadband shock-associated noise using Reynolds-averaged Navier-Stokes Solutions", PhD Thesis, 2009, The Pennsylvania State University.

[129] Veltin, J., Day, B. J. and McLaughlin, D. K., "Forward flight effect on small scale supersonic jet acoustics," AIAA Paper No. 2010-3924, 2010.

[130] Norum, T. D. and Shearin, J. G., "Effects of simulated flight on the structure and noise of underexpanded jets," NASA TP 2308, 1984.

[131] Norum, T. D. and Shearin, J. G., "Shock structure and noise of supersonic jets in simulated flight to Mach 0.4," NASA TP 2785, 1988.

[132] Papamoschou, D. and Mayoral, S., "Experiments on shielding of jet noise by airframe surfaces," AIAA Paper No. 2009-3326, 2009.

[133] Kuo, C.-W., Veltin, J., and McLaughlin, D. K., "Effects of jet noise source distribution on acoustic far-field measurements," AIAA Paper No. 2010-474, 2010.

[134] Bridges, J. and Wernet, M. P., "Turbulence associated with broadband shock noise in hot jets," AIAA Paper No. 2008-2834, 2008.

[135] Ahuja, K. K, "Designing clean jet noise facilities and making accurate jet noise measurements", *International Journal of Aeroacoustics*, Vol. 2, No 3 & 4, 2003, pp. 371-412.

[136] Bass, H. E., Sutherland, L. C., and Zuckerwar, A. J., "Atmospheric absorption of sound: Update," *J. Acoust. Soc. Amer.*, Vol. 88, No. 4, 1990, pp. 2019–2021.

[137] Bass, H. E., Sutherland, L. C., Blackstock, D. T., and Hester, D. M., "Atmospheric absorption of sound: Further developments," *J. Acoust. Soc. Amer.*, Vol. 97, No. 1, 1995, pp. 680–683.

[138] Bruel & Kjaer, *INSTRUCTIONS AND APPLICATIONS: Eighth-inch Condenser Microphone*, Brüel & Kjær, Naerum, Denmark, 1967.

[139] Bruel & Kjaer, “Product Data: 1/8" Pressure-field Microphone Type 4138”, *Product Data Sheet BP 2030* [online database], URL: http://www.bksv.com/doc/bp2030.pdf [cited 15 April 2009].

[140] Harris, C. M., “Absorption of sound in air versus humidity and temperature,” *J. Acoust. Soc. Amer.*, Vol. 40, 1966, pp. 148-159.

[141] American National Standards Institute, “Method for the Calculation of the Absorption of Sound by the Atmosphere,” ANSI S 1.26-1995 (Revision of ANSI S 1.26, 1978).

[142] McKinley, R. L., *et al.*, “Methods for the measurements of noise emissions from high performance military jet aircraft,” DRAFT BSR/ASA S12.70-201X, 6 May 2010.

VITA

Ching-Wen Kuo

Ching-Wen Kuo was born on August 9th, 1978 in Taipei, Taiwan to Tao-Ming Kuo and Mei-Yun Chen. He graduated from Taipei Municipal Huajiang High School in June 1996 and received his bachelor degree in Mechanic Engineering from National Chung Cheng University in June 2000. He then attended National Cheng Kung University where he obtained his Master of Science degree in Aerospace Engineering in June 2002. He served in the army from August 2002 to February 2004 for the fulfillment of the citizen obligation. In August 2005, he came to The Pennsylvania State University to pursue the Ph. D. degree in the Aerospace Engineering department. He is a student member of the American Institute of Aeronautics and Astronautics.